The Effect of EDM Wire Cutting on the Fatigue Properties of 4340 Steel

---

A thesis

submitted in fulfilment

of the requirements for the Degree

of

Master of Engineering

in the

University of Canterbury

Wei Hsien Yvonne Yeo

August 1999

ABSTRACT

Electric discharge machining (EDM) is a metal removal process that has seen increasing use in the recent years. EDM is replacing the use of conventional machining in certain applications due to its ability to machine conductive materials of any hardness into highly complex shapes. One such application is the manufacture of structural components for skis used by Antarctica-bound Hercules aircraft. As fatigue properties are important for structural components used in the aeronautical industry, the effect of EDM on fatigue properties is significant. Literature indicates that EDM causes degradation in fatigue properties; however, there is insufficient information relating EDM wire cutting (EDWC) (the process to be used) to fatigue.

Results indicate that EDWC is greatly detrimental to fatigue properties. Fatigue limits of EDWC specimens are reduced from approximately 900MPa (ground specimens) to 300MPa. Numerous cracks in the surface and sub-surface of the specimens, together with a surface roughness of 3μm R_a, indicate that surface topography contributes to the reduction in fatigue limit. A phase change in the surface layer and the presence of a residual tensile stress are also possible contributing factors.

The effect of shot peening after EDWC is also investigated, as there is little information on this subject. Shot peening after the EDWC process has returned the fatigue limit to its initial value, and in some cases has even increased it

(1000MPa). This result is attributed to the introduction of residual compressive stresses in the surface. The use of EDWC alone to manufacture the aircraft structural components is not practical. By adding the shot peening process after EDWC, the manufacturing process can become a viable alternative to conventional machining.

ACKNOWLEDGEMENTS

I would like to thank the following people without whose help the project would not have succeeded.

Mr J. Thomson from Air New Zealand Ltd (project initiator)

Dr. M Cowling (supervisor)

Dr. M. Pugh (supervisor)

Dr. J. Smaill (supervisor)

Mr. D. Thomas from Air New Zealand Ltd

All the technicians from the Mechanical Engineering department

Air New Zealand Ltd (supplying the test materials)

Family and friends for their support

CONTENTS

LISTS OF FIGURES

LISTS OF TABLES

CHAPTER 1: INTRODUCTION

Electric discharge machining (EDM) is a non-conventional metal removal process with the ability to machine conductive materials of any hardness into complex shapes[1]. Using conventional machining processes such as milling and grinding to machine materials in the hardened state is economically unviable. Components have to be machined in the unhardened stage, before being hardened. The hardening process can produce distortion in the components that has to be removed by hand. EDM removes the difficulties with distortion by machining the components in their hardened state. This advantage makes EDM more attractive than conventional machining in certain applications. One application for which EDM might prove beneficial is the manufacture of structural components for skis used by Antarctica-bound Hercules aircraft.

The structural components used for the skis are currently manufactured by conventional machining from large billets of 300M (4340M) high strength steel. EDM wire cutting (EDWC) has been suggested as an alternative production method that would have the advantage of a shorter machining time and a reduction in the amount of scrap metal produced. EDWC has, however, been shown to produce degradation of fatigue properties[1].

Shot peening is suggested as a finishing process for EDWC components. Literature indicates that shot peening can be used to restore the fatigue life lost through EDM[2]. However, data relating to the effects of EDWC and shot peening

on fatigue is insufficient to ascertain the suitability of the processes for the production of the ski structures.

This research was initiated by Air New Zealand Ltd in 1995 as a Third Professional Year Project (Project No 12/95)[3], but was uncompleted in 1995 as a result of problems with the experimental equipment. This research work is a continuation and expansion of the project.

4340 steel and 300M steel have very similar compositions and properties. Therefore 4340 steel can be used as a cheaper alternative to 300M steel. The materials are hardened, then machined using the EDWC process through Air New Zealand Ltd. One-third of the specimens were shot peened and another third ground. The specimens were then tested at the University of Canterbury and the results analysed.

Chapter 2, 3 and 4 describes the background theory relevant to this research. The results obtained are summarised in Chapter 5. The complete set of results is given in the appendices. Chapter 6 discusses the reasons behind the results and their implications, while Chapter 7 summarises the findings and gives some recommendations for the use of this research.

CHAPTER 2: FATIGUE

In the ASTM standards, fatigue is defined as "the process of progressive localized permanent structural change occurring in a material subjected to conditions that produce fluctuating stresses and strains at some point or points and that may culminate in cracks or complete fracture after a sufficient number of fluctuations." The failure of the material normally occurs at stress levels that should, under static loading, give infinite lives[4]. Few mechanical and structural components are, however, subjected to constant loads throughout their entire service lives; therefore fatigue failures constitute the most common source of failures in structures[5,6]. Over the last twenty years, fatigue failures have accounted for approximately 80% of in service catastrophic fractures[7].

2.1 Macrofractography of Fatigue Failures

The examination of a fatigue fracture surface usually shows a number of common features[8]. There are two distinct zones present: a fatigue zone and a final rupture zone.

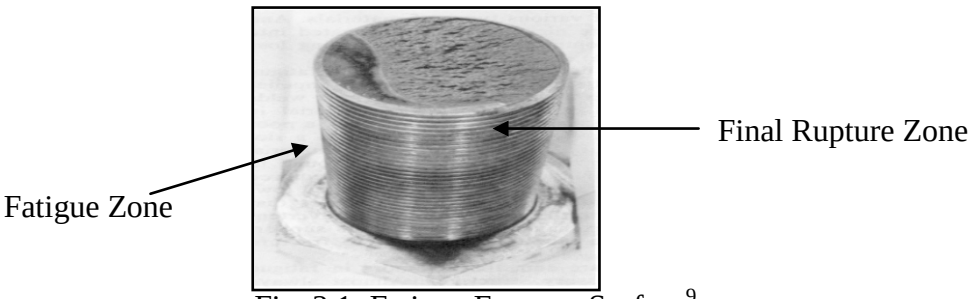

Fig. 2.1: Fatigue Fracture Surface[9]

There are a few characteristics that are unique to the fatigue zone. The fracture surface is generally flat, indicating the absence of any appreciable amounts of gross plastic deformation. Another characteristic is the presence of crack arrest lines (also referred to as "clam shell" or "beach" markings)[8].

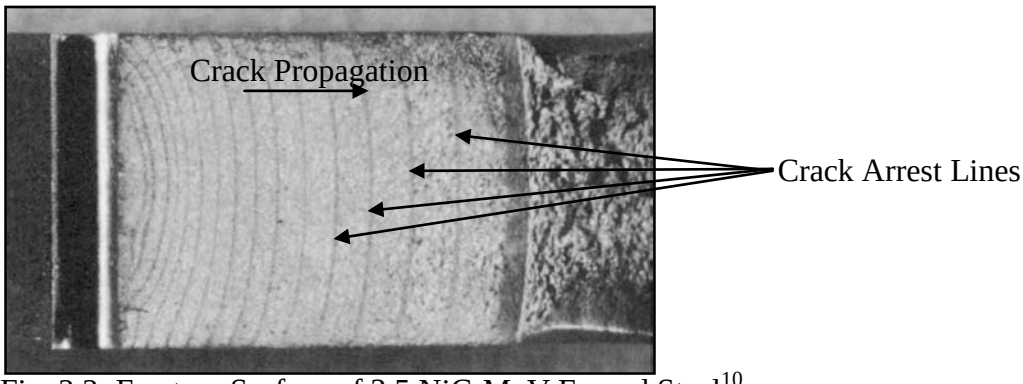

Fig. 2.2: Fracture Surface of 3.5 NiCrMoV Forged Steel[10]

The crack arrest lines are attributed to periods of crack growth and are believed to occur due to the oxidation or corrosion of the crack surface during the dormant periods (crack arrest periods)[11]. These markings are normally only present in fracture surfaces of failures that have been exposed to air over a long time period. Fracture surfaces of failures produced in the laboratory do not display these markings. The markings are seen to be perpendicular to the direction of crack propagation, making them a useful guide to identifying the fracture initiation site[8].

Another set of fracture surface markings that are present in the fatigue zone are ratchet lines. Ratchet lines are vertically orientated curved black lines that separate sets of crack arrest lines. These lines represent the junction surfaces between adjacent crack initiation sites. In a multi-crack initiation fracture, the cracks do not always form on the same plane. The linkage of the cracks causes the

creation of vertical steps on the fracture surface. As the cracks propagate to form a single major crack, the ratchet line disappears. The presence of the ratchet lines is due to factors such as the applied stress and the number of possible crack initiation sites[8].

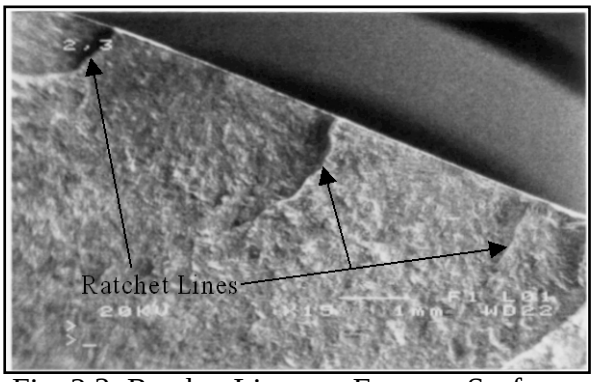

Fig. 2.3: Ratchet Lines on Fracture Surface

The final rupture zone is produced by the catastrophic separation of the part or the specimen. The fracture surface in the final rupture zone is rougher in texture than that in the fatigue zone. The roughness of the final rupture zone indicates that an appreciable amount of plastic deformation does occur in this zone.

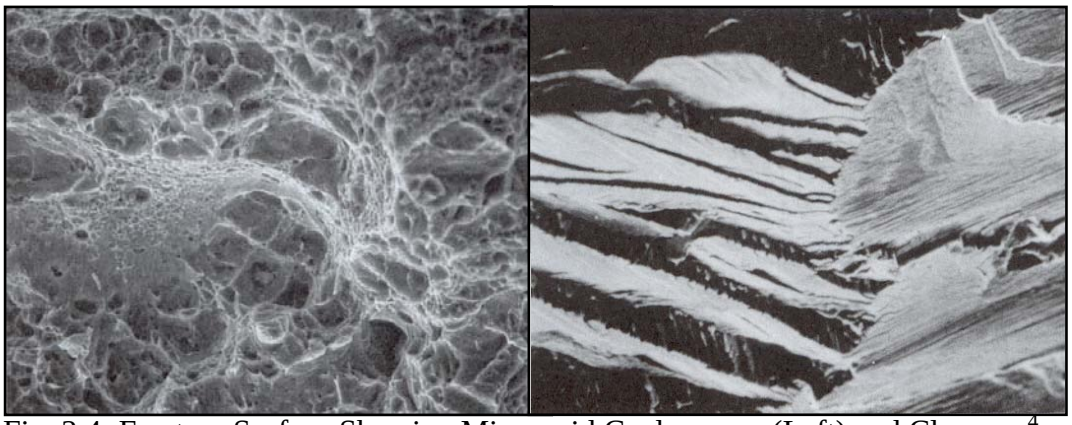

Fig. 2.4: Fracture Surface Showing Microvoid Coalescence (Left) and Cleavage[4]

The mode of the final fracture is usually by microvoid coalescence (indicated by tear dimples) or by cleavage[8,11].

2.2 Fatigue Failure Process

The fatigue failure process can be divided into several stages[4,5,12]:

I. Cyclic plastic deformation prior to fatigue crack initiation

II. Microcrack initiation

III. Microcrack propagation

IV. Macrocrack propagation

V. Final failure

Stages I to III of the fatigue process, normally known as macrocrack initiation, will be explained in detail. Stages IV and V are of less relevance to this research work and will not be described further.

2.2.1 Prior Cyclic Plastic Deformation

Except for a few cases of special stress distribution (see 2.4.1), most fatigue cracks initiate at the surface of a component. For a smooth specimen, the magnitude of the externally applied stress or strain-cycle amplitude may be large enough to lead to the initiation of microcracks[4].

The cyclic straining process can cause the surface to roughen through the motion of near-surface dislocations[78]. When a dislocation emerges at the surface of the component, a slip step of one Burgers vector is created. A perfect reversal of loading on the same plane cancels this step. In service, slip occurs in numerous

slip planes and perfect reversal is not possible. The accumulation of slip steps produces a roughening of the surface, thus leading to crack initiation[4].

This imperfect reversal of slip planes is the basis for the mechanism described by Cottrell and Hull to explain the features known as intrusions and extrusions that are seen on the surface of components undergoing fatigue loading[4]. A sequential step on two intersecting planes occurs.

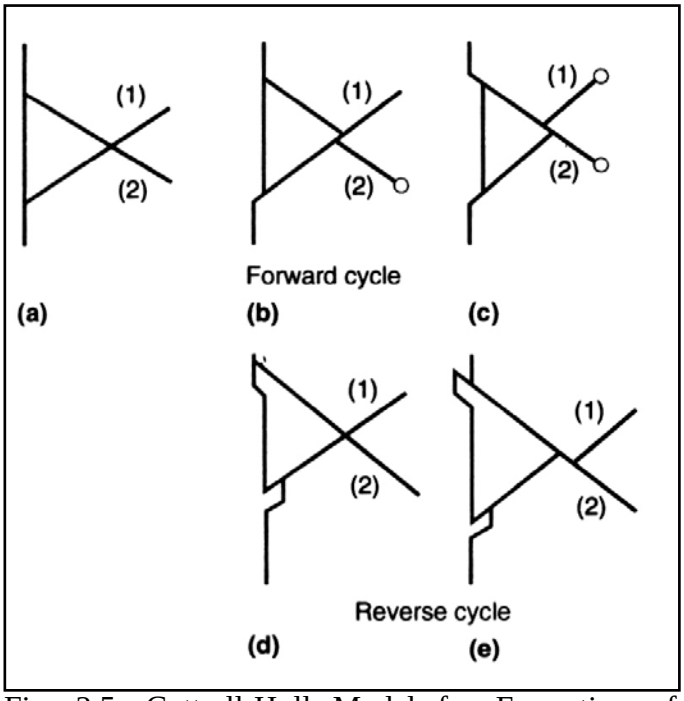

Fig. 2.5: Cottrell-Hull Model for Formation of Intrusions and Extrusions[13]

In the first half cycle, one slip system then the other operates to produce two slip steps of the same sign (Figure 2.5c). In the second half cycle, both slip system work again, giving rise to an intrusion and extrusion pair (Figure 2.5e)[4,13].

This model has been modified to allow the generation of intrusion-extrusion pairs in the absence of cross-slip, that is, only one slip system is operative. The

formation of an intrusion-extrusion pair is theorised to be the result of an avalanche from neighbouring slip bands containing excesses of dislocations of opposite sign[14].

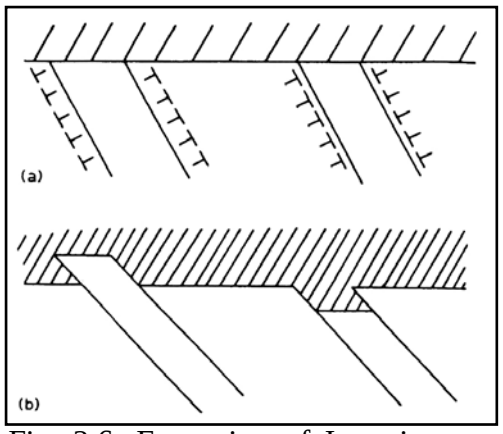

Fig. 2.6: Formation of Intrusion-Extrusion Pairs[13]

Paired dislocation pile-ups originate from cyclic straining. When the dislocations pile-ups reach a critical value, avalanches occur leading to the formation intrusions or extrusions[13].

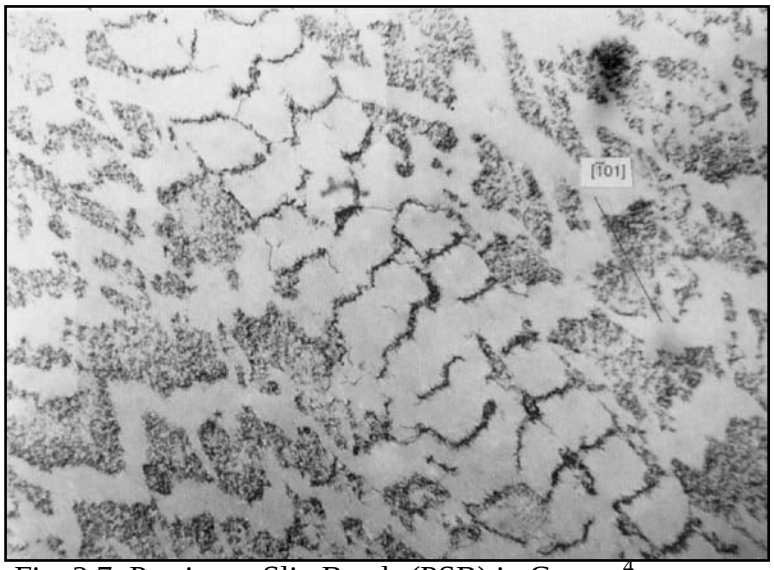

Fig. 2.7: Persistent Slip Bands (PSB) in Copper[4]

A form of coarse slip that can be produced by avalanches is persistent slip bands (PSB). PSBs are characteristic of materials subjected to cyclic deformation[15]. The slip bands are regions of localised deformation arising from the intense dislocation activity that occurs[15].

PSBs are said to be persistent in the sense that they are not removed by electropolishing[16]. Slip bands that have been removed, on further cyclic straining, form again at the same places[17]. A model that has been suggested for the formation of the PSBs follows.

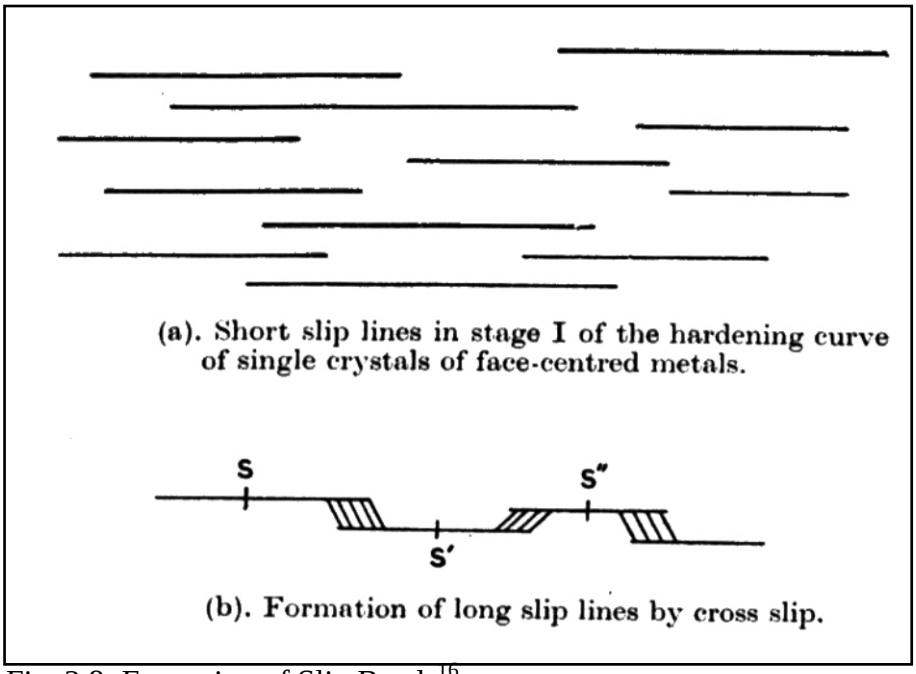

Fig. 2.8: Formation of Slip Bands[16]

The first stage of slip is the formation of numerous short slip lines. After a sufficient stress is reached, cross slip occurs. Cross slip releases the pile-up of dislocations at the ends of the slip lines, allowing more dislocations to be

generated. As more dislocations are generated, the slip bands increase and begin to merge by cross slip to form coarse slip bands[16].

Temperature has been found to affect the formation of the slip bands. An increase in temperature decreases the stress that is required for cross slip to occur, thus encouraging the formation of slip bands[16]. The application of anodic films on the surface is seen to block the formation of slip bands. Dislocations that pile-up at the surface do not concentrate enough stress to break through the anodic film. The formation of slip bands is therefore obstructed[18].

Not all materials form slip bands during fatigue. One such material is titanium. In titanium, the fatigue cyclic strain is in the linear elastic range. The dislocations are virtually immobile and slip is negligible. The only indication of the formation of a crack is a faint line that extends across one or two grains. This line is seen as a surface step at times, and a depression at other times[19]. It is possible that this slipless cracking may be due to cyclic slip that cannot be noted through the scanning electron microscope (SEM).

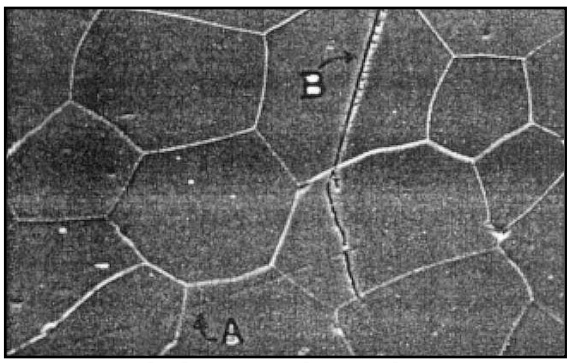

Fig. 2.9: Slipless Cracking Showing Faint Line (A) and Crack (B)[19]

During cyclic deformation, cyclic hardening or cyclic softening may occur[20]. Annealed alloys normally cyclically hardened, while cold worked alloys cyclically softened[4,12]. As-quenched steels were noted to cyclically harden, while quenched and tempered steels were seen to cyclically soften. Cyclic hardening in the as-quenched steels is attributed to dynamic strain ageing[21].

In annealed low carbon steel, cyclic softening was noted before cyclic hardening occurred. The initial softening is due to the generation of mobile dislocations within plastically deformed zones[22]. The spread of these zones lead to further softening. The subsequent hardening is attributed to work hardening mechanisms[21]. For materials that cyclically harden then cyclically soften, the softening is believed to be caused by irreversible damage occurring either at the intersection of slip bands with the surface, or at pile-ups of dislocation (microcracking)[21]. Other factors that determine cyclic softening include the mechanical removal of dislocation pinning, or the mechanical generation of unpinned dislocations[12,21,22].

2.2.2 Microcrack Initiation

The total fatigue life of a specimen is defined as:

$$N_T = N_i + N_p \qquad \text{....Eqn (1)}$$

where N_T = Total fatigue life

N_i = Initiation life

N_p = Propagation life

The initiation life of a specimen is defined as the number of cycles required to develop a crack of a specific size and the propagation life is defined as the number of cycles required for the crack to develop to a critical size[8].

The initiation of fatigue cracks on a specimen has been found to occur frequently at the surface of the specimen[8,23,24]. In changing the surface condition of the specimen, it is possible to change N_i. If the core of the specimen is unchanged, N_p remains the same, making it possible to vary the total fatigue life of the specimen by varying the surface conditions.

In specimens with a smooth surface, the cracks have been observed to initiate along slip bands[18,25-30], in grain boundaries[30,31], in second phase particles[32] and at interfaces between the matrix and inclusions or second phase particles[26,33]. These observations have led to the proposal of various models for the initiation of fatigue microcracks. The models for microcrack initiation can be separated into five groups[4]:

I. Models that do not distinguish between intrusions and microcracks

II. Crack nucleation based on critical conditions for local brittle fracture

III. Condensation of vacancies

IV. Loss of coherency across a slip plane due to accumulation of defects

V. Nucleation of cracks in grain boundaries

2.2.2.1 Models that Do Not Distinguish between Intrusions and Microcracks

The Neumann model proposes the formation of cracks by coarse slip[14].

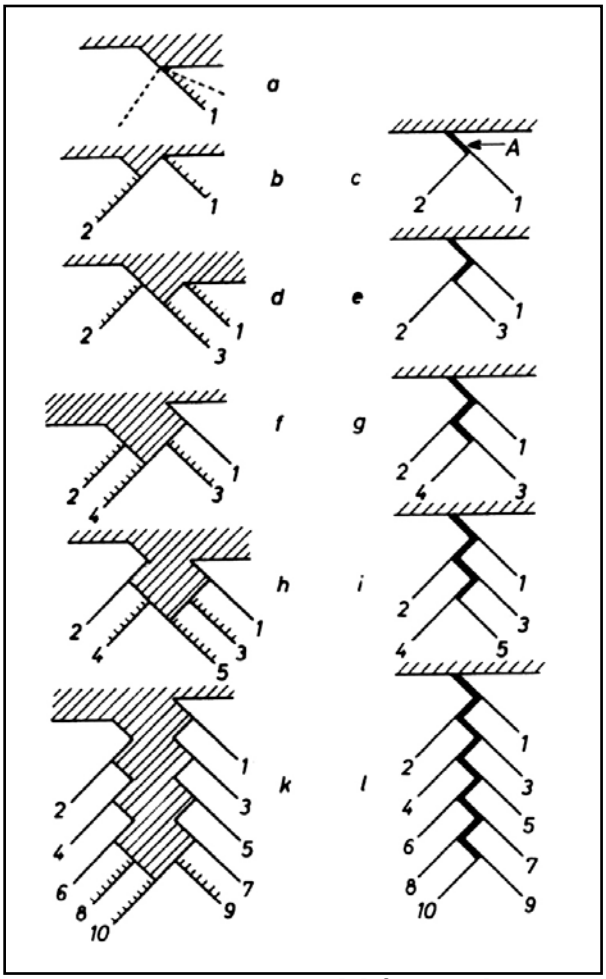

Fig. 2.10: Neumann's Model for Crack Initiation[14]

During the tensile phase of each cycle, excess dislocations of one sign on activated slip plane 1 led to the formation of a slip step (Figure 2.10a). The slip step acts as a stress raiser, leading to the activation of slip plane 2 (Figure 2.10b). In compression, the surfaces formed by slip plane 2 disappear due to reversal slip. The surfaces formed by slip plane 1, however, do not disappear. The surfaces at A touch macroscopically, ensuring that they can be separated without effort (Figure

2.10c). On the next tensile phase, slip plane 2 is activated as before. With the slip step formed by the activated slip plane 2 acting as a stress raiser, slip plane 3 is activated (Figure 2.10d). Compression leads to the surfaces formed by slip plane 2 touching macroscopically, thus producing a serrated crack (Figure 2.10e). This process continues leading to the growth of the crack.

2.2.2.2 Crack Nucleation Based on Critical Conditions for Local Brittle Fracture

Ni-base superalloy Udimet 720 Li is one material that supports this mechanism[32].

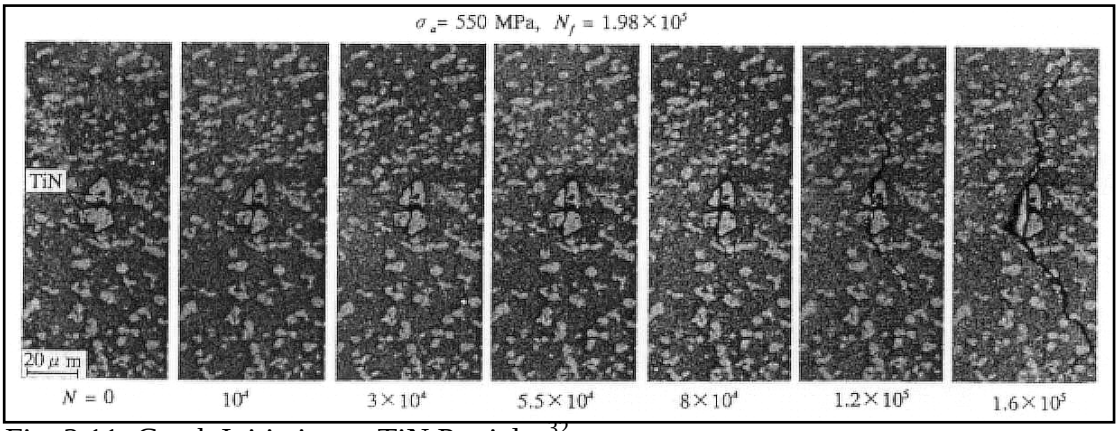

Fig. 2.11: Crack Initiation at TiN Particles[32]

The TiN particles in the alloy are brittle and unable to withstand the stress that is placed on the specimen. To relieve the stress, the TiN particles crack. Fatigue cracks then initiate from the cracked TiN particles.

2.2.2.3 Condensation of Vacancies

Cyclic deformation produces a high number of vacancies. The coalescence of the vacancies leads to the formation of microvoids or pores[4,23].

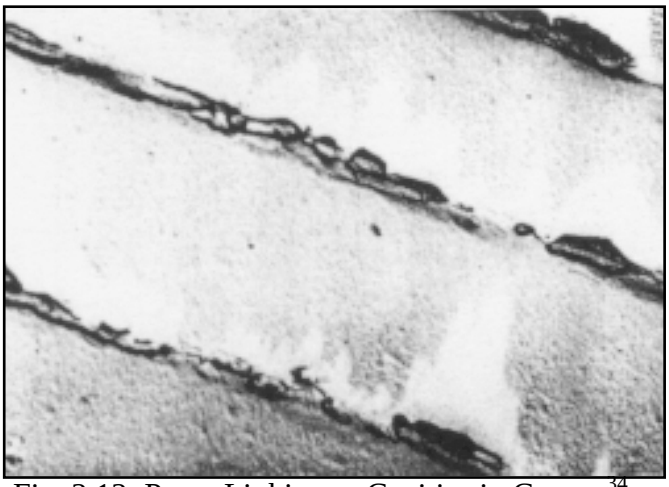

Fig. 2.12: Pores Linking to Cavities in Copper[34]

Continued generation of these microvoids or pores would lead to the destruction of the coherency of a plane. The microvoids or pores can then link to form microcracks[34].

2.2.2.4 Loss of Coherency across a Slip Plane due to Accumulation of Defects

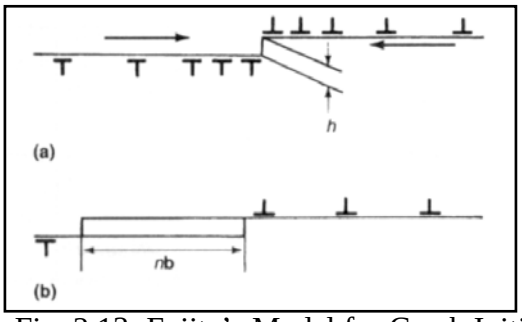

Fig. 2.13: Fujita's Model for Crack Initiation[4]

Fujita's model for crack initiation is based on the formation of cracks by the annihilation of dislocations in parallel slip planes[35].

During cycling, there is a pileup of dislocations of opposite signs on two parallel slip planes (Figure 2.13a), where *h* is the separation of the planes. When the two leading dislocations pass each other, there are two possible outcomes depending

on the value of *h*. When *h* is a few atomic spacings, the dislocations will annihilate in pairs and leave a small cavity. This annihilation occurs for *n* dislocations, leading to the formation of a microcrack with a length *n***b** (**b** is the Burgers vector). When h is relatively large (more than ten atomic spacings), the annihilation will not occur and the two rows of dislocations will pass each other.

Fujita's model has been modified by Mura[27,33,36,37]. One of the earliest modifications proposes that crack nucleation occurs when the strain energy of the dislocations exceeds the surface energy needed to open up the two faces of the crack[36]. In a later work, the crack size is set equal to the net displacement due to all piled-up dislocations at the time of the nucleation[27]. Mura shows that there exists a critical number of cycles beyond which the accumulation of dislocations become energetically unstable, leading to the annihilation of the dislocations and the formation of a crack[33,37].

2.2.2.5 Nucleation of Cracks in Grain Boundaries

Laird's model is based on slip band interaction with grain boundaries[30]. Laird proposes that the fatigue crack nucleation process is due to the formation of steps. The grain boundaries are required to have the following properties:

1. The trace of the boundaries lie at an angle in the range 30° to 90° with respect to the stress axis;
2. The boundaries join high misoriented grains;

3. The dominant slip system is directed at the intersection of the boundary with the surface.

Such a nucleation process is shown in Figure 2.14.

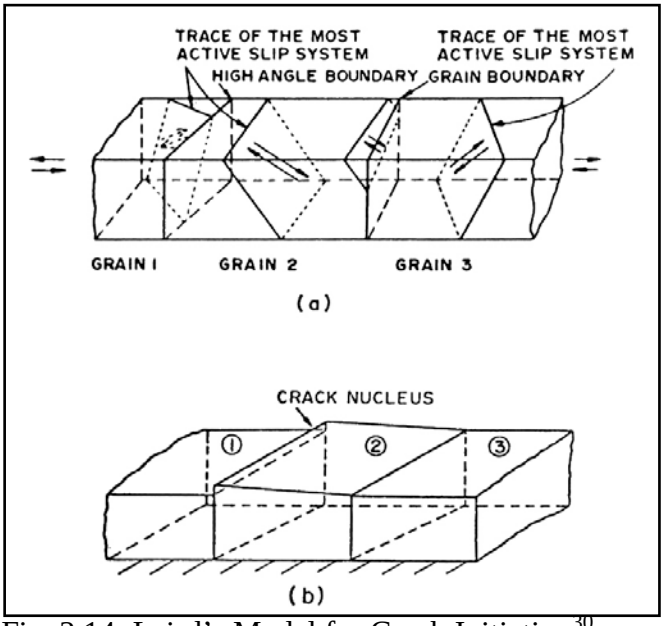

Fig. 2.14: Laird's Model for Crack Initiation[30]

A step can easily form at the grain boundary 1/2, but not at the boundary 2/3. The nucleation of the fatigue crack thus takes place at boundary 1/2.

2.2.2.6 Nucleation vs. Continuous Growth

The models that have been presented can be grouped into two categories. The first category explains the initiation of cracks as a gradual process, while the second describes initiation as a nucleation process[25]. Both categories have been proven and can easily be explained. For example, cracks are not seen in a specimen prior to *x* cycles. The cracks may form by nucleation; this would explain why they are not seen prior to *x* cycles. However, it can be argued that the cracks are formed by a continuous process that begins in the first cycle and that the cracks are too small

to be imaged prior to *x* cycles. Through crack size calculations and the observation of the formation of pit-shaped features, it has been shown that a nucleation process is the method by which cracks initiate[25].

2.2.3 Microcrack Propagation

Before the emergence of small crack theory in the mid 1970s, microcracks were proposed to propagate by coalescence or by propagation along crystallographic planes (referred to as Stage I)[4,12,26,31]. Stage I crack growth occurs principally by slip-plane cracking[4,28,29].

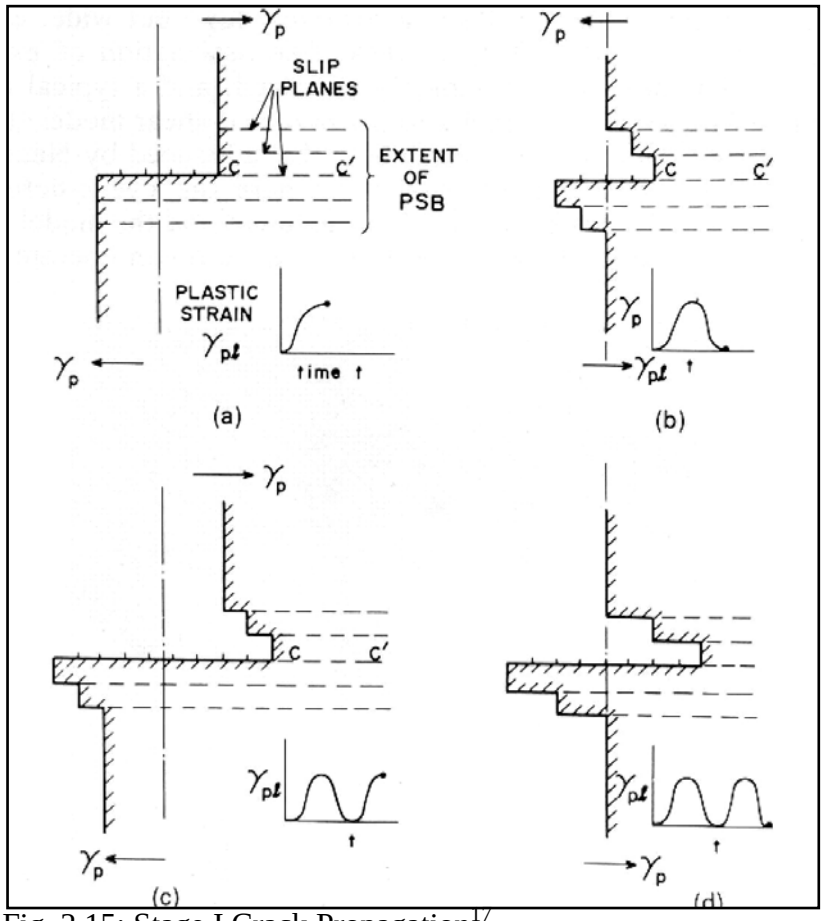

Fig. 2.15: Stage I Crack Propagation[17]

The presence of a notch is omitted in Figure 2.15a for clarity. The notch serves as a stress concentration point that focuses the slip in tension along C-C'. Here, a slip offset of five Burgers vectors is caused by the stress concentration. In the compression step, Figure 2.15b, the slip is distributed on the five slip planes, so that the C-C' slip is cancelled by one Burgers vector. In Figure 2.15c, tension is applied and the strain is again concentrated on C-C'. The next compression step shows a resultant offset of eight Burgers vectors. As the penetration of the crack is associated with an extrusion, the overall crack penetration is only four Burgers vectors[17].

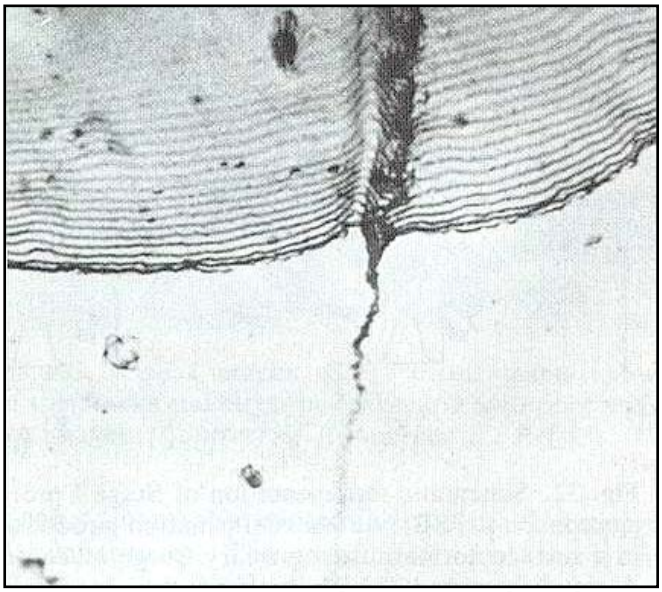

Fig. 2.16: Stage I Crack Associated with Extrusion[17]

The following model has been proposed for Stage I crack growth along grain boundaries by plastic blunting[30].

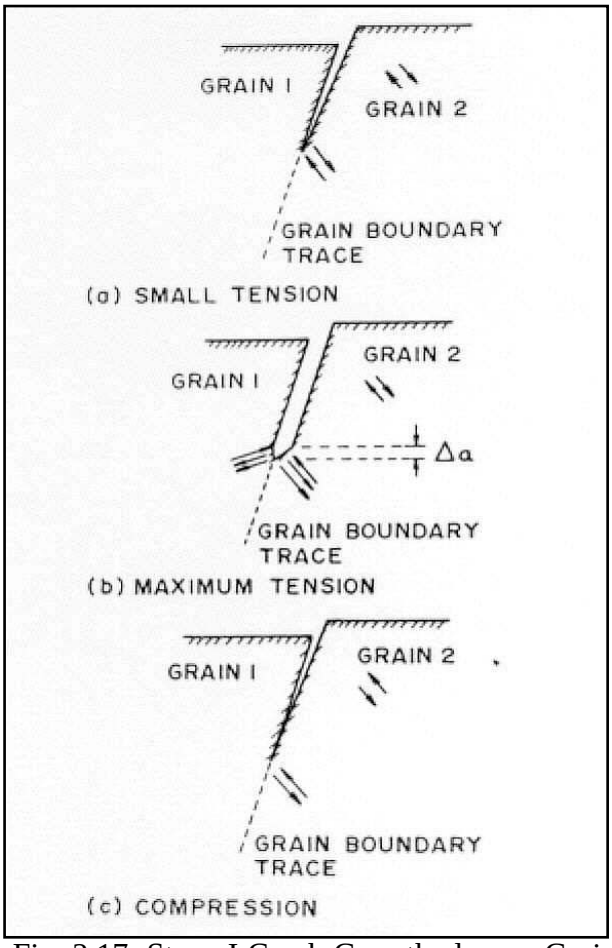

Fig. 2.17: Stage I Crack Growth along a Grain Boundary[30]

The requirements for this model include high angle boundary and slip motions directed at the intersection of a boundary with the surface. The crack is initiated at the boundary 1/2. Slip motions are indicated by the arrows in grain 2. Grain 2 is assumed to be oriented favorably for directed slip at the boundary. As the slip motions are associated with the most active slip system in grain 2, they are oriented to provide the greatest plastic deformation at the crack tip without requiring the stress concentration of the crack to initiate slip on other planes. At maximum tension, extensive shear occurs along the active slip system and the crack advances by Δa (Figure 2.17b). In compression, the load is reversed and the

slip at the crack tip is reversed. The new surface gained is conserved and crack growth is achieved[30].

The propagation of microcracks in some materials has been observed to occur rapidly[4,13,29]. When compared with macrocrack propagation with the same nominal crack driving force, microcrack propagation has been found to be up to 100 times faster in precipitation-hardened aluminum alloys[38]. The use of macrocrack analysis methods can, therefore, lead to an overestimation of structural life. Small crack theory has been developed to explain the increased propagation rates of small cracks (microcracks).

There are three types of small cracks that have been identified[4]:

I. Microstructurally small cracks

II. Mechanically small cracks

III. Physically small cracks

Microstructually small cracks are cracks with dimensions that are smaller than relevant microstructural dimensions, such as grain size or inclusion size, while cracks that are mechanically small are comparable to the scale of local plasticity. The third type of cracks are cracks that are just physically small[4,5,23]. The terms “small crack” and “short crack” have been used interchangeably in literature. However, they have recently acquired specific meanings. A “small” crack is a crack that is small in all dimensions, while a “short” crack is only small in all but one dimension[4,5,39]. Their differences are shown in Figure 2.18.

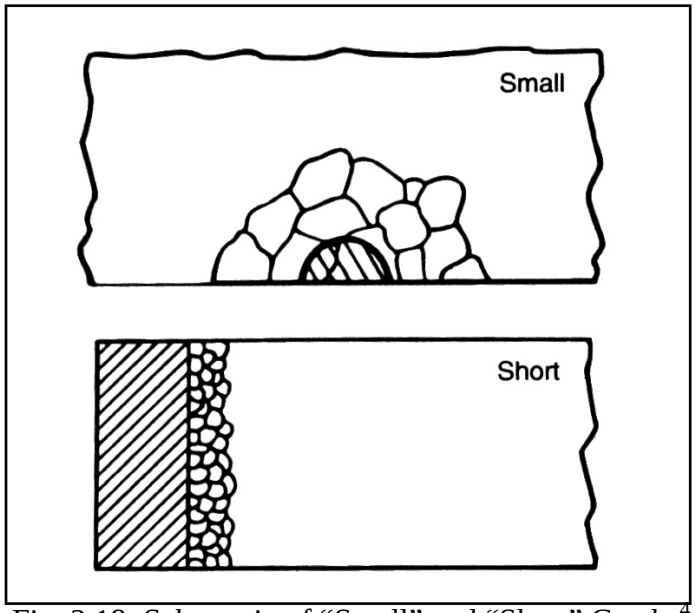

Fig. 2.18: Schematic of "Small" and "Short" Cracks[4]

The presence of small cracks is most noticeable when the cracks are so small that they interact with only one grain, or at most a few grains[39]. As the crack initiates at a preferred crystallographic plane, the local yield stress is lowered, leading to a fast growth rate[4]. However, due to the size of small cracks, microstructural features such as grain boundaries and inclusions have been observed to greatly influence the propagation of small cracks, leading to the acceleration, deceleration or arrest of the crack[29.32,39,40].

When approaching a grain boundary, small crack growth can be hindered by mechanisms that include the blocking of slip bands[41], the containment of the plastic zone within the grain, and reorientation and re-initiation of the crack as it travels into the next grain[5,40]. Crack deflection is proposed as an occurrence that happens when the crack tip interacts with the grain boundary. When a crack tip reaches the grain boundary, it reorients in the adjacent grain to advance on the most favourable slip system. Sometimes, the slip system is less favourable than

the initial system, thus leading to retardation in crack growth and maybe crack arrest[5,39].

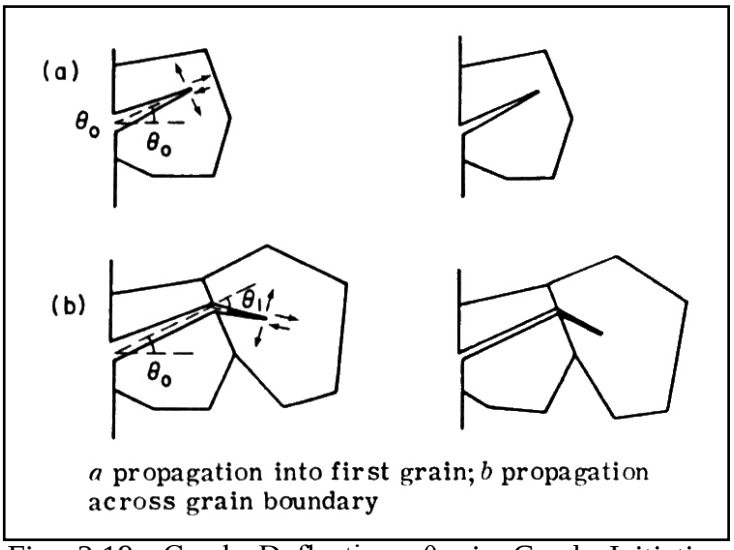

Fig. 2.19: Crack Deflection; θ_0 is Crack Initiation Angle and θ_1 is Angle of Deflection at First Grain Boundary[5]

Another factor that affects the growth rate of small cracks is crack closure[5,40]. Crack closure results from the constraint of the surrounding material on the plastic zone around the crack. As small cracks come into contact with a smaller plastic zone, the cracks would experience less closure, allowing a faster crack growth[5].

2.3 The S-N Curve

The S-N (stress-number of cycles) curve is used to display the results of fatigue testing over a range of stresses. There are two distinct types of S-N curves[20]. The S-N curve for most steels shows a well-defined fatigue limit[24,42]. The horizontal line on the S-N curve represents this limit. When stressed to below this limit, these steels can withstand an infinite number of load cycles without fracture[38].

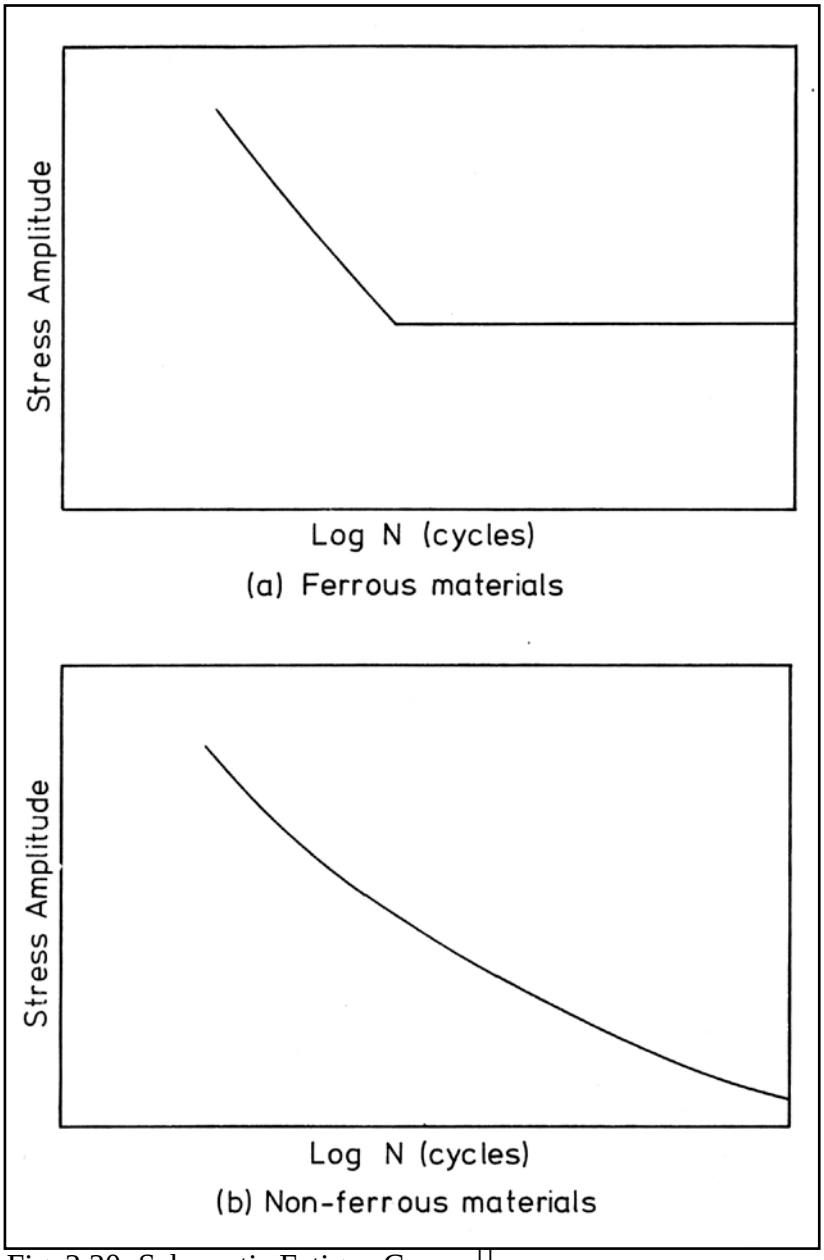

Fig. 2.20: Schematic Fatigue Curves[11]

In contrast, most non-ferrous alloys do not exhibit well-defined fatigue limits[20,38]. For these alloys, a minimum fatigue life is specified. The corresponding stress is taken to be the fatigue strength. The fatigue strength is the stress below which fatigue does not occur within the time period[42]. Running the material for a higher

number of cycles at the same stress would see the possibility of fatigue fracture occurring.

The presence of the fatigue limit in the S-N curve for most steels have been attributed to the ability of the steels to harden by strain ageing[11,38,43]. Strain ageing is when dislocations are pinned by mobile nitrogen atoms within the materials. An increase in stress is required to unpin the dislocations before the dislocations can begin moving again. The material dynamically strain ages as fatigue loading occurs. The accumulation of fatigue damage and the strain ageing process are seen as competitive processes. The fatigue limit occurs when the strain ageing process outpaces the damage process[11]. Some aluminium alloys have been noted to display the fatigue limit[44].

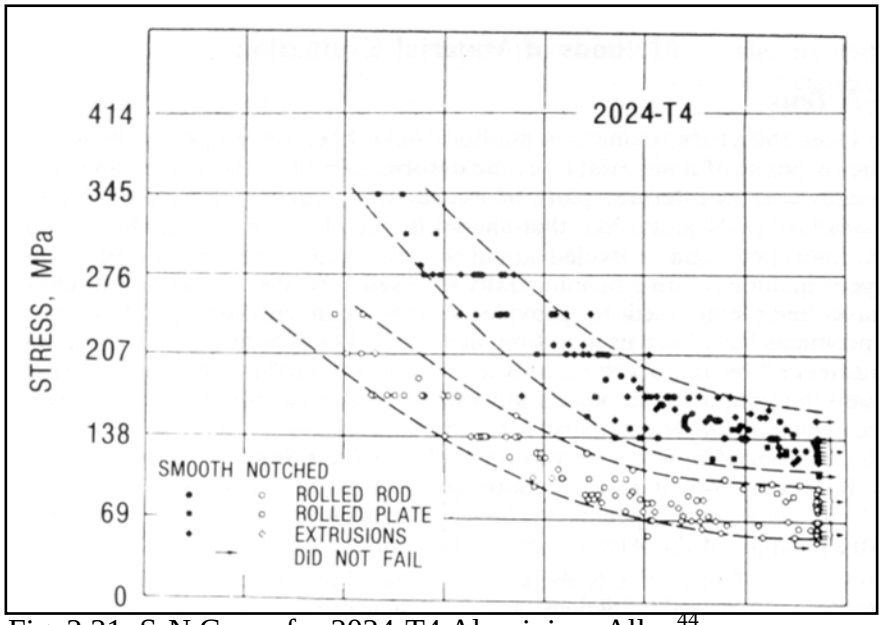

Fig. 2.21: S-N Curve for 2024-T4 Aluminium Alloy[44]

The S-N curve is influenced by several factors. Some of these factors include the type of material tested, its microstructure and the test environment. A well-

defined S-N curve is more likely to be obtained in tests on a soft ductile material. Harder materials normally show greater scatter, which is further emphasized by the presence of stress concentrations[45]. The grain size of the material affects its fatigue limit. An increase in grain size decreases the fatigue limit[46].

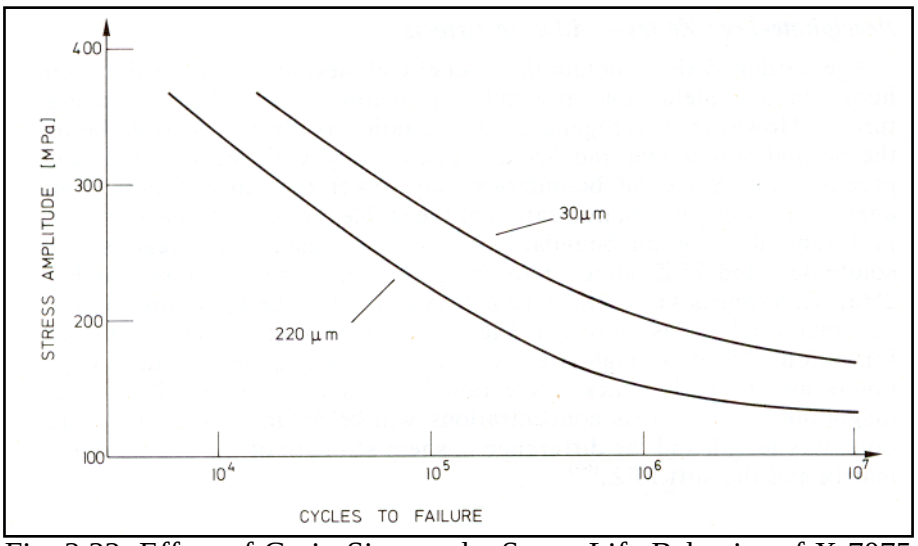

Fig. 2.22: Effect of Grain Size on the Stress-Life Behavior of X-7075 Alloy[46]

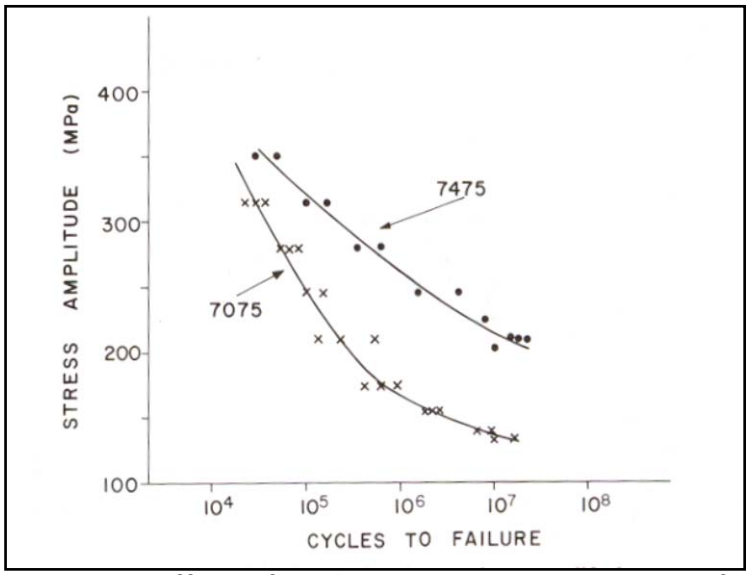

Fig. 2.23: Effect of Inclusion Density on Stress-Life Behavior of 7XXX Alloy: High-Inclusion Density 7075 Alloy, Low-Inclusion Density 7475 Alloy[46]

An increase in the amount of inclusions also decreases the fatigue limit[46].

The test environment also influences the S-N curve of a material[44]. The presence of a corrosive environment is detrimental to the fatigue limit of the material tested. If the material has been exposed to a corrosive environment before testing, the effect of the corrosion on the fatigue limit of the material is also detrimental[47].

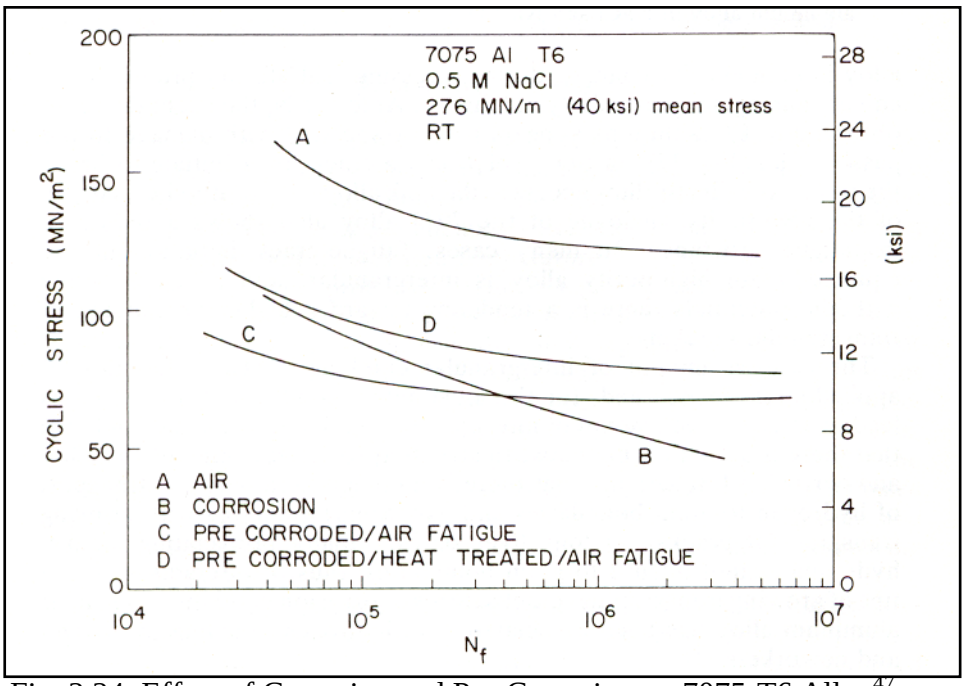

Fig. 2.24: Effect of Corrosion and Pre-Corrosion on 7075-T6 Alloy[47]

2.4 Factors that Influence Fatigue

There are many factors that can affect the fatigue behavior of a material. Some of the factors mentioned in Section 2.3 include microstructure and test environments. One important factor that has yet to be mentioned is the surface layer. Fatigue can be greatly influenced by the surface layer, due to the effect of the surface layer on crack initiation[4,48]..

The surface layer of a material includes the surface and a small layer of the material below the surface. A change in the surface affects crack initiation, while a change in the layer below the surface also influences crack propagation.

Cracks initiate at sites where cyclic deformations are higher than average - that is, areas of plastic-strain concentrations, such as stress concentrations[48]. Machining a surface can produce scratches on the surface that act as stress concentrations, leading to a reduction in the number of cycles required for crack initiation. Similarly, corrosive environments lead to pitting in the surface that act as points of stress concentrations[4].

The introduction of residual stresses on the surface influences the fatigue properties of a material. As the residual stresses are developed in the subsurface layers of the material, both crack initiation and propagation are affected. Residual stresses, when superimposed with the applied fatigue loads, change the mean stress applied[4,38,49]. A residual tensile stress is, therefore, detrimental to the fatigue process, while a residual compressive stress is beneficial. Residual compressive stresses have been observed to shift the site of crack initiation from the surface of the material to the subsurface[50,51]. A subsurface initiation would indicate that inclusions are the major source of failure[51]. Subsurface initiations generate a dark circular area around the crack initiation point; this area has been identified as an area of slow crack propagation[51].

A phase or chemical composition change at the surface of a material can affect fatigue depending on the resistance of the changed surface to fracture[4]. Changing the surface layer leads to a change in the hardness of the surface. The material can then be treated as a core with either a hard or soft coating. A core with a hard coating would allow the material to cope with a higher load before fracture, while a core with a soft coating would fail at a lower load. Cracks initiate in the soft coating at a lower stress level. These cracks act as a stress concentration for the higher strength core, leading to a drop in fatigue strength[52,53].

2.5 Processes to Modify Fatigue Properties

There are several surface treatments that are used to modify the fatigue properties of a material. Grinding, polishing, nitriding, surface rolling, aluminum cladding and shot peening are examples of such processes[52]. Some of the surface treatments affect fatigue by the removal of surface defects that may act as stress concentrations, while some introduce residual compressive stresses. Others change the physical properties of the surface to delay the onset of fatigue. Some surface treatments, however, have to balance beneficial against detrimental factors. One such surface treatment is grinding. Grinding removes surface defects that may act as stress concentrations. However, the grinding process introduces a residual tensile stress in the surface. Even with the residual tensile stresses, grinding has been found to improve the fatigue limit[4].

CHAPTER 3: ELECTRIC DISCHARGE MACHINING

Electric discharge machining (EDM), also known as 'electro-erosion' or spark erosion, is a non-traditional method of removing metal[1]. EDM was introduced over thirty years ago. The introduction of new materials, along with the need for the ability to produce more complex shapes and tighter tolerances, has led to the development of the EDM process.

3.1 Description of Process

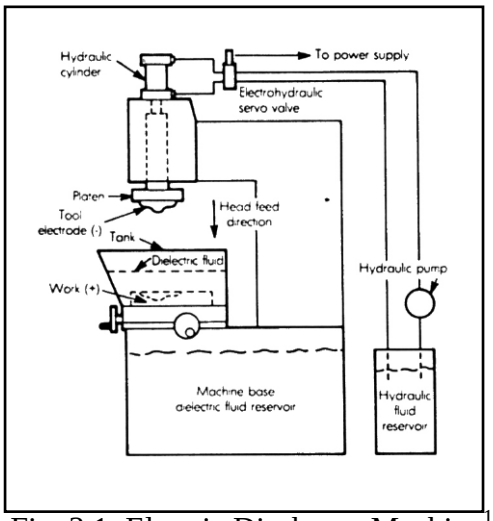

Fig. 3.1: Electric Discharge Machine[1]

EDM involves the use of a series of recurring electrical discharges (sparks) between one electrode (the cutting tool) and another electrode (the workpiece) to remove metal. The two electrodes, separated by a small gap of 0.0005 to 0.020 in (0.0127 to 0.508mm)[54], are immersed in a dielectric fluid. The dielectric fluid in the gap is partially ionized under the pulsed application of a high voltage, enabling a spark to pass between the cutting tool and the workpiece. The spark

causes a minute portion of the workpiece to melt, or vaporize, at the surface, resulting in the formation of a crater. Rapid recurrence of sparks erodes the workpiece to the electrode shape. The minute particles of metal and chips are then flushed away from the surface of the workpiece by the dielectric fluid.

3.2 Principles of Operation

There have been several theories that have been presented in an attempt to explain the erosion effect of the spark. One theory suggests that the electric field separates the material particles of the workpiece as it exceeds the force of cohesion in the lattice of the material. This theory neglects any thermal effects and experimental evidence does not support this theory[1].

Another theory is based on 'jets of flame'. These are formed by various electrical effects of the discharge and are said to be responsible for the removal of metal by melting the metal. This theory neither agrees with experimental data nor gives a good explanation for the erosion effect of the spark[1].

The theory that is best supported by experimental evidence suggests that the high intensity of the discharge current generates a temperature of over 10,000^{o}C, which, in turn, melts or vaporizes the metal [1,55-57].

The discharge mechanism is divided into three stages[1]. The first stage (Figure 3.2.a,b) is known as the preparatory stage. Here, the electric field ionizes the dielectric fluid, thus forming a conductive channel. The second stage (Figure

3.2.c,d) is characterized by the discharge itself, which causes the heating of the channel (10,000°C - 50,000°C[1]), which is hot enough to melt or even vaporize the metal. The final stage (Figure 3.2.e,f) is the ejection of the eroded metal.

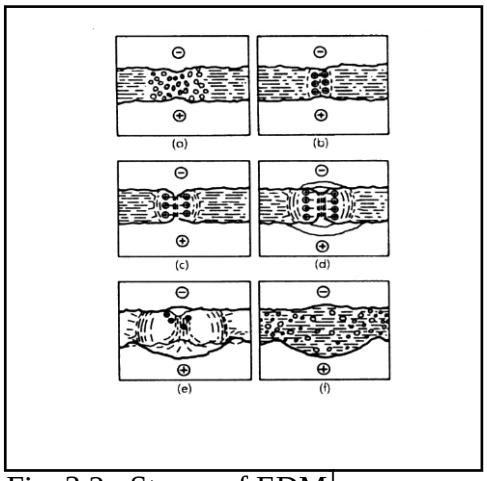

Fig. 3.2 : Stages of EDM[1]

The ejection of the eroded metal may start during the second stage and continue after the discharge. A crater may be observed on the workpiece and, to a smaller extent, on the cutting tool (see Section 3.3.1). The thermic effect is therefore demonstrated to be a main factor of the spark erosion[1].

3.3 Electrode Wear

Electrode wear is an important factor that has to be considered. Wear produces inaccurate machining as it occurs at the leading edge of the electrodes, thus producing tapered cavities[1].

When copper, iron and other low melting point materials are used as electrodes, the temperature produced by the spark is higher than the melting point of the

electrodes. The molten metal droplets are blasted away, thus causing electrode wear. The melting point of graphite is much higher; the heat generated is insufficient to melt graphite, thus ensuring less wear.

There are three kinds of metal removal[1]:

I. Vaporization

II. Liquid metal droplets

III. Thermal shock

Vaporization is when the metal has to be removed as it boils. Liquid metal droplets is when the metal is melted and removed in droplet form by high pressure at the electrode face. Thermal shock is when the material comes off in small particles due to the thermal shock gradients between the melting surface and the cold material behind the surface.

The ratios of the three kinds of metal removal depend on several factors, such as the workpiece material properties, the size of the cut, and other machine variables. The surface finish can therefore be controlled by the ratios of the three kinds of metal removal.

3.4 Dielectric Fluid

The dielectric fluid fulfils three functions[1,55,58].

I. It acts as an insulator between the electrode and the workpiece until the required conditions are achieved, after which it acts as a conductor.

II. It is a coolant and must cool the workpiece, electrode and "chips".

III. It is a flushing medium for the removal of the "chips" from the workpiece.

The most commonly used dielectric fluid is petroleum-based hydrocarbon oil[1]. These oils have a high flash point and very low viscosity. Additives are used to inhibit the formation of gas bubbles and remove the characteristic of the petroleum odour. Another advantage of oil is its constant dielectric resistance, which allows a discharge gap of 0.005mm and less. This makes it suitable for fine machining with a thin wire electrode[1]. One disadvantage is that hydrocarbon oils leave a slight carbon residue, which acts as a barrier to sparking.

For some applications, better results can be obtained using silicone fluids. In machining titanium, higher removal rates, less electrode wear and better surface finishes are obtained[1]. One disadvantage in using silicone fluids is their high cost; however this disadvantage may be minimised by mixing the silicone fluid with a less expensive dielectric[59].

Another dielectric fluid that can be used is a powder mixed oil. This oil has been found to improve finishing efficiency and to provide mirror finished surfaces. One major disadvantage is the presence of powder precipitate[6].

Other dielectric fluids that can be used include deionized water, kerosene, and polar liquids such as aqueous solutions of ethylene glycols[1].

The effectiveness of the process depends on the cleanliness of the dielectric fluid[55]. The presence of particles can interfere with the smooth and effective working of the process, especially during the machining of accurate work within small spark-gaps. Metal particles and carbon formed due to the breakdown of the dielectric fluid can cause inaccurate sparking to occur[55,59]. The presence of a carefully controlled, small amount of contamination can be beneficial in stabilizing the EDM process for high-amperage, low-frequency roughing operations[1,59].

3.5 Types of EDM and Their Applications

3.5.1 Electric Discharge Spark Erosion

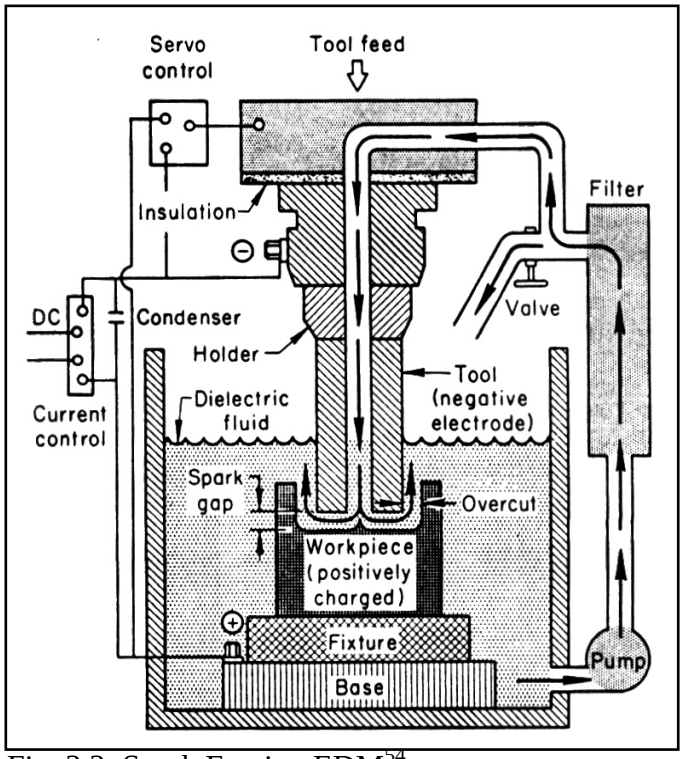

Fig. 3.3: Spark Erosion EDM[54]

Spark erosion is the most common type of EDM process. The electrode is shaped to the opposite of the final cavity machined on the workpiece. The electrode is mounted on a machine ram and fed into the workpiece to obtain three-dimensional machining. The most common application for spark erosion EDM is in the production of dies. Complex features, such as small or odd-shaped holes and intricate contours, can be easily produced[1].

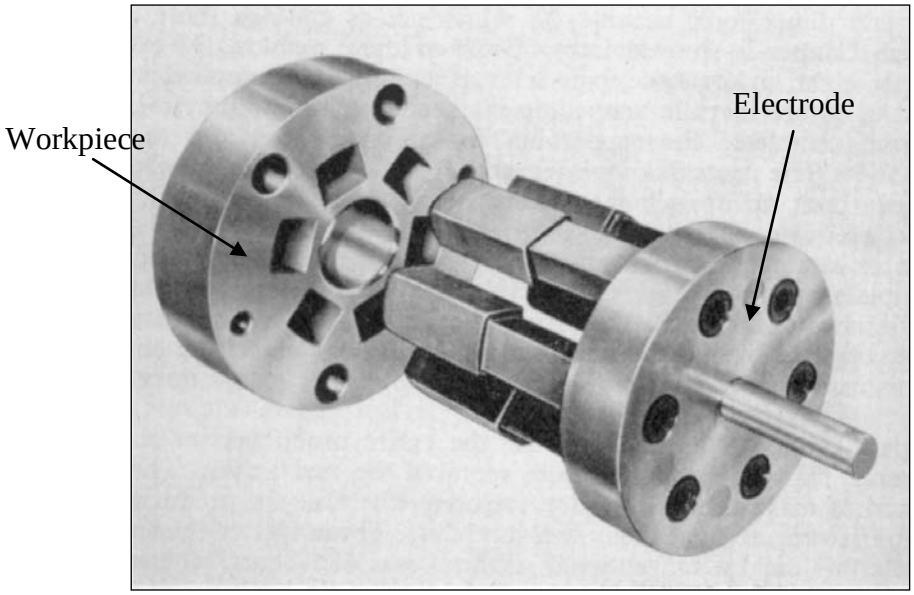

Fig. 3.4: Electrode Assembly and Spark-Eroded Press Tool for Punching Clutch Linings[60]

Machining procedures such as electrode rotation and orbiting electrode have been developed to improve flushing of the dielectric fluid.

3.5.1.1 Electrode Rotation

The EDM machine used includes a precision spindle, a drive mechanism and a speed control[1]. The electrode rotates as it is being lowered towards and through the workpiece. This rotating motion circulates the dielectric fluid through the gap between the electrode and the workpiece, thus improving flushing and increasing cutting speed. The quality of the hole produced is superior to that of a stationary electrode. This method is limited to the production of round holes[1,60]and internal threads[61].

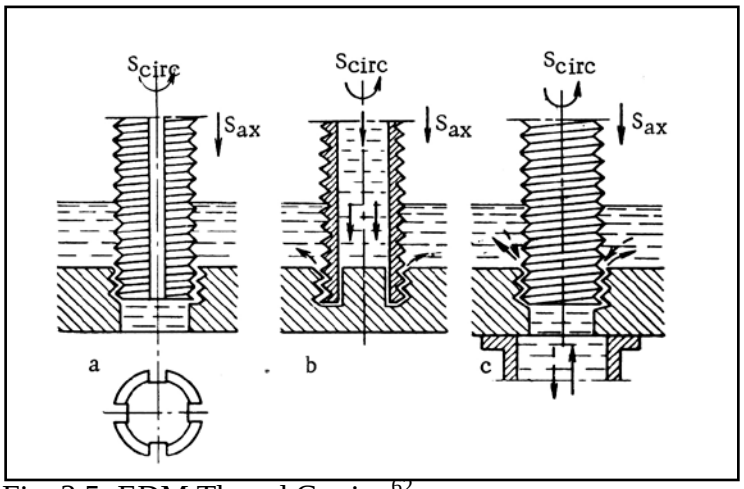

Fig. 3.5: EDM Thread Cutting[62]

3.5.1.2 Orbiting Electrode

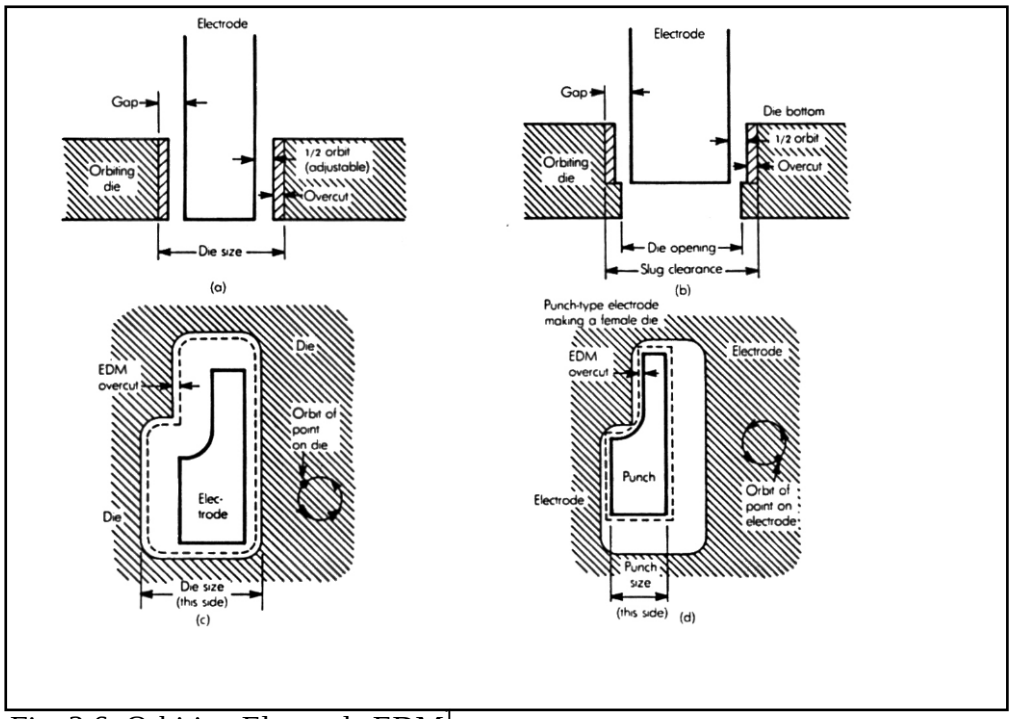

Fig. 3.6: Orbiting Electrode EDM[1]

In this process the electrode does not rotate, but moves in a prescribed orbit. The relative motion between the electrode and the workpiece during orbiting circulates the dielectric fluid, thus improving flushing. The final size of the hole is dependent on the size of the electrode and the size of the orbit. Orbiting electrode

EDM is therefore a good process for producing low-volume, close-tolerance jobs at a low electrode manufacturing cost[1].

3.5.2 Electric Discharge Wire Cutting (EDWC)

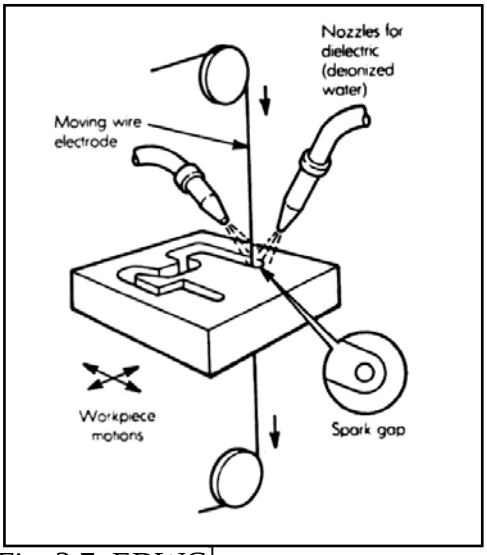

Fig. 3.7: EDWC[1]

The major difference between electric discharge spark erosion and EDWC is the type of electrode that is used. In EDWC, the electrode is a wire, which is fed through the workpiece[1,3,63,64]. The workpiece remains stationary and the horizontal movement of the wire determines the shape of the hole. This process requires a starter or threading hole for the wire. EDWC is normally used to produce stamping and extrusion dies, complex-shaped blanks and templates, and special form inserts. With the use of numerical control (NC) programs, skilled workers are not required. This is the type of EDM process used in this research work.

3.5.3 Electric Discharge Grinding (EDG)

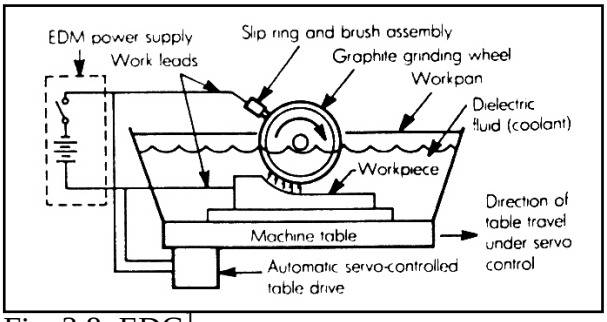

Fig. 3.8: EDG[1]

In EDG, the electrode is a rotating wheel. The metal is removed by electrical discharges passing through the gap between the wheel and the workpiece. The reverse form of the wheel face is transferred to the workpiece surface[1,55]. The main application for EDG is grinding hard materials. These materials include carbide form tools, hardened steel gear racks, tungsten carbide inserts and hardened lamination dies[1].

3.6 Effects of EDM

3.6.1 Macroscopic Effect

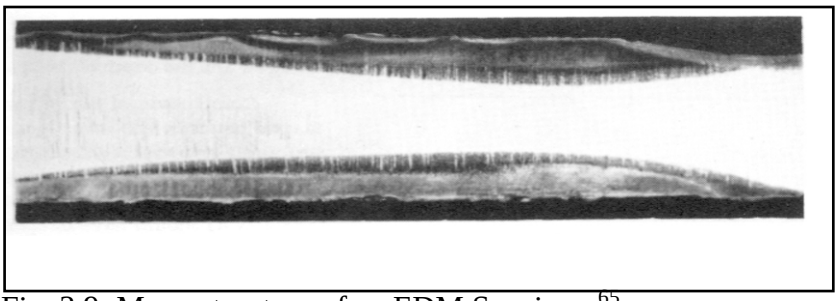
Fig. 3.9: Macrostructure of an EDM Specimen[65]

EDM has been reported to cause changes in the surface layers of the machined specimen. In a cross-section of the specimen, the macrostructure consists of 3 zones – a central zone and two darker edge zones. The central zone consists of the original material. The edge zones are regions that have been thermally affected regions by the EDM process[65].

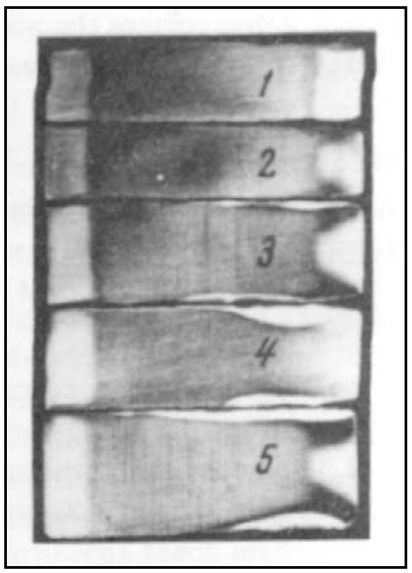

Fig. 3.10: Variation of Zones with Increasing Cutting Currents[65]

Figure 3.10 shows that the size of each zones depends on the cutting conditions. An increase in current leads to an increase in the heat generated, thus increasing the size of the zones. In steels and alloys that experience no structural changes during heating and cooling, there are no edge zones are present.[14]

3.6.2 Microscopic Effect

The surface of the machined part is produced through metal vaporization by sparks, resulting in the formation of many craters. The size of the craters formed,

and hence the surface finish, is dependent on the energy of the discharge[1,55,66]. Surface roughness of the machined surface varies from 0.005μm R_a to 6.3μm R_a[1,63]. No matter how fine a surface roughness is obtained, the surface of the part is covered with numerous craters, giving a similar appearance to the surface of the moon[63,67,68]. Ideally, the dielectric fluid carries away all the melted material from the machined surface. In practice, not all of the melted material is removed by the dielectric fluid. A limited volume of material re-solidifies on the surface, forming a shiny skin, known as the recast layer, which is dissimilar to the macroscopic zone mentioned above[1,58,60,63,66]. This produces surfaces as shown below.

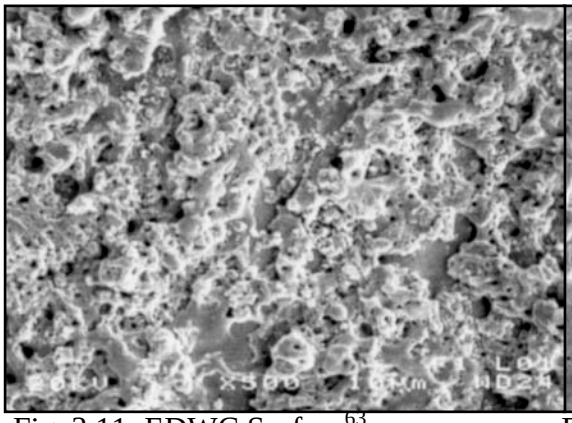

Fig. 3.11: EDWC Surface[63]

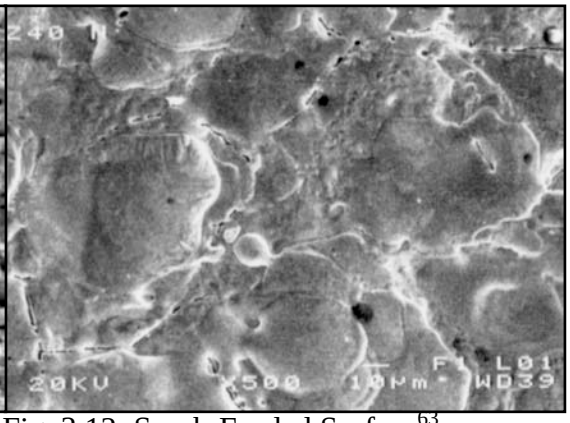

Fig. 3.12: Spark-Eroded Surface[63]

Figures 3.13 and 3.14 show the cross-sections of machined workpieces. The recast layer can be seen as the light band in Figure 3.13. The recast layer is non-uniform across the section and varies from a thickness of 0.002mm to 0.38mm[1,63,66]. The difference in color of the recast layer and the original material in Figure 3.13 shows that the structure of the recast layer differs from that of the original material[63,66]. The recast layer is harder than the parent material. This recast layer causes an increased resistance to wear, but a reduction in strength[1,66]. A darker

zone is present just below the recast layer, where the material has been tempered[60].

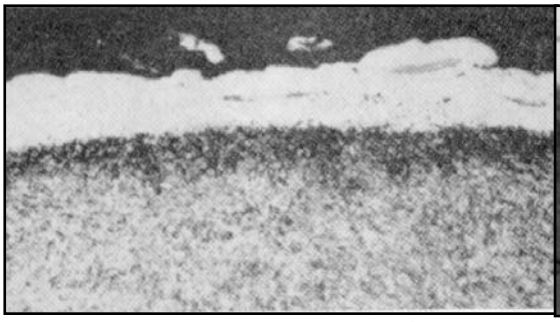

Fig. 3.13: Recast Layer (Optical Microscope)[60]

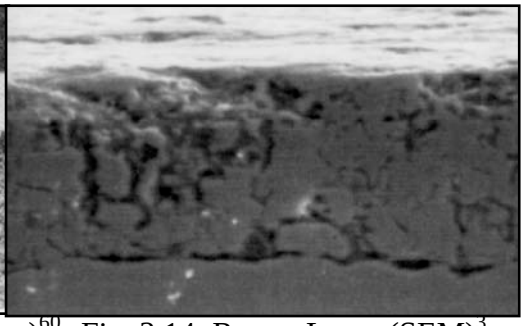

Fig. 3.14: Recast Layer (SEM)[3]

Figure 3.14 shows the recast layer as seen on the scanning electron microscope (SEM). The layer has a fused structure and is riddled with holes[66]. The presence of these holes is detrimental to the fatigue strength of the workpiece. When the workpiece is stressed, the holes act as stress concentrations, encouraging the initiation of cracks[63].

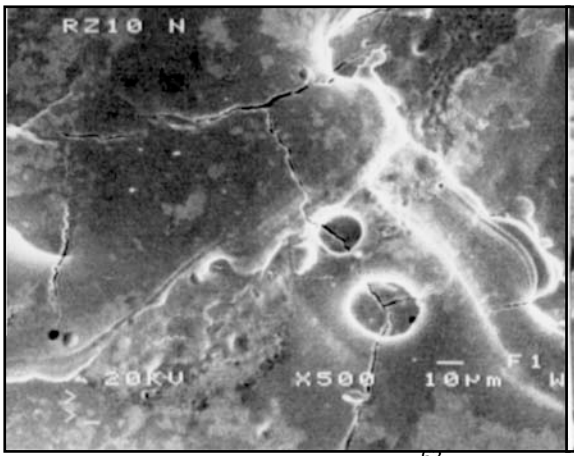

Fig. 3.15: Spark-Eroded Surface[63]

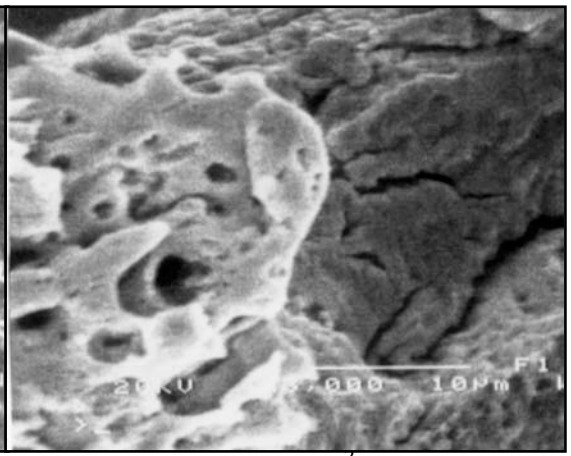

Fig. 3.16: EDWC Surface[3]

EDM machined workpieces exhibit numerous cracks on the surface[1,3,63,66]. These cracks may be seen in Figures 3.15 and 3.16. The molten metal that has not been

carried away by the dielectric fluid has re-solidified on the surface of the workpiece. The molten metal left on the surface (the recast layer) is cooled rapidly by the dielectric fluid, and shrinkage occurs. Cooler sections on the surface resist this shrinkage, causing tensile stresses on the surface of the specimen. The recast layer has a lower resistance to tensile stresses, leading to the formation of microcracks[63,66].

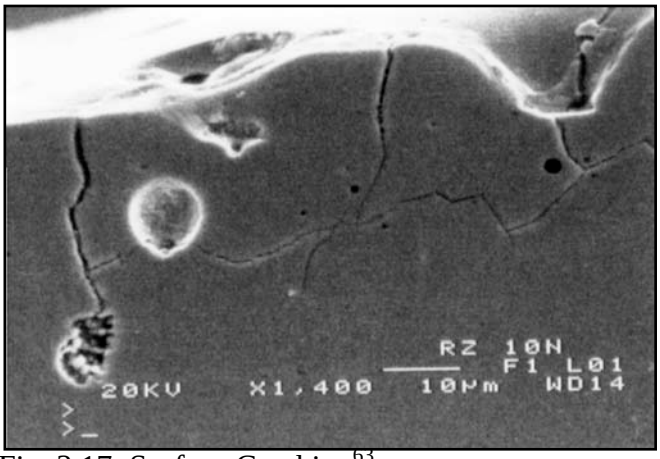

Fig. 3.17: Surface Cracking[63]

Figure 3.17 shows the cross-section of a spark-eroded workpiece with a network of microcracks that extend from the surface of the workpiece[1,63]. Shrinkage in the surface due to the rapid cooling of the recast layer produces tensile stresses in the surface. As a result of this stress, cracking occurs in the surface[1].

The existence of these microcracks on the surface is detrimental to the fatigue strength[1,3,66]. The microcracks act as stress concentrations when stressed and are sites for the initiation of propagating cracks that lead to failure[1,3,63,66]. In the absence of these microcracks, the fatigue strength is still lower. The drop in

fatigue strength can be attributed to the residual tensile stresses in the surface layer[64,66,69,70].

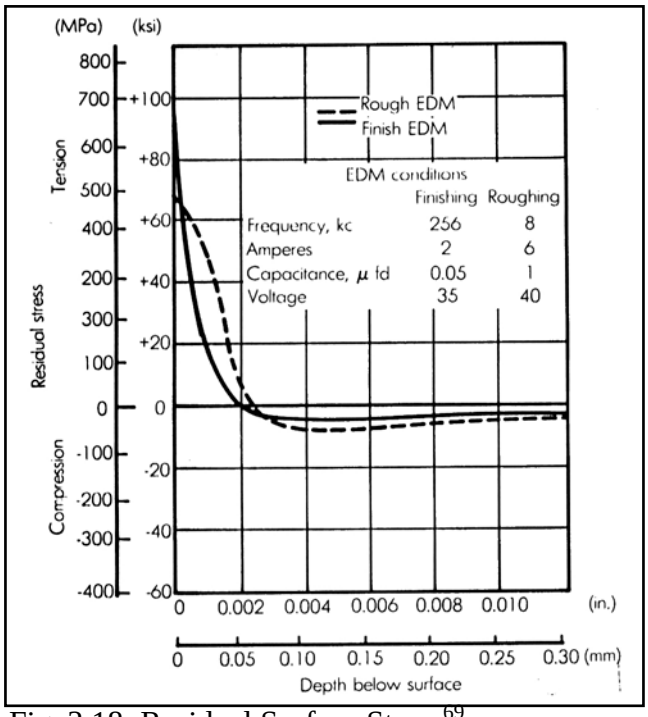

Fig. 3.18: Residual Surface Stress[69]

Figure 3.18 shows the variation of residual tensile stresses from the EDM machined surface down towards the bulk material as measured using x-ray diffraction. The recast layer shrinks during re-solidification. This shrinkage is resisted by the bulk material, leading to tensile stresses in the recast layer and compressive stresses in the bulk material adjacent to the recast layer. Therefore, the tensile stress, at a certain depth in the bulk material, changes to a compressive stress[66].

The heat-affected zone is another characteristic of the EDM process. The light band in Figure 3.19 is the recast layer. Beneath the recast layer is the heat-affected zone. The heat-affected zone in Figure 3.19 shows a distinct change in structure.

This does not always occur[1,63,68]. Figure 3.20 does not show a distinct difference in structure between the heat-affected zone and the original material.

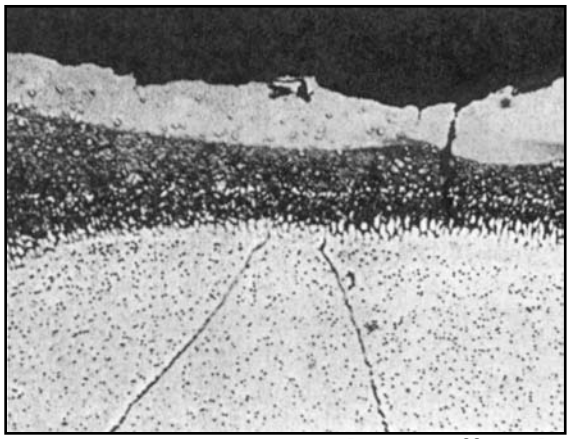

Fig. 3.19: Recast Layer and Heat-Affected Zone[69]

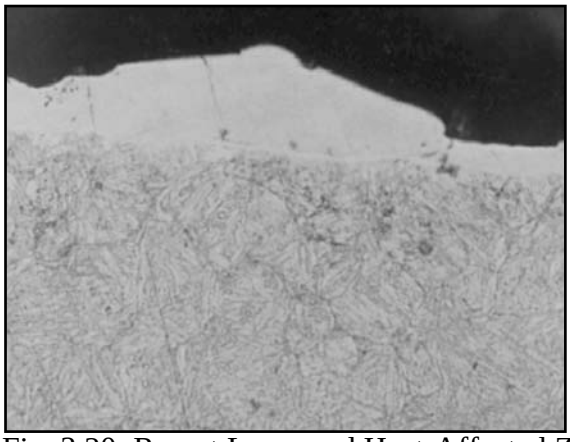

Fig. 3.20: Recast Layer and Heat-Affected Zone[63]

Hardened metals that are heated to a temperature lower than the critical level may be annealed. If however the temperature is above the critical level, the metal is re-hardened. For martensitic steels, the structure in the heat-affected zone and the original structure differ little[63,65]. It is therefore difficult to distinguish the heat-affected zone from the bulk material.

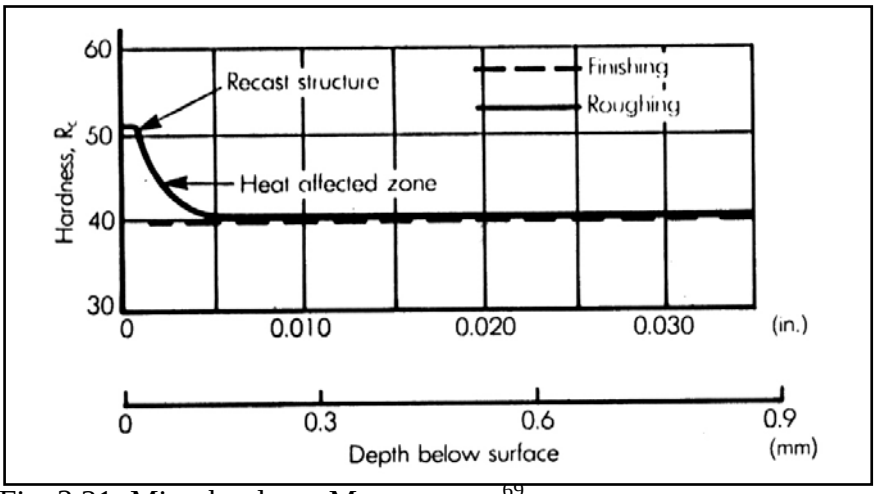

Fig. 3.21: Microhardness Measurement[69]

One way of defining the depth and the presence of the heat-affected zone is to test the hardness of the material[63,69]. Figure 3.21 indicates that there is a total heat-affected depth of approximately 0.15mm. Another way of differentiating the heat-affected zone from the bulk material is by examining the fracture surface. The heat-affected zone would show a fine crystalline structure that is similar to that of hardened carbon steel, while the bulk material would have a large grain structure[65].

Table 3.1 shows a summary of the types of surface characteristics that may be obtained for different metal removal processes. Electrochemical machining (ECM) and chemical milling (CHM) are the other two non-traditional metal removal methods included.

Material	Conventional Metal Removal Methods		Nontraditional Removal Methods		
	Milling, Drilling, or Turning	Grinding	EDM	ECM	CHM
Steels:					
Nonhardenable	R	R	R	R	R
1018	PD	PD	MCK	SE	SE
	L & T		RC	IGA	IGA
Hardenable	R	R	R	R	R
4340	PD	PD	MCK	SE	SE
D6AC	L & T	MCK	RC	IGA	IGA
	MCK	UTM	UTM		
	UTM	OTM	OTM		
	OTM				
Tool Steel	R	R	R	R	R
D2	PD	PD	MCK	SE	SE
	L & T	MCK	RC	IGA	IGA
	MCK	UTM	UTM		
	UTM	OTM	OTM		
	OTM				
Stainless (martensitic)	R	R	R	R	R
410	PD	PD	MCK	SE	SE
	L & T	MCK	RC	IGA	IGA
	MCK	UTM	UTM		
	UTM	OTM	OTM		
	OTM				
Stainless (austenitic)	R	R	R	R	R
302	PD	PD	MCK	SE	SE
	L & T		RC	IGA	IGA
Precipitation hardening	R	R	R	R	R
17-4 PH	PD	PD	MCK	SE	SE
	L & T	OA	RC	IGA	IGA
	OA		OA		

Table 3.1: Surface Characteristics Resulting from Various Metal Removal Processes[69]

Key:

R Roughness of surface

PD Plastic deformation and plastically deformed debris

L & T Laps and tears and crevice-like defects

MCK Microcracks

SE Selective etch

IGA Intergranular attack

UTM Untempered martensite

OTM Overtempered martensite

OA Overaging

RC Recast, respattered metal, or vapor deposited metal

3.7 Post-Operation Processes

The surface characteristics that the EDM process generates are detrimental to workpieces that are subject to high dynamic stresses in service. The two main methods of overcoming this problem are by removing the surface layer or by negating the effects of the residual tensile stresses[54].

The surface layer can be removed by conventional methods such as mechanical milling, polishing and abrasive finishing. Other methods of surface layer removal include chemical milling, electropolishing and electrochemical machining[1,63,71]. In order to neutralize the effects of the residual tensile stresses and increase the fatigue strength of the workpiece, the surface can be peened or burnished to produce a residual compressive stress in the surface[54,70].

3.8 Advantages and Limitations of EDM

The EDM process utilizes sparks to remove metal. The electrode tool does not touch the workpiece at all. No physical force is exerted on the workpiece, making it ideal for the machining of thin and fragile workpieces that cannot withstand conventional mechanical cutting forces[1,55]. Metal removal by this process is independent of the hardness of the workpiece[1,55,63,72,73]. Hardened materials can undergo heat treatment processes before being machined, thus eliminating workpiece distortions that are caused by the heat treatment process[1,55,56,63,74]. The EDM process is, however, limited to electrically conductive workpieces[1,63,73].

Another advantage of the EDM process is the ability to machine complex shapes without the need for costly cross-sectional construction. Workpieces that contain narrow, deep cavities with intricate contours or holes can be easily produced[1,3,54-56,60,61,63,67,75].

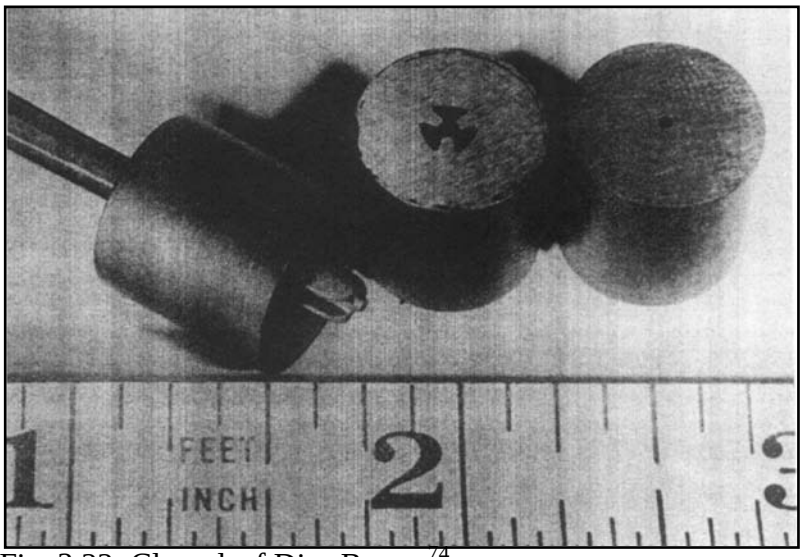

Fig. 3.22: Cloverleaf Dies Button[74]

These difficult features can be machined to a high accuracy and uniformity in tight clearances for irregular shapes can be achieved[54,55,60,61,67,74]. The complete product is burr-free, eliminating the need for a finishing process to smoothen any rough edges, thus reducing cost and time[1,56,61,74]. The surface patterns that the EDM process leaves on the workpiece have been shown to have an enhanced oil retention capability. This capability makes EDM a very good process for the finishing of parts such as plain bearings[55,73].

EDM is a low cost procedure as electrodes can be machined out of relatively inexpensive materials such as carbon[3,72,74]. Actual parts can be used as electrodes to produce electrodes for manufacture, reducing electrode-machining costs.

However, the low electrode tool life and the high costs of accurate electrode tools mean that conventional mechanical methods may be preferable[54].

Modern EDM machines have many new features that contribute to broadening the process capability. One of these features is the NC motion control, in which the EDM process is automated, removing the need for skilled operators. The machine can also be left to run on its own without the need for supervision[1,3,72,67].

CHAPTER 4: SHOT PEENING

Shot peening is a method of cold working that involves the impingement of a stream of shot on the surface of a workpiece at high velocities[6,73]. The peening of a surface is not a new process; it has been in use for thousands of years in the production of armour, weapons and tools[2]. Shot peening has now gained widespread acceptance in the automobile, aeronautic and aerospace industries as an effective means to combat fatigue[76].

4.1 Description of Process

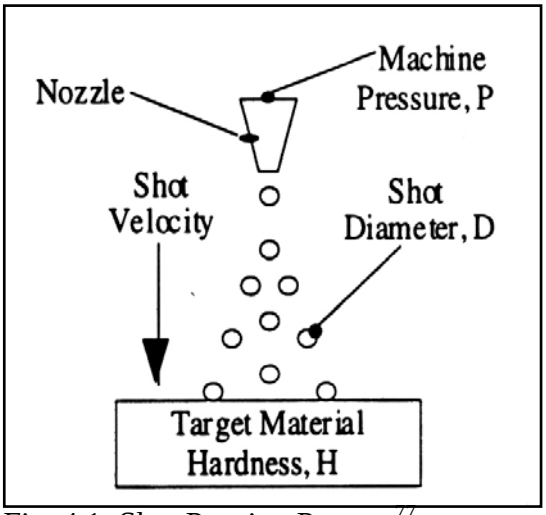

Fig. 4.1: Shot Peening Process[77]

Shot peening utilises a stream of spherical shot particles to impact the surface of a workpiece at a high velocity. The shots are normally propelled by compressed air or by centrifugal force onto the surface of the workpiece[6,73]. The used shot is then removed to a shot-recycling unit, where the shot is recycled and re-classified. Usable shot is then sent to the shot propulsion unit to be reused.

When the shot particles hit the surface of the workpiece, an indentation is formed on the surface. This is a consequence of plastic deformation. This plastic deformation normally extends to a depth of 0.13mm to 0.25mm (0.005in to 0.02in)[6]. The material below this depth has not been altered, but is still continuous with the material that has been deformed. This results in a compressive stress at the surface, with an associated tensile stress being present in the material below the surface[2,6,78-80]. If an external load is applied to the component, the resultant stress at the surface is equivalent to the sum of the residual surface stress and the surface stress at the surface associated with the externally applied load. As fatigue cracking is sensitive to tensile stress, the fatigue life is improved[2,6,78].

4.2 History of Peening

Peening is a process that has been in use for hundreds of years. Known as hammer hardening, a ball pein hammer was used to work harden a surface, such as that of weapons and shields. Some copper spearheads were seen to penetrate armour with ease while others did not. Similarly, blacksmiths who hammer peened the tension side of carriage springs noted that this increased the life and load carrying capacity of the springs. This greater wear resistance and improved resilience in the part was noticed, but the mechanisms behind the effect were unknown[2].

In the 1920s, analytical methods were employed to study the effects of particles striking a surface as compared to that of a single pointed ball pein hammer. In the late 1920s, General Motors was involved in the use of blast cleaning to remove

corrosion from car valve springs. These springs were observed to have a longer fatigue life then springs that had not been blast cleaned. John O. Almen, who was working at General Motors, investigated this phenomenon and concluded that the blast cleaning process was the cause of the extended lives. General Motors began using shot peening in production, to extend the lives of valve springs in car engines[2,78,81].

In a bid to control the shot peening process in production, Almen manufactured thin strips, out of the same materials, as a comparator to the springs. The strips, now known as the Almen strip ('A' strip), were subjected to the same shot peening process as the springs. The changes in the curvature of the strips were then used as an indicator for the peening process[2,6,73,79].

Two other strips were later introduced to allow the control of a larger range of peening conditions. The 'N' strip was introduced in the 1950s for controlling lighter peening conditions on aerospace components. In the 1960s, the 'C' strip was manufactured for more aggressive peening parameters. Apart from these three standard strips, other strips produced from different alloys and of different sizes are in use in industry today[2,6,73,81].

Although shot peening had been seen to cause fatigue strength improvements of 20% - 30% since the 1940s, shot peening was only applied as a remedial treatment for components that had failed during service[2]. In the late 1970s, a review of the shot peening process was carried out. The results of this review

spread rapidly throughout the world's aerospace industries, leading to the recognition of shot peening as a process that can greatly enhance the fatigue life of components. This review coincided with an increasing demand for lighter and more fuel-efficient aircraft. Improvements in the process predictability and reliability of shot peening were required[80].

4.2.1 Equipment

Shot peening began as a manual technique. Hand held equipment was replaced by mechanised methods when the automotive industry began using shot peening. Use of mechanisation made the shot peening process repeatable. The process has now been simplified by the addition of CNC controls[82] and the use of shot peening programs, such as PEPCOM, to run the operation[83].

The accuracy of the Almen gauges is also continually being improved to achieve a consistent in quality[84]. Some advancements have also led to shot peening becoming a more environmentally friendly process. One example is to use a dust-free process[85].

4.2.2 Media

In the 1930s, chilled iron grit was used for blast cleaning. The first main change to the shot peening process was the change in the shape of the shot to a sphere. In the 1950s, cast steel shot was introduced as chilled iron grit was seen to shatter too quickly. In the 1960s, glass beads were introduced to allow for the peening of thin

ferrous materials and materials that might be contaminated by ferrous shot. In the 1970s, high hardness steel shot was introduced. In the 1980s, ceramic shot was introduced to fill the gap between the steel shots, which lasted for several thousand cycles, and the glass shot, which lasted only a few cycles. There are other types of shot that are now available for special applications, but cast steel shot is still the most commonly used[2,6,73].

4.2.3 Applications

The first application of shot peening was to address fatigue problems in the automotive industry[2,78,81]. Initially, the peening process was used on leaf and coil springs. The range of applications soon expanded to include gears, shafts, fasteners and oil drilling equipment. The success of shot peening was such that it spread to the aerospace industry. Landing gears, structural members and compressor and turbine blades were peened[73].

In the late 1940s, the Almen strip principle was used as the basis for the forming of aerodynamic components through shot peening[2]. This process was known as peen forming. The peen forming process is largely automated. The part is usually thin in section and selectively peened on one side to produce its final shape[6,73,79]. A variation of peen forming is peen straightening. Peen straightening is used to correct the distortion that is produced in parts due to machining or heat treatment[6,73,79].

In the 1960s, shot peening was found to improve the resistance of a part to stress corrosion cracking[2]. One such example is hydraulic reservoirs in aircraft landing gears. Shot peening has also been found to be effective against fretting corrosion, and is used to combat fretting corrosion on bolt and fastener holes on aerospace structures[73].

4.3 Effects of Peening

Shot peening is a process that uses a stream of shot particles travelling at a high velocity to bombard the surface of a component. When each shot particle impacts the metal surface, plastic deformation occurs, thus producing a slight, round depression on the surface[2,6,79,80]. The material that has been plastically deformed only extends about 0.013mm to 0.50mm (0.005in to 0.02in) beneath the surface[6,73]. Below this stretched layer is the bulk material that is unaffected by this indentation. Due to continuity, residuals stresses are generated by the shot peening process[2].

Figure 4.2 shows how residual stresses can be created. Imagine bar A as the surface layer and bar B as the bulk material. When the component is peened, the surface layer, bar A, plastically deforms and stretches. To rejoin both bars now, their lengths would have to be adjusted. Bar A would have to be shortened, while bar B lengthened. The final assembly would have a compressive stress in the surface and a tensile stress in the bulk material. The creation of these stresses is what happens when the component is shot peened[2].

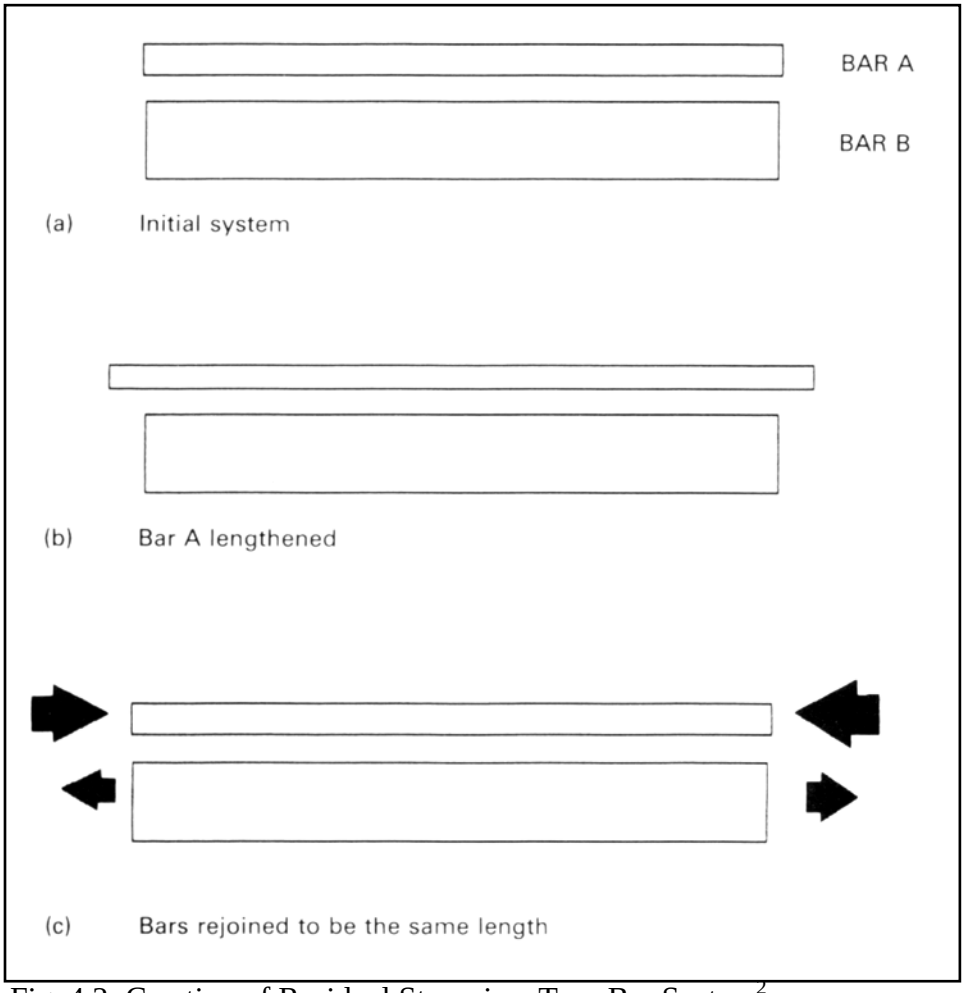

Fig. 4.2: Creation of Residual Stress in a Two-Bar System[2]

For thin materials, shot peening on only one side of the material would cause a convex curve to form with the peened surface on the outside. Here, the layer that is unaffected by the peening is too thin to completely resist the elongation of the peened side, thus resulting in curvature. This is the basis of the Almen strips, which are used to monitor the process. Peen forming and peen straightening have been developed on this principle as well[73,79].

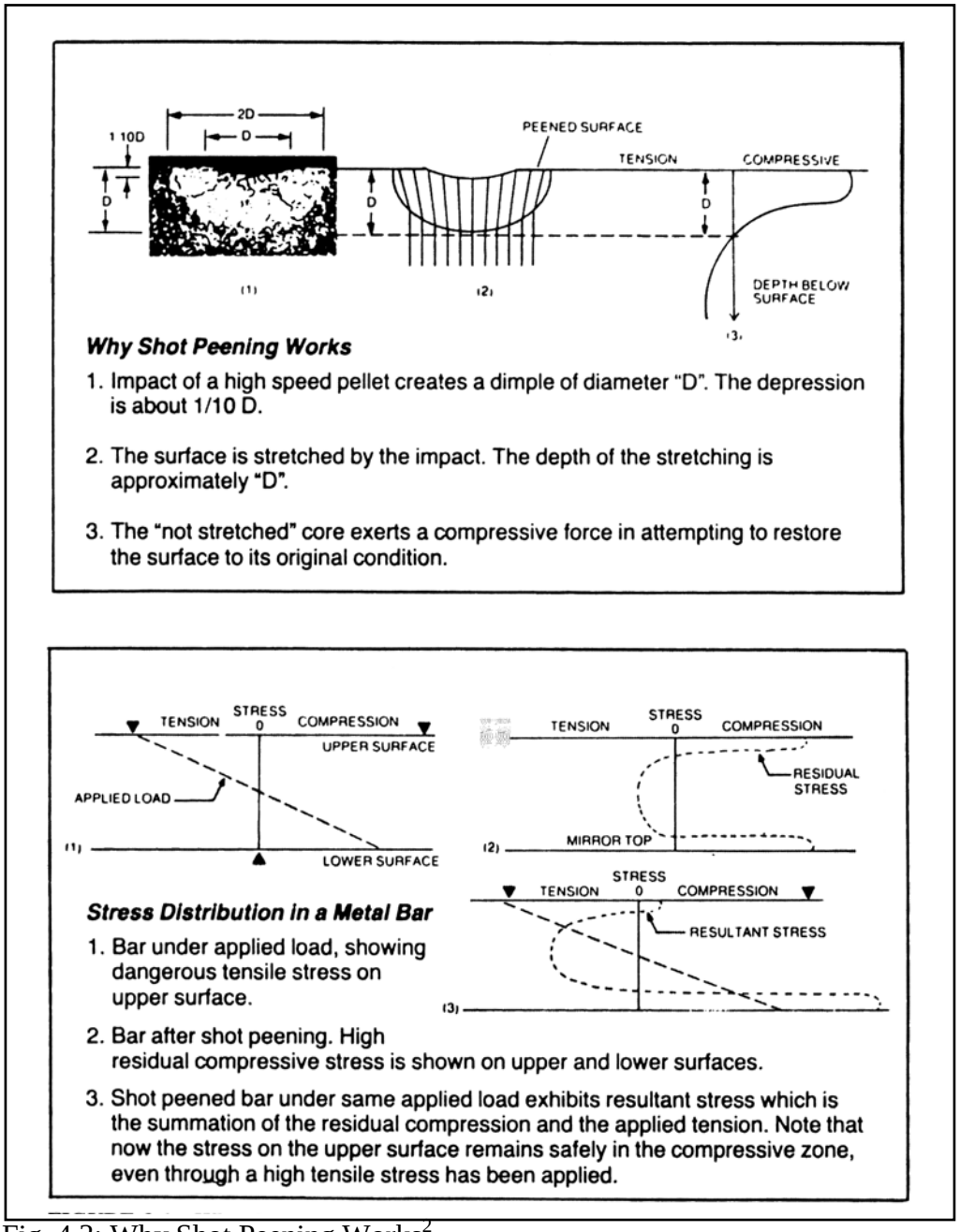

Fig. 4.3: Why Shot Peening Works[2]

The residual stress in the surface layer of a component that has been shot peened is compressive[2,6,73,78,79,80]. Figure 4.3 shows how shot peening increases the fatigue life of a component. Cracks propagate from the surface of a component under repeated tensile stresses associated with the loading. When the component is shot peened, a residual compressive stress is created in the surface. When a load

is applied, tensile stresses do not develop to form a crack on the critical surface area until the residual compressive stresses induced by the shot peening process have been overcome. The allowable stress level is increased, thus increasing the fatigue life of the component[6,73,78]. Shot peening has been found to increase the fatigue life of components by up to 50%[79,87].

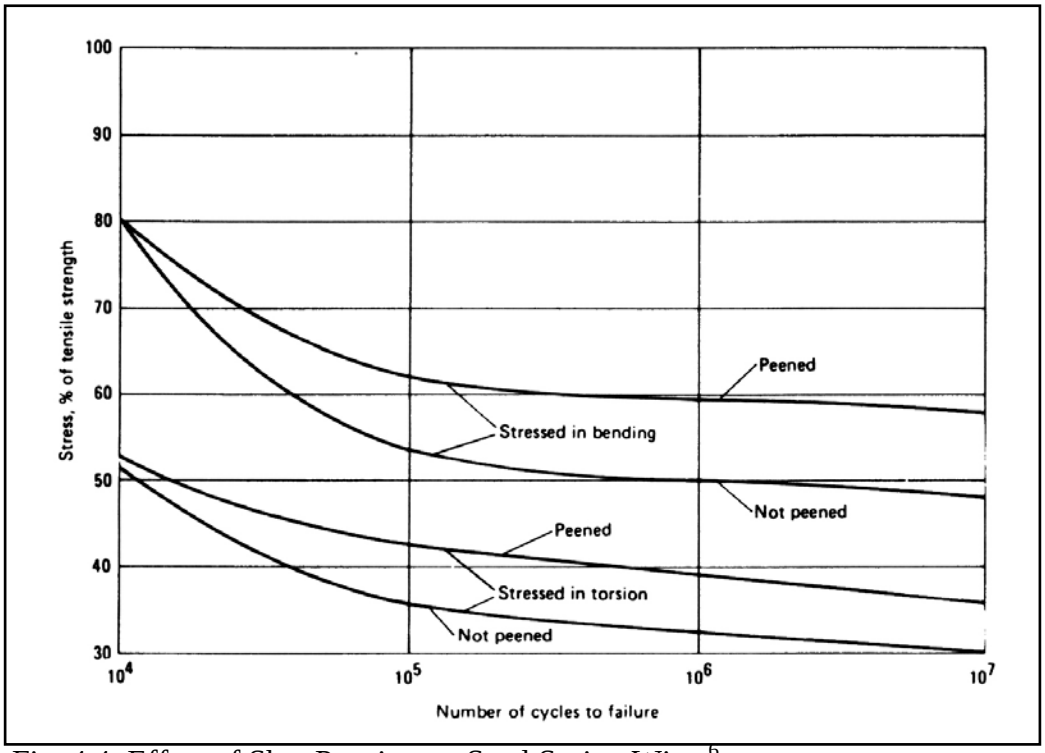

Fig. 4.4: Effect of Shot Peening on Steel Spring Wires[6]

A side effect that occurs due to shot peening is the stress relief that may occur in the component. Manufacturing processes, such as grinding and milling, lead to the creation of residual tensile stresses in the surface layer of the component. These tensile stresses would contribute to the early failure of the component. Shot peening changes these undesirable tensile stresses to compressive stresses, thus further improving the component's fatigue life[6,73,78].

Surface imperfections found on machined components include pits, scratches and other surface defects. The shot peening process blends these imperfections, thus effectively removing them as stress concentration points[6,73]. However, the surface finish may not have improved. After peening, overlapping dimples cover the surface. As a general rule, shot peening would improve the surface roughness of the component if its initial surface roughness is above 125 RMS. This surface roughness value is also dependent on process parameters, such as material type, hardness and the shot size[87].

Overpeening, or peening a component for too long a time, has been seen to be detrimental to the component and potentially dangerous. In adverse conditions, pockets of localized corrosion may occur on the surface[80]. Another point to note is that although shot peening is very effective in improving the fatigue life of a component, it is less effective in preventing fatigue failures that initiate from defects that are present beneath the surface[80].

4.4 Major Factors

Shot peening is affected by three major factors: the peening media, the peening intensity and the coverage[2,6,73,87]. The nature of the anticipated mode of fracture, the geometry and metallurgy of the component to be shot peened affects how each factor should be determined[2,87].

4.4.1 Peening Media

4.4.1.1 Materials

There are several different types of peening shot. The most commonly used shot is cast steel shot[2,6,73,80]. Shots made from cast steel have good ductility and a low initial cost. There are two common hardness levels: regular and hard. The shot hardness required is dependent on the hardness of the component to be peened. The disadvantage of hard cast shot is that they break down rapidly and an efficient system to remove the broken particles must be employed[2,6].

Conditioned cut wire shot breaks down slower than cast steel shot, although the initial cost is higher[2,73]. Steel wire is chopped into cylinders where the length equals the diameter. These cylinders are then blasted repeatedly to round off the cut edges[2,6]. One advantage of cut wire shots is that the shots rarely break into sharp half spheres that would nick the surface of the component being peened[2].

Glass beads are used where ferrous contamination of the peened component would be detrimental[2,6,73]. The beads are manufactured from high grade glass and are designed to provide a desired finish[2,80]. Glass beads are used to peen very thin sections. As glass beads are available in sizes down to 0.05mm (0.002in), very tight radii, such as threads in screws can be easily peened[2].

Ceramic beads are manufactured from a mixture of zirconium, silicon and aluminium oxides at a high temperature[2,80]. The beads produce acceptable

intensities and are more durable than glass beads, making them ideal for applications where no foreign metal can be tolerated[2,73].

4.4.1.2 Shot Shape

Through his investigations on shot blasting, Almen discovered that the use of spherical shot particles rather than angular and grit type particles made the peening process more effective[2]. The shape of shot is currently monitored visually. An example of shot shapes is shown in Figure 4.5. The first row shows shapes that are considered normal in appearance and uniformity. The impressions produced would be circular and uniform in size. The second row of shapes show shot shapes that is unacceptable as the shot is not uniform and would produce irregular impressions on the component. The third row includes shot shapes that contain sharp edges. These edges are detrimental to components being peened[2].

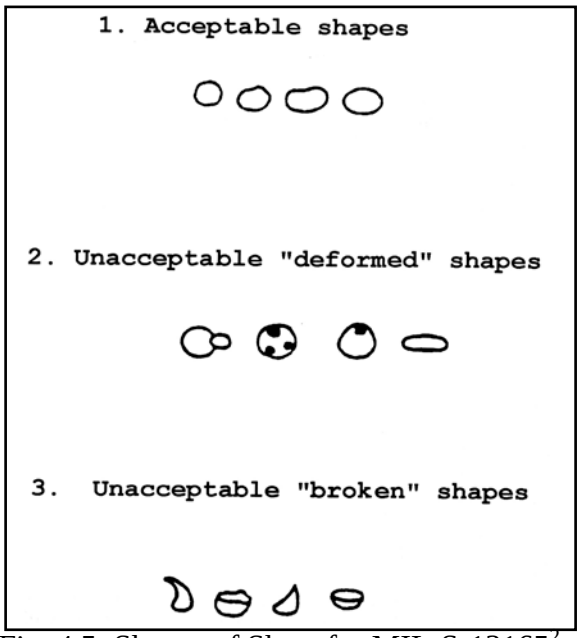

Fig. 4.5: Shapes of Shots for MIL-S-13165[2]

The breakdown of shot is inherent in the process of shot peening. The resulting broken shot can be detrimental; therefore the shape of the shot must be screened throughout the peening process. Figure 4.6 compares the surface that is produced by peening with broken shot and regularly shaped shot.

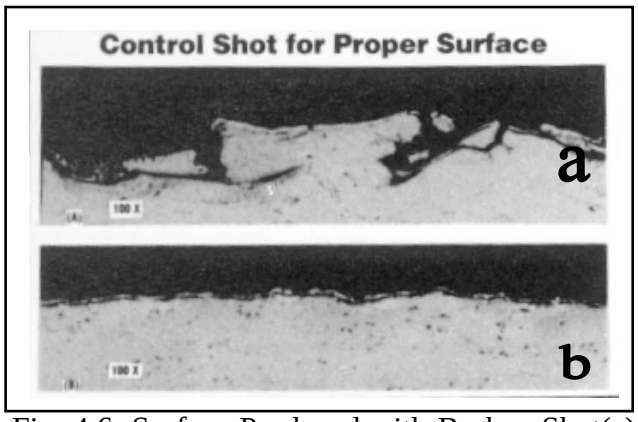

Fig. 4.6: Surface Produced with Broken Shot(a) and Regular Shot(b)[87]

Peening with broken-regular shot mixtures can increase fatigue life, however, to do so would require an increase in the weight of the broken shot mixture used. This increase would, in turn, lead to an increase in the cost of the process[88].

4.4.1.3 Shot Size

The size of the shot used must be monitored in order to control the outcome of the peening process. The shot is passed through a set of five test sieves to determine the size distribution of the shot. The bulk of the shot will typically pass through the second sieve but be retained by the fourth sieve[2].

There are several conditions that determine that size of the shot that is used in peening. The geometry of the component is the main constraint[73]. Figure 4.7(A)

shows that if the diameter of the shot used is larger than twice the radius of a groove, full coverage will not be achieved. Figure 4.7(B) show the maximum shot size (d = ½R) that would make peening the root radius of a thread effective[6,87].

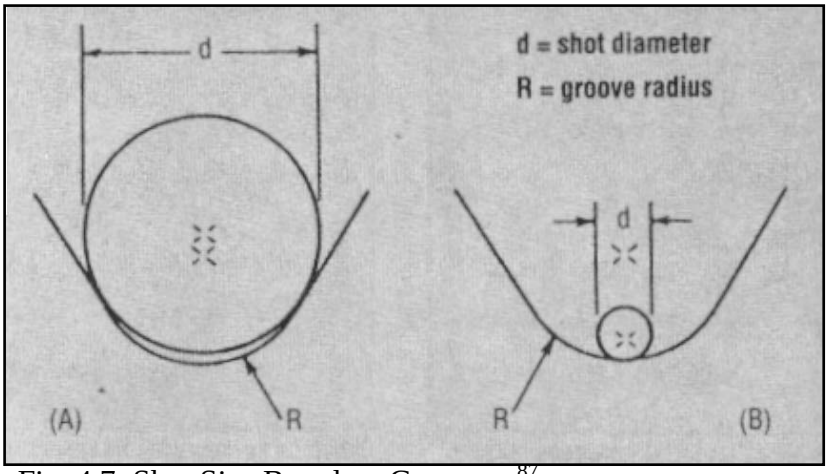

Fig. 4.7: Shot Size Based on Geometry[87]

Changing the size of the shot affects the intensity of the peening process[6,89]. With all other process parameters constant, an increase in the diameter of the shot increases the peening intensity of the process. The increase in peening intensity causes an increase in the depth of the compressed layer of the component[6,90]. The final surface roughness of the component has been found to increase with increasing shot size[90]. However, the coverage and the compressive stresses induced are decreased with an increase in shot size[6,91].

4.4.2 Intensity

The peening intensity is used to describe the overall effect of peening[73]. In the 1930s, Almen recognized the importance of process consistency. He arranged to manufacture strips as a comparator. He observed that if one side of a strip was

peened, it would curve, convex on the peened side. The curvature is due to the introduction of compressive stresses and the stretching of the peened side. The amount of curvature on the strip varies with different process conditions. If the shot size is larger, the curvature is greater. Similarly, if there is a greater shot velocity, the curvature increases. However, once the surface of the test strip is totally covered in peening dimples, further peening shows little additional curvature. Using this information, Almen developed the system that is named after him[2,87].

The Almen system consists of mainly three elements: the test strip, the holding block and the Almen gauge. Figure 4.8 shows the three standard test strips that are used for the measurement of peening intensity.

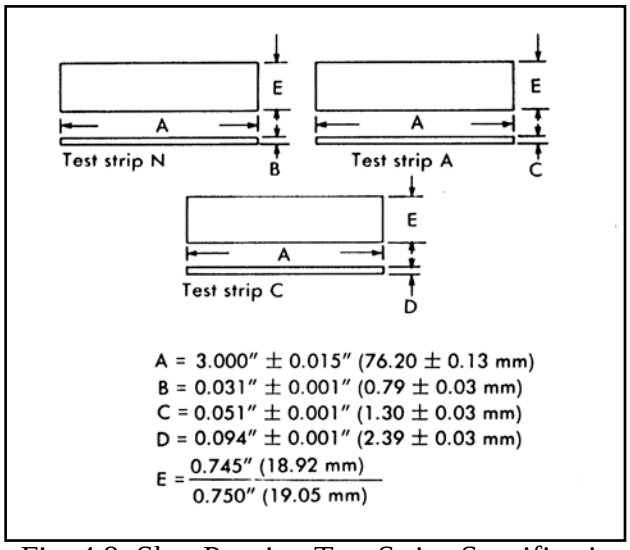

Fig. 4.8: Shot Peening Test Strips Specifications[73]

The ‘A’ strip is used to measure peening intensities that produce arc heights of 0.15mm to 0.569mm (0.006in to 0.0224in). Intensities producing arc heights of less than 0.15mm (0.006in) are measured using the ‘N’ strip, while intensities

greater than 0.61mm (0.0.024in) are measured using the 'C' strip[2,73,81]. Test strips are normally produced from steel[79], although other materials such as aluminium and Inconel have been used. Producing strips of material other than steel is rarely done, as intensities obtained using the standard strips have been found to relate adequately to most peening applications[2].

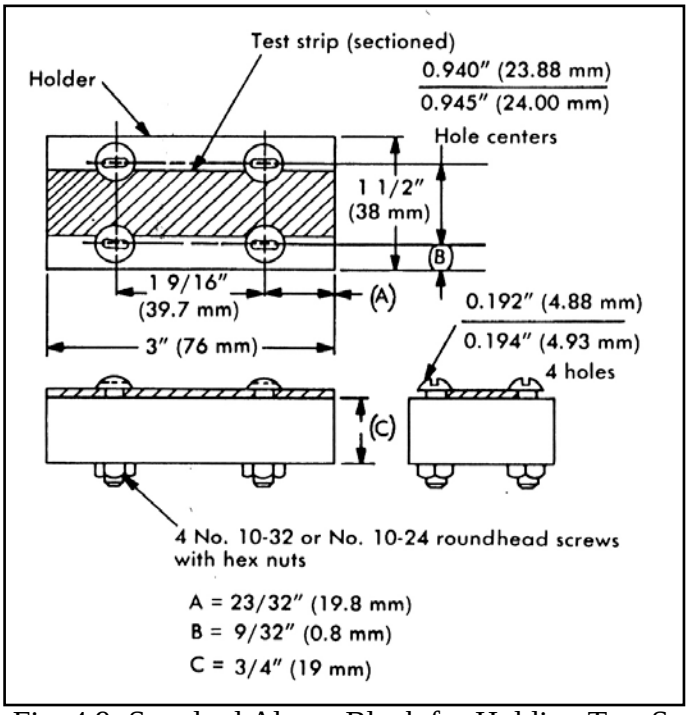

Fig. 4.9: Standard Almen Block for Holding Test Strips[73]

The test strip is held in a standard Almen holding block as shown above. The holding block is loaded in the machine at a location where the peening is critical. The test strip is peened for a short time period, then removed from the holding block. The curvature of the strip is measured using an Almen gauge and recorded on a chart.

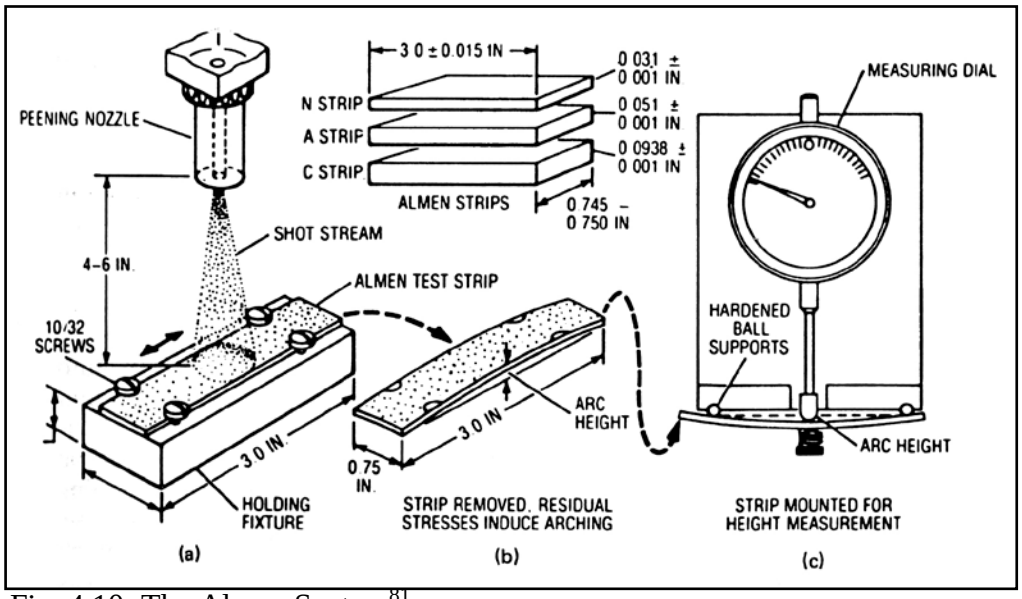

Fig. 4.10: The Almen System[81]

The process is repeated with new test strips at increasing time periods until the resultant curve flattens out. When doubling the exposure time yields only a 10% increase in arc height, saturation is said to have occurred. This exposure time is known as the saturation time[2,80,81,87]. The saturation time is also the approximate time required for the Almen strip to receive 100% surface denting, or 100% coverage[92].

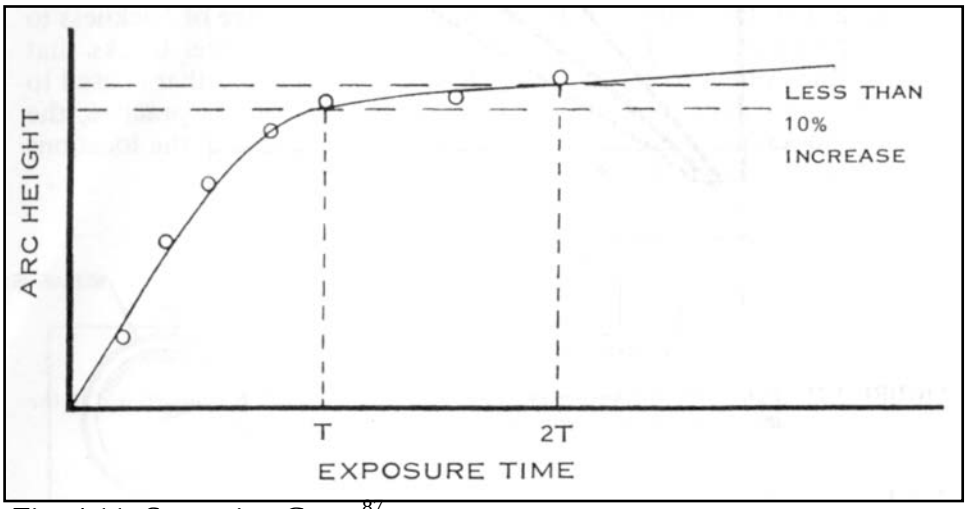

Fig. 4.11: Saturation Curve[87]

4.4.3 Coverage

Surface coverage is defined as the percentage of the original part surface that is covered by the indentations of the individual shot particles. Full or 100% coverage is achieved when the original surface is totally replaced by the peening dimples and over 100% coverage is achieved if the peening process continues after 100% coverage is reached[2,6,73]. Coverage is an important factor as a little less than 100% coverage can result in a reduction in fatigue life. An increase in coverage from 200% to 600%, however, only leads to an increase of 9% for fatigue life[91]. If 200% coverage is insufficient, further shot peening will not solve the problem. In industry, the coverage varies from 80% to 100% for spring applications and 200% in the aircraft industry[73].

There are four methods of measuring coverage. The first is by visual examination with a tenfold magnification. Although not quantitative, visual examination is widely used[2,6,80,81]. Situations where this method is not very accurate include the examination of gears, where the dimples in the critical tooth root radii are almost impossible to distinguish[2].

An alternative method is the use of Dyescan tracer liquids, as in the Peenscan® process[2,73]. The tracer liquid is painted, sprayed or dipped onto the part. After drying, the part is peened for about half the estimated time required to obtain full coverage. The part is then removed and examined under black (UV) light. Any tracer liquid that is not removed by the peening process is highly visible. The

exposure time is then increased until full coverage is obtained - that is, no tracer liquid is left on the part.

The Straub method involves the use of an Almen strip[6,73]. The strip is exposed to the shot and then magnified to 50 diameters in the field of a metallograpic camera. The images of the indented area are traced with a sharp pencil onto transparent paper, then measured with a planimeter. The ratio of the indented area to the total area is determined. This method is time consuming, and it assumes that the area selected is representative of the whole strip.

Another method that uses the Almen strip depends upon the hardness of the Almen strip and the component. This method is fairly quick and accurate. The Almen strip is exposed for the time that is estimated to be required to achieve 100% coverage. Another Almen strip is exposed for twice the length of time for the first one. The arc heights are measured. If the change in arc heights is found to be more than 10%, it indicates that the first Almen strip did not reach saturation[73]. This method is fairly indicative for components that are of the same hardness. However, for components that are of a different hardness, the saturation time would vary from that of the Almen strip, with a softer material requiring a shorter time.

4.5 Post-Operation Processes

Shot peening is normally used as a finishing process[6]. If a surface finish finer than that of the peened component is required, certain processes may be used. These processes are limited by the amount of heat that is produced and the amount of material removed[6,87].

The effectiveness of shot peening is greatly dependent on the compressive stresses that are produced at the surface of the peened component. High temperatures generated during the post-peening process act to relieve the compressive stresses[6,87]. Moreover, the compressive layer is relatively thin, and no more than 10% of the compression depth should be removed during subsequent grinding[87]. Light honing and lapping can be carried out if required[6,87].

Straightening or cold forming should be avoided, as these processes introduce residual tensile stresses, which reduce or eliminate the effect of shot peening. Peen straightening and peen forming should be used instead[6].

Steel that has been peened has a clean and chemically active surface that is highly susceptible to corrosion. This problem can be addressed by the application of a rust preventative. Stainless steels that have been peened using steel shot can be contaminated by iron particles, which cause rusting. Further peening with glass beads removes the contamination and increases the fatigue life of the peened part[6,93].

CHAPTER 5: EXPERIMENTAL PROCEDURE AND RESULTS

5.1 Test Specimens

300M steel is essentially a silicon-modified 4340 steel with a higher carbon and molybdenum content and added vanadium. The increased silicon content provides deeper hardenability and better resistance to softening at higher temperatures[94]. Although 300M steel is the material used to produce the structural components, 4340 steel is a cheaper alternative that can be used as a basis for comparison. The chemical compositions of the two steels are shown below.

	4340 Steel	300M Steel
Carbon	0.38 – 0.43	0.40 – 0.46
Manganese	0.60 – 0.80	0.65 – 0.90
Silicon	0.20 – 0.35	1.45 – 1.80
Nickel	1.65 – 2.00	1.65 – 2.00
Chromium	0.70 – 0.90	0.70 – 0.95
Molybdenum	0.20 – 0.30	0.30 – 0.45
Vanadium	-	0.05 (min)

Table 5.1: Composition of 4340 Steel and 300M Steel[94]

4340 steel is heat treated to a hardness of 51 to 52 R_c. The microstructure of 4340 steel is primarily martensite and is shown in Figures 5.1 and 5.2.

Fig. 5.1: Microstructure of Heat Treated 4340 Steel at 230X

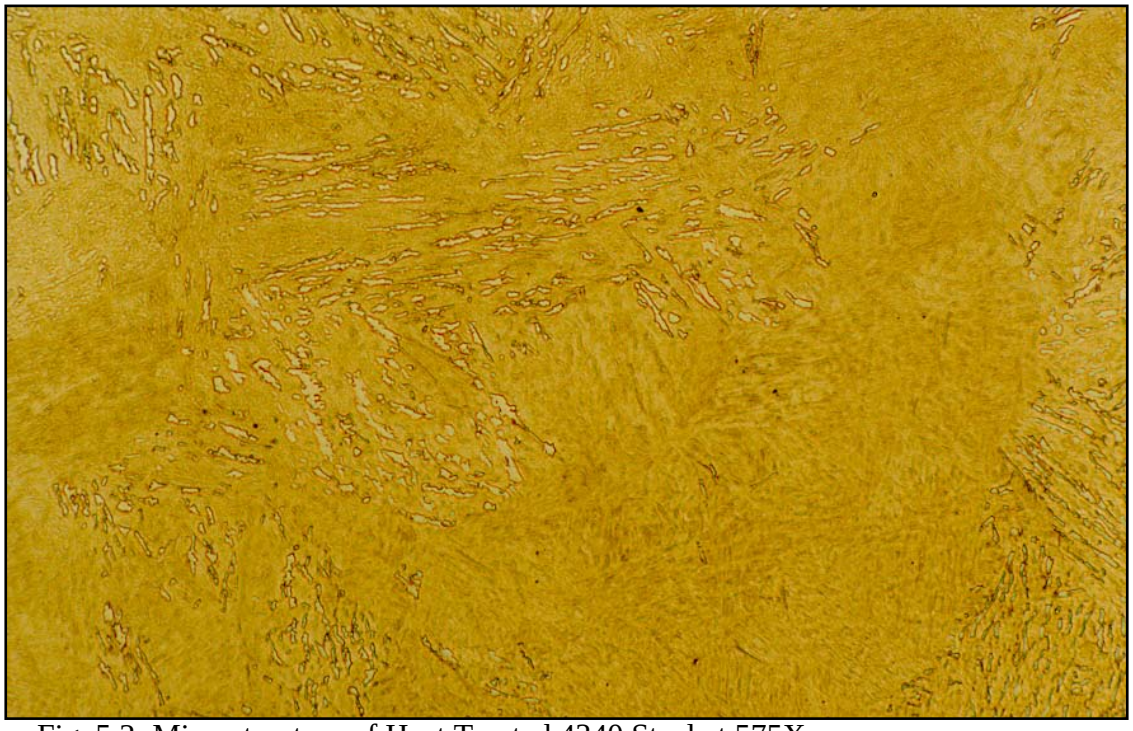

Fig. 5.2: Microstructure of Heat Treated 4340 Steel at 575X

The dimensions of the test specimens were taken from Project 12/95[3]. The width of each specimen is 20mm; the height is 10mm and the length is 75mm. Each

edge of each specimen has a radius of 2mm. Two-thirds of the tests specimens were machined to size by EDWC. Of the two-thirds, half the specimens were shot peened to 0.01A, while the other half were left in the EDWC condition. The remaining third of the specimens were EDWC before they were ground to size.

5.2 Fatigue Tests

Four-point bend testing on the test specimens was carried out on an Amsler High Frequency Vibrophone machine (Figure 5.3). The Vibrophone machine is used to determine the fatigue properties of a material through fluctuating and alternating tensile, compressive or shear stresses. The machine runs on the resonance principle; the test frequency coinciding with the natural frequency of the oscillating elements. The test frequency for the test specimens varies from 120Hz to 140Hz. The mean load used for the EDWC test specimens was 15kN, while the mean load used for the EDWC, then shot peened specimens and the machined specimens was 25kN. These values were determined in Project 12/95[3] using a Goodman diagram (Figure 5.5). Any change in the mean stress would result in a change in the alternating stress amplitude used.

The four-point bend test is used so that the maximum strain occurs within the area of the central two points. Fatigue will initiate from this area and the corresponding stresses can be calculated. The results of the fatigue tests are shown in Figures 5.6 to 5.8. The values for the fatigue limits are based on reverse bending and can vary from results obtained from rotating bending tests.

Fig. 5.3 Amsler High Frequency Vibrophone Machine[3]

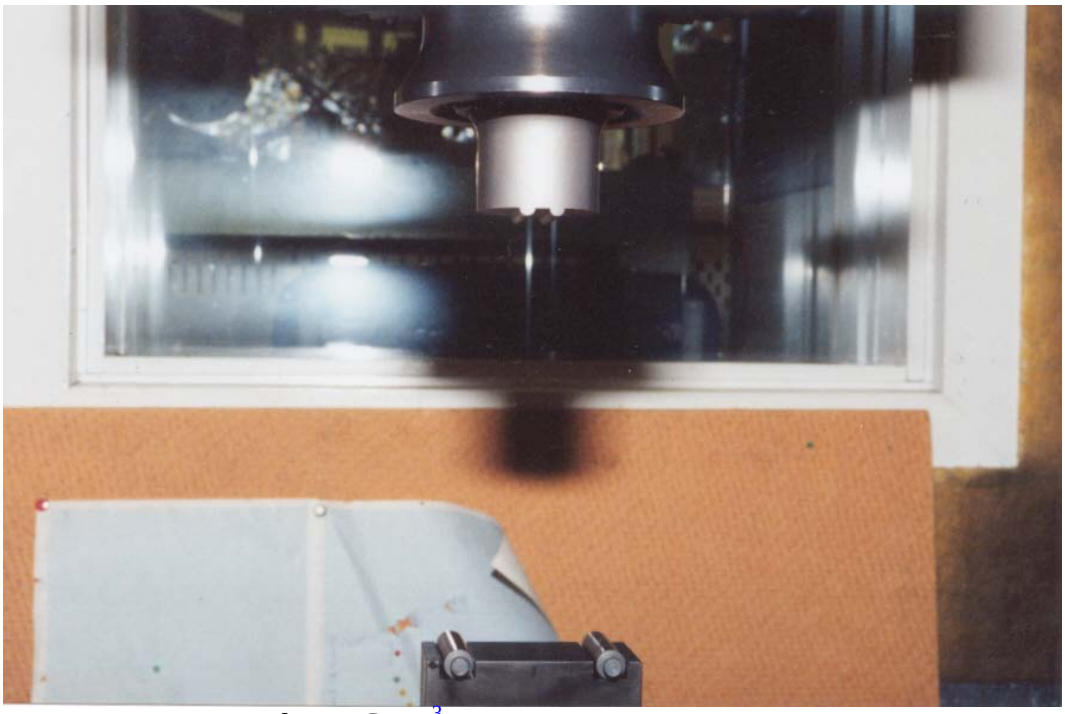

Fig. 5.4: 4-Point Bend Test Grips[3]

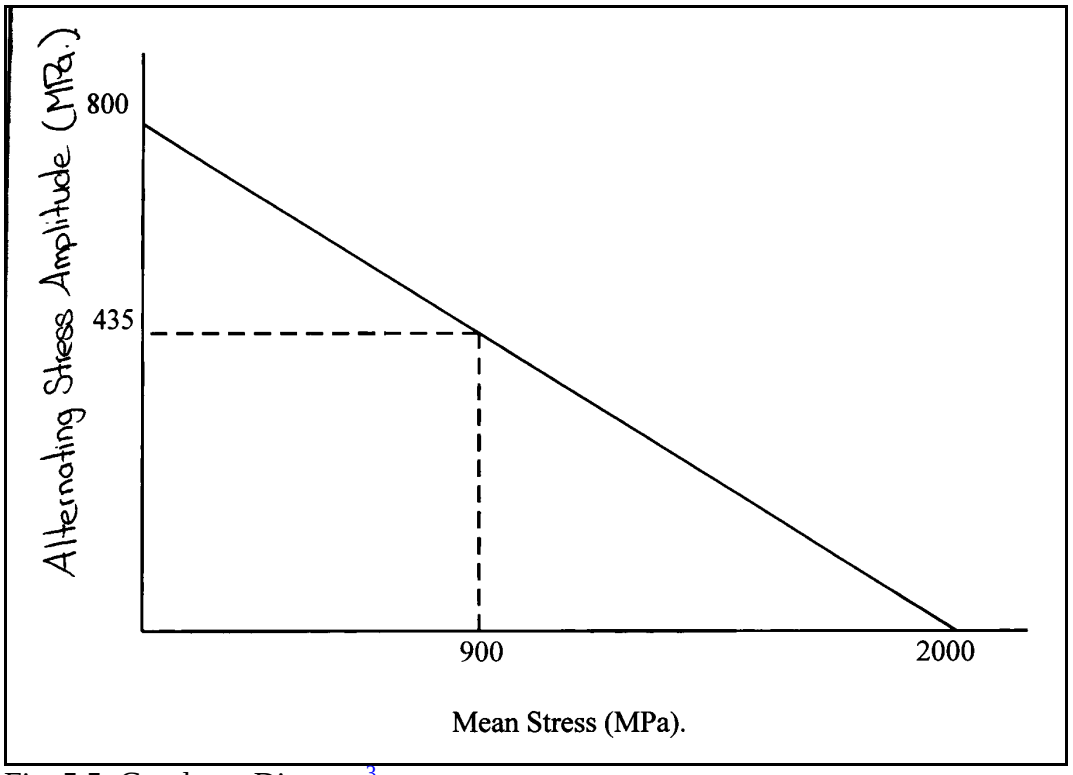

Fig. 5.5: Goodman Diagram[3]

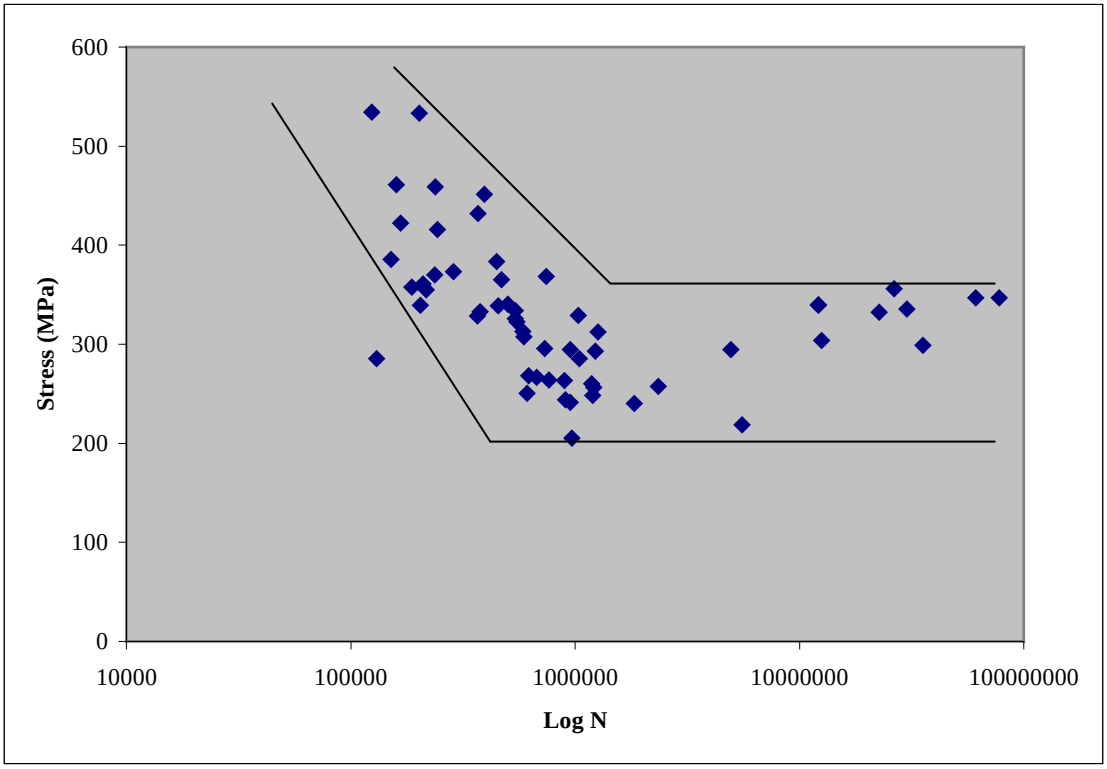

Fig. 5.6: S-N Graph for Rough EDWC Test Specimens

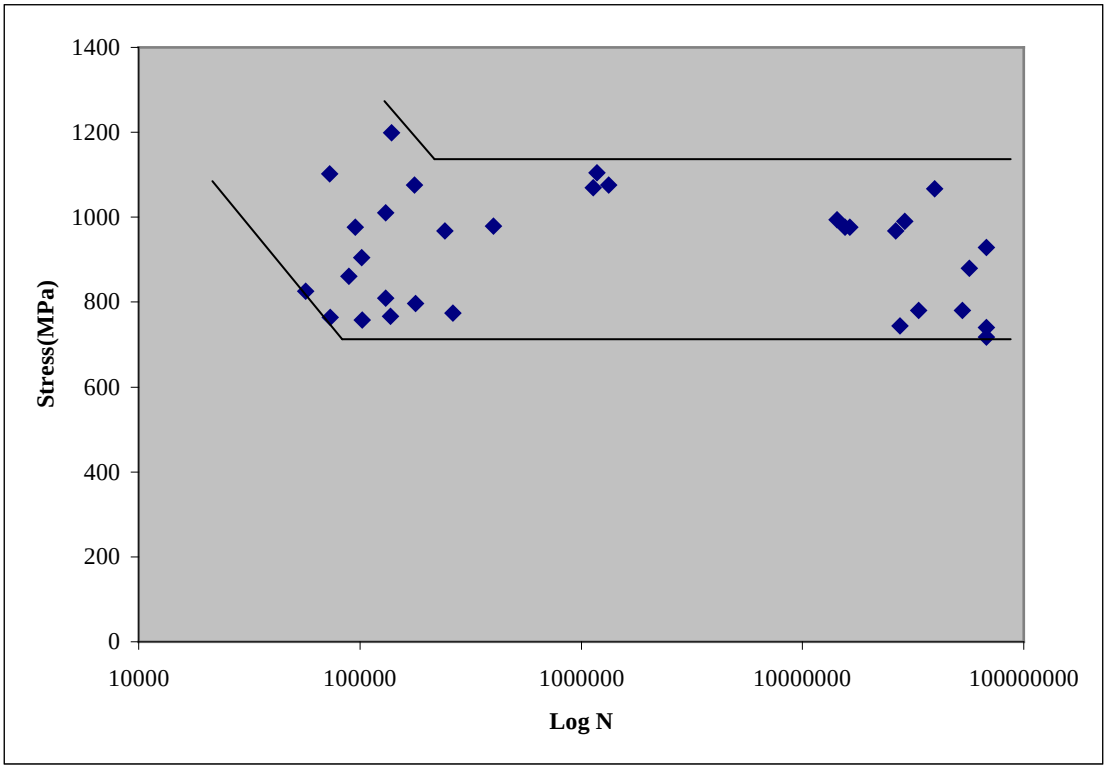

Fig. 5.7: S-N Graph for Rough EDWC and Shot Peened Test Specimens

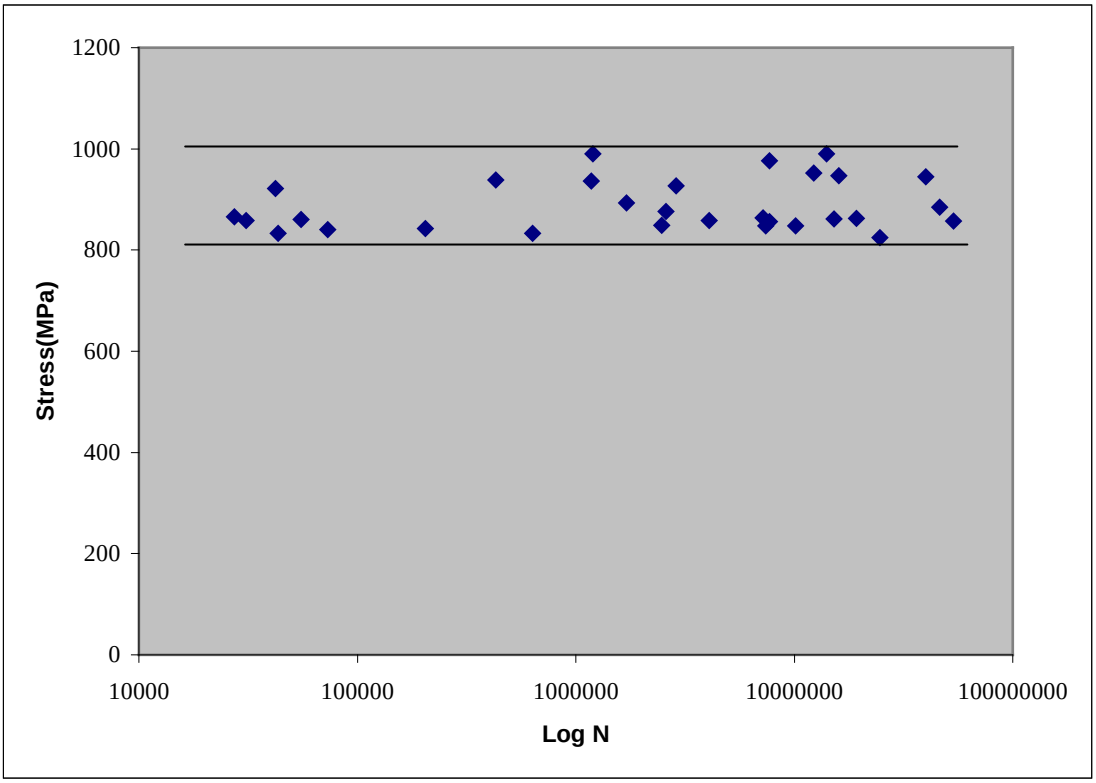

Fig. 5.8: S-N Graph for Machined Test Specimens

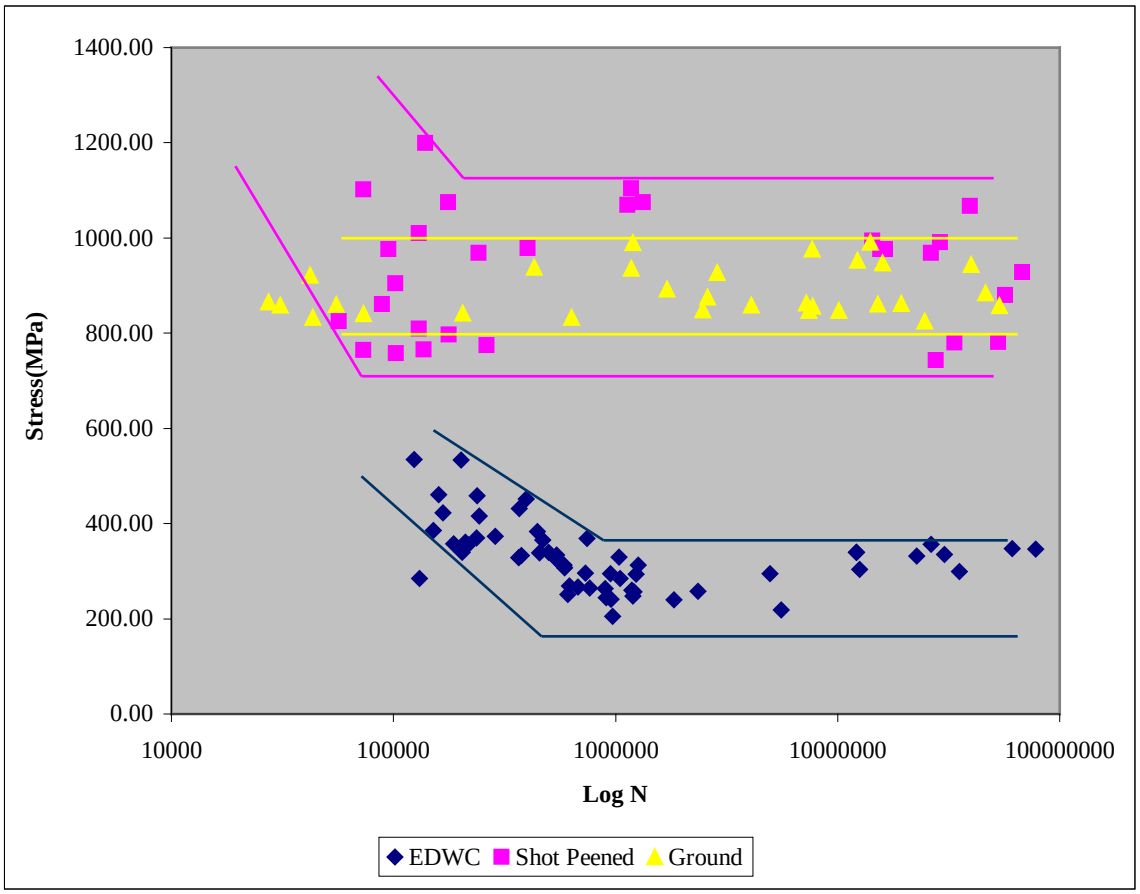

Fig. 5.9: S-N Graphs

The fatigue limits of the three sets of test specimens can be compared in Figure 5.9. The EDWC specimens show a fatigue limit of aproximately 200MPa to 350MPa. The EDWC specimens that have been shot peened have a fatigue limit of approximately 700MPa to 1100MPa. The ground specimens have a fatigue limit of 800MPa to 1000MPa. The scatter of data is observed to be much greater for the shot peened specimens than for the other specimens.

5.3 Scanning Electron Microscopic Examination

The fracture surfaces of the specimens were examined under the scanning electron microscope (SEM). The crack initiation sites for the specimens were

photographed. Figures 5.10 to 5.19 are examples of the crack initiation sites observed for each of the three sets of specimens.

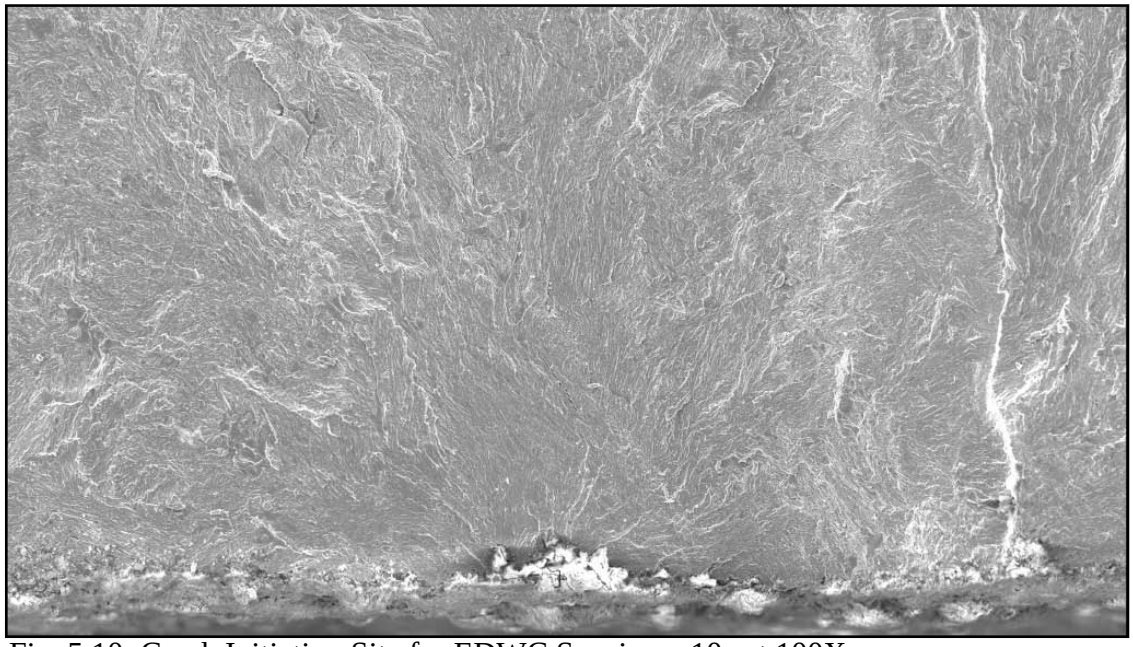

Fig. 5.10: Crack Initiation Site for EDWC Specimen 10a at 100X

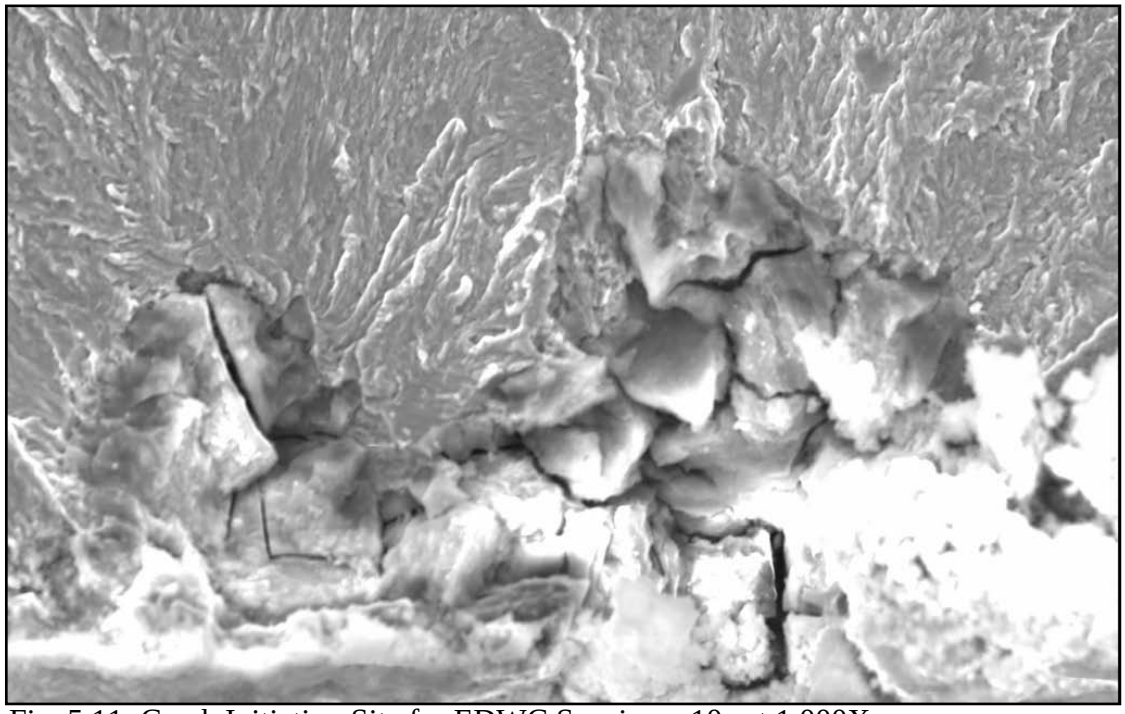

Fig. 5.11: Crack Initiation Site for EDWC Specimen 10a at 1,000X

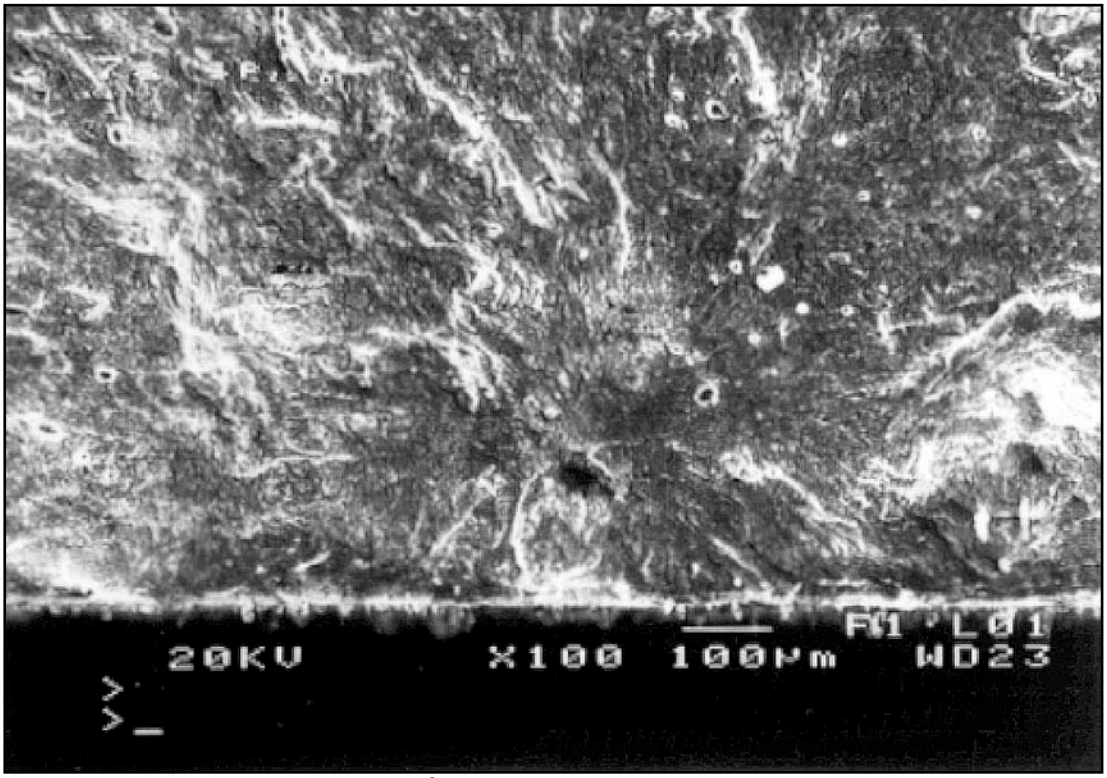

Fig. 5.12: Crack Initiation Site for Shot Peened Specimen 7a at 100X

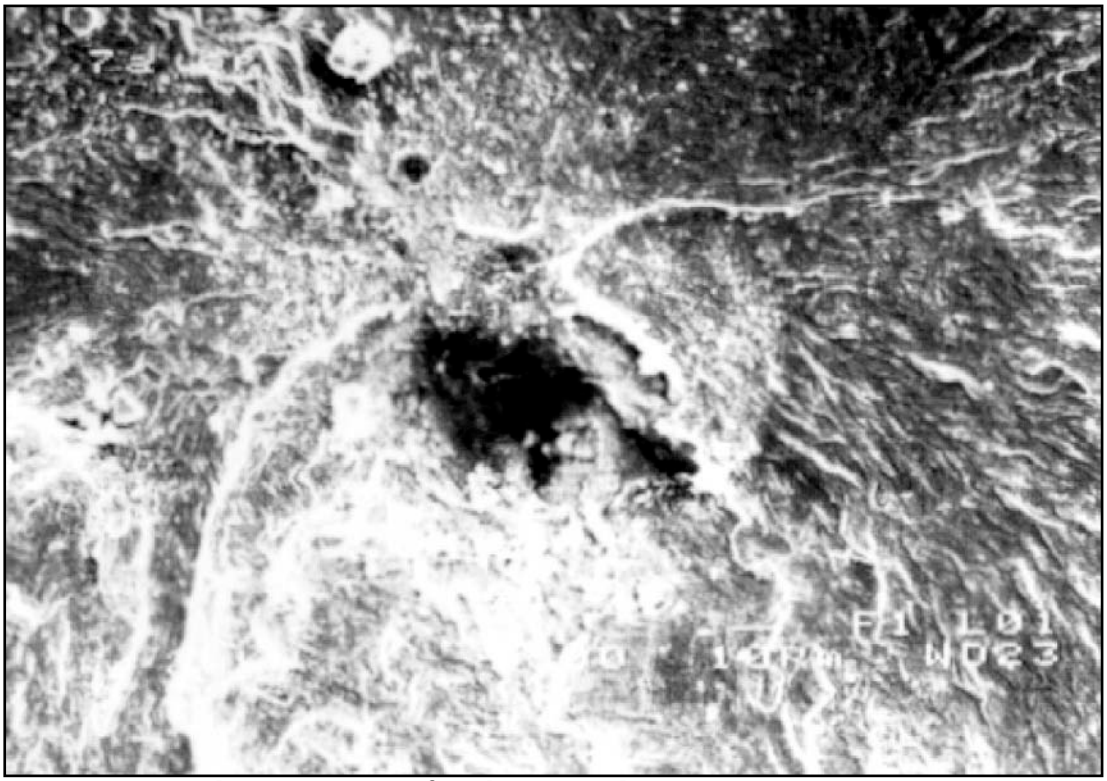

Fig. 5.13: Crack Initiation Site for Shot Peened Specimen 7a at 1,000X

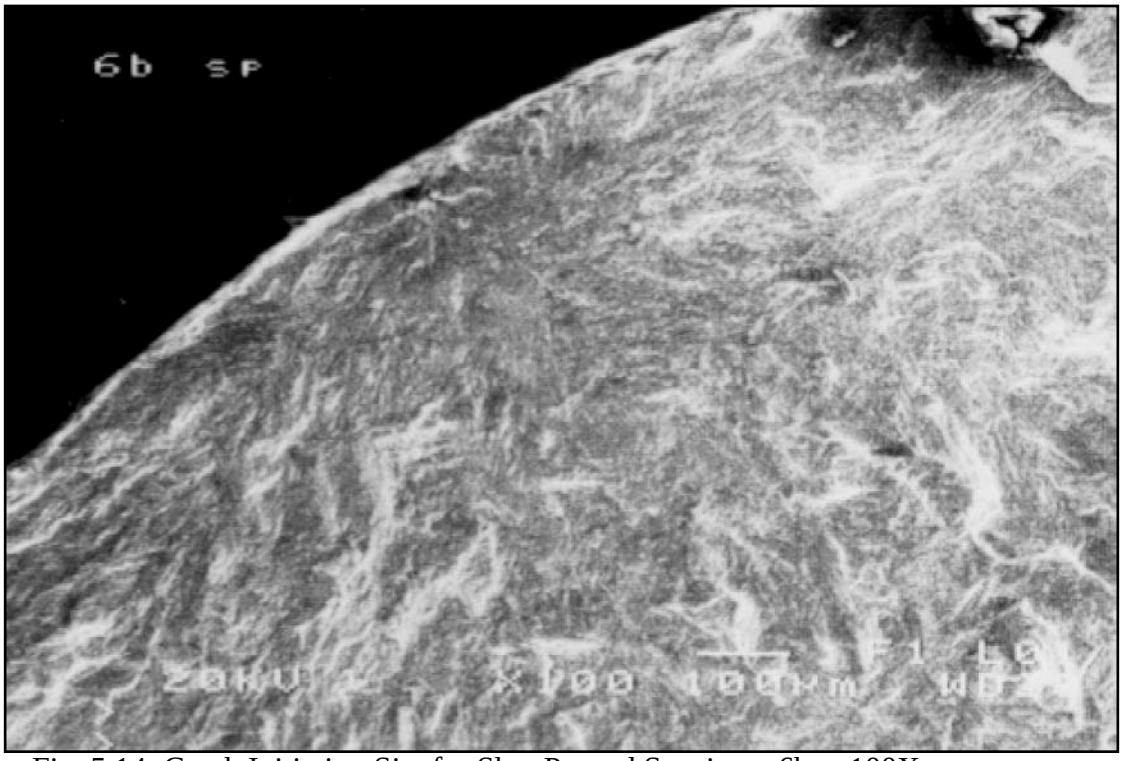

Fig. 5.14: Crack Initiation Site for Shot Peened Specimen 6b at 100X

Fig. 5.15: Crack Initiation Site for Shot Peened Specimen 6b at 500X

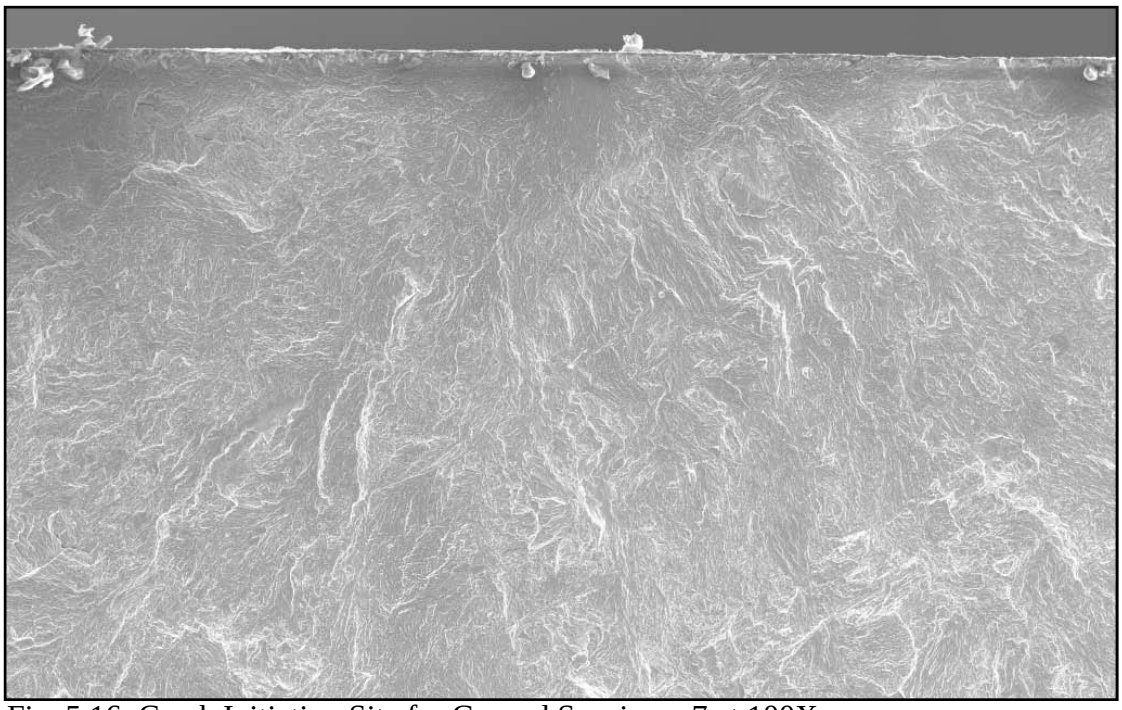

Fig. 5.16: Crack Initiation Site for Ground Specimen 7 at 100X

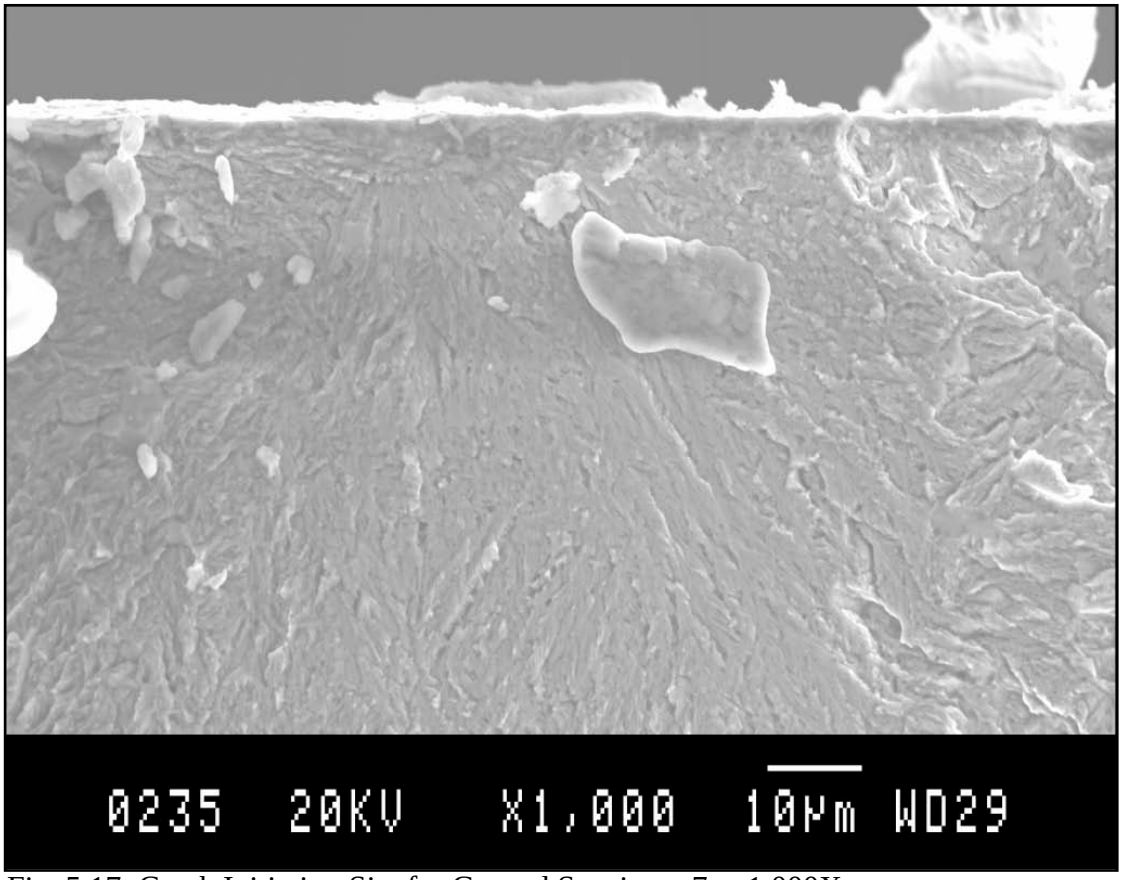

Fig. 5.17: Crack Initiation Site for Ground Specimen 7 at 1,000X

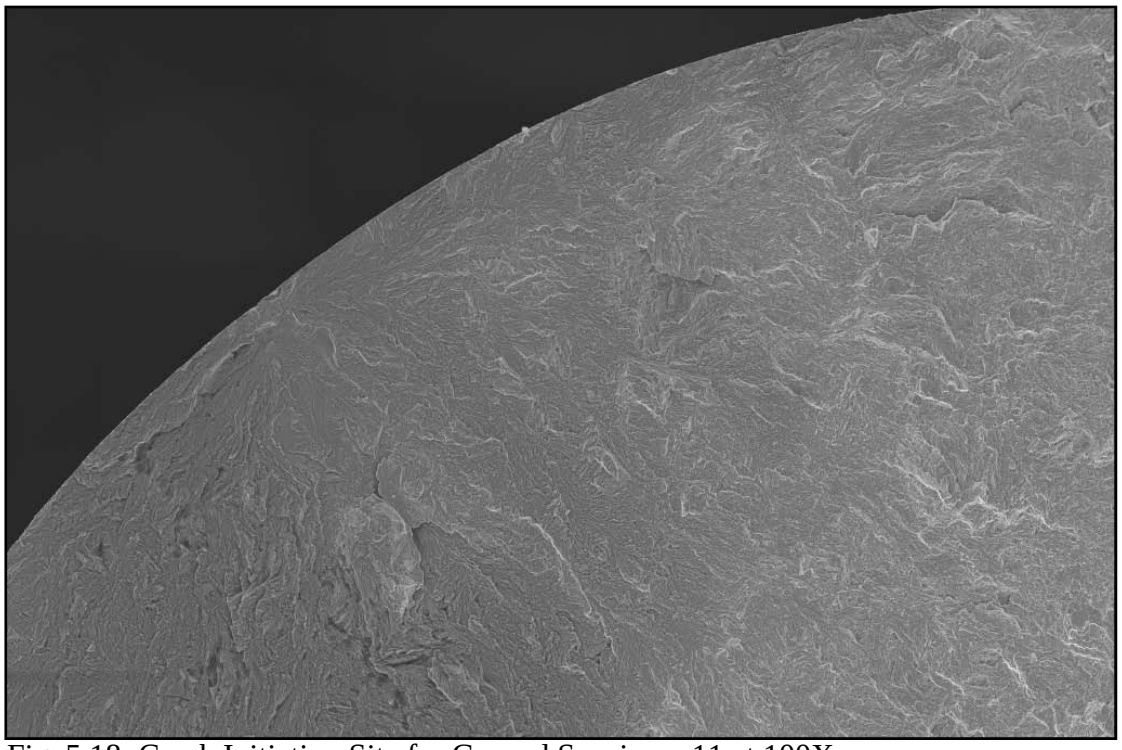

Fig. 5.18: Crack Initiation Site for Ground Specimen 11 at 100X

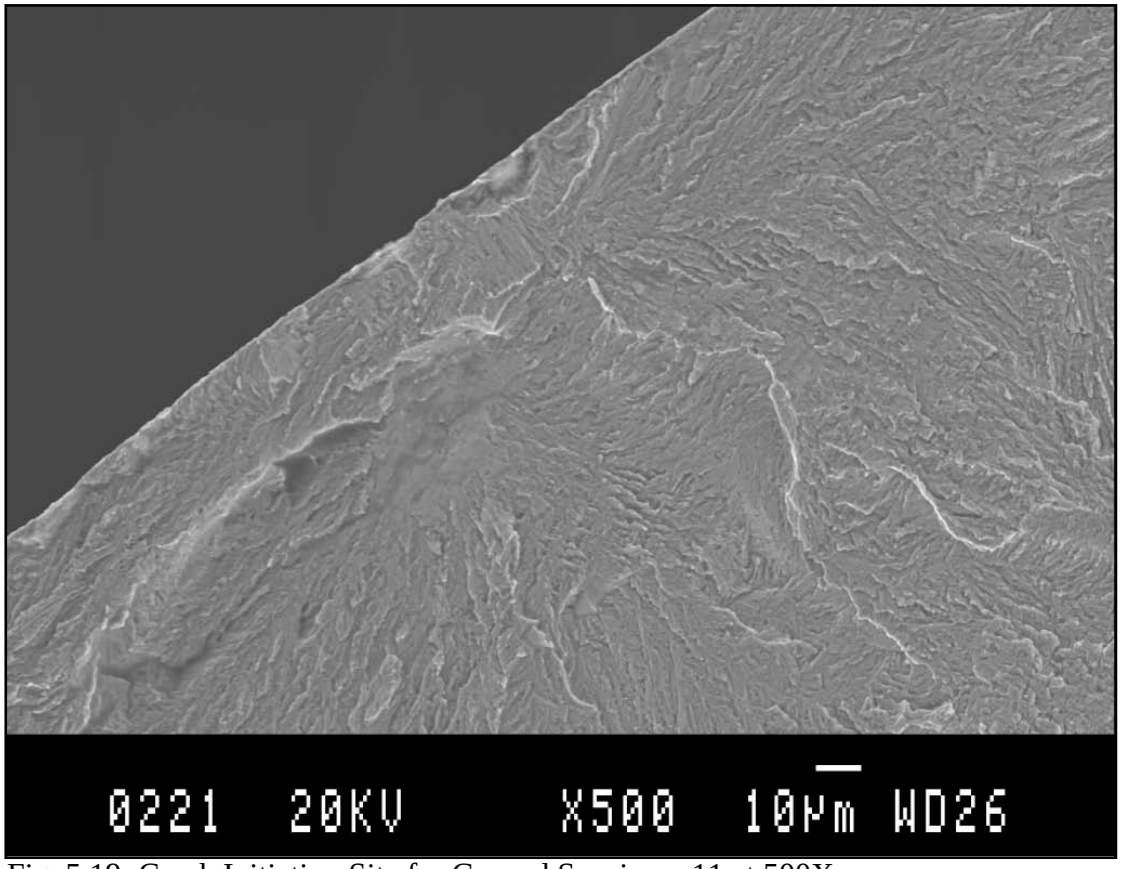

Fig. 5.19: Crack Initiation Site for Ground Specimen 11 at 500X

The SEM images show the different crack initiation sites for the three sets of specimens. The EDWC specimens are observed to initiate from the surface. The fatigue cracks can be seen to initiate from surface defects. The shot peened specimens exhibit a variety of possible crack initiation sites. There are a few sub-surface crack initiations, despite the fact that surface defects are present. Some specimens showed surface crack initiations. A few specimens exhibit cracks initiating from surface defects at the corners. The ground specimens generally display surface crack initiation sites. Cracks initiating from the corners were also observed for some ground samples.

The machined surfaces of the specimens were also examined under the SEM. Figures 5.20 to 5.22 are representative of the surfaces of the specimens.

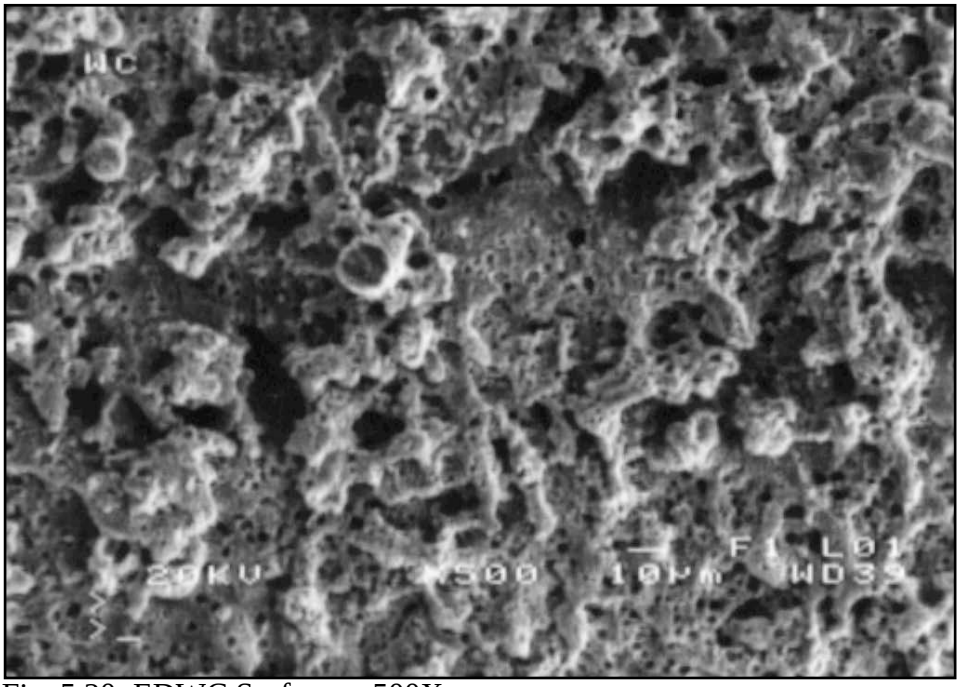

Fig. 5.20: EDWC Surface at 500X

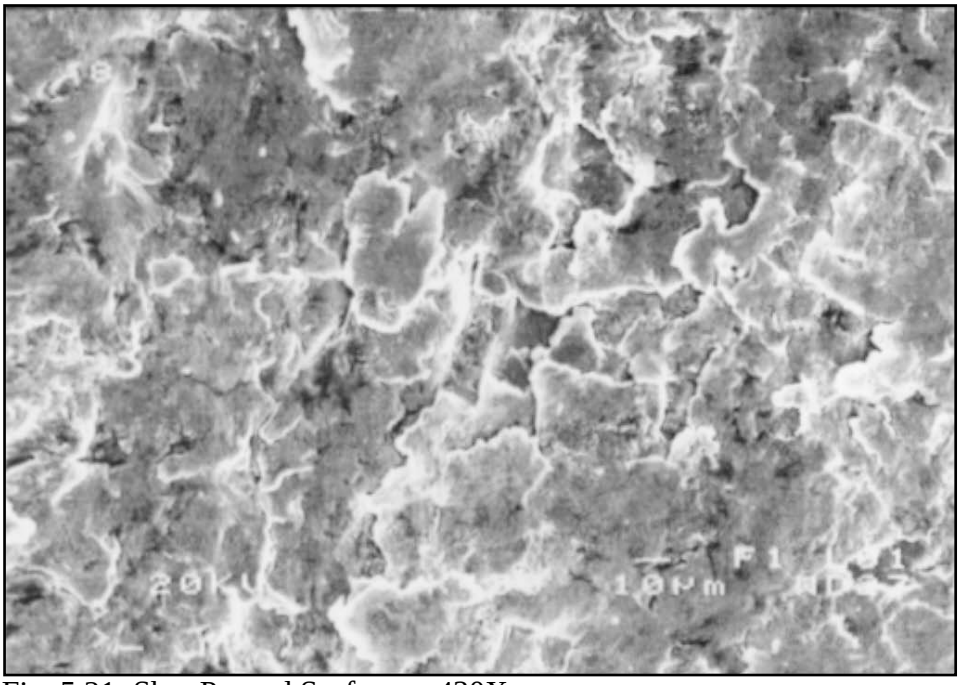

Fig. 5.21: Shot Peened Surface at 430X

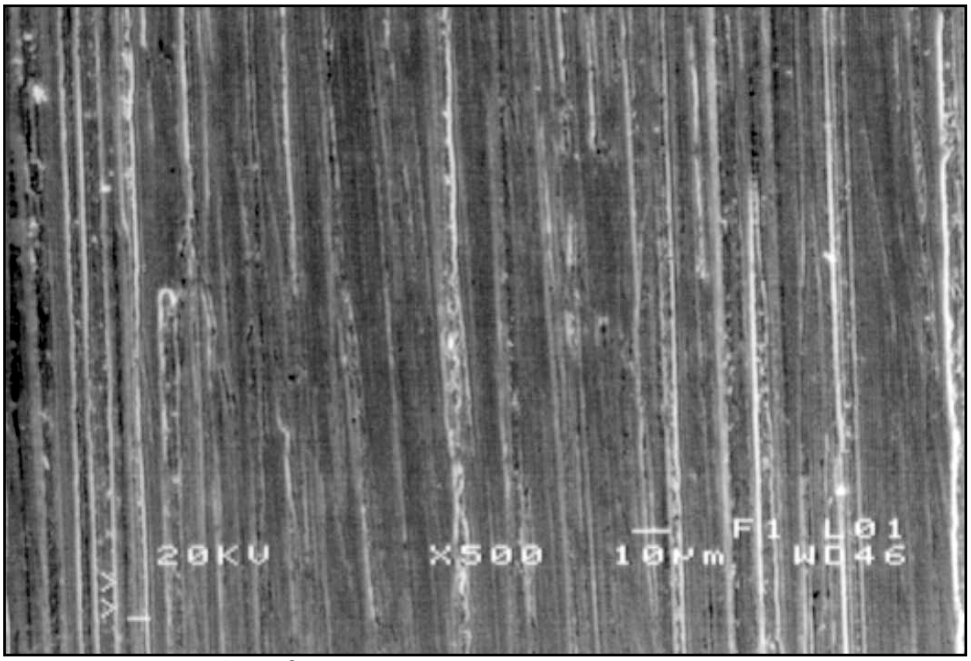

Fig. 5.22: Ground Surface at 500X

5.4 Microhardness

Microhardness testing was carried out on some specimens that were mounted and polished. The testing was done on a Leco M-400-H1 hardness testing machine that was fitted with a Knoop indenter. The resulting indentations produced by the Knoop indenter are shown in Figure 5.23.

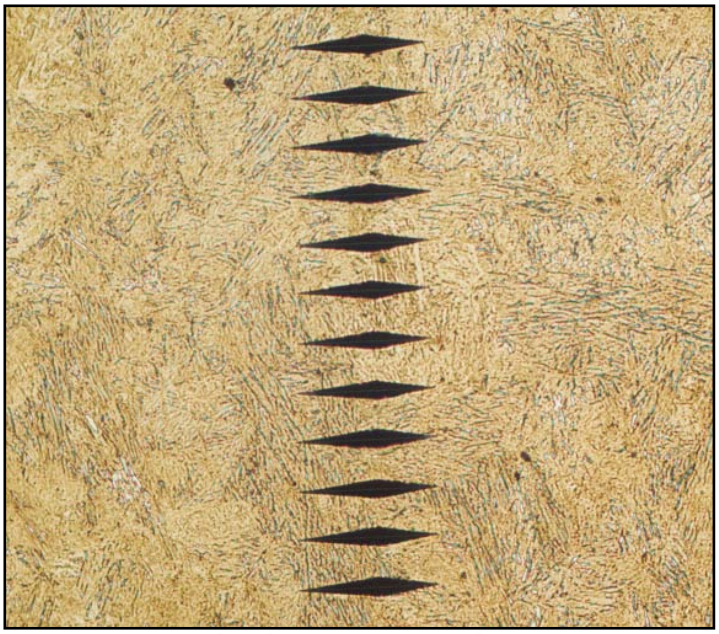

Fig. 5.23: Microhardness Testing Indentations

The load used for the microhardness testing was 200g. The indentations have been place 0.03mm apart to prevent interference due to the plastic deformation produced by the indentations. The width of the indentations have been measured and converted to R_c. Figure 5.21 show the results obtained for the specimens tested.

The microhardness values for the three different sets of specimens are shown in Figure 5.24. The curves are observed to be similar with a slight drop in hardness

at the edge of the specimens. The hardness of the specimens levels out at a depth of approximately 0.2mm. The hardness is found to be approximately $52R_c$.

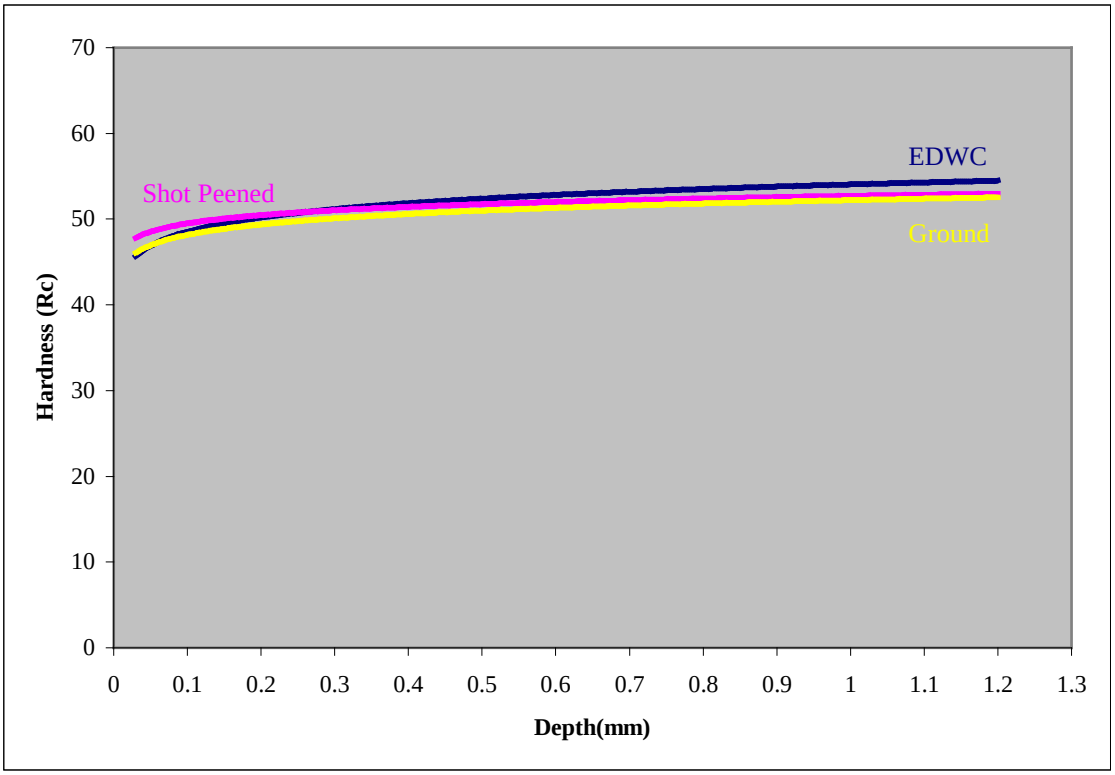

Fig. 5.24: Graph of Microhardness vs Specimen Depth

5.5 Surface Roughness

The surface roughness of the specimens was measured using a Rank Taylor-Hobson Talysurf 10 surface texture measuring instrument. Surface roughness was measured horizontally widthwise and lengthwise. The average values are shown in Table 5.2.

	Surface Roughness (μm R_a)	
	Length	Width
EDWC	3.19	3.23
Shot Peened	1.01	1.06
Ground	0.19	0.42

Table 5.2: Surface Roughness

The surface roughness of the EDWC specimens is approximately 3.2μm R_a, while the shot peened specimens have a surface roughness of 1μm R_a. There is little variation of surface roughness for both the EDWC specimens and the shot peened specimens, regardless of the direction of measurement. The surface roughness of the ground specimens is highly dependant on the direction of measurement. The surface roughness is approximately 0.4μm R_a when measured across the specimen, while it is 0.2μm R_a when measured along the specimen.

CHAPTER 6: DISCUSSION

6.1 Fatigue Test and SEM Analysis

The fatigue limit of polished 4340 steel specimens is 795MPa for air melted and 965MPa for vacuum arc remelted steel[94]. The fatigue testing of the ground specimens have shown a fatigue limit varying from 820MPa to 990MPa. An examination of the fracture surfaces using the SEM was carried out on all the specimens. Specimens with cracks that had initiated from the corners were included. On close examination, it was observed that the corner crack initiations all began at a surface defect. The surface defect could be a scratch that has been left by the polishing process, which acted as a stress concentration point, initiating cracking. An example is shown below.

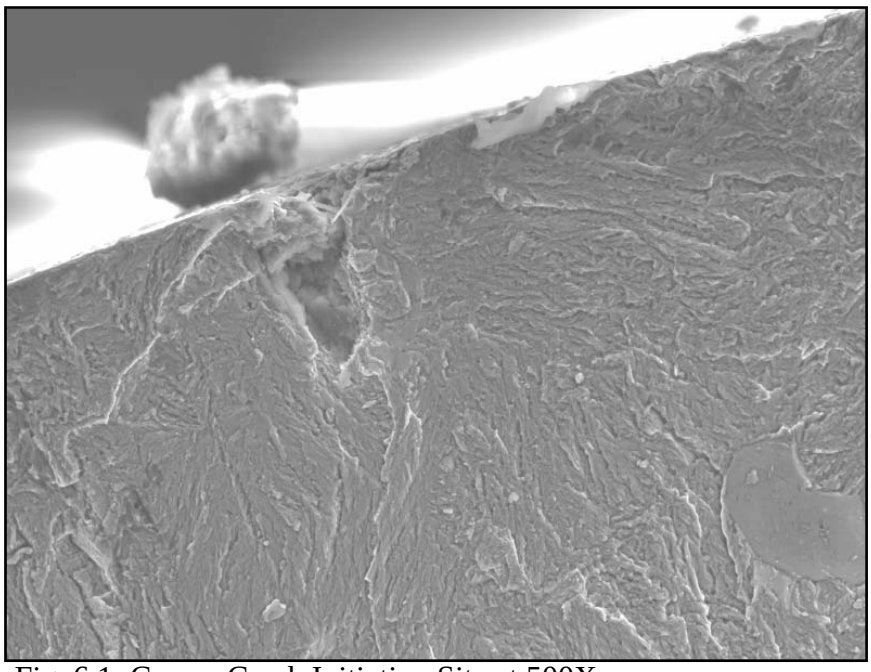

Fig. 6.1: Corner Crack Initiation Site at 500X

Those specimens that did not have corner crack initiation were observed to have surface crack initiations. Some cracks initiated from a surface defect.

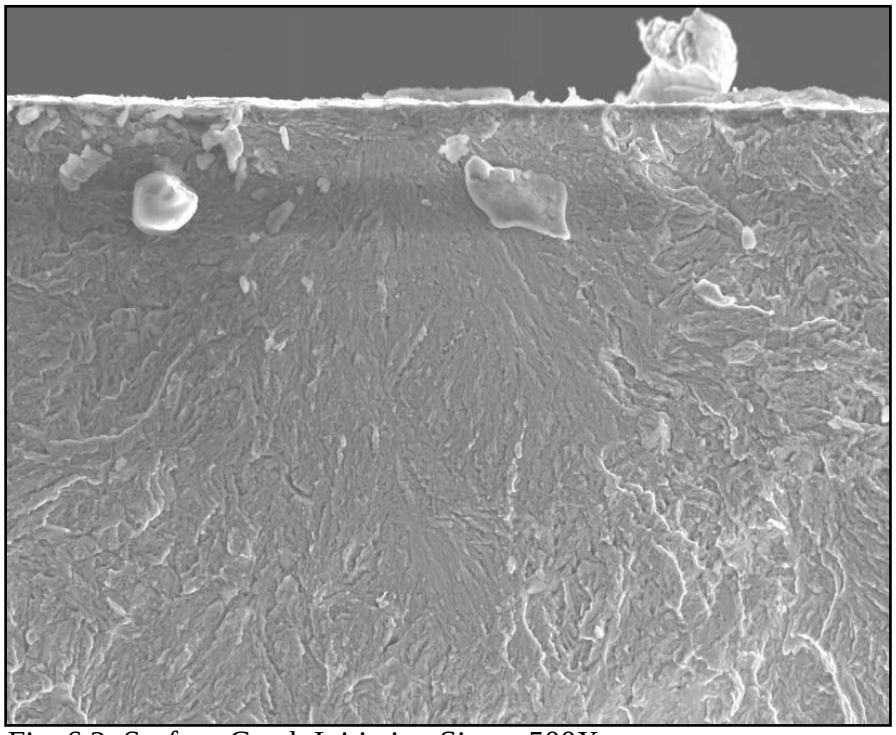

Fig. 6.2: Surface Crack Initiation Site at 500X

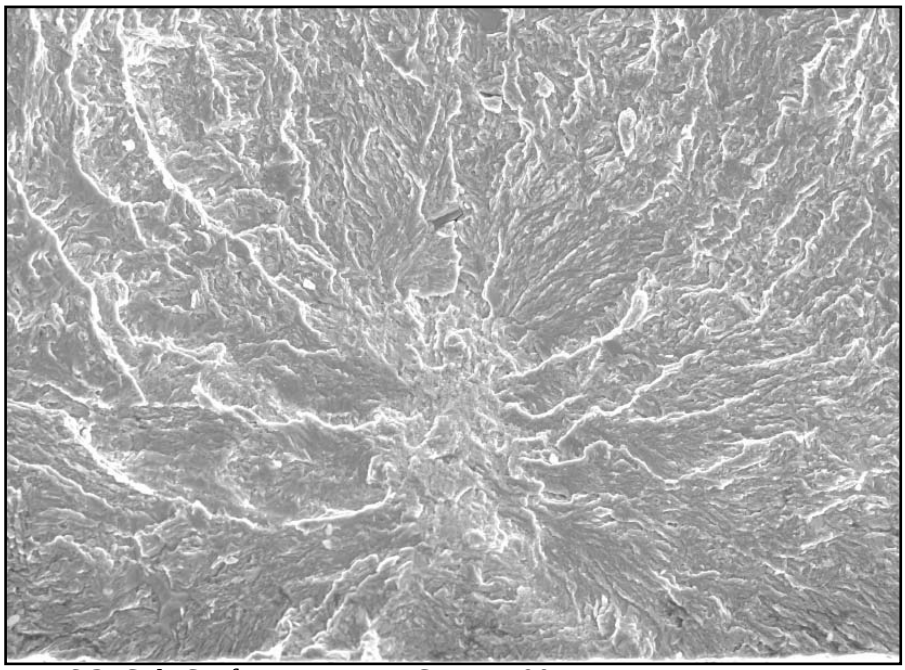

Fig. 6.3: Sub-Surface Initiation Site at 500X

Sub-surface initiation sites were observed in a few of the ground specimens. Figure 6.3 shows one such example. The mechanism by which the surface and sub-surface cracks had initiated is difficult to determine by SEM analysis alone.

The fatigue limit obtained for the EDWC specimens ranged from 200MPa to 350MPa. The scatter of data for these specimens was slightly less than that of the ground specimens. The lessening in scatter could be attributed to the reduced variation of crack initiation sites for the EDWC specimens. The SEM analysis showed that for all non-corner crack initiation specimens, there was a single site from where the cracks initiated. These sites were surface defects that were produced by the EDWC process.

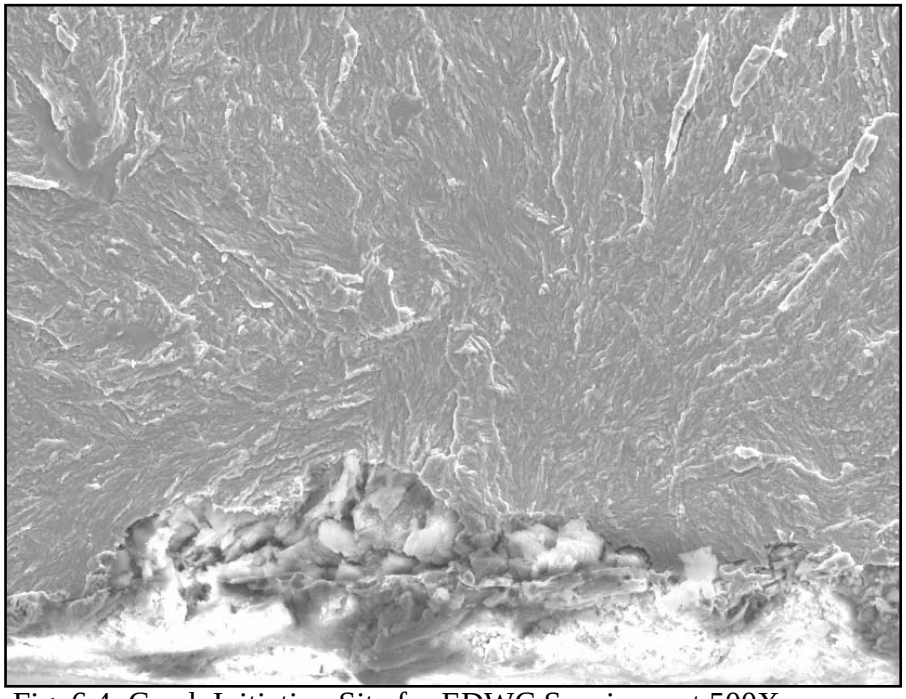

Fig. 6.4: Crack Initiation Site for EDWC Specimen at 500X

The value of the fatigue limit obtained for EDWC specimens shows that the EDWC process causes degradation in the fatigue properties of the specimens. There are three possible factors that contribute to this degradation:

I. Surface topography

II. Phase changes in the surface layer

III. Residual tensile stresses

Surface topography includes the surface roughness and all other surface features. The EDWC process produced a surface finish inferior to that of ground specimens. From the testing using the Talysurf, the surface roughness of EDWC specimens was 3.2μm R_a, while the surface roughness of ground specimens was an average of 0.2μm R_a to 0.3μm R_a. On a smooth surface, cyclic deformation occurs to produce roughening of the surface. These irregularities can then act as crack initiation sites. EDWC specimens are already "rough", thus no cyclic deformation is required. The SEM examination of the machined surface shows the presence of several surface defects (Figure 6.5).

The EDWC process produces a surface that is covered with craters. The material that had been vaporized and not removed by the dielectric fluid re-solidifies on the surface, producing an uneven surface that is full of holes. There are also many microcracks that are present extending from the surface of the specimen into the bulk material.

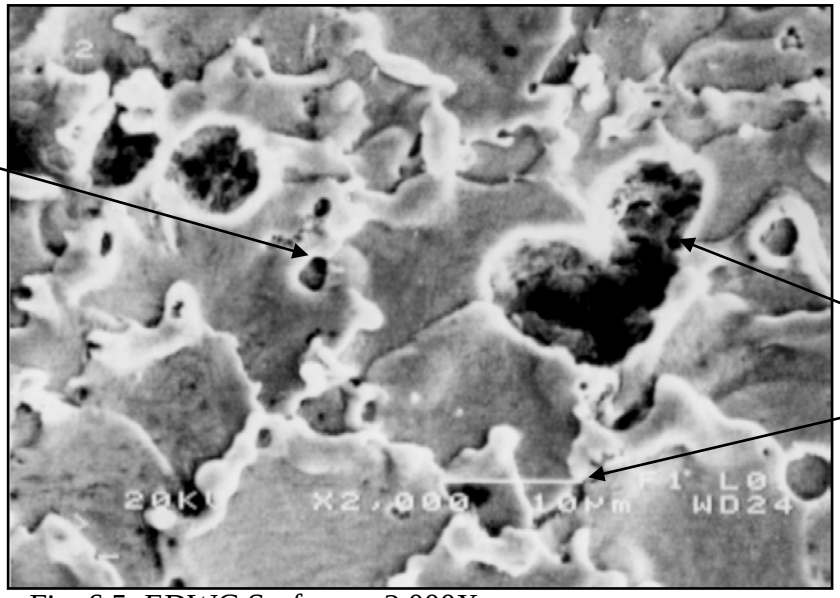

Fig. 6.5: EDWC Surface at 2,000X

An examination of an EDWC specimen through an optical microscope (Figure 6.6) shows that there are many cracks present. The surface of the specimen is very uneven with protruding areas. These protrusions are examples of sites that can act as stress concentrations; initiating fatigue cracks at lower stresses.

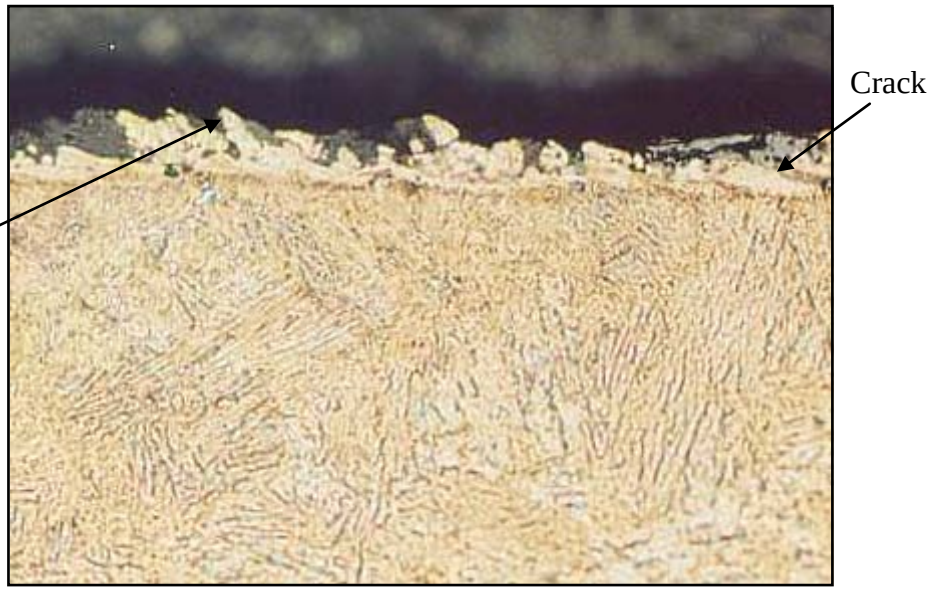

Fig. 6.6: EDWC Specimen at 230X

Equation (1) states that the total fatigue life is equal to the sum of the crack initiation life and the crack propagation life. The presence of the cracks implies that the crack initiation life is nil. Fatigue cracks can easily propagate from the existing cracks. The crack initiation life is totally eliminated, reducing the total fatigue life to be equivalent to the crack propagation life.

A phase change in the surface layer can lead to a reduction in the total fatigue life. Figure 6.6 shows that the surface layer of the specimen had a different colour to that of the bulk material. The lighter colour indicates the recast layer. The recast layer contains many defects and is more brittle than the bulk material[1]. Below the recast layer is the heat-affected zone. In 4340 steel, the heat-affected zone cannot be easily distinguished from the parent material, as there is no phase change. As mentioned above, there are many cracks that extend through the recast layer, which makes the structure of the recast layer irrelevant to crack initiation.

EDWC produces a residual tensile stress on the surface of the specimen[69]. This residual stress is due to the heating and cooling of the surface during the EDWC process. A residual stress on the surface of a specimen changes the mean stress that is applied on the specimen during fatigue. As the residual stress is tensile, the mean tensile stress that is applied on the specimen is increased. This increased mean tensile stress allows crack initiation and propagation to occur much more easily. Smaller stress amplitudes produce the same fatigue life as a specimen that has a lower mean tensile stress applied[64,66,69,70].

Shot peening after the EDWC process affected the fatigue limit of the specimen. The fatigue limit of specimens that had been shot peened after the EDWC process ranged from 700MPa to 1100MPa. The scatter of data for these specimens was considerable. The large variation in the data can be linked to crack initiation in these specimens. The SEM examination of the fracture surfaces showed cracks initiating from several different types of initiation sites.

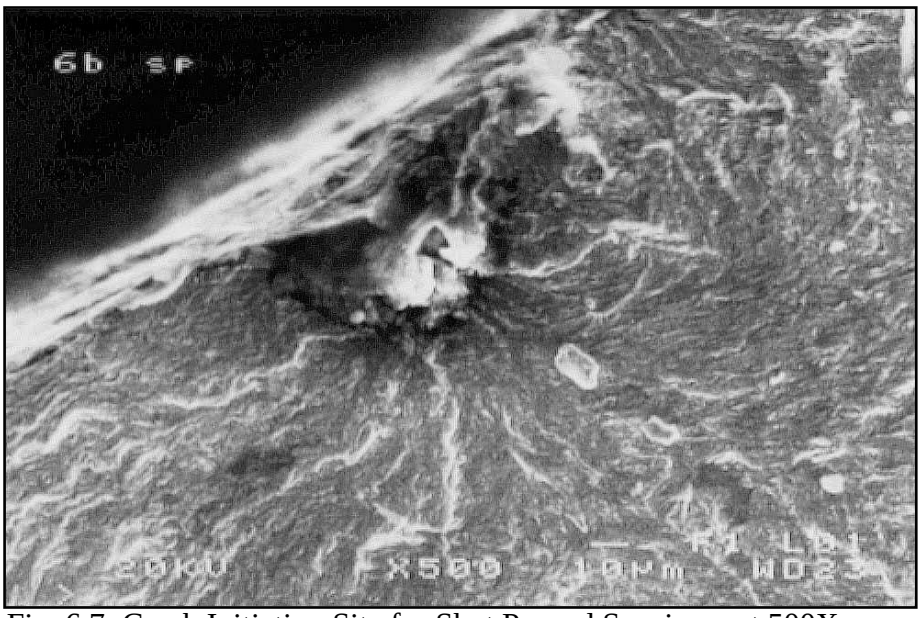

Fig. 6.7: Crack Initiation Site for Shot Peened Specimen at 500X

Figure 6.7 shows a corner crack initiation site. Shot peened specimens with corner crack initiations had the cracks initiating from a surface defect. A dark semi-circular area was observed around the crack initiation site.

Figure 6.8 shows a surface crack initiation site. This surface initiation site has its origins in a surface defect. Only a few of the shot peened specimens had cracks that initiated in this manner. These specimens gave the lowest fatigue life values. A slightly darker area was also present around the crack initiation site.

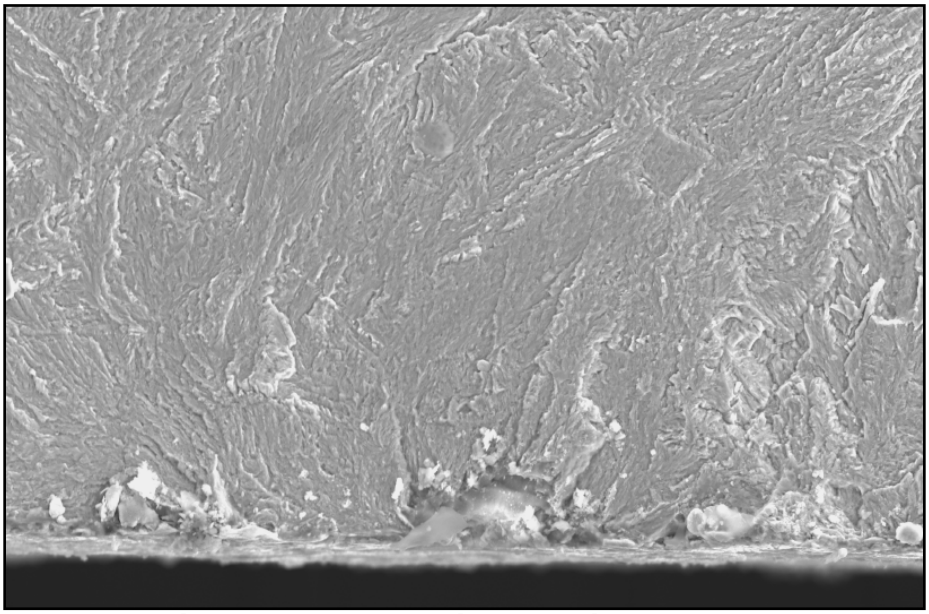

Fig. 6.8: Crack Initiation Site For Shot Peened Specimen at 500X

Another surface crack initiation site is observed in Figure 6.9. Although surface defects are present, the fatigue crack initiated from the free surface instead of from a surface defect. There is also a darker area that is observed to surround the crack initiation site.

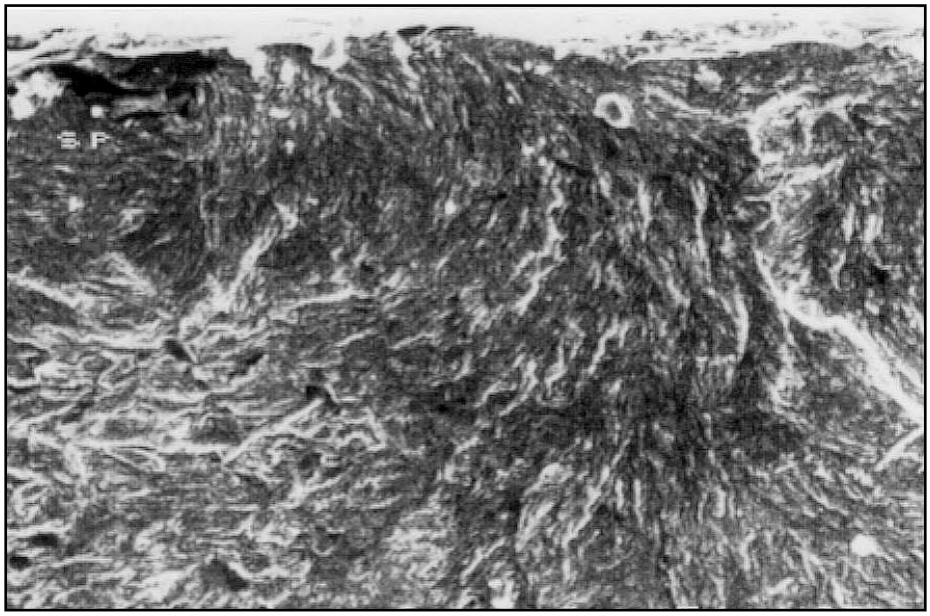

Fig. 6.9: Crack Initiation Site For Shot Peened Specimen at 500X

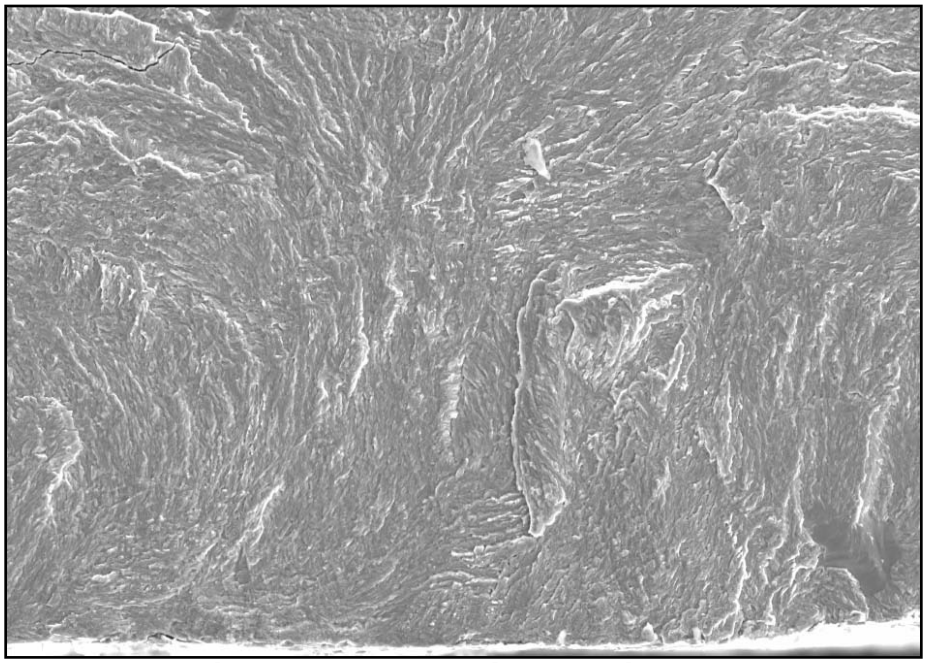

Fig. 6.10: Crack Initiation Site For Shot Peened Specimen at 500X

Sub-surface crack initiation sites were also observed. Some sub-surface initiations sites initiated from sub-surface defects, such as cracks and inclusions. Figure 6.10 shows a sub-surface initiation site that did not initiate from a defect.

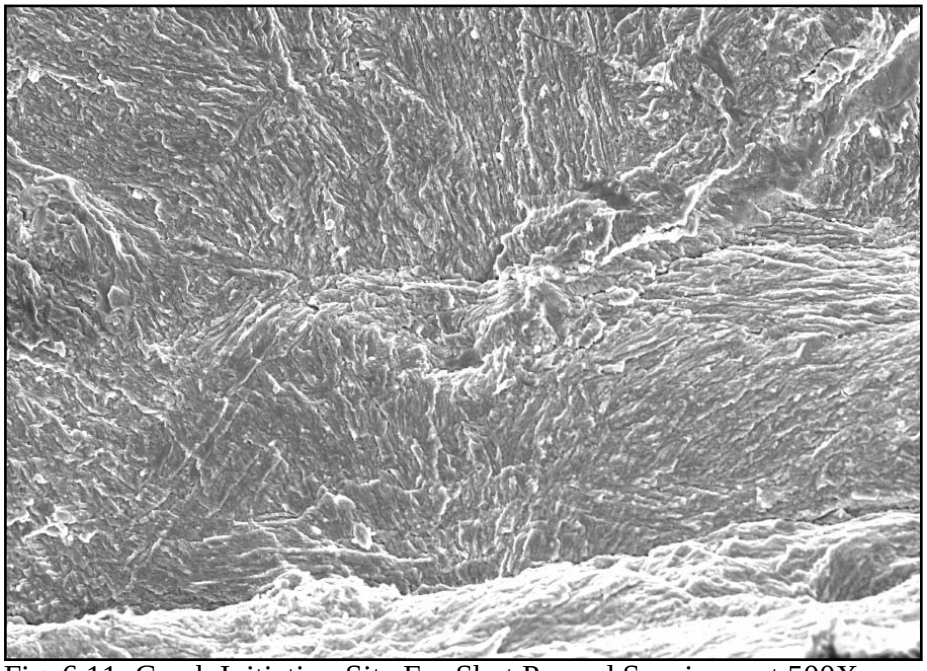

Fig. 6.11: Crack Initiation Site For Shot Peened Specimen at 500X

The most commonly observed crack initiation sites were found to be sub-surface initiation sites with a sharp lip present (Figure 6.11). The angle of the lip made it difficult to determine the role that the lip plays in crack initiation. The lip could be due to the brittleness of the recast layer. After initiation, the crack propagates away from the initiation site. The stress that is applied could have resulted in a sudden fracture of the recast layer. A dark semi-circular area is again observed around the crack initiation site.

The increase in fatigue limit indicates that shot peening restores the fatigue life that is lost through the EDWC process. Some of the three factors that lead to the degradation of fatigue life for EDWC specimens are modified by the shot peening process.

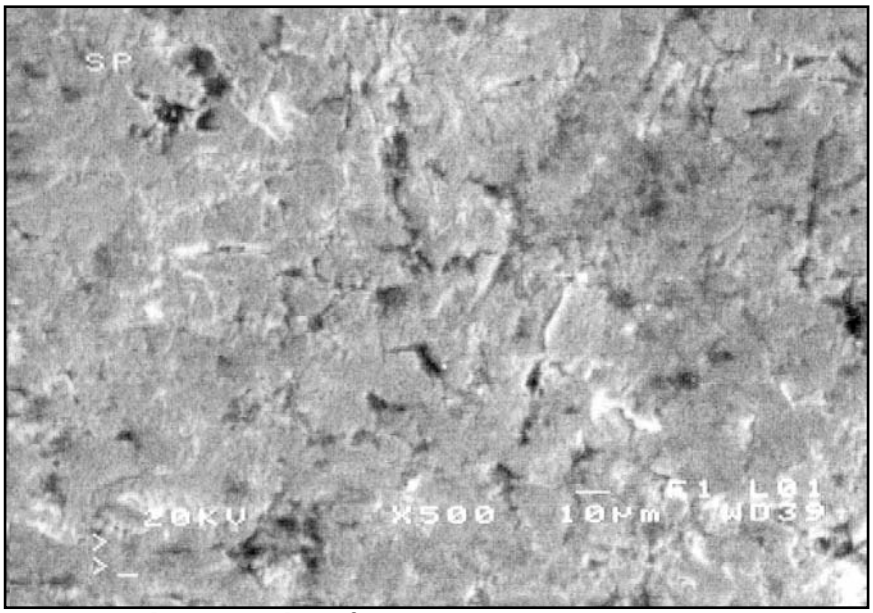

Fig. 6.12: Shot Peened Surface at 500X

The surface roughness of the shot peened specimens is approximately 1μm R_a. This value is less than that of EDWC specimens. The SEM examination of the shot peened surface displayed a flattened surface (Figure 6.12).

During the shot peening process, particles impact the surface of the specimen. The numerous "protruding" areas on an EDWC specimen surface are subsequently flattened by the impacting particles, thus producing a "squashed" appearance. The flattening of the surface is equivalent to a decrease in the measured roughness of the surface. The cracks are, however, still present (Figure 6.13).

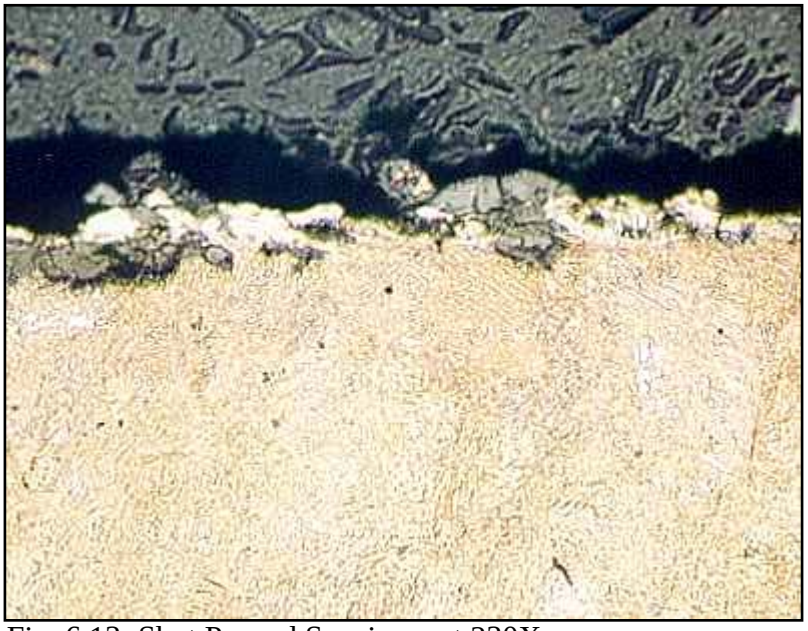

Fig. 6.13: Shot Peened Specimen at 230X

A phase change in the surface layer was not observed visually. Moreover, as discussed above, the presence of cracks in the recast layer would cause the structure of the recast layer to be irrelevant to crack initiation and propagation.

Residual tensile stresses brought about by the EDWC process are removed by shot peening. Residual compressive stresses are introduced into the surface layers of specimens. Figure 6.14 shows a representation of the stresses present in a specimen that has been shot peened.

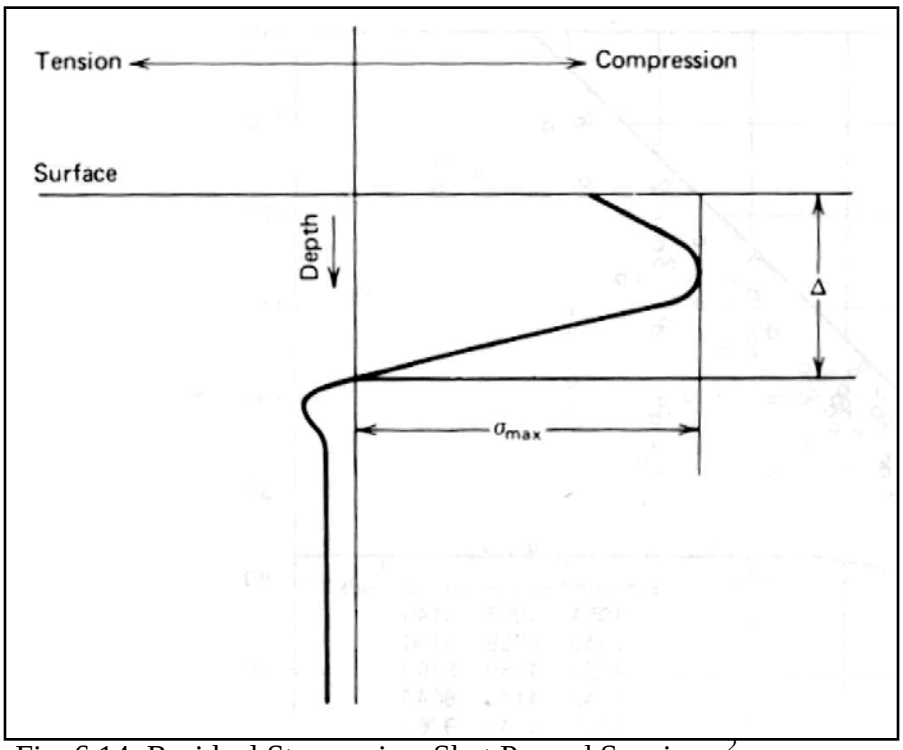

Fig. 6.14: Residual Stresses in a Shot Peened Specimen[2]

Theory suggests that a residual compressive stress reduces the mean tensile stress applied to the specimen. This reduction indicates that higher stress amplitudes can be applied to the specimen before a fatigue crack initiates, thus increasing the fatigue limit of the specimen. In normal static loading, tensile stresses do not develop on the surface until the residual compressive stresses have been overcome; therefore the allowable stress level is increased.

Residual compressive stress also affects the propagation rates of fatigue cracks. A sufficient degree of tensile stress is required for the cracks to propagate. Residual compressive stress reduces the tensile stress applied, leading to a decrease in crack propagation rates. This effect has been described in literature[51] and can be seen as a dark area around the crack initiation site. Within the dark area, crack propagation rates are reduced, while outside the dark area, propagation rates accelerate.

Residual compressive stresses are also observed to alter the site of crack initiation from the surface of the material to the subsurface[50,51]. As mentioned above, many sub-surface initiation sites had been observed for the shot peened specimens.

6.2 Microhardness Test

The results obtained for the microhardness tests indicate that the specimens display a lower hardness closer to the surface. The hardness increases with depth and levels out at approximately $52R_c$. Theoretically, the hardness of the EDWC specimens and the shot peened specimens should show an increased hardness closer to the surface. The results have indicated otherwise. Similarly, in work by Fordham et al[95] and Project 83/95[63], the hardness of EDWC specimens was noted as showing a similar drop near the surface.

The EDWC specimens have a recast layer and a heat-affected zone that should have caused an increase in the hardness of the surface layer. The microhardness

measurements were taken at a minimum of 0.03mm from the surface. It is likely that if the recast layer is thinner than 0.03mm, the hardness of the recast layer is not registered on the microhardness tests[95]. Similarly, the heat-affected zone can be too narrow. Of the available analysis methods, the thickness of the heat-affected zone can only be determined by microhardness testing. The thickness of the heat-affected zone is thus assumed to be too narrow to be picked up by the microhardness testing.

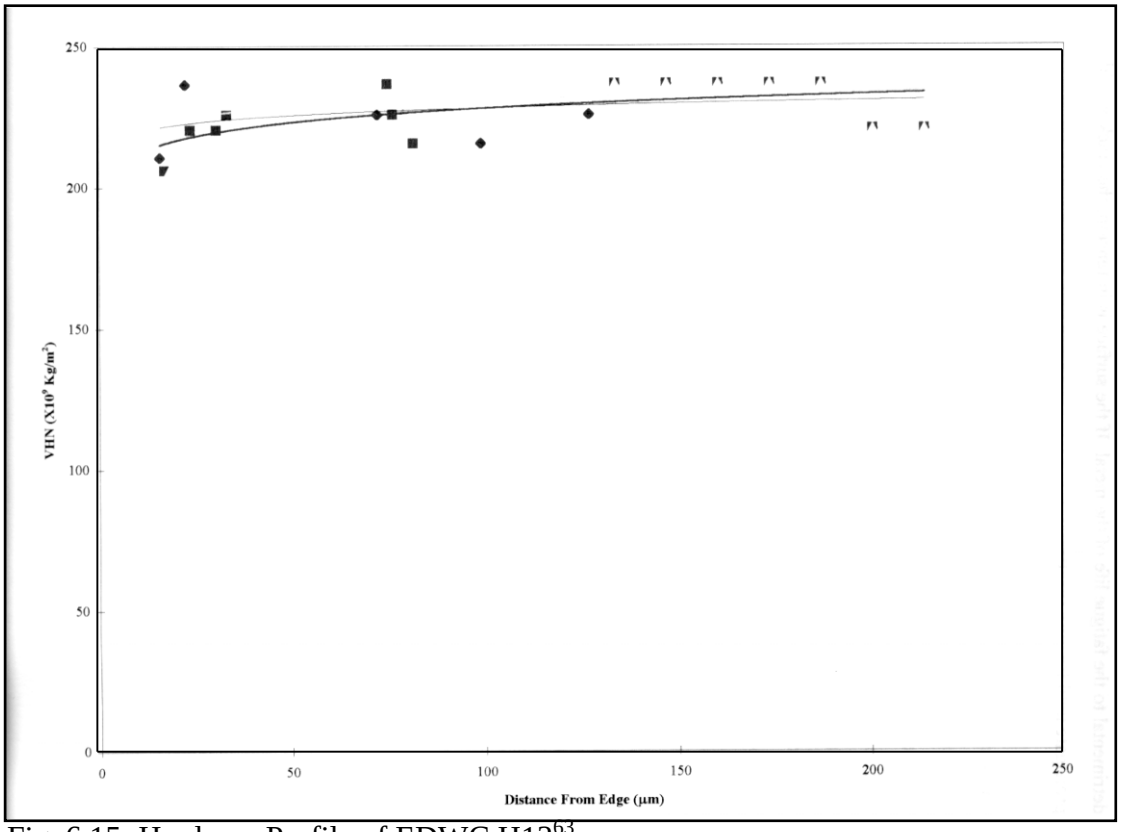

Fig. 6.15: Hardness Profile of EDWC H13[63]

Shot peened specimens also display a hardness profile similar to that of EDWC specimens. There is a lower hardness near the surface. Due to the presence of a residual compressive stress, an increase in the hardness near the surface is

expected. Shot peening a specimen to 0.10A gives a residual compressive depth of 0.15mm (Figure 6.16).

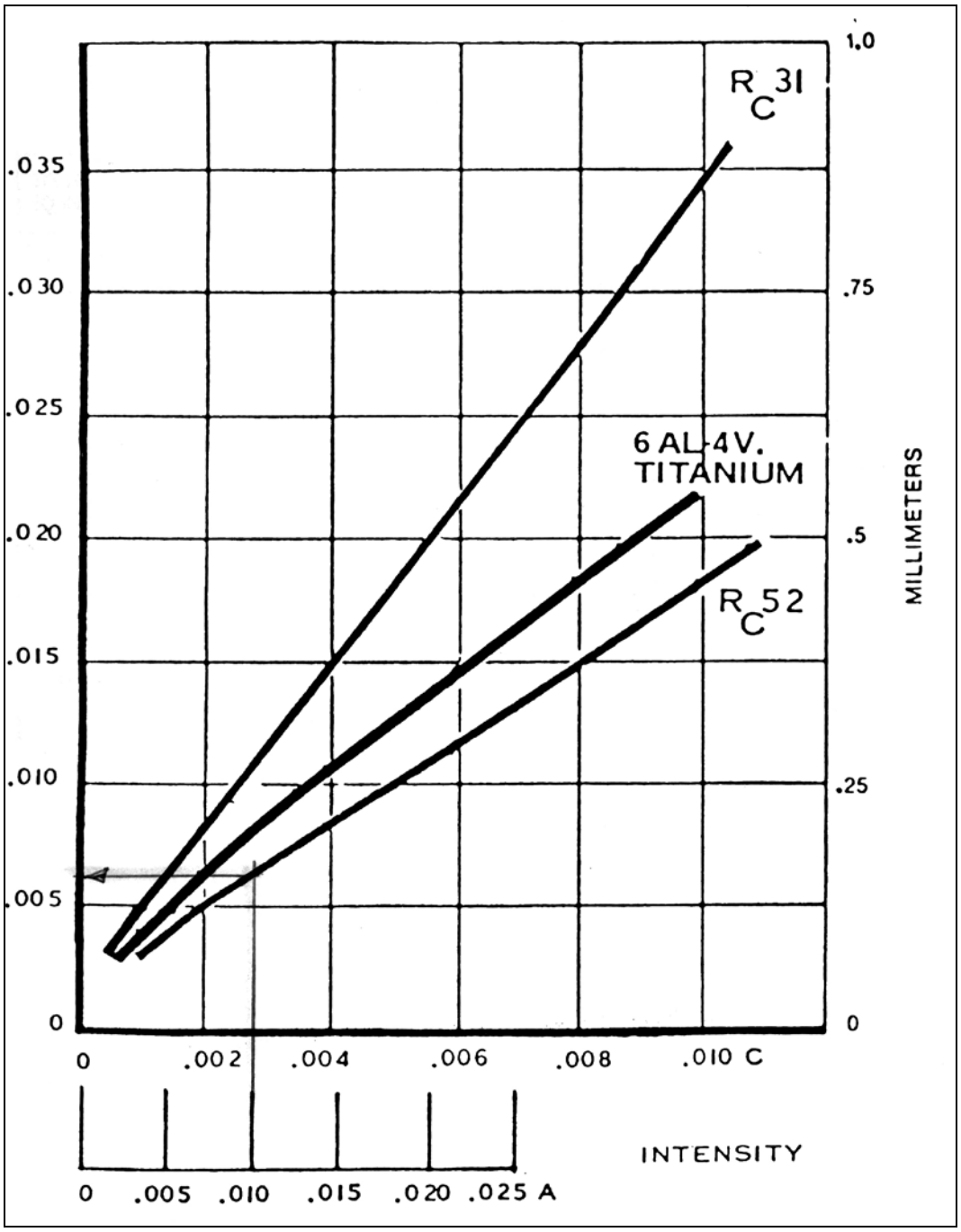

Fig. 6.16: Depth of Compression vs Almen Arc Height

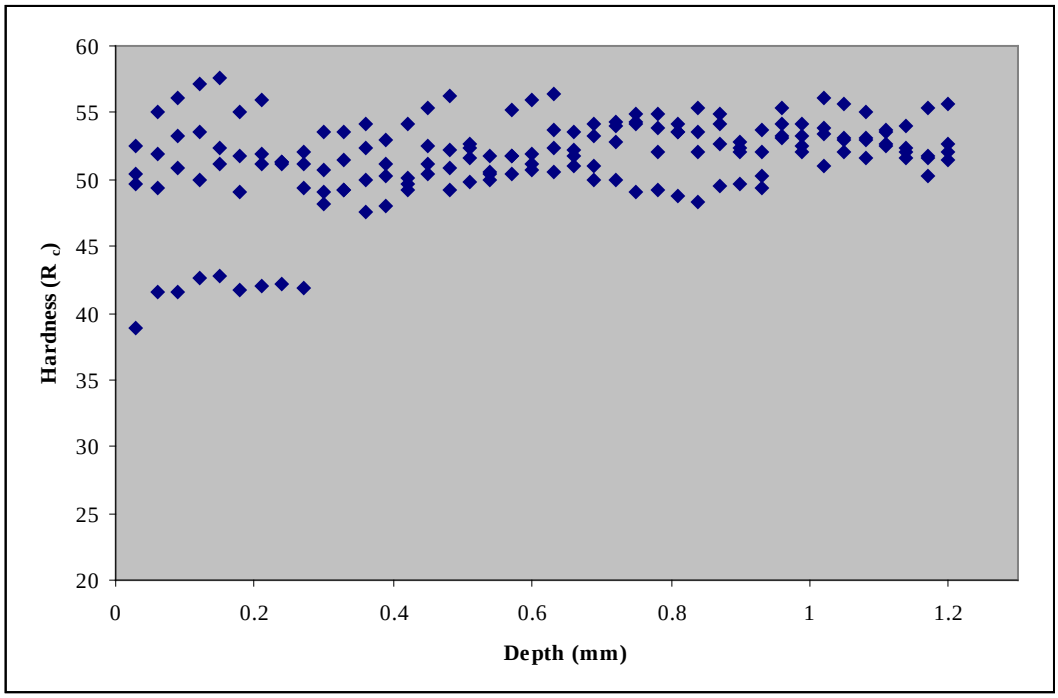

Fig. 6.17: Hardness Profile of Shot Peened Specimens

Figure 6.17 shows the hardness data points obtained for the shot peened specimens. There are nine hardness values that are very much lower than the other points. Removing these points would produce a curve that is almost horizontal. The microhardness testing machine is highly sensitive; therefore the nine hardness values could easily have been influenced by other factors.

The ground specimens were not expected to display any influences on the hardness profile. A slight drop in hardness near the surface may be present due to residual tensile stresses introduced from the machining process. This trend is shown in the results.

The hardness profiles for all three sets of specimens have shown a drop in the hardness near the surface. The hardness was expected to be higher near the

surface; therefore it seems there are other factors that affect the hardness values closer to the surface. Such factors might include the flatness of the surface, how parallel the surface is to the testing bed and possibly external factors such as vibrations.

6.3 Surface Roughness

The surface roughness of the EDWC specimens is approximately 3.2μm R_a, whether measured across or along the surface. The SEM examination of the EDWC specimen shows a surface consisting of many holes and cracks (Figure 6.18). There is little evidence to indicate the direction of the machining process; therefore the surface roughness values produced are not directional with respect to machining.

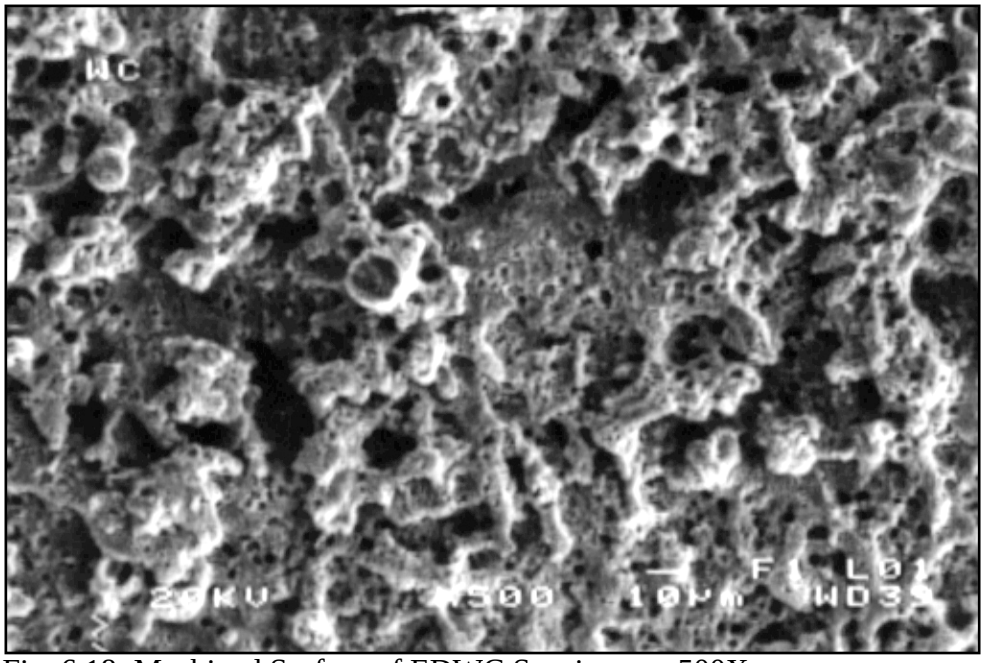

Fig. 6.18: Machined Surface of EDWC Specimen at 500X

Shot peened specimens produced a surface roughness of 1μm R_a. Shot peening utilises spherical particles to impact on the surface of the specimen, blending surface defects. The shot peening reduced the height of the protruding areas, giving the observed flattened look and reducing the measure surface roughness (Figure 6.19).

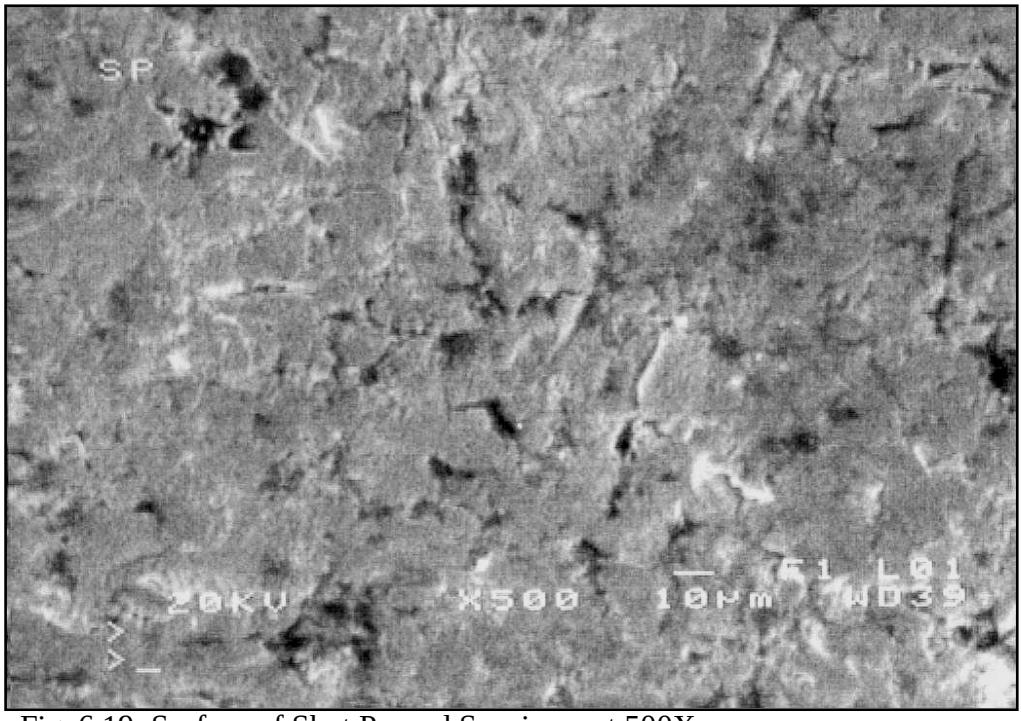

Fig. 6.19: Surface of Shot Peened Specimen at 500X

The surface roughness obtained for ground specimens have been found to vary along and across the surface. Along the surface, the surface roughness is 0.2μm R_a, while across the surface, a value of 0.4μm R_a is obtained. This variation can be explained by the SEM examination of the surface.

As shown in Figure 6.20, the surface of the ground specimen is shown to be directional. The machining tool evidently travelled from either top to bottom or

vice versa. This caused of the varying surface roughness for the ground specimens.

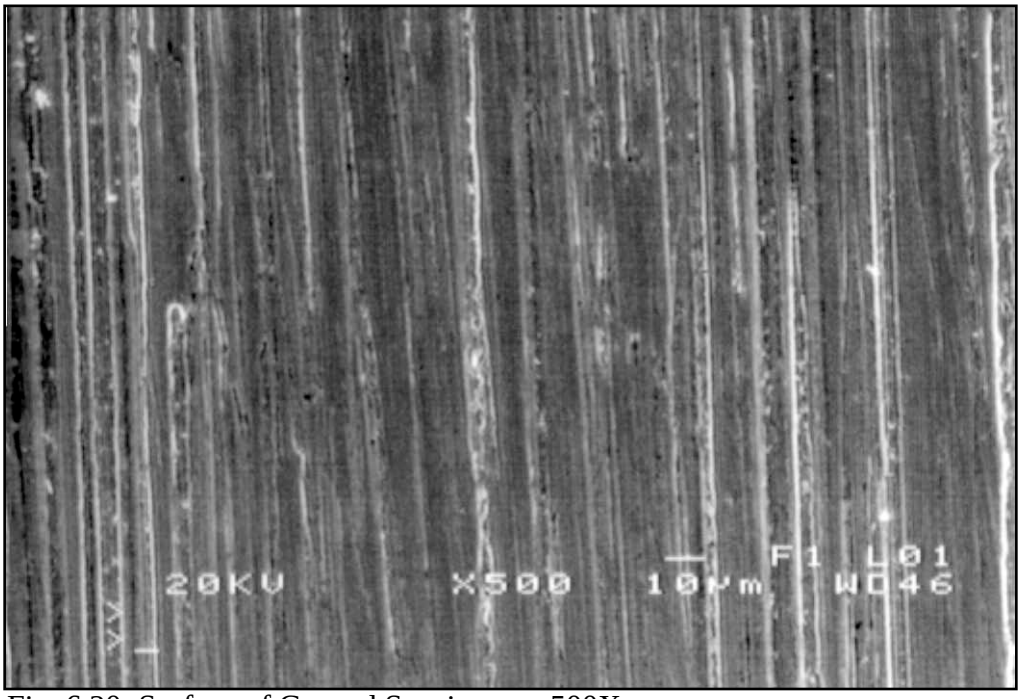

Fig. 6.20: Surface of Ground Specimen at 500X

CHAPTER 7: CONCLUSION AND RECOMMENDATIONS

7.1 Conclusion

EDWC is a non-conventional metal removal process that is seeing increased usage in industry. One possible application of EDWC is the manufacture of aircraft structural components. Fatigue properties are important for structural components used in the aeronautical industry. The effect of EDWC on fatigue properties and the possible benefits shot peening may provide are investigated.

The EDWC process has been found to be greatly detrimental to the fatigue properties of the components produced. The fatigue limit of EDWC specimens is reduced to approximately 30% of that for a ground specimen. The presence of numerous microcracks in the surface and sub-surface of the specimens, together with a surface roughness of 3μm R_a, indicate that surface topography contributes greatly to the reduction in fatigue limit. Other possible contributing factors include a phase change in the surface layer and the presence of a residual tensile stress.

Some EDWC specimens have been shot peened before testing. The shot peening process has restored the fatigue limit, and in some cases has even improved it. There are numerous cracks still present in the surface and the sub-surface of the specimens, although the surface roughness is reduced to 1μm R_a. Optical

examinations were incapable of detecting a phase change between the surface layer of a shot peened specimen and that of the EDWC specimen. The most likely cause for the restoration of the fatigue limit is the introduction of a residual compressive stress.

7.2 Recommendations

The fatigue limit of components is significantly reduced by the use of EDWC. It is difficult to ascertain a precise reason for this observation; however a likely reason is that the surface defects produced by the process are acting as stress concentrations, hence accelerating fatigue crack initiation. The extent of the effects of the heat-affected zone on the fatigue limit is uncertain. Microhardness testing has proved incapable of determining the depth of the heat-affected zone. Further work might include the removal of the recast layer, and testing to determine the effect of the heat-affected zone on the fatigue limit. X-ray diffraction might also be employed to determine the depth of any residual tensile stresses present.

Shot peening an EDWC specimen leads to the recovery of the fatigue limit that had been lowered. The residual compressive stresses introduced by the shot peening process have been attributed to this recovery. The role of a smoother surface and possible modifications to surface defects on changing the fatigue limit can be further explored. A large scatter in the values of the fatigue limit is observed. Methods of reducing the scatter of the fatigue limit can be investigated

by examining methods to reduce the possible types of crack initiation sites. One such method may be to remove the surface defects by the removal of a thin layer from the surface of the specimen prior to testing.

Although the results that have been obtained are encouraging, more testing needs to be done to confirm the positive effect of shot peening on EDWC specimens. There are only a few other research works that have investigated the effect of shot peening on EDM. Even in these cases, the EDM process used is not EDWC, but EDM spark erosion.

1. (1983). *Tools and Manufacturing Engineers Handbook (4th Edition)*. Vol 1.

2. Marsh, K. J. (1993). *Shot Peening: Techniques and Applications*.

3. Conera, E. (1995). *The Effect of EDM Wire Cutting on the Fatigue Properties of 300M Steel*. Christchurch, New Zealand, University of Canterbury. (3rd Pro Project Report: Mechanical Engineering: 12/95)

4. (1996). *ASM Handbook*. Vol 19.

5. Suresh, S. and Ritchie, R. O. (1984). *Propagation of Short Fatigue Cracks*. International Metals Reviews, Vol 29 No 6, p445.

6. (1994). *ASM Handbook*. Vol 5.

7. Kyriacou, S. (1996). *Shot Peening Mechanics: A Theoretical Study*. 1996 ICSP Conference Proceedings, p505.

8. Hertzberg, R. W. (1996). *Deformation and Fracture Mechanics of Engineering Materials (4th Edition)*.

9. Cooper, T. D. and Kelto, C. A. (1979). *Fatigue in Machines and Structures – Aircraft*. Fatigue and Microstructure, p49.

10. Kondo, Y. and Endo, T. (1987). *Prediction of Corrosion Fatigue Strength in Long Life Regions*. Current Research on Fatigue Cracks, p298.

11. Erasmus, L. A. (1972). *The Effects of Strain Ageing on Fatigue Damage in Low Carbon Steels*. Cape Town, South Africa, University of Cape Town. (Thesis: PhD: Mechanical Engineering)

12. Cowling, J. M. (1986). *Fatigue Cracking in Nitrided Steels*. Research Reports in Material Science, Series 1.

13. Fine, M. E. and Ritchie, R. O. (1979). *Fatigue-Crack Initiation and Near-Threshold Crack Growth*. Fatigue and Microstructure, p245.

14. Neumann, P. (1969). *Coarse Slip Model of Fatigue*. Acta Metallurgica, Vol 17, p1219.

15. Venkataraman, G., Chung, Y. W. and Mura, T. (1991). *Application of Minimum Energy Formalism in a Multiple Slip Band Model for Fatigue – I. Calculation of Slip Band Spacings*. Acta Metallurgica, Vol 39 No 11, p2621.

16. Mott, N. F. (1958). *A Theory of the Origin of Fatigue Cracks*. Acta Metallurgica, Vol 6, p195.

17. Laird, C. (1979). *Mechanisms and Theories of Fatigue*. Fatigue and Microstructure, p149.

18. Alden, T. H. and Backofen, W. A. (1961). *The Formation of Fatigue Cracks in Aluminum Single Crystals*. Acta Metallurgica, Vol 9, p352.

19. Douglas, D. E. and Wood, W. A. (1972). *Slipless Fatigue in Titanium*. Journal of the Institute of Metals, Vol 100, p73.

20. Mitchell, M. R. (1979). *Fundamentals of Modern Fatigue Analysis for Design*. Fatigue and Microstructure, p385.

21. Thielen, P. N, Fine, M. E. and Fournelle, R. A. (1976). *Cyclic Stress Relations and Strain-Controlled Fatigue of 4140 Steel*. Acta Metallurgica, Vol 24, p1.

22. Sarma, V. S., Padmanabhan, K. A., Gueth, A. and Koeth, A. (1999). *Low Cycle Fatigue Behaviour of Low Carbon Microalloyed Steel: Microstructural Evolution and Life Assessment*. Material Science and Technology, Vol 15, p260.

23. Sudarshan, T. S. and Louthan Jr, M. R. (1987). *Gaseous Environment Effects on Fatigue Behaviour of Metals*. International Metals Reviews, Vol 32 No. 3, p121.

24. Cox, H. L. (1950). *Fracture by Fatigue*. The Fracture of Metals, p42.

25. Sriram, T. S., Chih-Ming K. E. and Chung, Y. W. (1993). *Fatigue Deformation of Silver Single Crystals: STM Evidence for Crack Nucleation, Measurements of Slip Irreversibility and Verification of a New Scaling Relationship for Fatigue Life*. Acta Metallurgica, Vol 41 No.8, p2515.

26. Funkenbusch, A. W. and Coffin, L. F. (1978). *Low-Cycle Fatigue Crack Nucleation and Early Growth in Ti-17*. Metallurgical Transactions A, Vol 9A, p1159.

27. Venkatarman, G., Chung, Y. W., Nakasone, Y. and Mura, T. (1990). *Free Energy Formulation of Fatigue Crack Initiation Along Persistent Slip Bands: Calculation of S-N Curves and Crack Depths*. Acta Metallurgica, Vol 38 No 1, p31.

28. Vinogradov, A., Hashimoto, S. and Miura, S. (1995). *Crack initiation and Propagation in <110> Oriented Copper Single Crystals Under Cyclic Deformation*. Acta Metallurgica, Vol 43 No 2, p675.

29. Kim, Y. H., Mura, T. and Fine, M. E. (1978). *Fatigue Crack Initiation and Microcrack Growth in 4140 Steel*. Metallurgical Transactions A, Vol 9A, p1679.

30. Kim, W. H. and Laird, C. (1978). *Crack Nucleation and Stage I Propagation in High Strain Fatigue – II. Mechanism*. Acta Metallurgica, Vol 26, p789.

31. Kim, W. H. and Laird, C. (1978). *Crack Nucleation and Stage I Propagation in High Strain Fatigue – I. Microscopic and Interferometric Observations*. Acta Metallurgica, Vol 26, p777.

32. Goto, M. and Knowles, D. M. (1998). *Initiation and Propagation Behaviour of Microcracks in Ni-Base Superalloy Udimet 720 Li*. Engineering Fracture Mechanics, Vol 60 No1, p1.

33. Venkataraman, G., Chung, Y. W. and Mura, T. (1991). *Application of Minimum Energy Formalism in a Multiple Slip Band Model for Fatigue – II.*

Crack Nucleation and Derivation of a Generalised Coffin-Manson Law. Acta Metallurgica, Vol 39 No 11, p2631.

34. Wood, W. A., Cousland, S. McK. and Sargant, K. R. (1963). *Systematic Microstructural Changes Peculiar to Fatigue Deformation*. Acta Metallurgica Vol 11, p643.

35. Fujita, F. E. (1958). *Dislocation Theory of Fracture of Crystals*. Acta Metallurgica, Vol 6, p543.

36. Tanaka, K. and Mura, T. A (1981). *Dislocation Model for Fatigue Crack Initiation*. Journal of Applied Mechanics, Vol 48, p97.

37. Mura, T. A (1994). *Theory of Fatigue Crack Initiation*. Materials Science and Engineering, Vol 176A, p61.

38. Suresh, S. (1992). *Fatigue of Materials*.

39. Chan, K. S. and Lanford, J. (1988). *The Role of Microstructural Dissimilitude in Fatigue and Fracture of Small Cracks*. Acta Metallurgica, Vol 36 No1, p193.

40. D. L. McDowell, An Engineering Model for Propagation of Small Cracks in Fatigue, Engineering Fracture Mechanics (Vol 56 No 3), p.357 (1997).

41. Morris, W. L., James, M. R. and Buck, O. (1981). *Growth Rate Models for Short Surface Cracks in Al 2219-T851*. Metallurgical Transactions A, Vol 12A, p57.

42. Askeland, D. R. (1990). *The Science and Engineering of Materials, (2nd Edition)*. p166.

43. Jin, C. C. (1980). *The Effects of Strain Ageing and Grain Size on Fatigue in Low Carbon Steel*. Christchurch, New Zealand, University of Canterbury (Thesis: PhD: Mechanical Engineering).

44. Sanders Jr, T. H. and Stanley, J. T. (1979). *Review of Fatigue and Fracture Research on High-Strength Aluminum Alloys*. Fatigue and Microstructure, p470.

45. Buck, O. and Alers, G. A. (1979). *New Techniques for Detection and Monitoring of Fatigue Damage*. Fatigue and Microstructure, p101.

46. Starke Jr., E. A. (1979). *Cyclic Plastic Deformation and Microstructure*. Fatigue and Microstructure, p205.

47. Duquette, D. J. (1979). *Environmental Effects I: General Fatigue Resistance and Crack Nucleation in Metals and Alloys*. Fatigue and Microstructure, p335.

48. Bayoumi, M. R. and Abdellatif, A. K. (1995). *Effect of Surface Finish on Fatigue Strength*. Engineering Fracture Mechanics, Vol 51 No 5, p861.

49. Kobayashi, M., Murakami, Y., Makino, T., Toriyama, T., Kurihara, Y. and Ebara, R. (1991). *Fatigue Strength Prediction of Automobile Suspension Spring Steels: Explicit Analysis of Nonmetallic Inclusions, Shot Peening, Decarburized Layer, Surface Roughness and Corrosion Pits*. Impact of

Improved Material Quality on Properties, Product Performance, and Design – Symposium Winter Annual Meeting, MD-Vol 8, p171.

50. Starker, P., Wohlfahrt, H. and Macherauch, E. (1979). *Subsurface Crack Initiation During Fatigue as a Result of Residual Stresses*. Fatigue of Engineering Materials and Structures, Vol 1, p319.

51. Larsson, M., Melander, A., Blom, R. and Preston, S. (1991). *Effects of Shot Peening on Bending Fatigue Strength of Spring Steel SS 2090*. Materials Science and Technology, Vol 7, p998.

52. Forrest, G. (1955). *The Effect on Fatigue of Notches, Surface Finishes, Etc*. The Fatigue of Metals, p40.

53. Paskiet, G. F., Boone, D. H. and Sullivan, C. P. (1972). *Effect of Aluminide Coating on the High-Cycle Fatigue Behaviour of a Nickel-Base High-Temperature Alloy*. Journal of the Institute of Metals, Vol 100, p58.

54. Kahles, J. F. (1967). *Metals Handbook (8th Edition)*. Vol 3, p227.

55. (1960). *Spark Machining*. Machinery's Yellow Back Series No. 46.

56. Smith, G. V. (1967). *Progress in Spark-Erosion Machining*. Conference on Electrical Methods of Machining and Forming, p119.

57. Nekrashevich G. and Bakuto, I. A. (1965). *Present State of the Theoretical Concept of the Electric Erosion of Metals*. Electrospark Machining of Metals, Vol 3, p17.

58. *Understanding EDM Surface Integrity*, AGIETRON Corporation.

59. Bloom, J. A. (1963). *EDM- Dielectric Selection and Dielectric Filtering*. Advanced Electro Metal Removal (Electric Machining) Book 2, SP63-22.

60. (1968). *Spark Machining (Part 2)*. Machinery's Yellow Back Series No. 46.

61. Kaefer, M. H. (1963). *Machining Tube Grids and Other Electronic Components - A Production Application for EDM*. Advanced Electro Metal Removal (Electric Machining) Book 2, SP63-43.

62. Gularyan, K. K. (1964). *Electrospark Threading Methods*. Electrospark Machining of Metals (Vol 2), p102.

63. Yeo, W. H. Y. (1995). *Surface Integrity in Electric Discharge Machining*. Christchurch, New Zealand, University of Canterbury. (3rd Pro Project Report: Mechanical Engineering: 83/95).

64. Cheng, W., Finnie, I., Gremaud, M. and Prime, M. B. (1994). *Measurement of Near Surface Residual Stresses Using Electric Discharge Wire Machining*. Journal of Engineering Materials and Technology, Vol 116, p1.

65. Mogilevskii, Z., Linetskii, Y. L. and Chepovaya, S. A. (1965). *Macroscopic Investigation of Changes in the Structure of the Surface Layers of Steels and Alloys Caused by Electrospark Cutting*. Electrospark Machining of Metals, Vol 3, p103.

66. Aleksandrov, P. (1965). *Residual Stresses and the Long-Term and Fatigue Strengths of Heat-resistant Materials after Electrospark Machining*. Electrospark Machining of Metals, Vol 3, p98.

67. Ogikubo, F. *Wire-EDM for Precision Press Die Parts*. Sodick.

68. Lazarenko, B. R. and Lazarenko, N. I. (1964). *Technological Characteristics of Electrospark Machining of Current Conducting Materials*. Electrospark Machining of Metals, Vol 2, p1.

69. (1983). *Tools and Manufacturing Engineers Handbook (4th Edition)*. Vol 1, p129.

70. *Shot Peening Applications (6th Edition)*. Metal Improvement Company Inc. p15.

71. Fukao, S. *Mold Manufacturing Method by EDMing without Polishing*.

72. Christiana, J. J. (1963). *EDM-Spark Drilling*. Advanced Electro Metal Removal (Electric Machining) Book 2, SP63-47.

73. (1983). *Tools and Manufacturing Engineers Handbook (4th Edition)*. Vol 1.

74. Holm, A. E. (1963). *Application of EDM for Die Sinking and Punch Fabrication*. Advanced Electro Metal Removal (Electric Machining) Book 2, SP63-23.

75. Kotora Jr, J. and Strack, D. (1963). *Fabrication of Neutron Chopper Mark IV Using the Electrical Discharge Machining Process*. Advanced Electro Metal Removal (Electric Machining) Book 2, SP63-31.

76. Fathalla, R., Inglebert, G. and Castex, L. (1998). *Prediction of Plastic Deformation and Residual Stresses induced in Metallic Parts by Shot Peening*. Materials Science and Technology, Vol 14, p631.

77. Nevarez, I. M., Nelson, D. V., Esterman, M. and Ishii, K. (1996). *Shot Peening and Robust Design for Fatigue Performance*. 1996 ICSP Conference Proceedings, p517.

78. Eckersley, J. S. and Ferrelli, B. (1992). *Using Shot Peening to Multiply the Life of Compressor Components*. Proceedings of the 1992 International Compressor Engineering Conference.

79. (1996). *Peen Forming – A Look Under the Surface*. The Shot Peener, Vol 10 Iss 3, p6.

80. Williams, S. (1992). *Practical Application of Shot Peening*. The Shot Peener, Vol 5 Iss 4, p1.

81. Champaigne, J. (1992). *Controlled Shot Peening*, Peening Reference Manual Vol 2, p1.

82. Baiker, A. G. (1997). *CNC Shot Peening Machining Specialized for the Aviation Industry*. The Shot Peener, Vol 11 Iss 2, p30.

83. Baiker, A. G. (1997). *Peening Efficiency Program PEPCOM 1.0*. The Shot Peener Vol 11 Iss 1, p30.

84. Champaigne, J. (1992). *Almen Gage Accuracy*. The Shot Peener, Vol 6 Iss 3, p14.

85. (1997). *Dust-free Abrasive Blasting On-Site*. The Shot Peener, Vol 11, Iss 2, p37.

86. Larsson, M., Melander, A., Blom, R. and Preston, S. (1991). *Effects of Shot Peening on Bending Fatigue Strength of Spring Steel SS 2090*. Materials Science and Technology, Vol 7, p.998.

87. Lawerenz, M. and Ekis, I. (1993). *Creating an In-House Shot Peening Specification for Gears Part 1*. The Shot Peener, Vol 6 Iss 4, p13.

88. Straub, J. (1997). *The Importance of Uniformity in the Application of the Shot Peening Treatment.* The Shot Peener, Vol 11 Iss 1, p10.

89. Champaigne, J. (1992). *Almen Strip as Process Control for Shot Peening*. The Shot Peener, Vol 6 Iss 1, p1.

90. Hozapfel, H., Wick, A., Vohringer, O. (1996). *Effect of Shot Peening Parameters on the Properties of Surface Layers in AISI 4140 in Different Heat Treatment Conditions*. The Shot Peener, Vol 10 Iss 1, p6.

91. Archer, F. (1995). *Shot Peening of Carburized Gears: Influence of Main Shot Peening Parameters*. The Shot Peener, Vol 8 Iss 4, p28.

92. Champaigne, J. (1993). *Shot Peening Intensity Measurement*. The Shot Peener, Vol 6 Iss 4, p1.

93. (1963). *Double Peening*. U.S. Patent 3,073,022.

94. (1982). *Military Specification Steel, Chrome-Nickel-Molybdenum (E4340) Bars and Reforging Stock*. MIL-S-50000.

95. Fordham, J. D., Pilkington, R. and Tang, C. C. (1997). *The Effect of Different Profiling Techniques on the Fatigue Performance of Metallic Membranes of AISI 301 and Inconel 718*. International Journal of Fatigue,Vol19 No 6, p487.

APPENDIX A: OPTICAL MICROSCOPY

Microstructure of 4340 Steel X 57.5

Microstructure of 4340 Steel X 230

Microstructure of 4340 Steel X 575

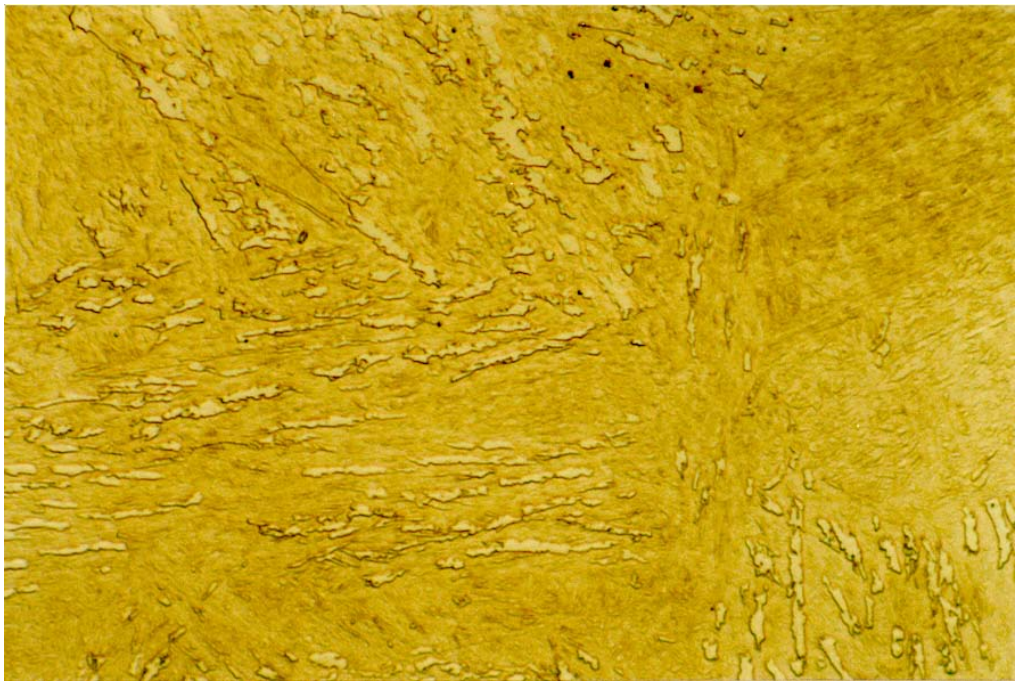

Microstructure of 4340 Steel X 1150

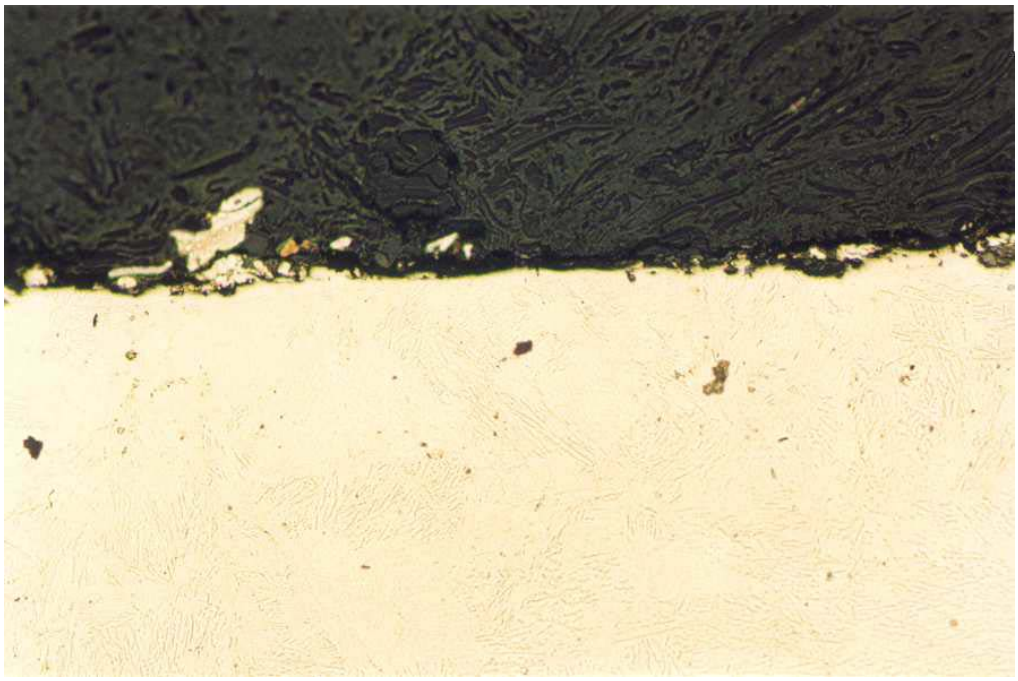

Edge of EDWC Specimen X 230

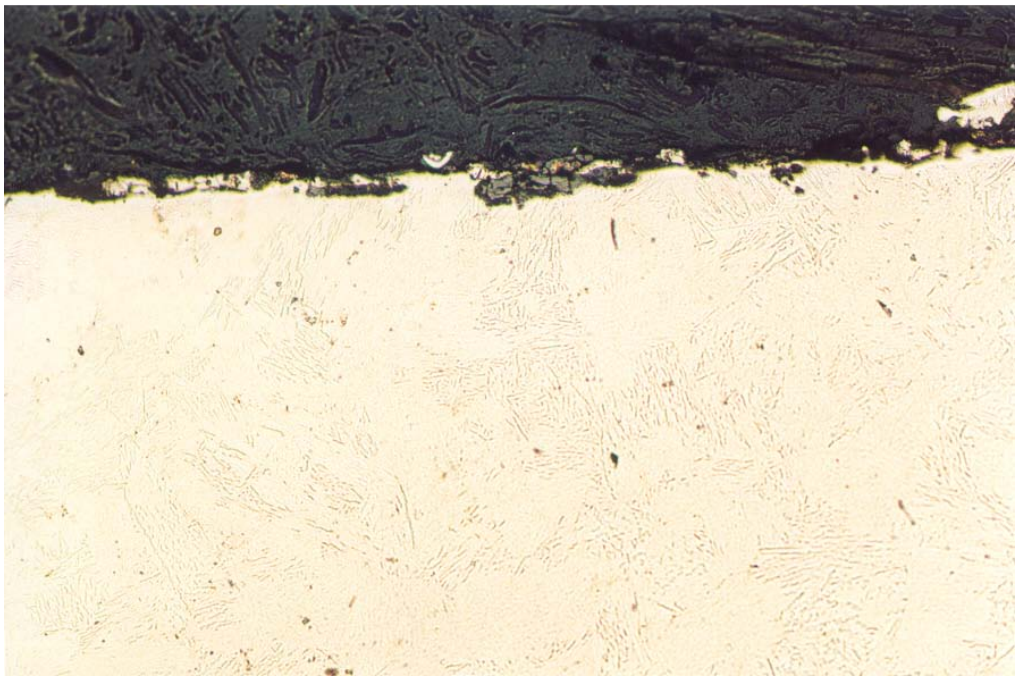

Edge of EDWC Specimen X 230

Edge of EDWC Specimen X 230

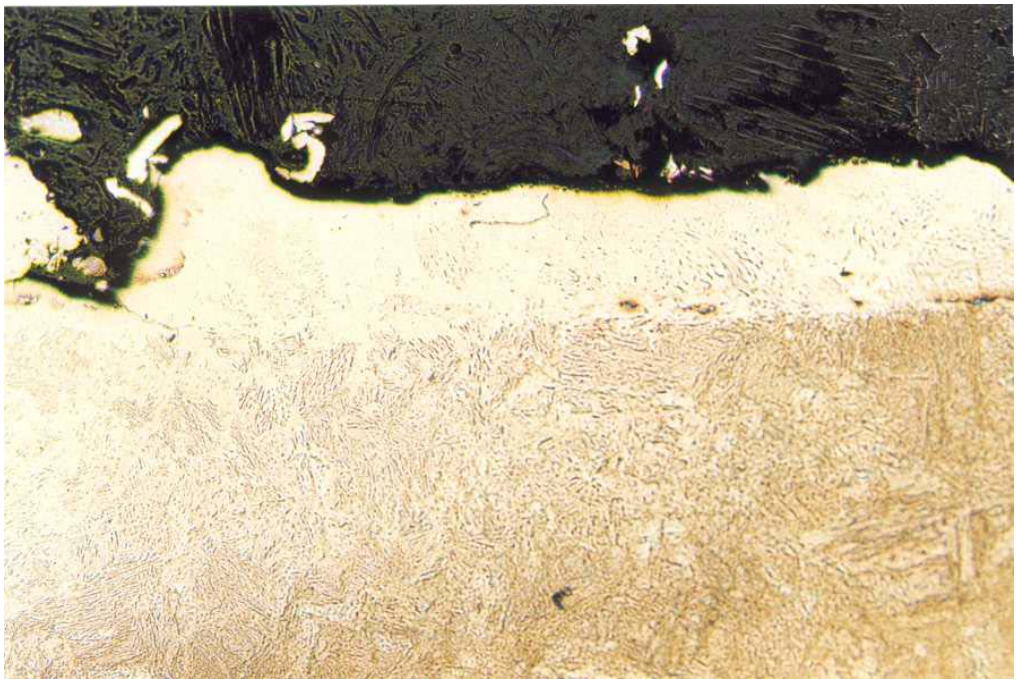

Edge of Shot Peened Specimen X 115

Edge of Shot Peened Specimen X 230

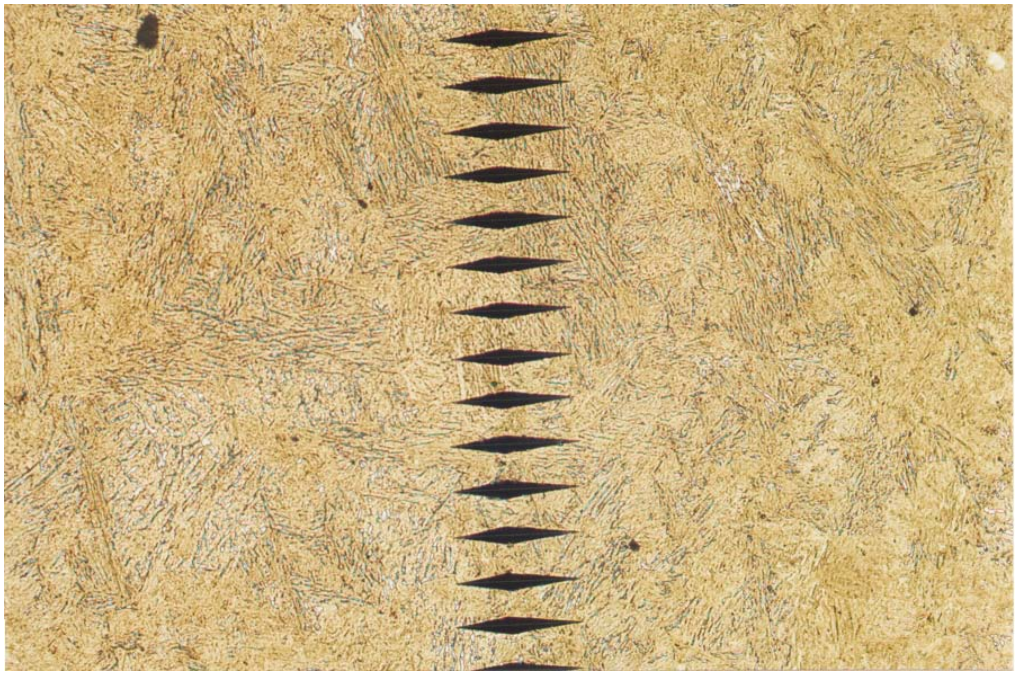

Microhardness Indentations X 230

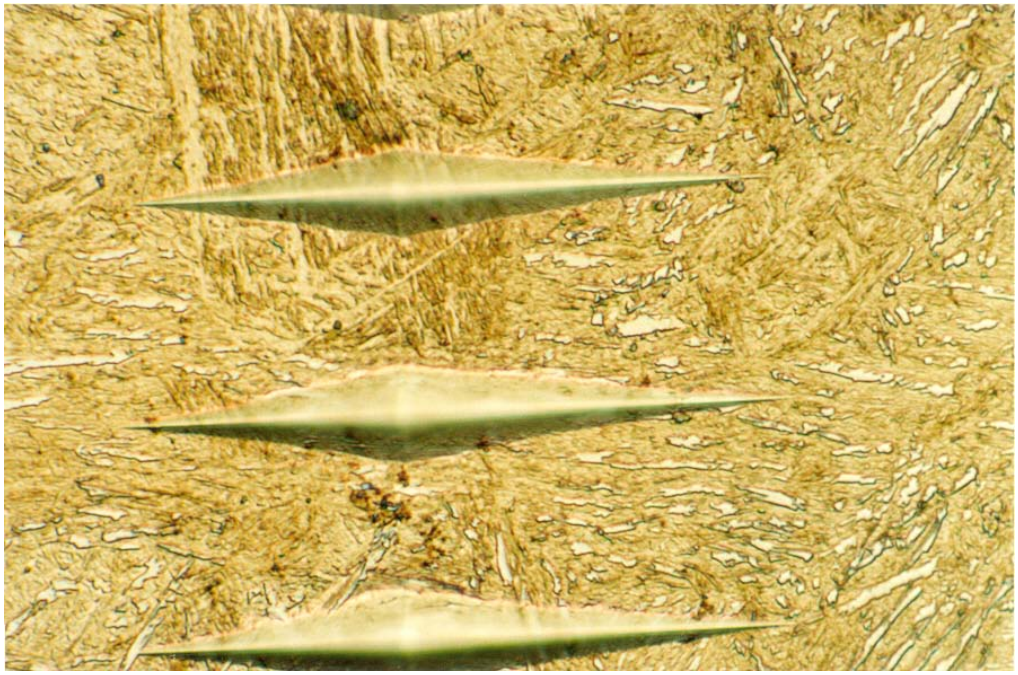

Microhardness Indentations X 1150

APPENDIX B: FATIGUE TESTING

Specimen	Width (mm)	Thickness (mm)	Mean Load (kN)	Load Range (kN)	No. of Cycles	Stress Range (MPa)	Frequency (Hz)	Time (hr)	
1,1	20.04	10.01	24.81	17.45	124100	534.45	129.4	0.27	
1,2	20.02	10.06	25.08	15.19	160000	461.08	127.7	0.35	
1,3	20.00	10.07	25.01	13.72	243000	416.04	129.5	0.52	
2,1	20.05	10.04	25.55	12.27	286800	373.37	129.5	0.62	
2,2	20.06	10.04	24.53	10.80	366400	328.47	130.1	0.78	
2,3	20.05	10.25	20.14	11.40	377500	332.83	130.2	0.81	
2,4	20.02	10.10	10.70	14.98	395200	451.47	125.8	0.87	
3,1	20.01	10.06	9.50	11.20	500300	340.13	121.5	1.14	
3,2	20.04	10.30	10.77	7.10	970000	205.38	124.6	2.16	
3,3	20.04	10.22	10.73	8.30	905700	243.87	122.3	2.06	
3,4	20.06	10.06	15.65	8.80	675800	266.58	125.2	1.50	
4,1	20.03	10.03	15.00	7.90	952400	241.11	126.2	2.10	
4,2	20.09	10.07	15.27	8.30	609700	250.56	126.6	1.34	
4,3	20.06	10.06	15.10	8.70	895800	263.55	125.6	1.98	
4,4	20.03	10.03	15.00	8.65	765800	264.00	126.6	1.68	
5,1	20.06	10.06	14.90	8.47	1212800	256.59	125.5	2.68	runout
5,2	20.09	10.30	14.85	8.60	1200000	248.15	124.3	2.68	runout
5,3	20.15	10.06	14.88	8.63	1186100	260.26	126.9	2.60	
5,4	20.06	10.05	14.79	9.70	949900	294.43	124.3	2.12	
6,1	20.00	10.06	14.99	9.74	731100	295.94	126.8	1.60	
6,2	20.04	10.16	14.42	9.03	619500	268.46	125.1	1.38	
6,4	20.05	10.03	15.07	17.10	270600	521.38	131.0	0.57	
7,1	20.06	10.02	15.14	18.15	227600	554.22	129.2	0.49	
7,2	20.06	10.08	14.63	13.02	412000	392.86	125.7	0.91	
7,3	19.99	10.02	15.03	20.40	140700	625.11	130.8	0.30	

Table B1: EDWC Specimens

Specimen	Width (mm)	Thickness (mm)	Mean Load (kN)	Load Range (kN)	No.of Cycles	Stress Range (MPa)	Frequency (Hz)	Time (hr)	
1a	20.00	10.00	14.74	19.50	130700	285.23	130.5	0.28	runout
1b	20.04	10.00	14.91	10.19	585100	312.72	129.9	1.25	
1c	20.09	10.03	14.48	9.69	4948000	294.86	12734.0	0.11	runout
2a	20.05	10.05	15.23	12.02	470800	365.03	132.0	0.99	
2b	20.10	10.07	14.74	11.07	541900	334.02	131.3	1.15	
2c	19.99	10.00	15.02	11.05	12152000	339.96	127.7	26.43	runout
3a	20.07	10.07	14.57	9.70	1234100	293.12	132.3	2.59	
3b	20.13	10.04	14.85	10.64	549900	322.48	130.4	1.17	
4a	20.02	10.06	14.96	8.49	2352300	257.70	132.3	4.94	
4b	20.07	10.03	14.83	10.10	590000	307.64	130.4	1.26	
5a	20.05	10.13	15.05	15.35	237900	458.83	131.3	0.50	
5b	20.08	10.10	14.86	9.50	1047200	285.23	133.4	2.18	
6a	20.09	9.91	14.86	13.85	368800	431.72	131.1	0.78	
6b	20.14	10.25	14.95	11.22	542700	326.11	130.1	1.16	
7a	20.14	10.09	14.52	17.77	201700	532.99	131.3	0.43	
7b	20.10	10.06	14.86	11.10	30200000	335.59	132.2	63.46	runout
8a	20.03	10.16	14.72	10.22	12560000	303.99	131.2	26.59	runout
8b	20.10	10.10	14.81	8.00	1836000	239.95	131.3	3.88	
9a	20.09	9.81	14.78	10.66	12160000	339.09	130.2	25.94	runout
9b	20.06	10.10	14.92	7.28	5562000	218.79	131.5	11.75	runout
10a	20.09	10.09	14.89	11.27	455500	338.87	131.5	0.96	
11a	20.07	10.00	14.87	10.20	1263000	312.56	132.5	2.65	runout
12a	20.08	10.06	15.01	10.88	1034000	329.26	132.9	2.16	runout
13a	20.05	10.05	14.64	12.63	445900	383.56	131.9	0.94	
14a	20.05	10.05	15.17	12.13	744600	368.37	132.1	1.57	runout

Table B2: EDWC Specimens

Specimen	Width (mm)	Thickness (mm)	Mean Load (kN)	Load Range (kN)	No.of Cycles	Stress Range (MPa)	Frequency (Hz)	Time (hr)	
1a	20.04	9.92	14.26	11.42	26373500	356.14	128.0	57.23	runout
8a	20.06	10.04	14.02	11.40	77925500	346.72	129.7	166.89	runout
8b	20.06	10.06	14.06	11.80	186800	357.46	128.7	0.40	
9a	20.08	10.07	14.07	11.75	216600	354.89	128.6	0.47	runout
9b	20.09	10.10	14.04	12.02	210200	360.71	125.8	0.46	
10a	20.03	10.19	14.34	11.23	22696000	332.07	129.4	48.72	runout
10b	20.06	10.33	14.03	11.81	204200	339.31	127.3	0.45	
11a	20.09	10.09	14.07	12.30	237300	369.84	128.9	0.51	
11b	20.10	10.09	13.88	12.84	151500	385.89	128.2	0.33	
12a	20.00	10.08	14.44	11.47	61172000	347.13	121.0	140.43	runout
12b	20.05	10.05	14.52	9.85	35437800	299.13	126.9	77.57	runout
12c	20.06	10.03	14.06	13.85	167100	422.08	125.2	0.37	

Table B3: EDWC Specimens

Specimen	Width (mm)	Thickness (mm)	Mean Load (kN)	Load Range (kN)	No.of Cycles	Stress Range (MPa)	Frequency (Hz)	Time (hr)	
1a	20	9.88	22.82	28.73	102000	905.04	127.7	0.22187	
1b	20.01	9.96	23.13	25	263600	774.55	130	0.56325	
1c	20.01	9.95	23.21	25.13	33590500	780.14	128.8	72.4433	interference
3a	19.95	9.99	25.96	24.8	137100	766.04	131.6	0.28939	
4b	20	9.95	27.05	24.38	102600	757.24	132.3	0.21542	
7b	19.97	9.93	26.16	25.51	177900	796.73	130.3	0.37925	
8a	20.09	9.95	23.07	25.26	52931000	781.06	130.2	112.927	runout
8b	19.99	9.92	26.3	26.4	56800	825.36	130.7	0.12072	runout
11a	19.97	9.95	22.75	26	130400	808.77	128.9	0.28101	
12a	19.94	10	26.37	24.78	73400	764.28	131	0.15564	
12b	20.05	10.11	23.08	28.69	89000	860.97	128.9	0.19179	

Table B4: Shot Peened Specimens

Specimen	Width (mm)	Thickness (mm)	Mean Load (kN)	Load Range (kN)	No.of Cycles	Stress Range (MPa)	Frequency (Hz)	Time (hr)	
1a	20.11	10.17	14.71	18.74	14360000	994.36	129.4	30.83	runout
1b	20.03	10.00	26.48	31.93	70300	1066.91	125.5	0.16	corner
1c	20.07	10.08	26.40	30.78	67850000	928.27	125.7	149.94	runout
2a	20.02	10.00	14.76	24.20	401900	978.79	127.7	0.87	runout
2b	20.06	10.01	25.83	31.99	1541300	1075.17	124.3	3.44	interference
2c	20.03	10.02	26.19	31.93	15580700	976.47	130.8	33.09	
3a	19.98	10.10	24.41	39.75	139100	1199.43	129.5	0.30	
3b	20.05	10.01	26.45	31.89	95000	976.22	126.9	0.21	
4a	20.07	9.83	24.55	38.03	100300	1199.43	129.5	0.22	corner
4b	20.04	10.18	26.38	32.69	241700	968.05	124.3	0.54	
5a	19.96	10.01	24.38	35.92	1327500	1075.17	130.1	2.83	runout
5b	20.09	10.23	26.90	30.08	56747000	879.88	126.8	124.31	runout
6a	20.07	10.01	24.40	36.02	73100	1101.55	130.2	0.16	
6b	20.08	9.99	26.46	31.57	93700	1010.09	125.1	0.21	corner
7a	20.07	9.77	24.74	35.62	4194700	1199.43	125.8	9.26	interference
7b	20.10	9.99	24.12	34.80	58300	1075.17	130.6	0.12	corner
8a	20.04	10.05	26.47	31.55	27650000	743.41	121.5	63.21	runout
8b	20.07	10.00	26.60	32.45	58000	554.10	131.0	0.12	corner
9a	20.03	9.99	25.90	31.86	1175000	1104.54	124.6	2.62	runout
9b	20.09	9.99	26.58	32.30	29040700	990.76	129.2	62.44	
10a	20.04	9.82	27.00	31.74	130400	1010.09	122.3	0.30	
11a	19.98	10.00	27.09	34.93	176300	1075.17	125.2	0.39	
12a	19.99	10.03	23.91	34.90	39532000	1067.30	126.2	87.01	runout
13a	19.99	9.99	24.08	34.68	16340000	976.22	126.6	35.85	runout
14a	20.07	9.99	24.48	34.20	26370000	968.05	125.6	58.32	runout
15a	20.04	9.99	24.43	29.47	1130000	1069.08	126.6	2.48	runout

Table B5: Shot Peened Specimens

Specimen	Width (mm)	Thickness (mm)	Mean Load (kN)	Load Range (kN)	No.of Cycles	Stress Range (MPa)	Frequency (Hz)	Time (hr)	
1	20.03	10.00	25.07	31.02	12300000	952.44	135.1	25.2899	runout
2	19.96	10.00	25.25	32.15	14025000	990.59	134.0	29.0734	runout
3	20.00	10.00	26.72	32.20	1199500	990.15	133.9	2.48838	
4	20.04	10.00	26.30	31.82	7687500	976.51	134.2	15.9122	
5	20.02	10.00	25.63	30.84	15980000	947.38	133.7	33.2004	runout
6	20.02	10.01	27.89	28.85	46328100	884.48	136.7	94.1398	interference
7	20.01	10.00	27.58	30.53	429400	938.33	136.0	0.87704	
8	20.02	9.99	26.92	30.68	39889300	944.36	133.9	82.751	runout
9	20.02	10.00	27.60	30.48	1175000	936.32	133.0	2.45405	runout
10	20.04	10.01	29.19	28.08	55400	860.02	132.8	0.11588	corner
11	20.02	10.00	27.10	27.11	634100	832.80	132.8	1.32635	
12	20.04	10.01	28.82	27.68	10147500	847.76	133.1	21.1777	
13	20.03	10.00	28.35	28.20	27400	865.85	135.0	0.05638	
14	20.03	10.00	27.63	27.95	30900	858.18	132.3	0.06488	
15	20.03	10.00	27.73	30.02	42200	921.73	135.6	0.08645	
16	20.02	10.00	27.80	26.85	24636900	824.81	134.7	50.8061	
17	20.03	10.01	28.56	28.58	2592500	875.77	134.9	5.33832	
18	20.02	10.02	29.12	27.70	7413800	847.53	135.1	15.2434	
19	20.03	10.01	29.07	29.13	1703300	892.62	133.1	3.55476	
20	20.02	10.00	28.30	30.19	2870000	927.42	135.2	5.89661	
21	20.04	10.00	27.11	27.15	43400	833.20	132.3	0.09112	
22	20.03	10.00	27.51	27.97	4088200	858.79	132.3	8.58361	
23	20.03	10.00	27.35	27.88	7713200	856.03	132.2	16.2069	
24	20.02	10.02	27.13	27.46	73100	840.19	133.2	0.15244	
25	20.02	10.00	27.20	27.42	204600	842.32	134.3	0.42318	
26	20.04	10.01	26.94	28.16	19292900	862.47	133.2	40.2338	
27	20.02	10.01	26.58	28.17	7213000	863.63	132.9	15.0761	
28	20.02	10.00	27.17	27.63	2468400	848.77	133.5	5.13608	
29	20.03	10.00	27.09	28.05	15186900	861.25	133.4	31.6236	
30	20.02	10.00	27.82	27.92	53560100	857.68	133.2	111.695	runout

Table B6: Ground Specimens

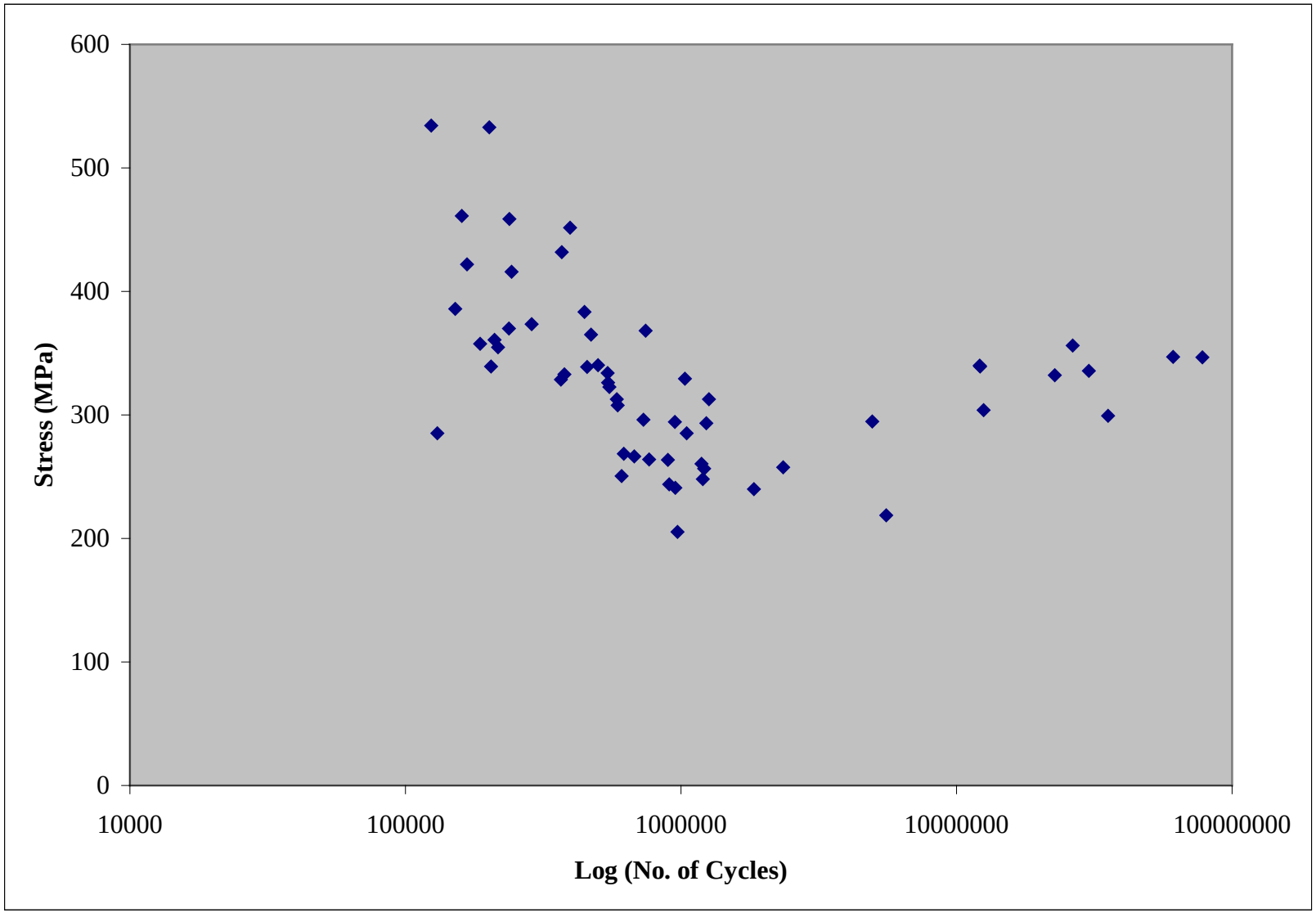

Fig. B1: S-N Graph for EDWC Specimens

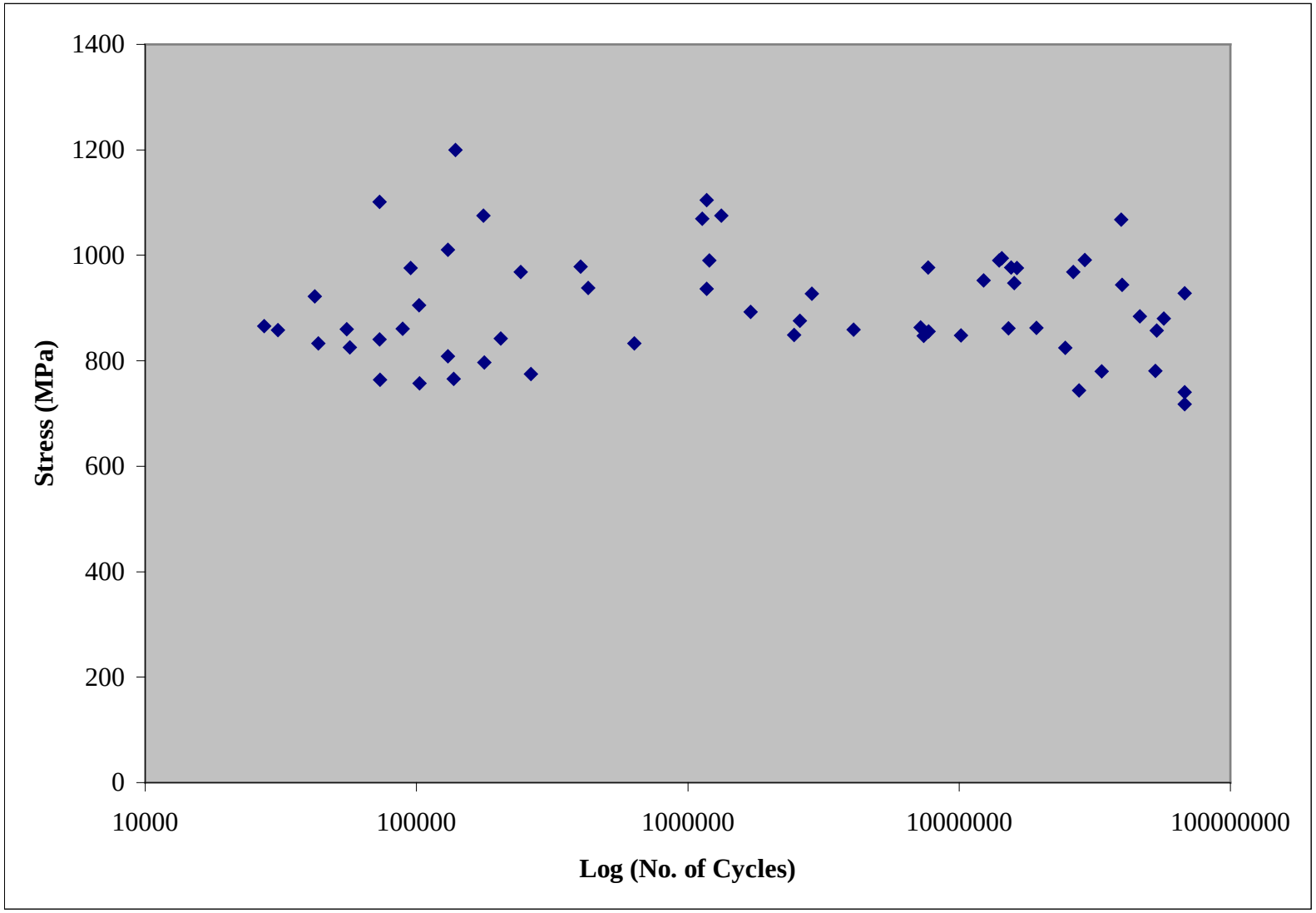

Fig B2: S-N Graph for Shot Peened Specimens

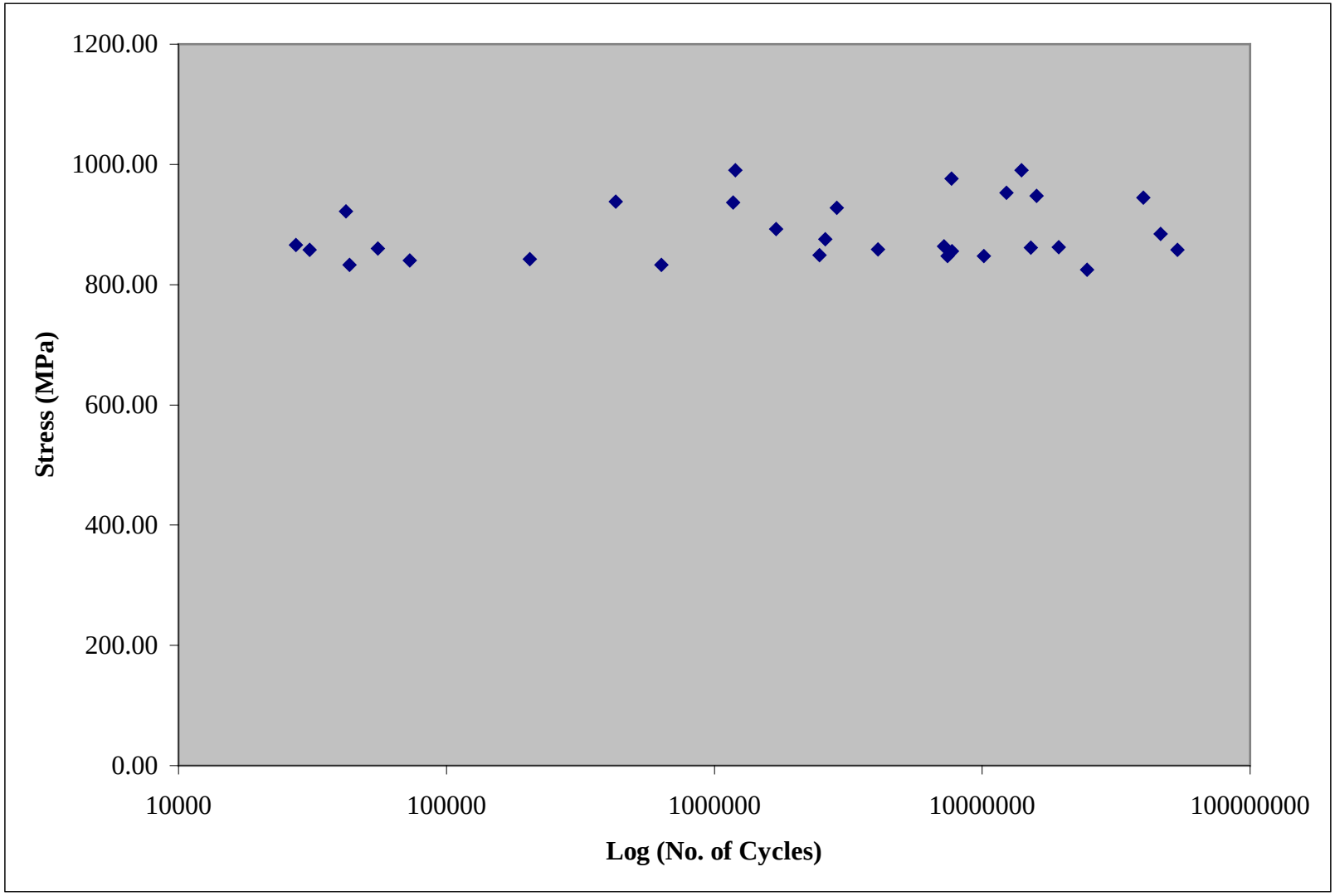

Fig B3: S-N Graph for Ground Specimens

APPENDIX C: SEM OF EDWC SPECIMENS

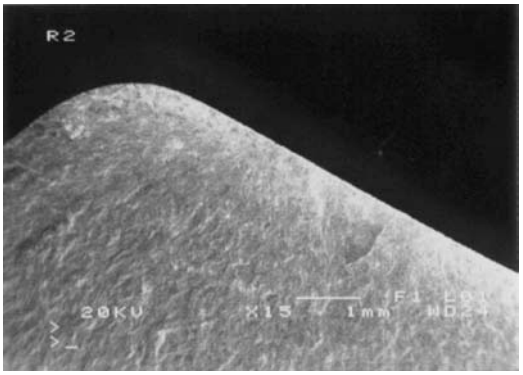

Specimen R2 X 15

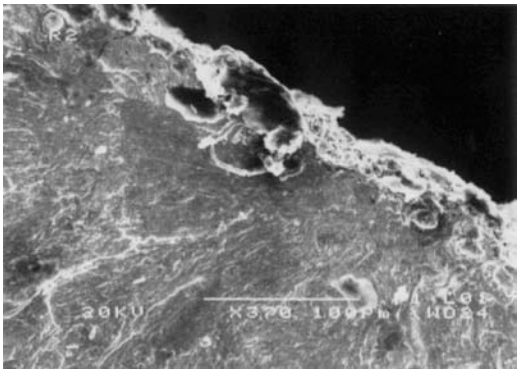

Specimen R2 X 370

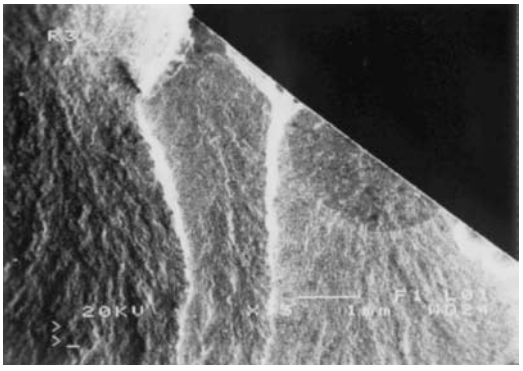

Specimen R3 X 15

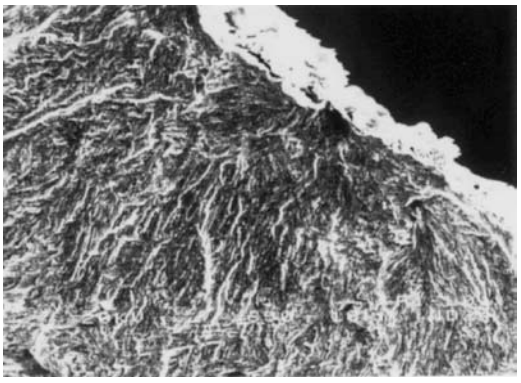

Specimen R3 X 650

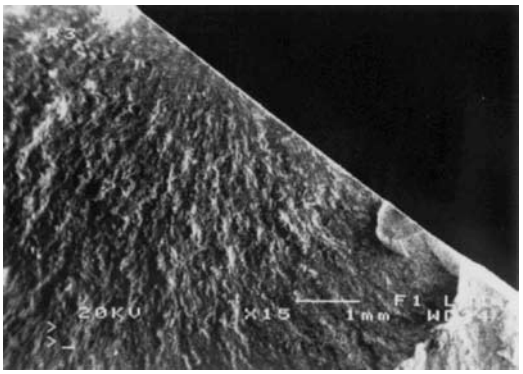

Specimen R3 X 15

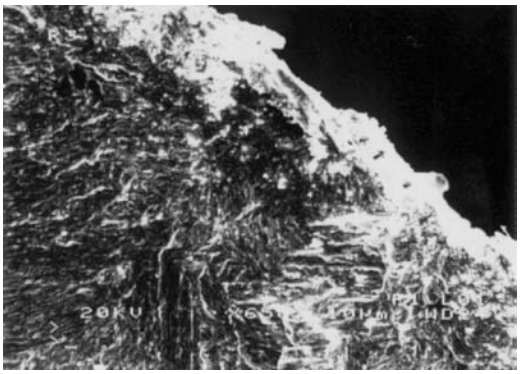

Specimen R3 X 650

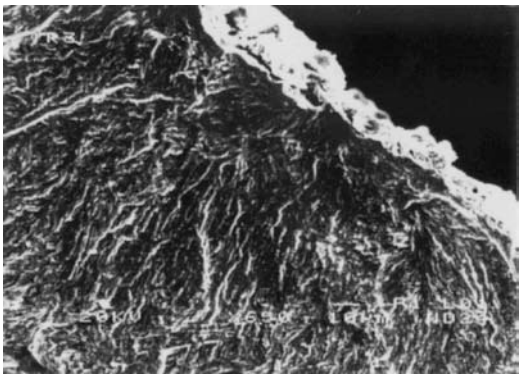

Specimen R3 X 650

Specimen 1,1 X 15

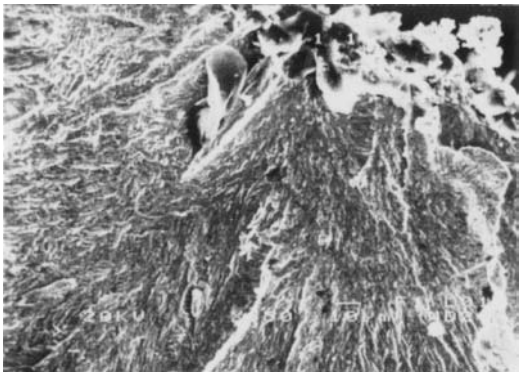

Specimen 1,1 X 650

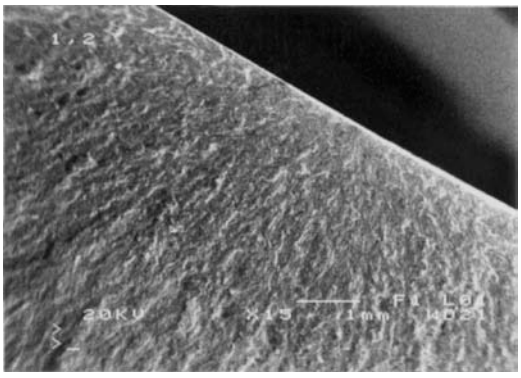

Specimen 1,2 X 15

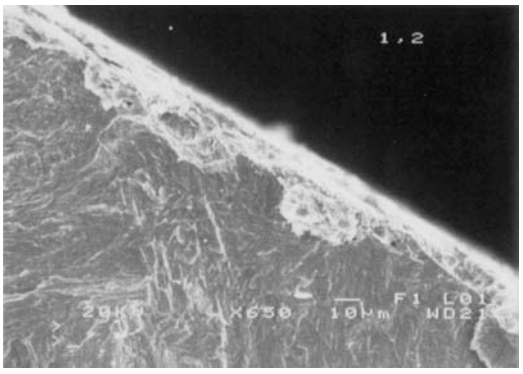

Specimen 1,2 X 650

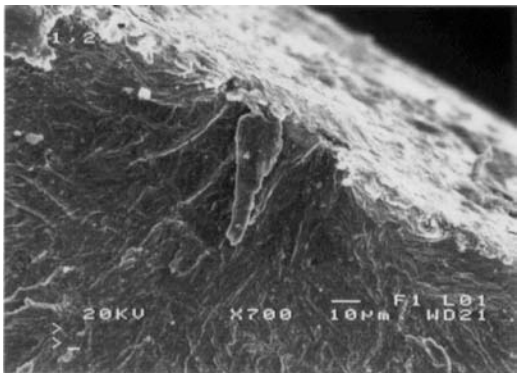

Specimen 1,2 X 700

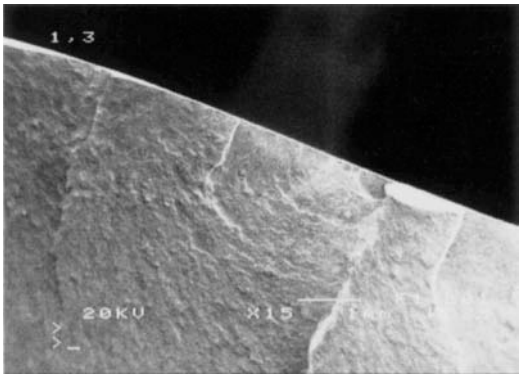

Specimen 1,3 X 15

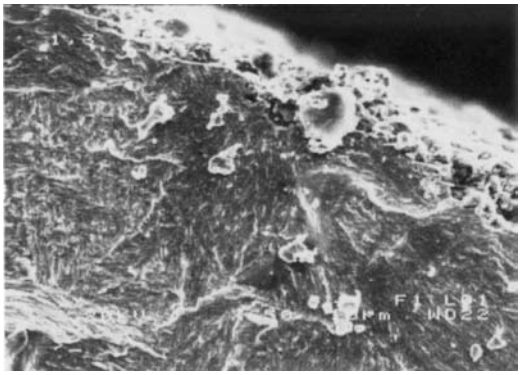

Specimen 1,3 X 650

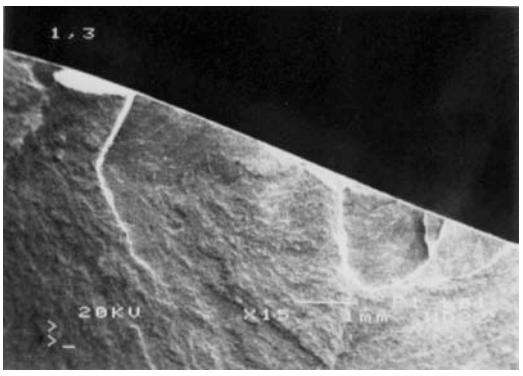

Specimen 1,3 X 15

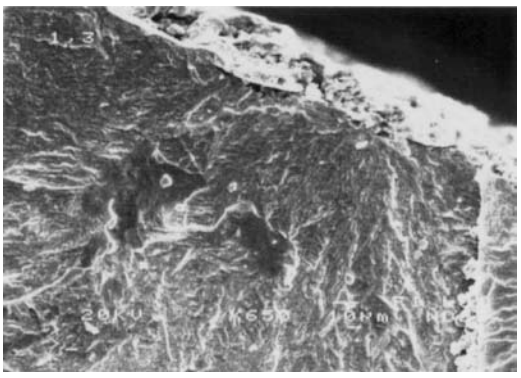

Specimen 1,3 X 650

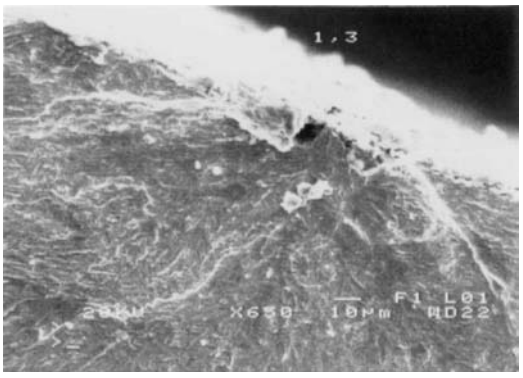

Specimen 1,3 X 650

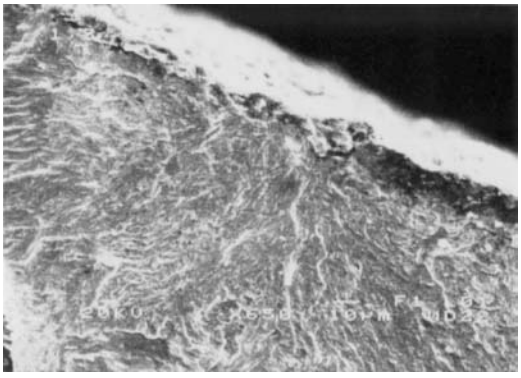

Specimen 1,3 X 650

Specimen 1,3 X 650

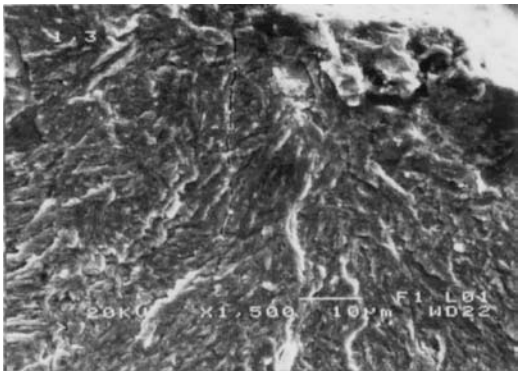

Specimen 1,3 X1,500

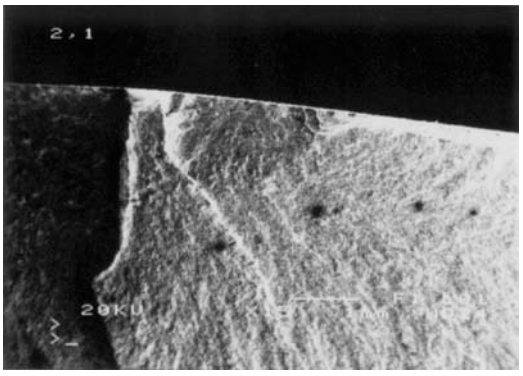

Specimen 2,1 X 15

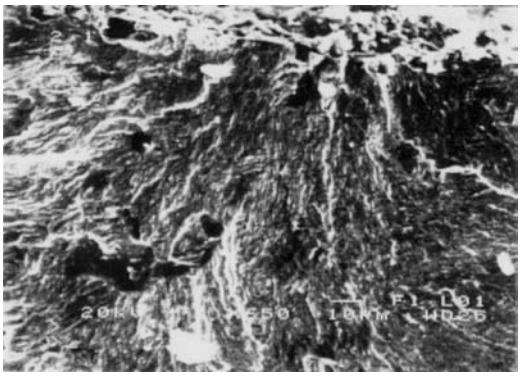

Specimen 2,1 X 650

Specimen 2,1 X 650

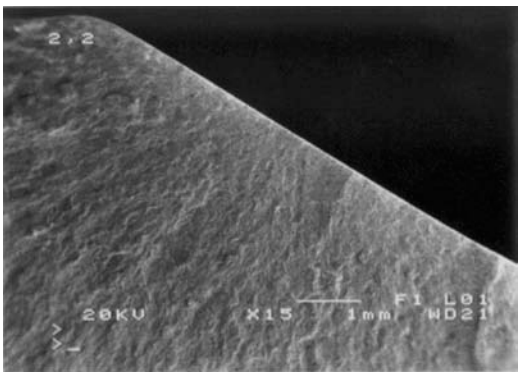

Specimen 2,2 X 15

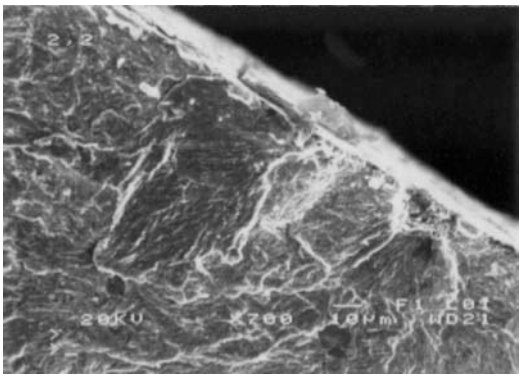

Specimen 2,2 X 700

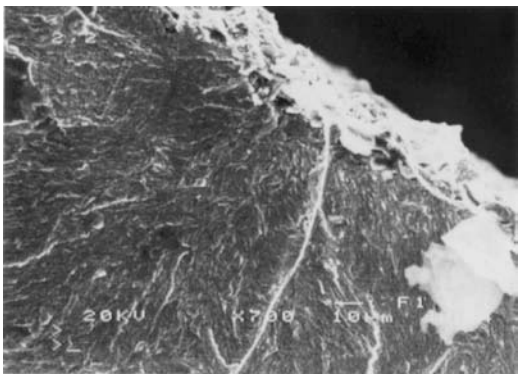

Specimen 2,2 X 700

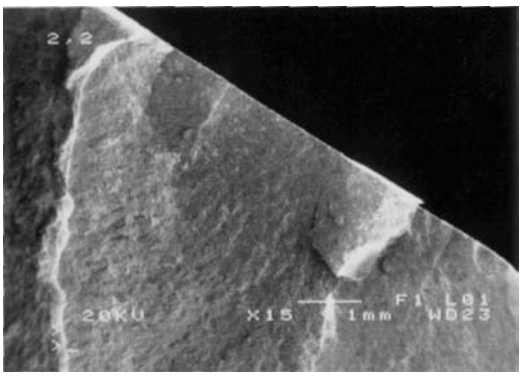

Specimen 2,2 X 15

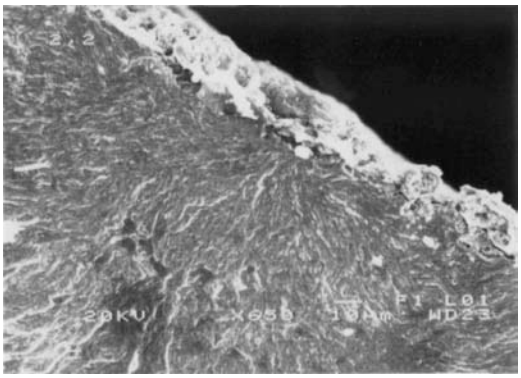

Specimen 2,2 X 650

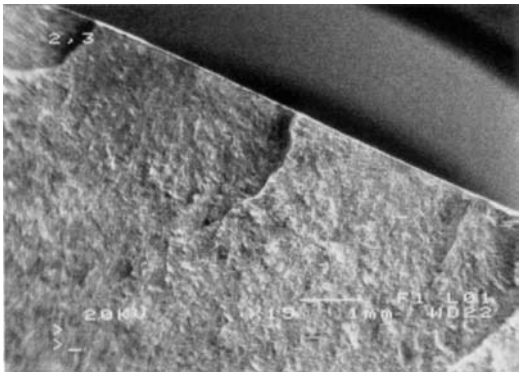

Specimen 2,3 X 15

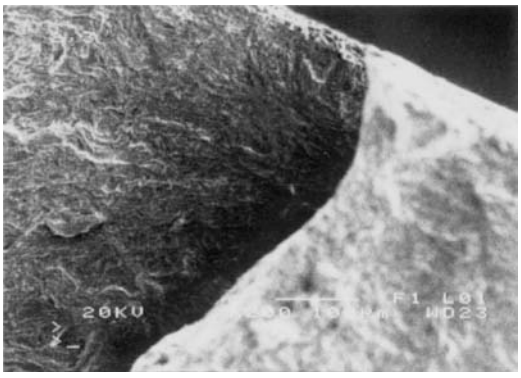

Specimen 2,3 X 200

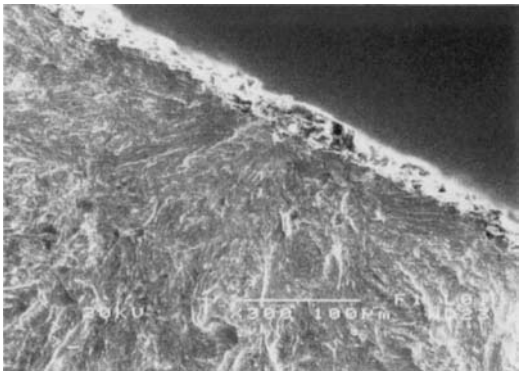

Specimen 2,3 X 300

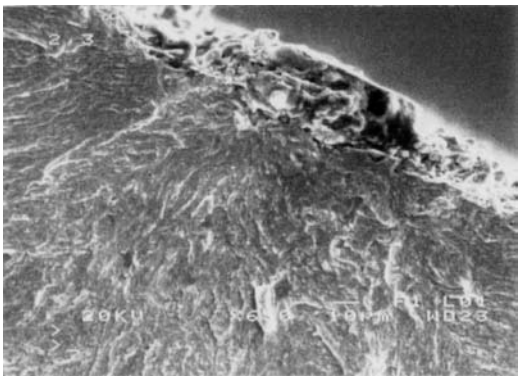

Specimen 2,3 X 650

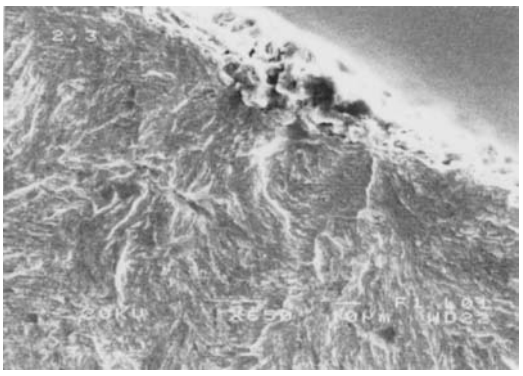

Specimen 2,3 X 650

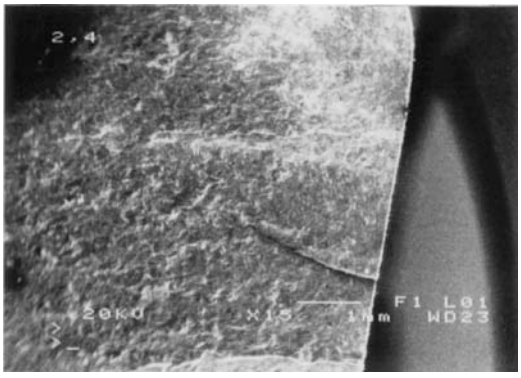

Specimen 2,4 X 15

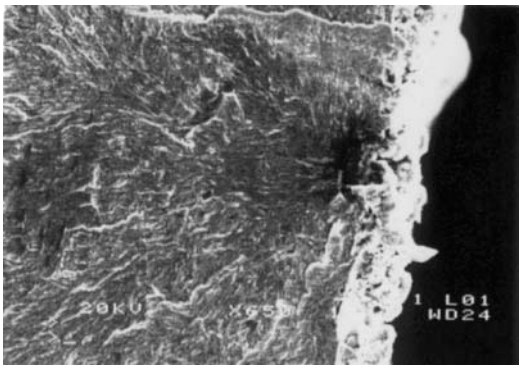

Specimen 2,4 X 650

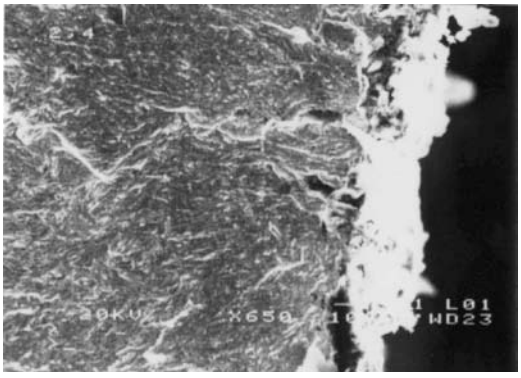

Specimen 2,4 X 650

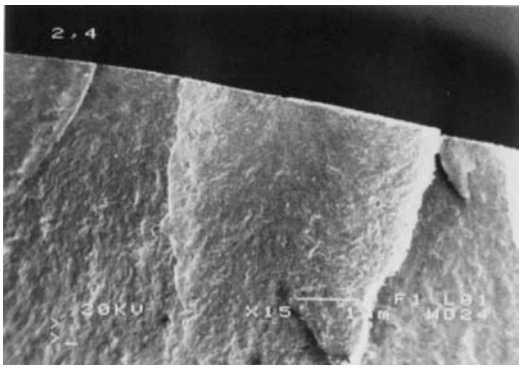

Specimen 2,4 X 15

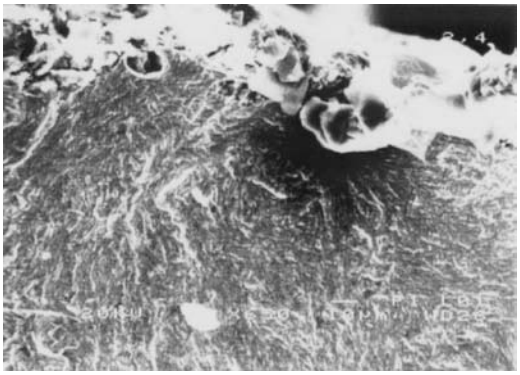

Specimen 2,4 X 650

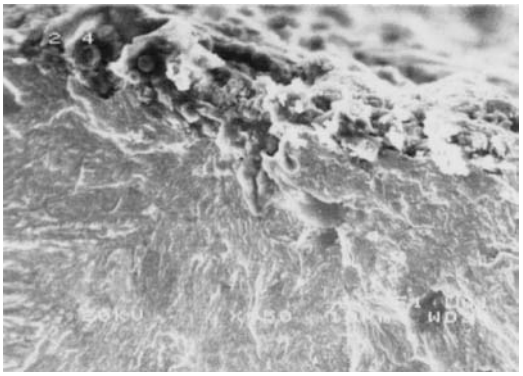

Specimen 2,4 X 650

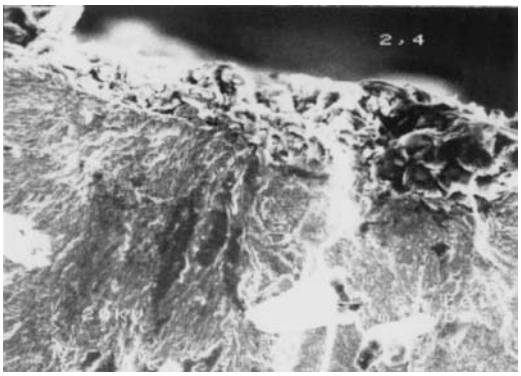

Specimen 2,4 X 650

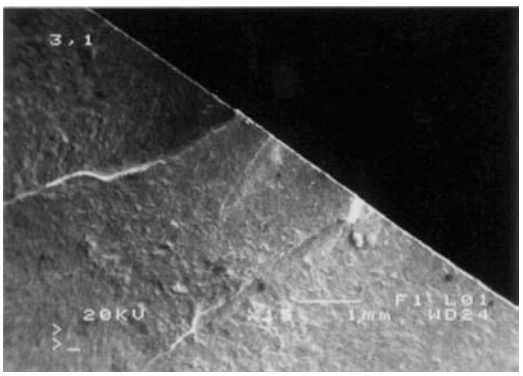

Specimen 3,1 X 15

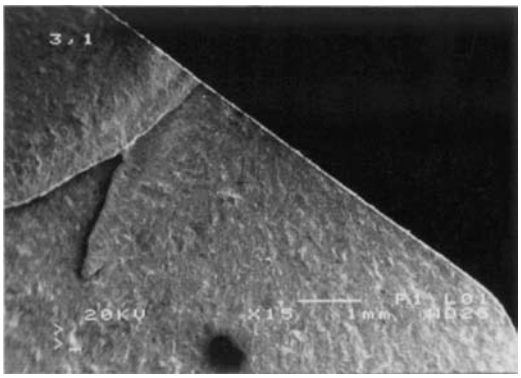

Specimen 3,1 X 15

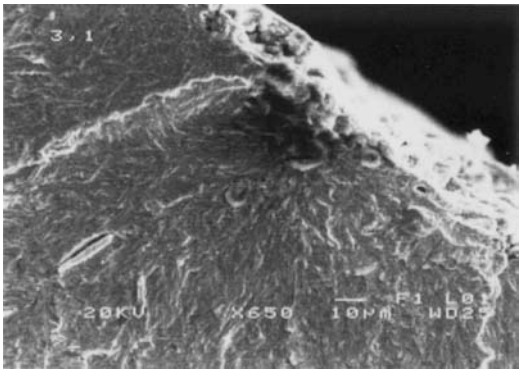

Specimen 3,1 X 650

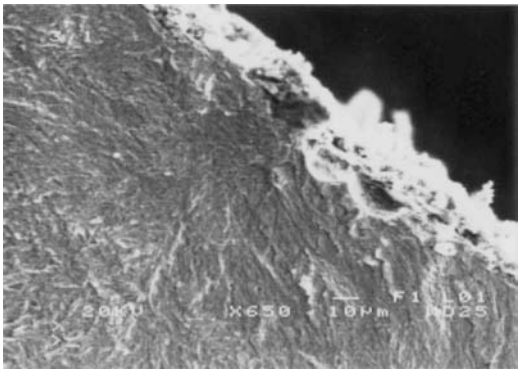

Specimen 3,1 X 650

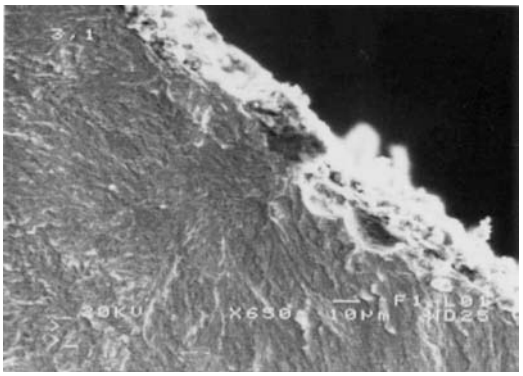

Specimen 3,1 X 650

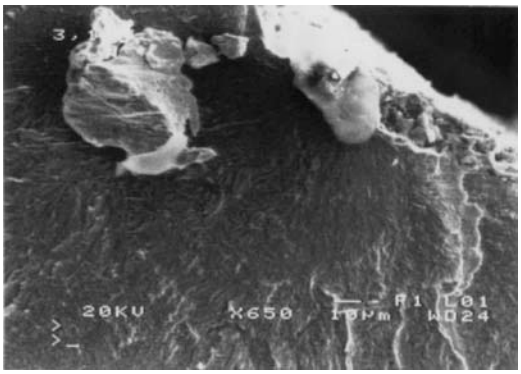

Specimen 3,1 X 650

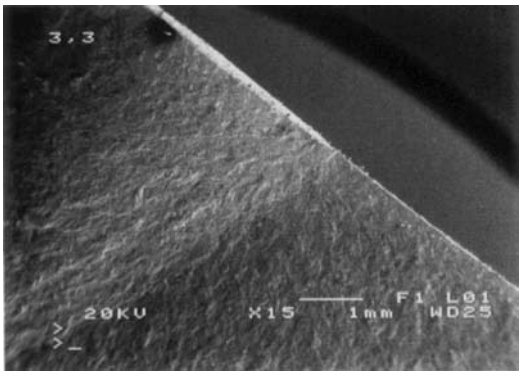

Specimen 3,3 X 15

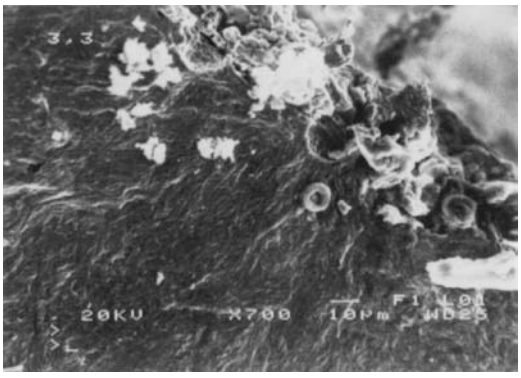

Specimen 3,3 X 15

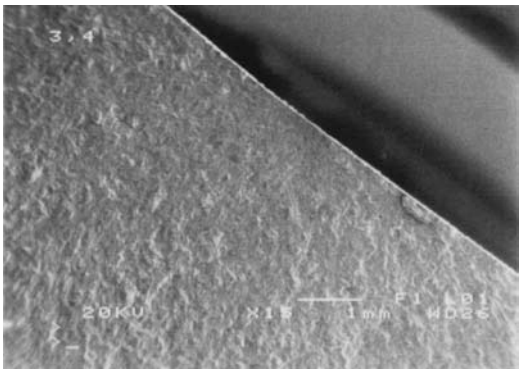

Specimen 3,4 X 15

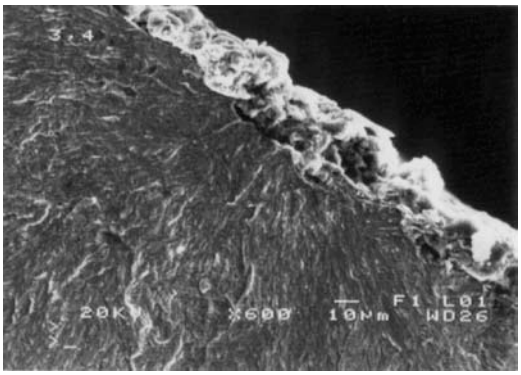

Specimen 3,4 X 600

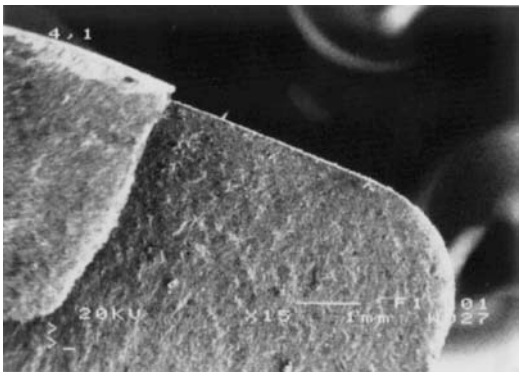

Specimen 4,1 X 15

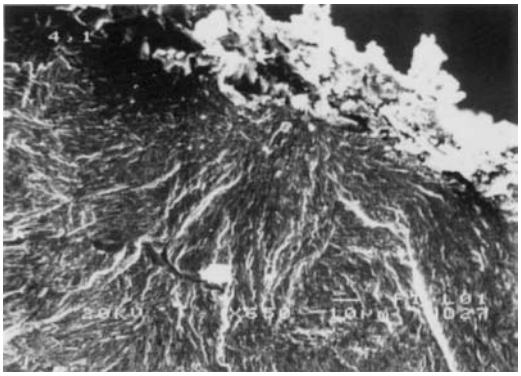

Specimen 4,1 X 650

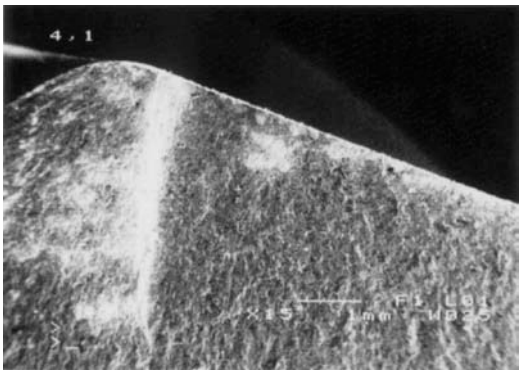

Specimen 4,1 X 15

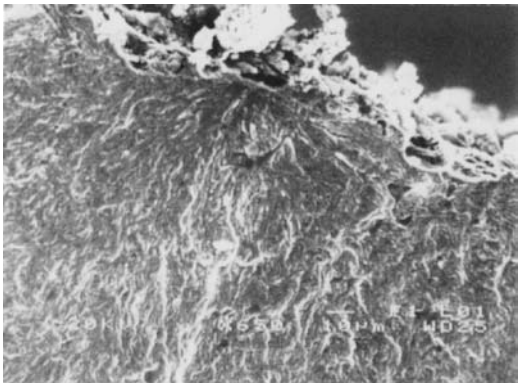

Specimen 4,1 X 650

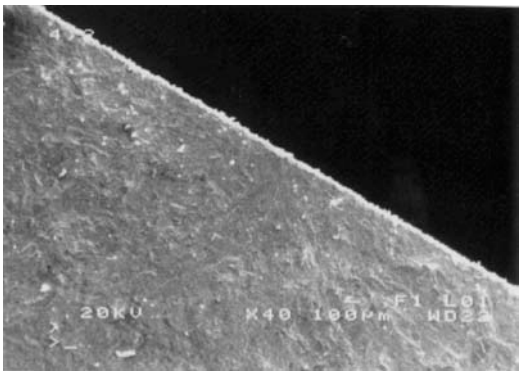

Specimen 4,2 X 40

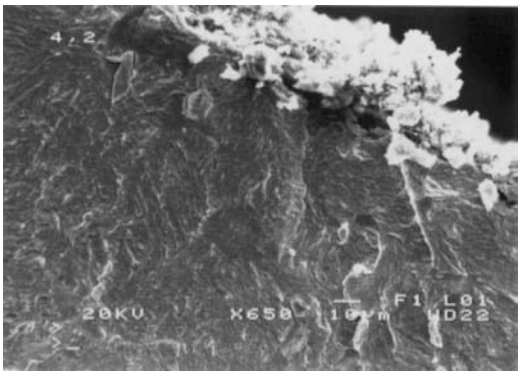

Specimen 4,2 X 650

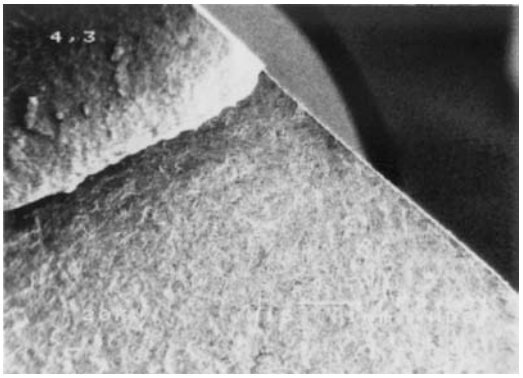

Specimen 4,3 X 15

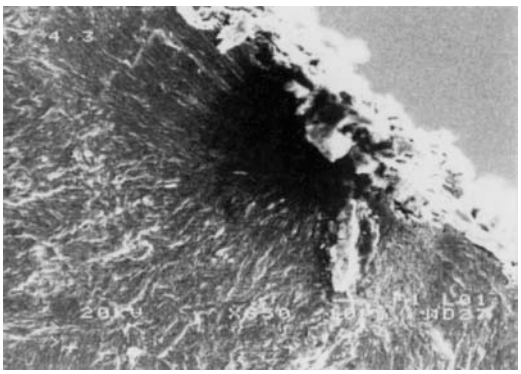

Specimen 4,3 X 650

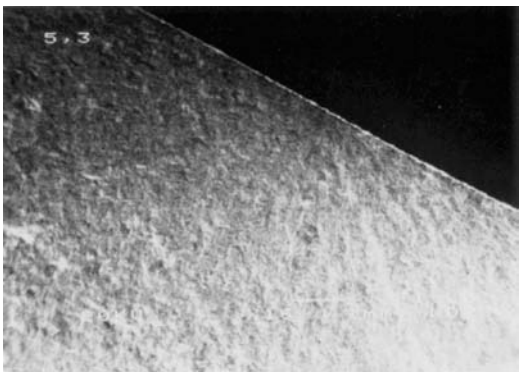

Specimen 5,3 X 16

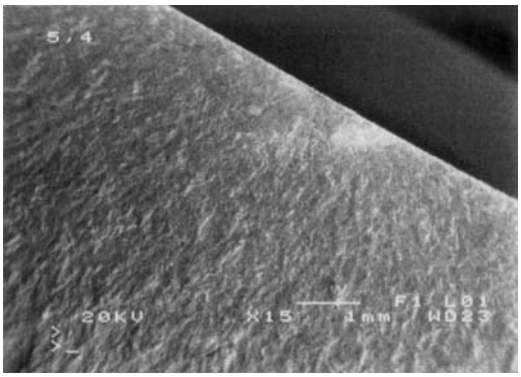

Specimen 5,4 X 15

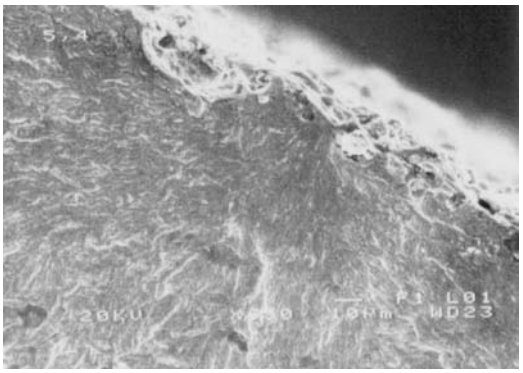

Specimen 5,4 X 650

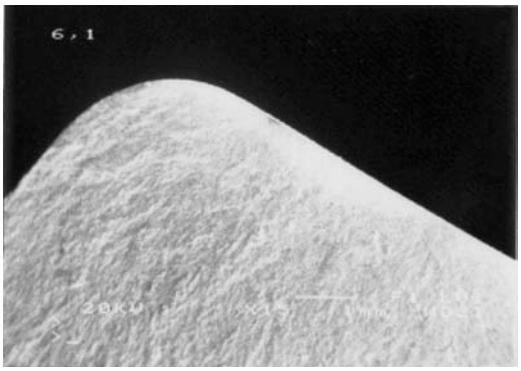

Specimen 6,1 X 15

Specimen 6,1 X 650

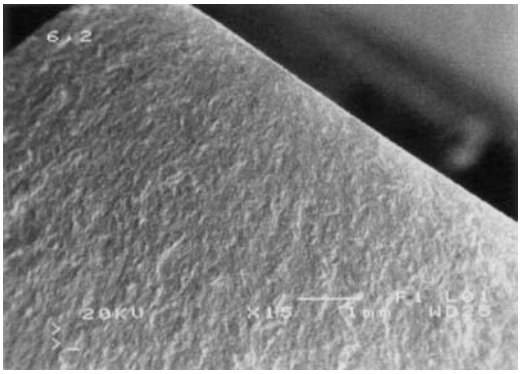

Specimen 6,2 X 15

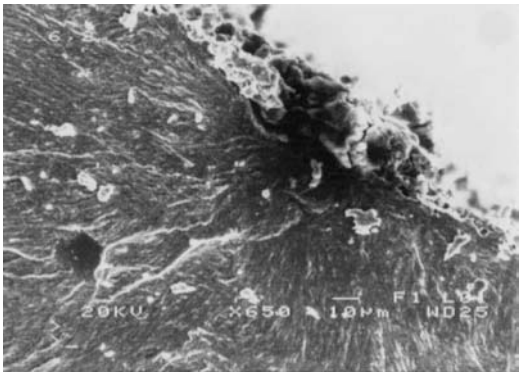

Specimen 6,2 X 650

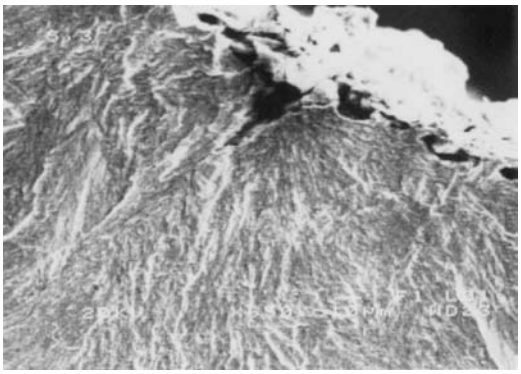

Specimen 6,3 X 650

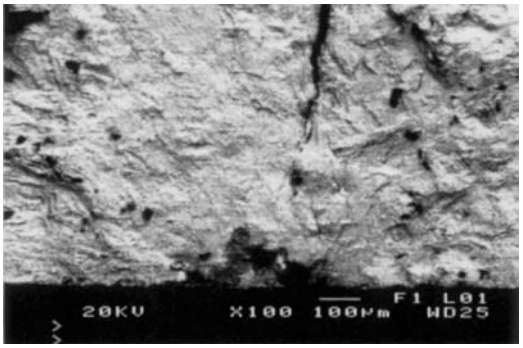

Specimen 1b X 100

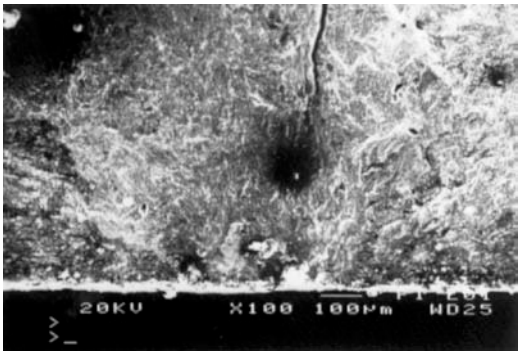

Specimen 1b X 100

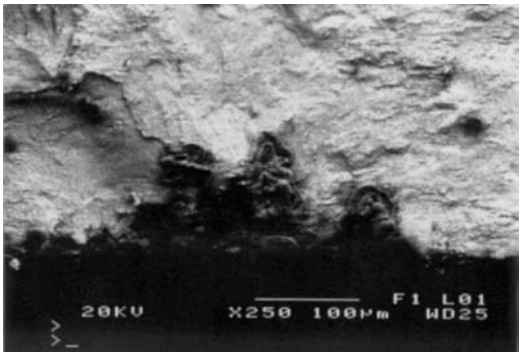

Specimen 1b X 250

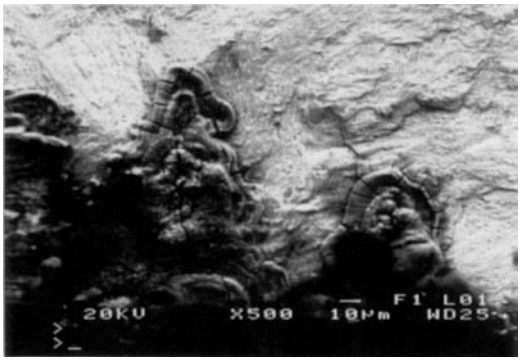

Specimen 1b X 500

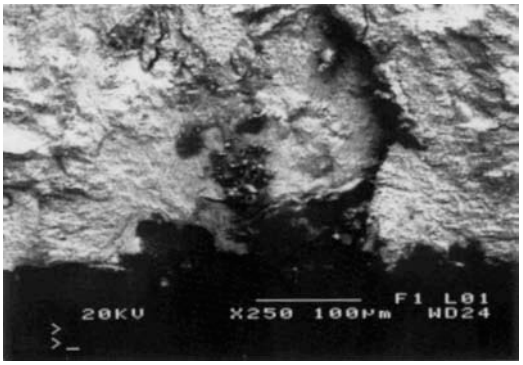

Specimen 1b X 250

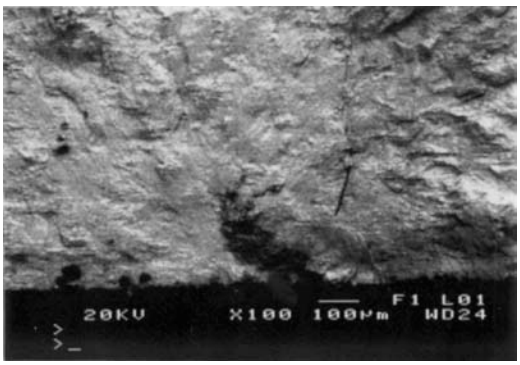

Specimen 1b X 100

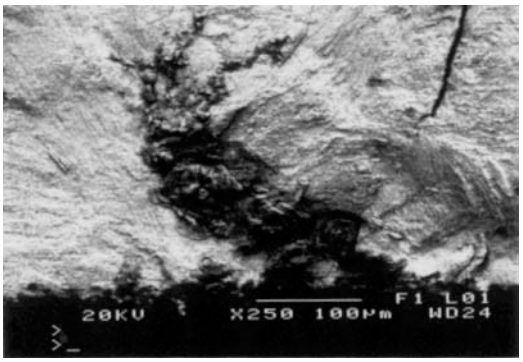

Specimen 1b X 250

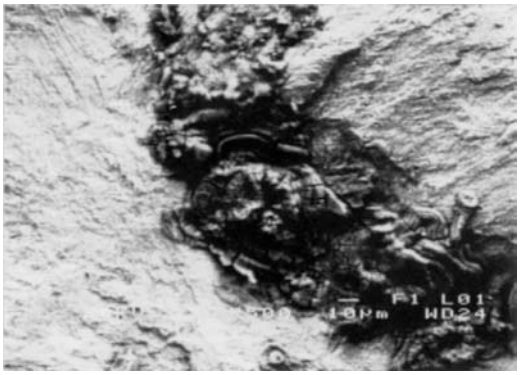

Specimen 1b X 500

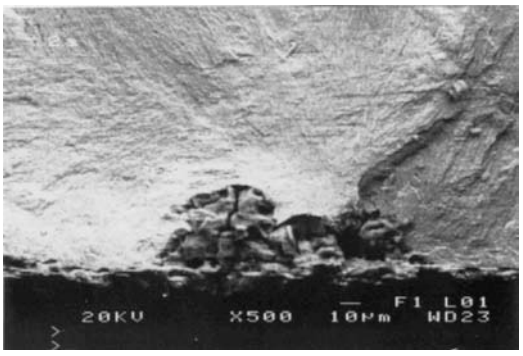

Specimen 2a X 500

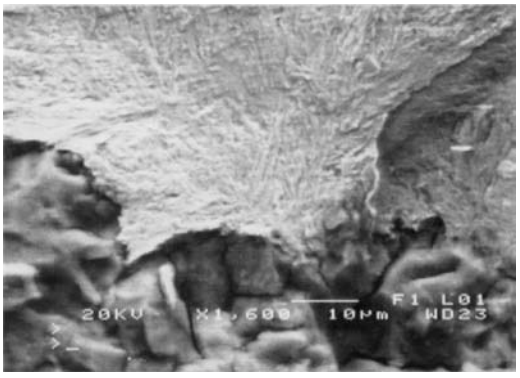

Specimen 2a X 1,600

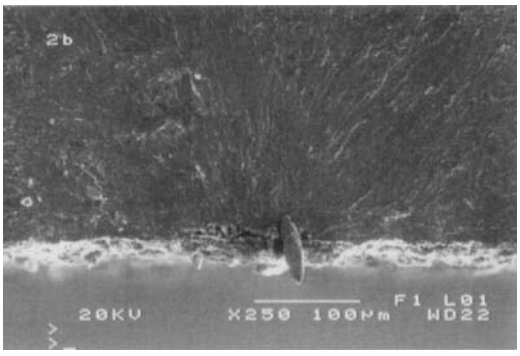

Specimen 2b X 250

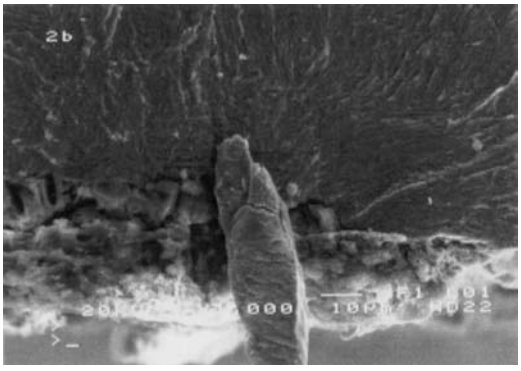

Specimen 2b X 1,000

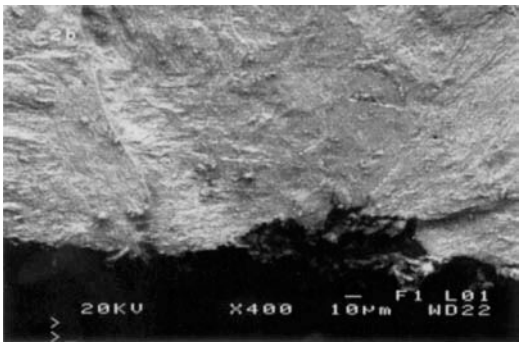

Specimen 2b X 400

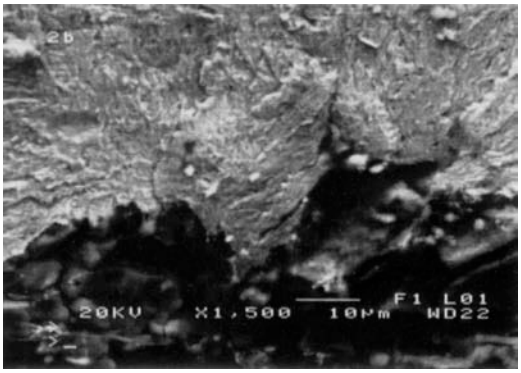

Specimen 2b X 1,500

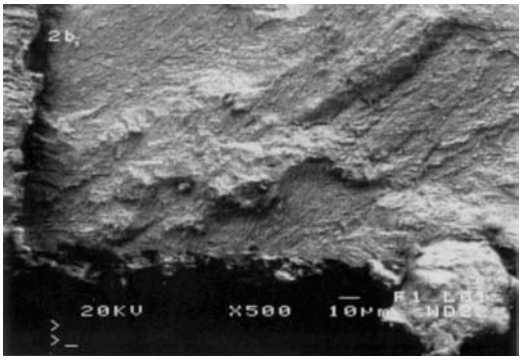

Specimen 2b X 500

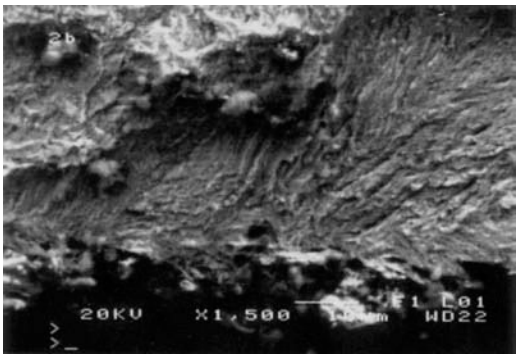

Specimen 2b X 1,500

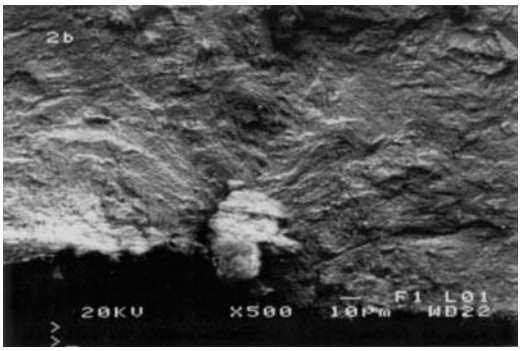

Specimen 2b X 500

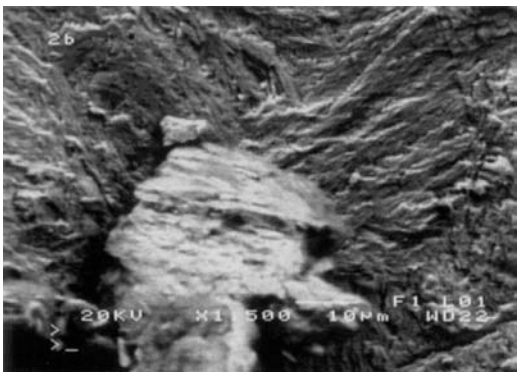

Specimen 2b X 1,500

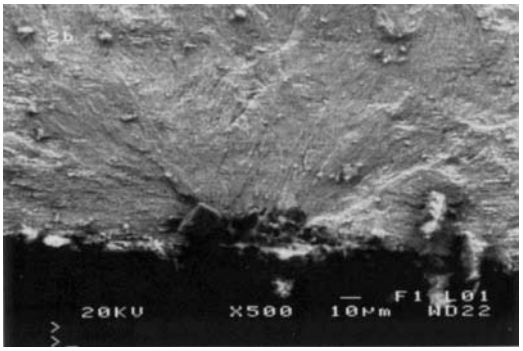

Specimen 2b X 500

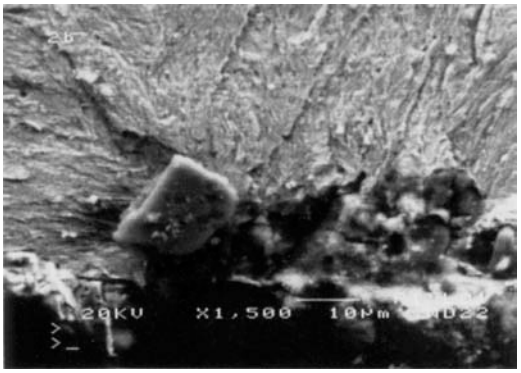

Specimen 2b X 1,500

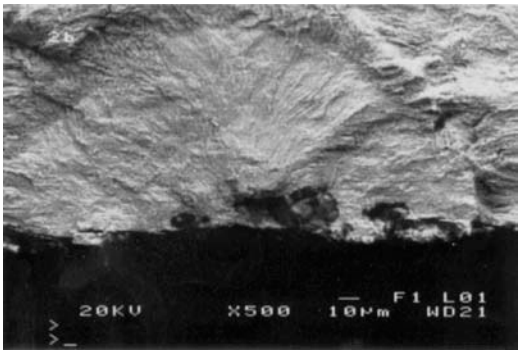

Specimen 2b X 500

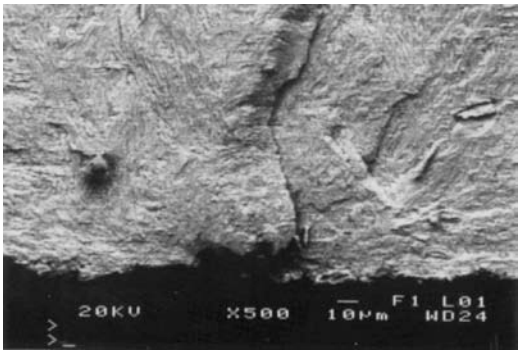

Specimen 2c X 500

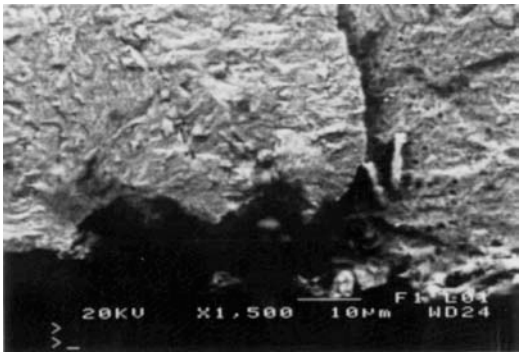

Specimen 2c X 1,500

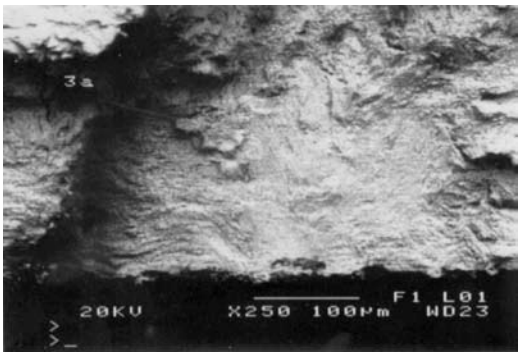

Specimen 3a X 250

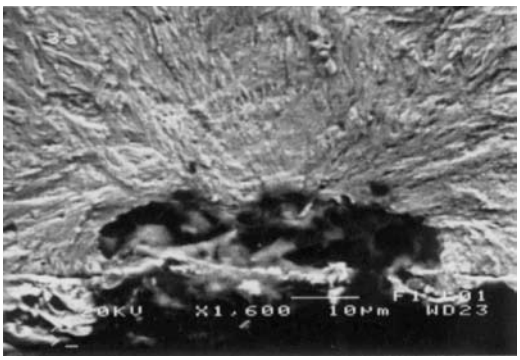

Specimen 3a X 1,600

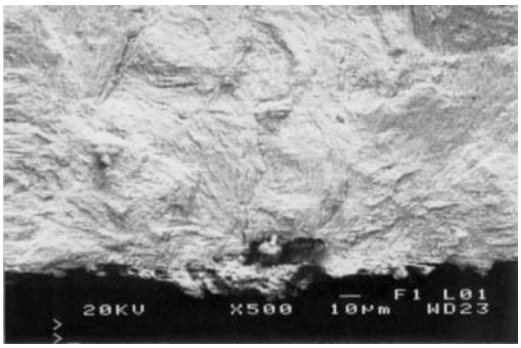

Specimen 3a X 500

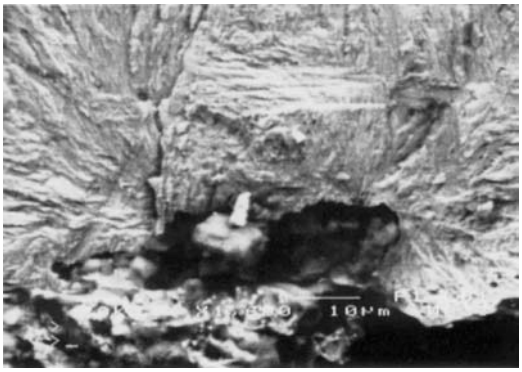

Specimen 3a X 1,600

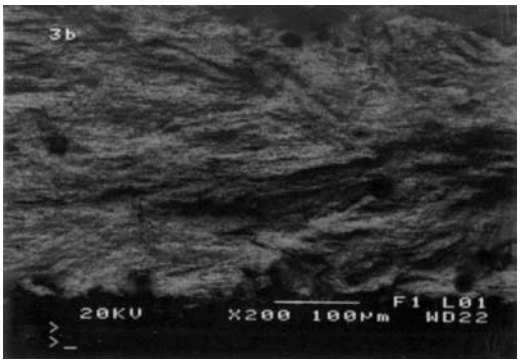

Specimen 3b X 200

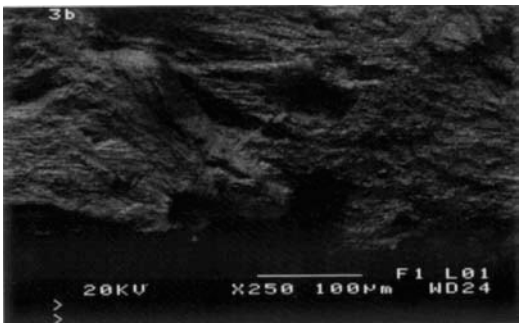

Specimen 3b X 250

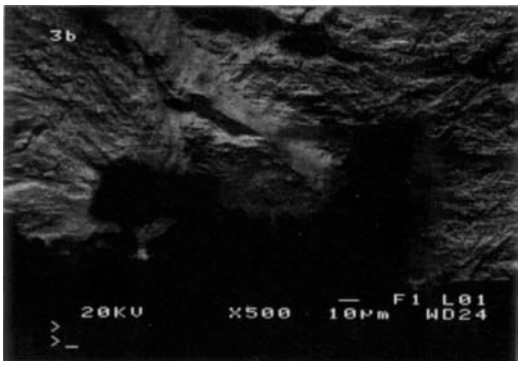

Specimen 3b X 500

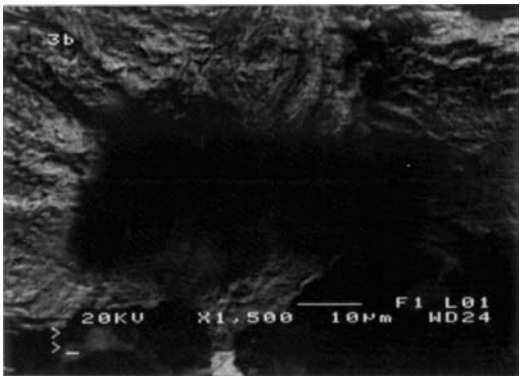

Specimen 3b X 1,500

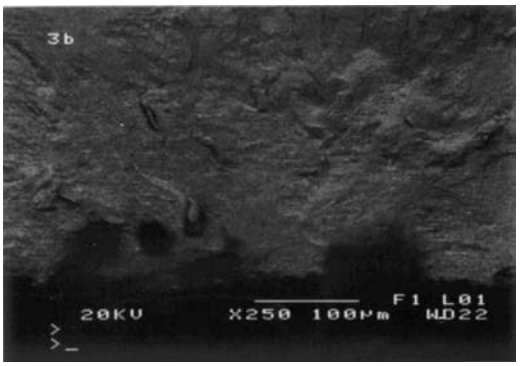

Specimen 3b X 250

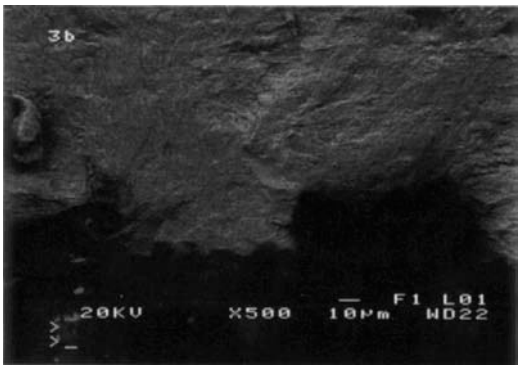

Specimen 3b X 500

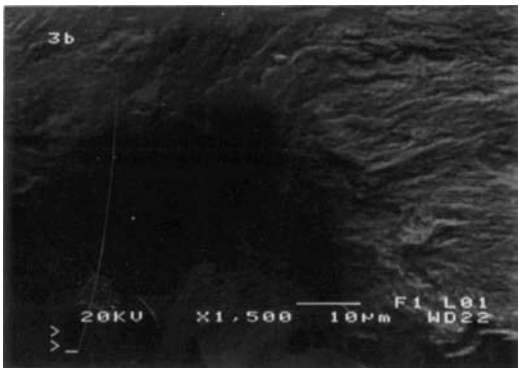

Specimen 3b X 1,500

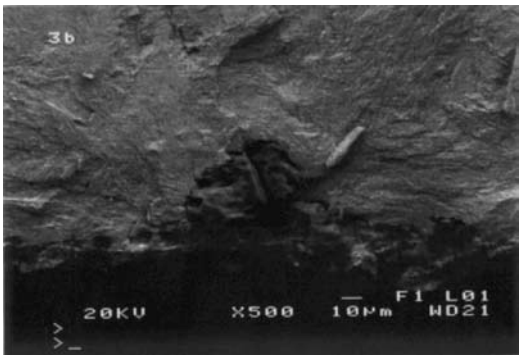

Specimen 3b X 500

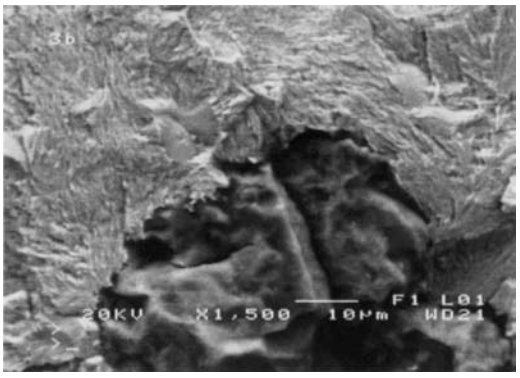

Specimen 3b X 1,500

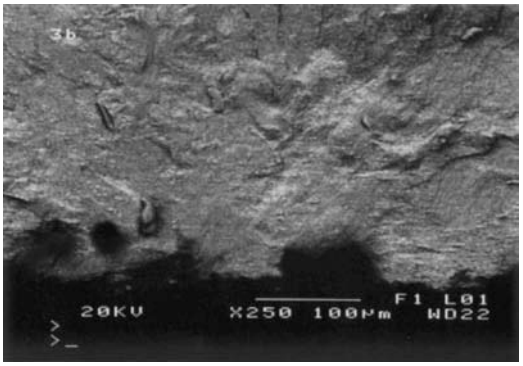

Specimen 3b X 250

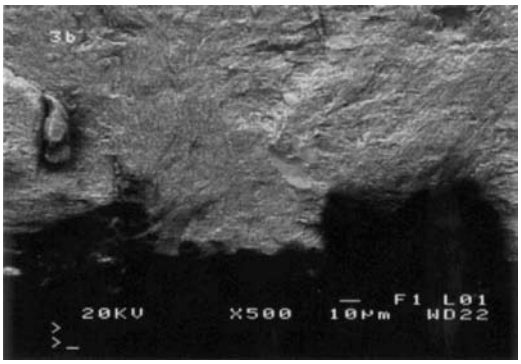

Specimen 3b X 500

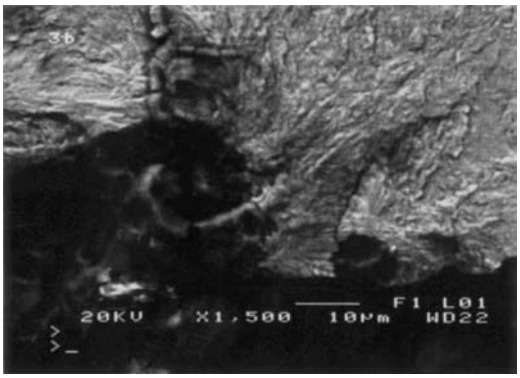

Specimen 3b X 1,500

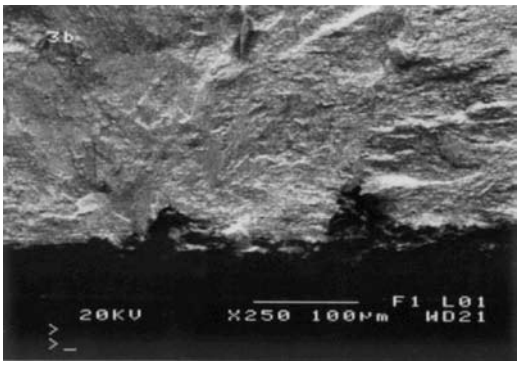

Specimen 3b X 250

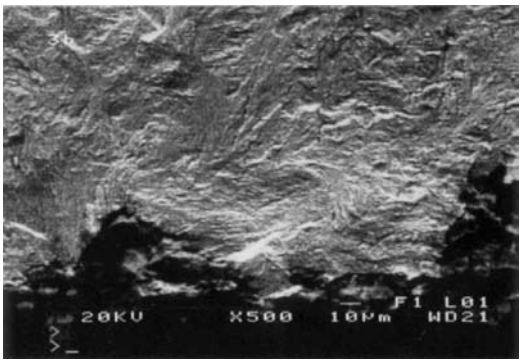

Specimen 3b X 500

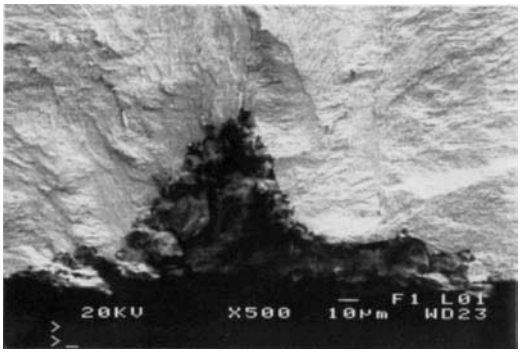

Specimen 4a X 500

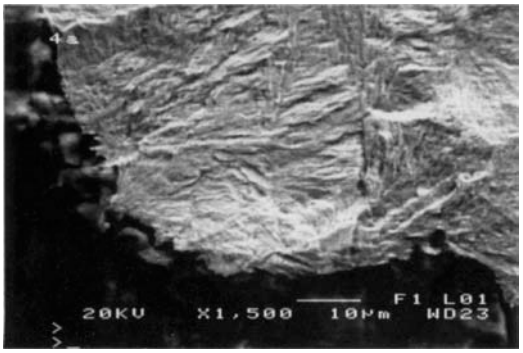

Specimen 4a X 1,500

Specimen 4b X 100

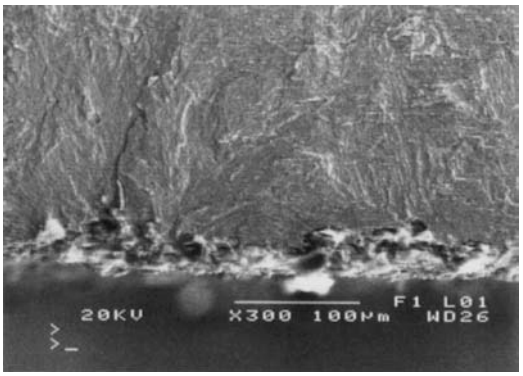

Specimen 4b X 300

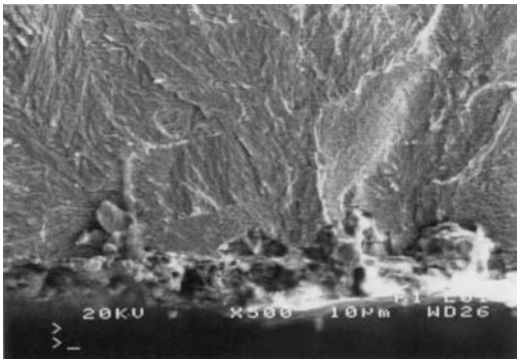

Specimen 4b X 500

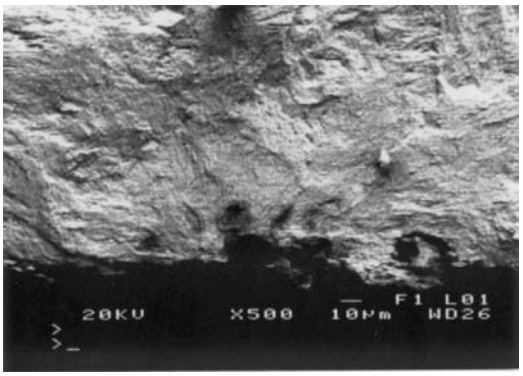

Specimen 4b X 500

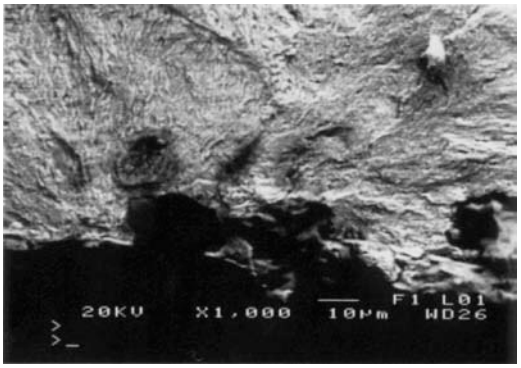

Specimen 4b X 1,000

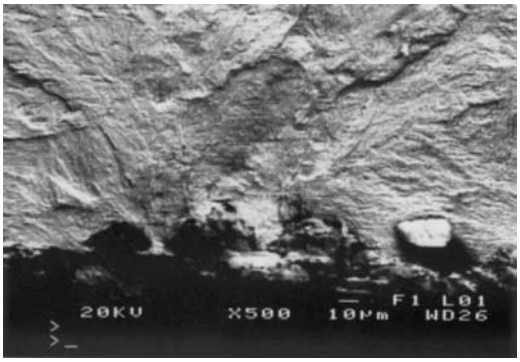

Specimen 4b X 500

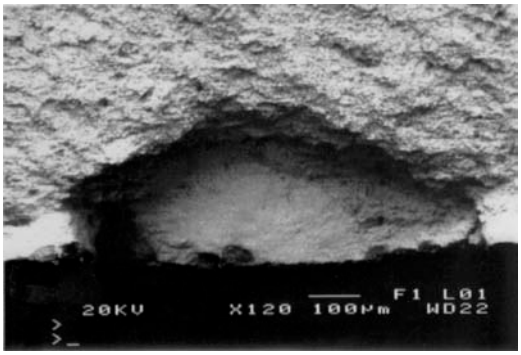

Specimen 5a X 120

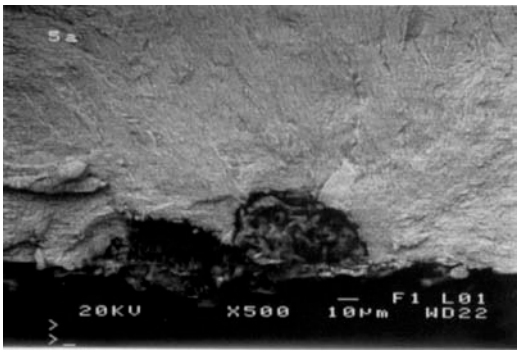

Specimen 5a X 500

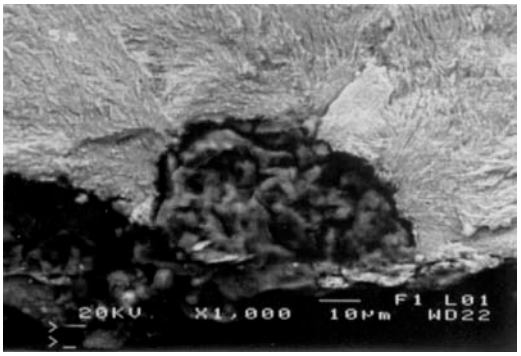

Specimen 5a X 1,000

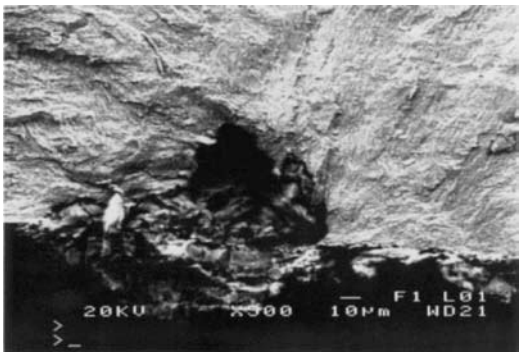

Specimen 5a X 500

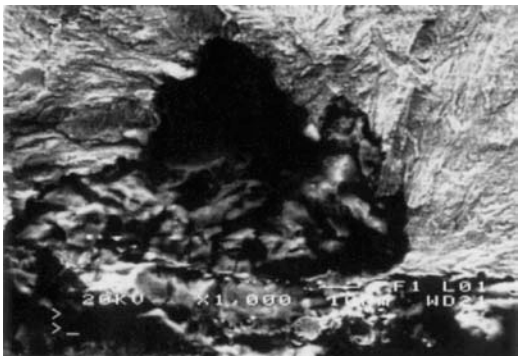

Specimen 5a X 1,000

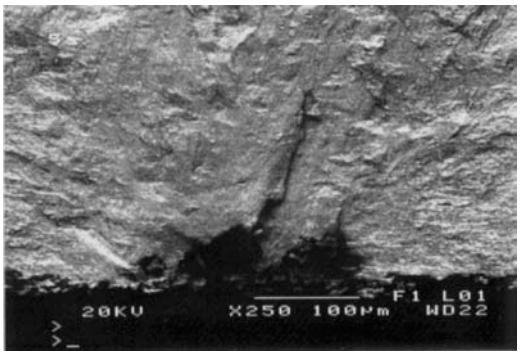

Specimen 5a X 250

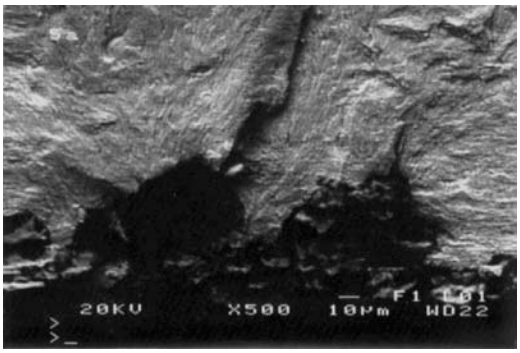

Specimen 5a X 500

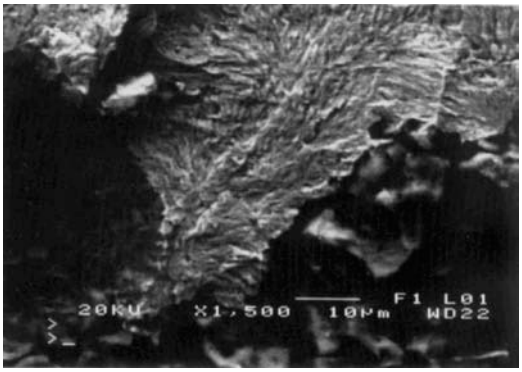

Specimen 5a X 1,500

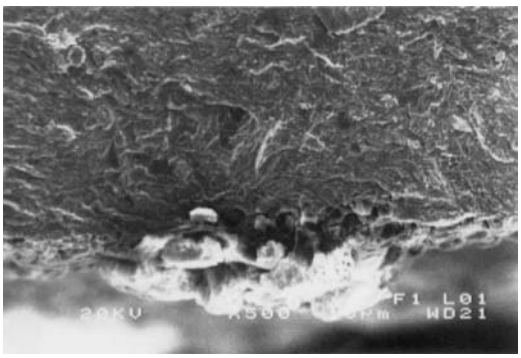

Specimen 5a X 500

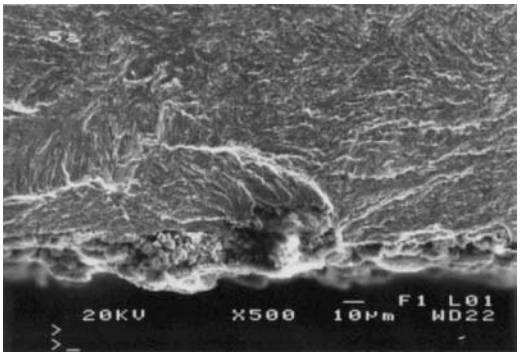

Specimen 5a X 500

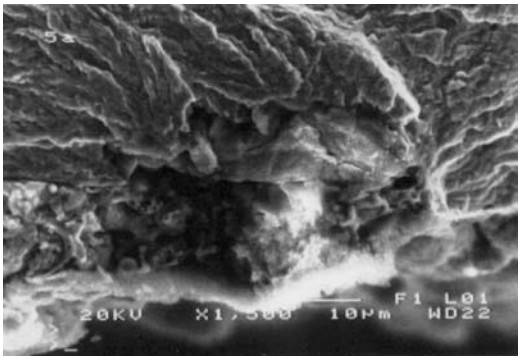

Specimen 5a X 1,500

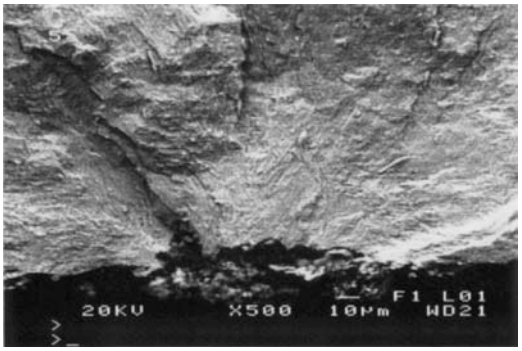

Specimen 5a X 500

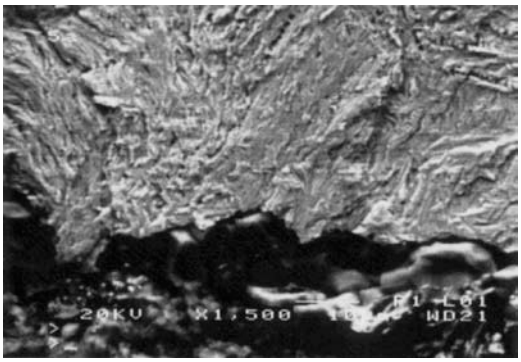

Specimen 5a X 500

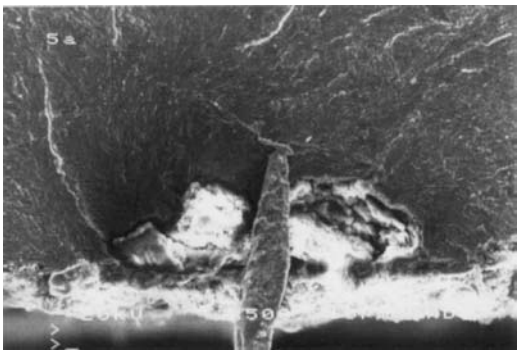

Specimen 5a X 500

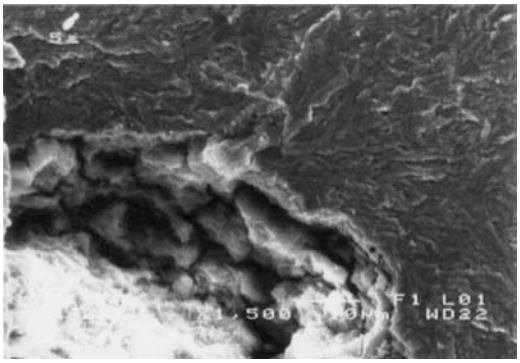

Specimen 5a X 1,500

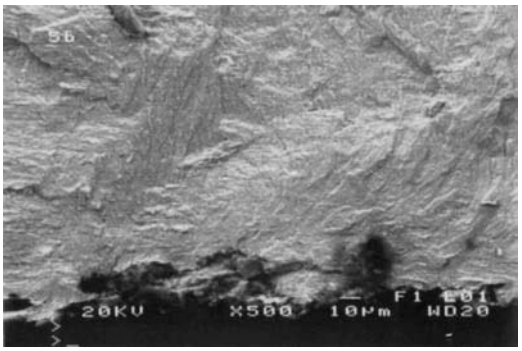

Specimen 5b X 500

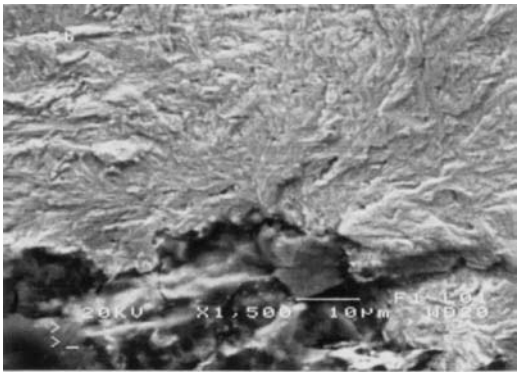

Specimen 5b X 1,500

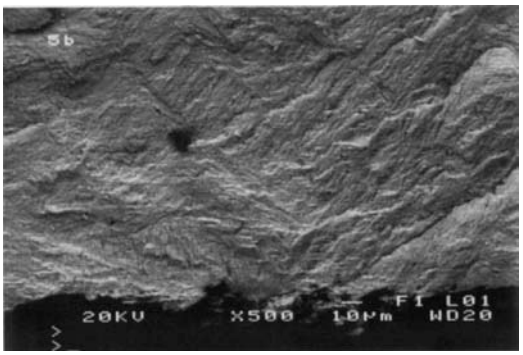

Specimen 5b X 500

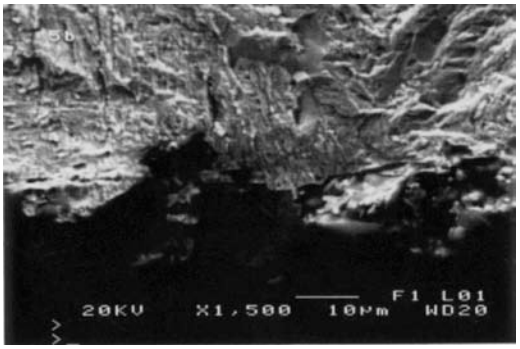

Specimen 5b X 1,500

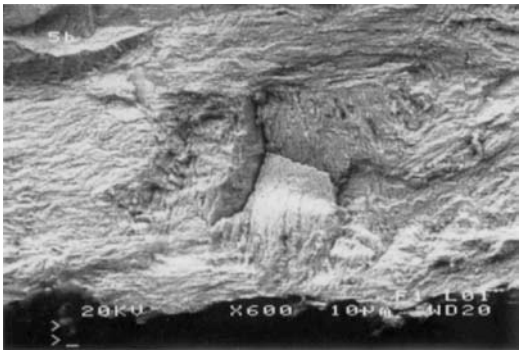

Specimen 5b X 500

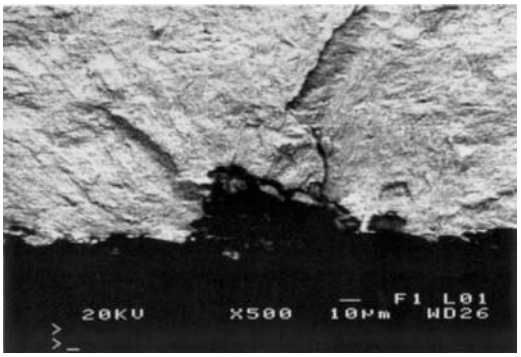

Specimen 6a X 500

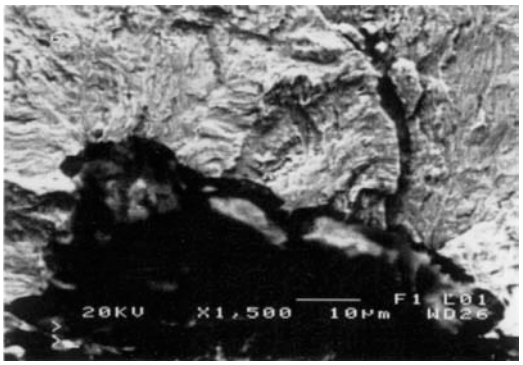

Specimen 6a X 1,500

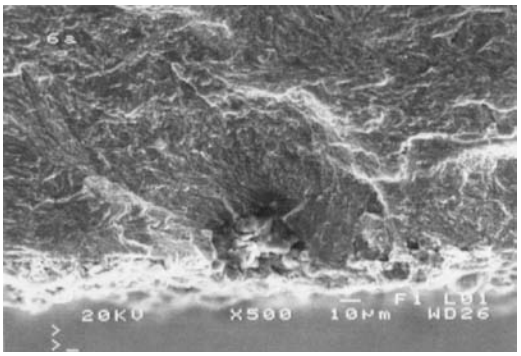

Specimen 6a X 500

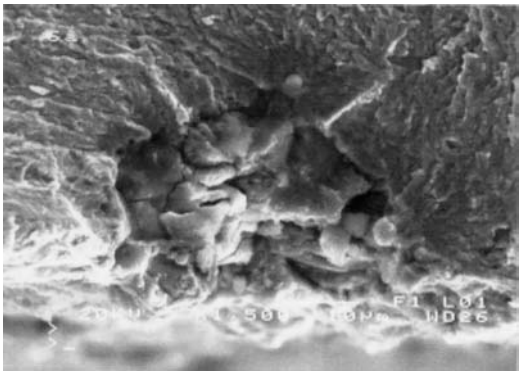

Specimen 6a X 1,500

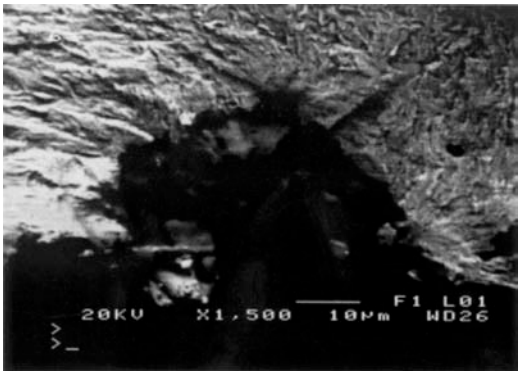

Specimen 6a X 1,500

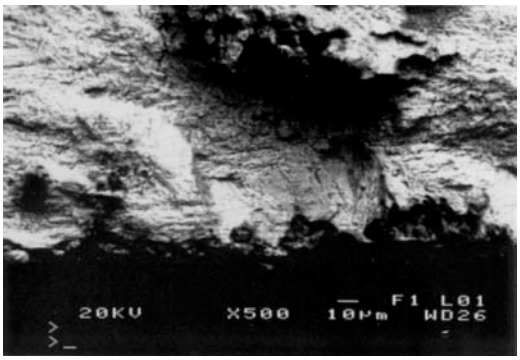

Specimen 6a X 500

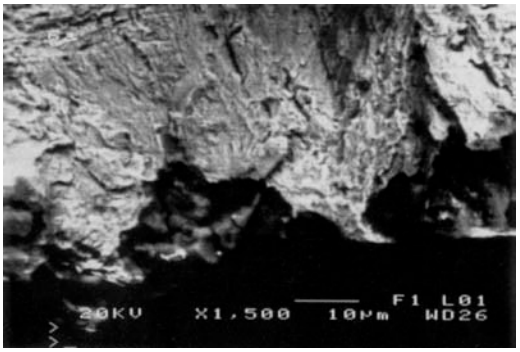

Specimen 6a X 1,500

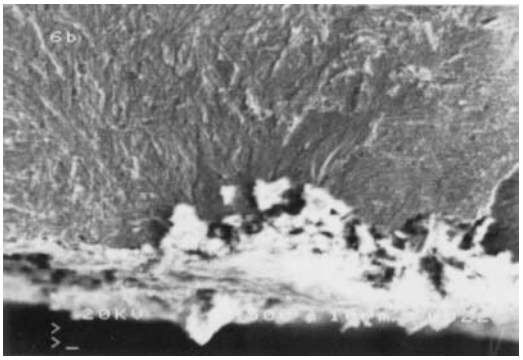

Specimen 6b X 500

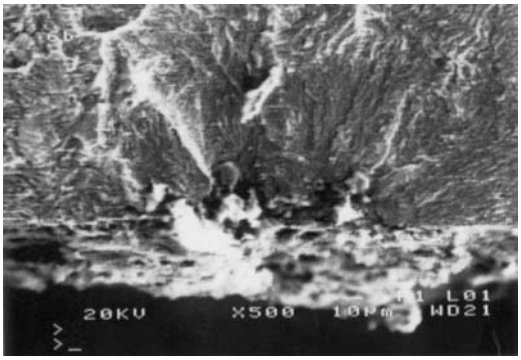

Specimen 6b X 500

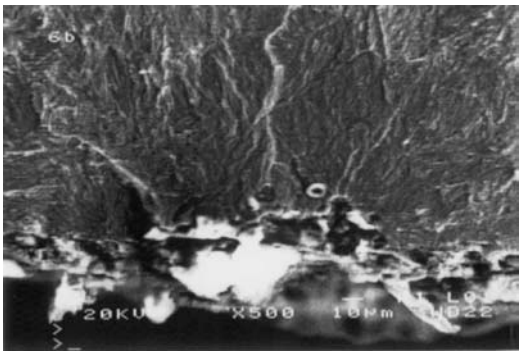

Specimen 6b X 500

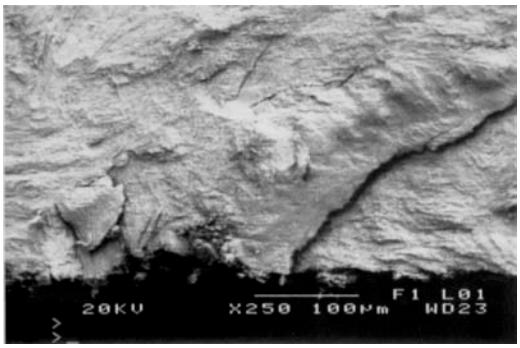

Specimen 7a X 250

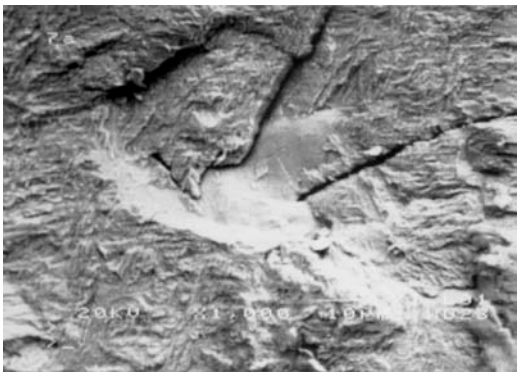

Specimen 7a X 1,000

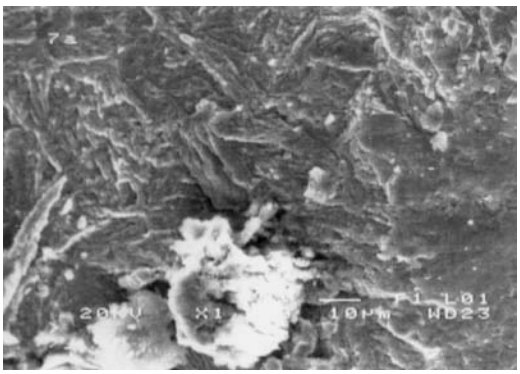

Specimen 7a X 1,000

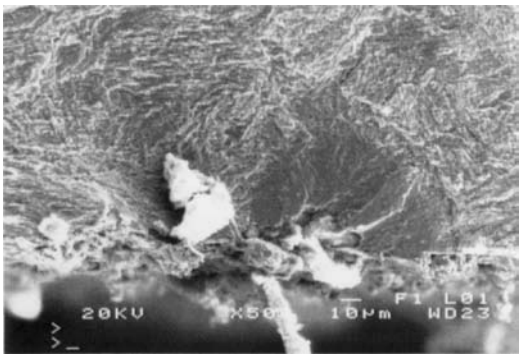

Specimen 7a X 500

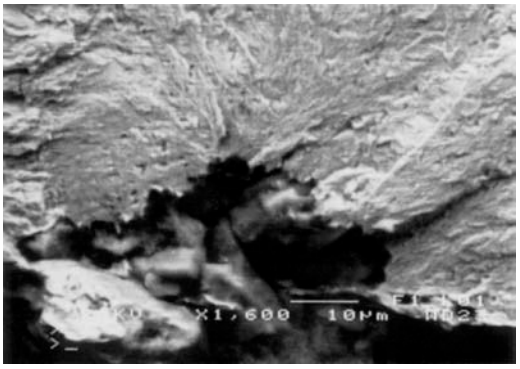

Specimen 7a X 1,600

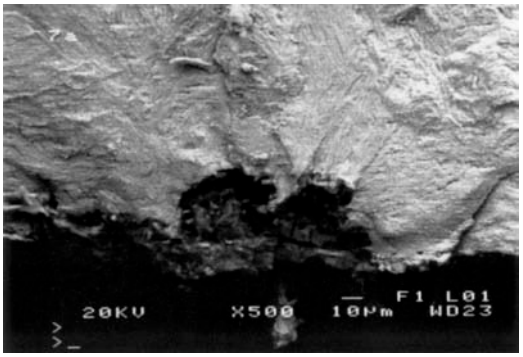

Specimen 7a X 500

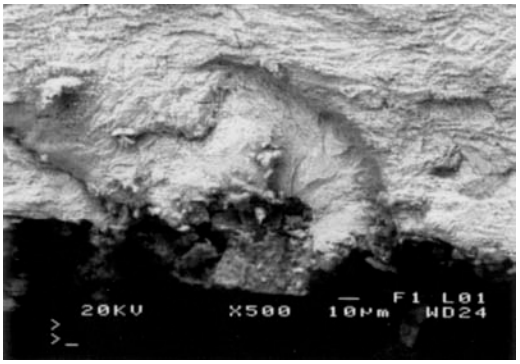

Specimen 7a X 500

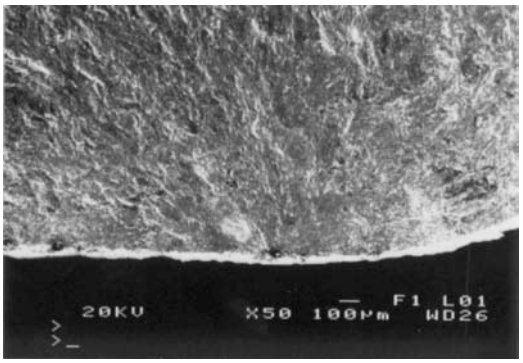

Specimen 8b X 50

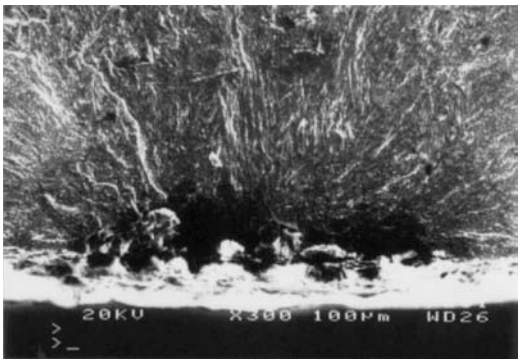

Specimen 8b X 300

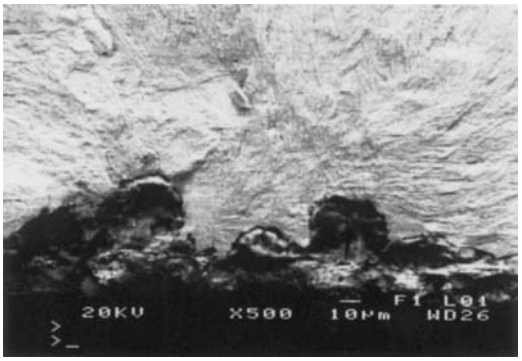

Specimen 8b X 500

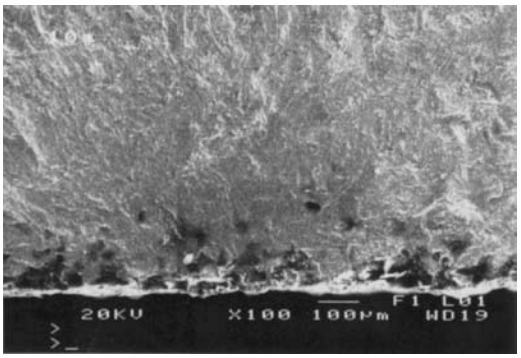

Specimen 10a X 100

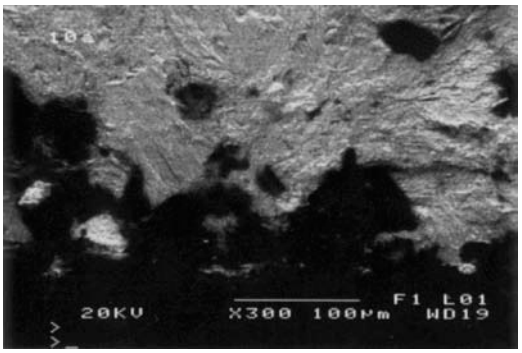

Specimen 10a X 300

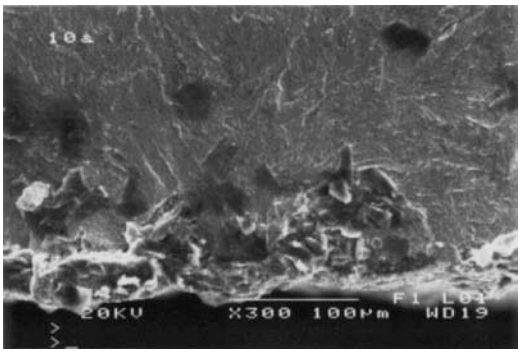

Specimen 10a X 300

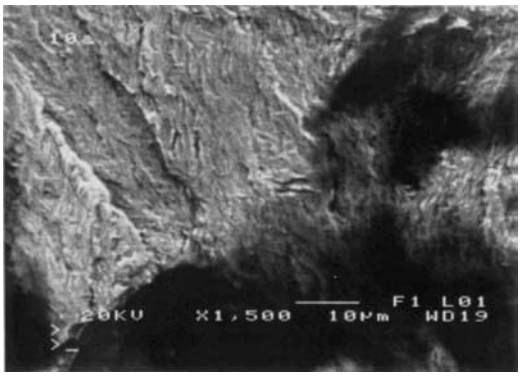

Specimen 10a X 1,500

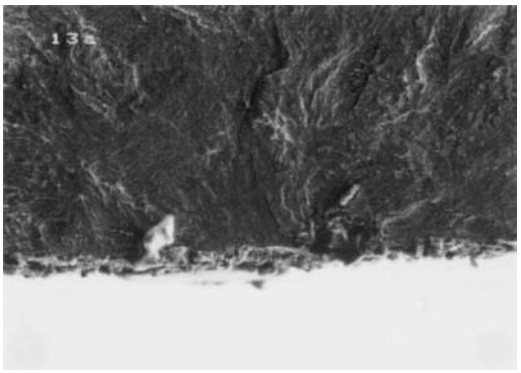

Specimen 13a X 250

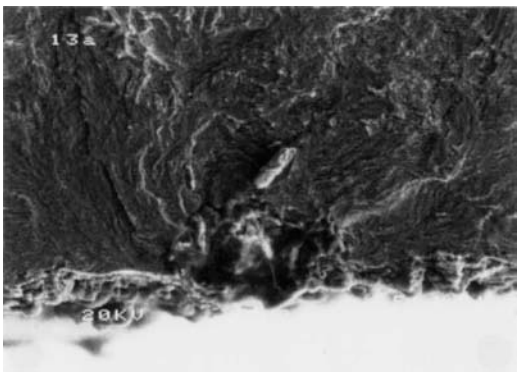

Specimen 13a X 500

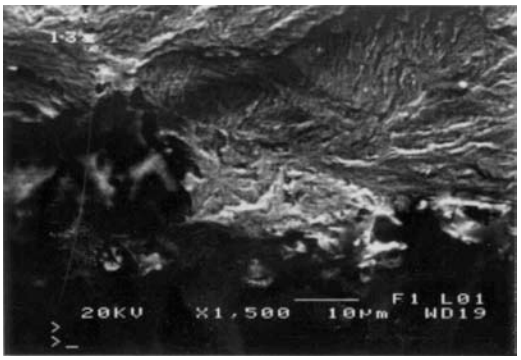

Specimen 13a X 1,500

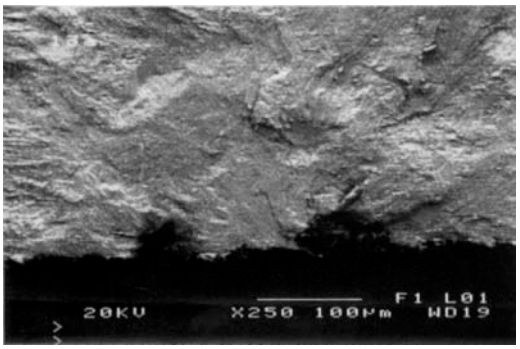

Specimen 13a X 250

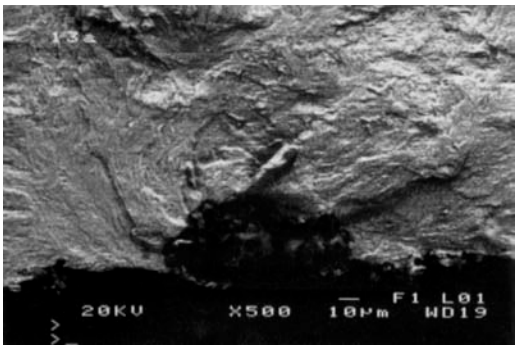

Specimen 13a X 500

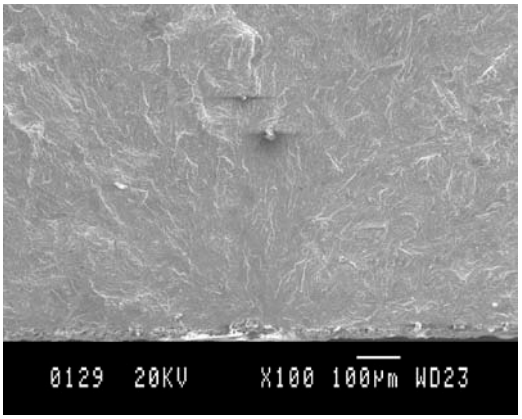

Specimen 1a X 100

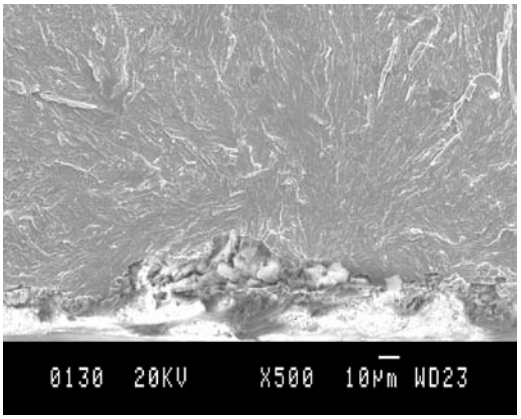

Specimen 1a X 500

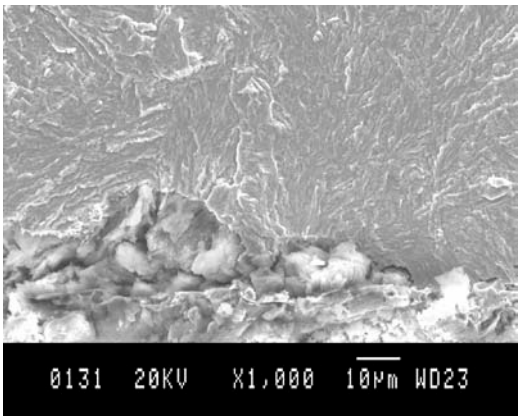

Specimen 1a X 1,000

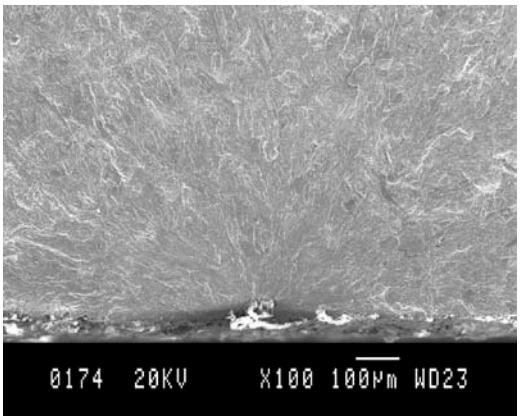

Specimen 8a X 100

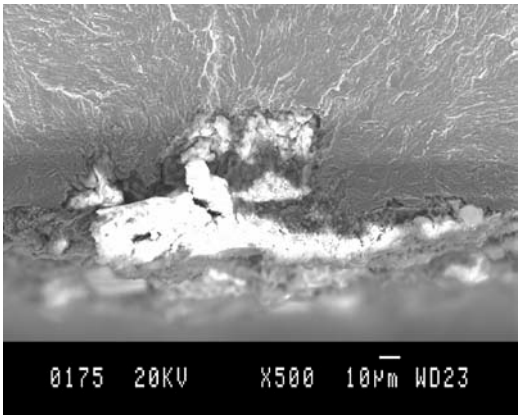

Specimen 8a X 500

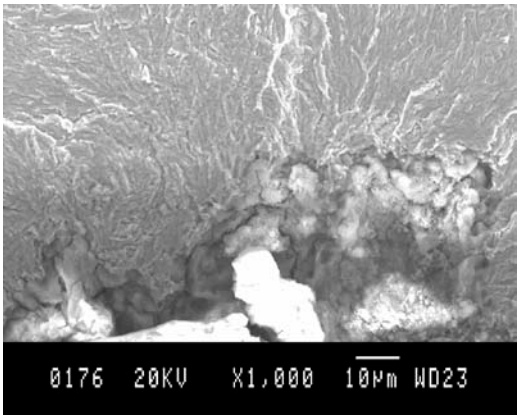

Specimen 8a X 1,000

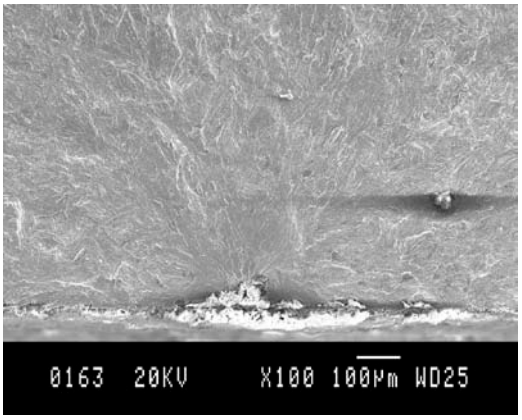

Specimen 8b X 100

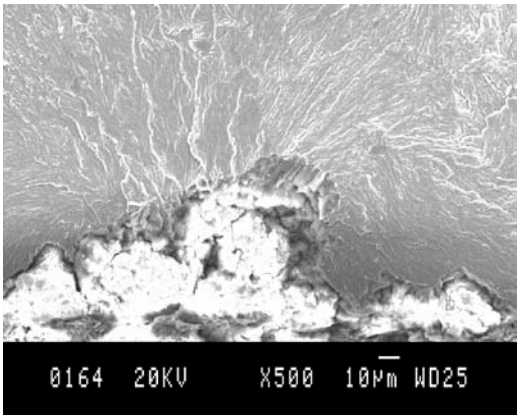

Specimen 8b X 500

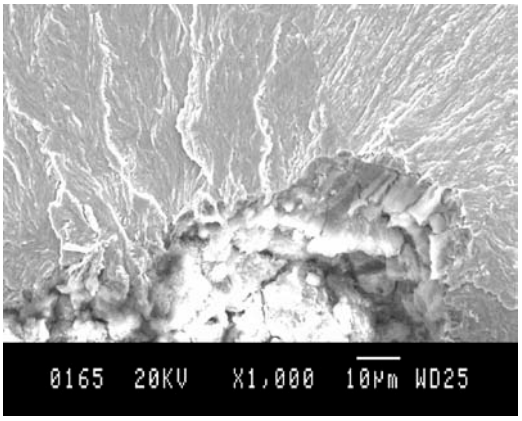

Specimen 8b X 1,000

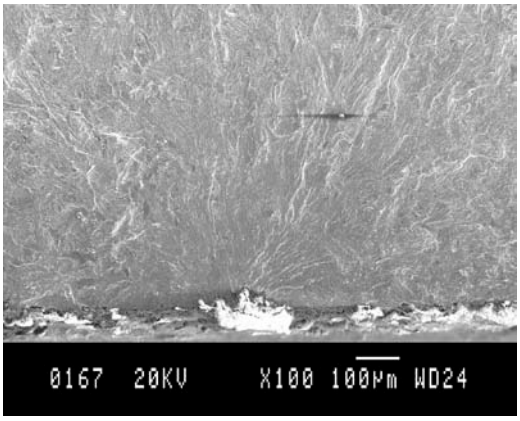

Specimen 9b X 100

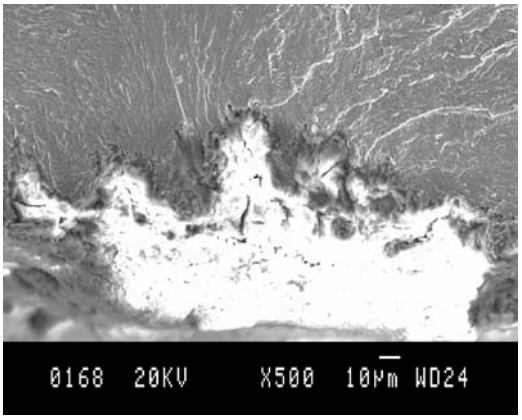

Specimen 9b X 500

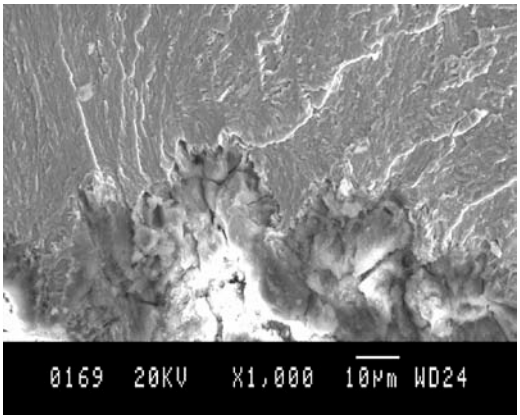

Specimen 9b X 1,000

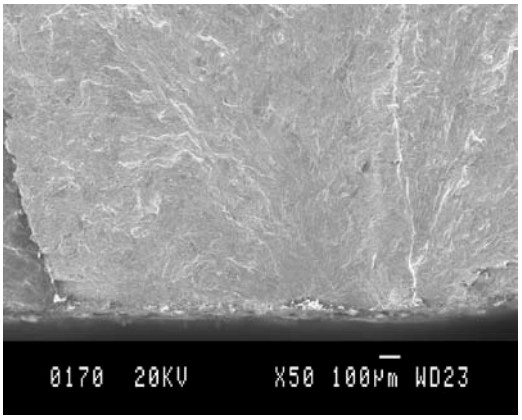

Specimen 10a X 50

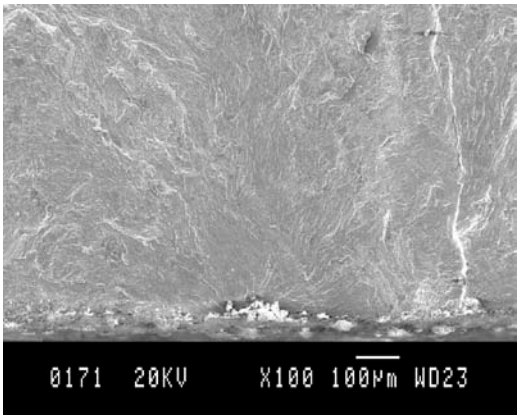

Specimen 10a X 100

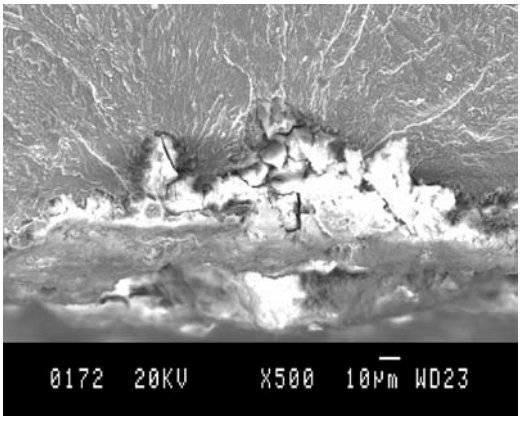

Specimen 10a X 500

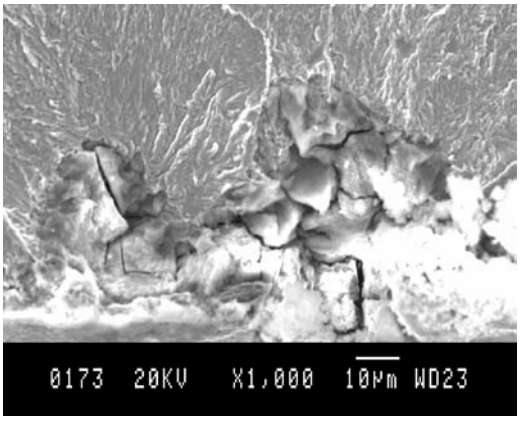

Specimen 10a X 1,000

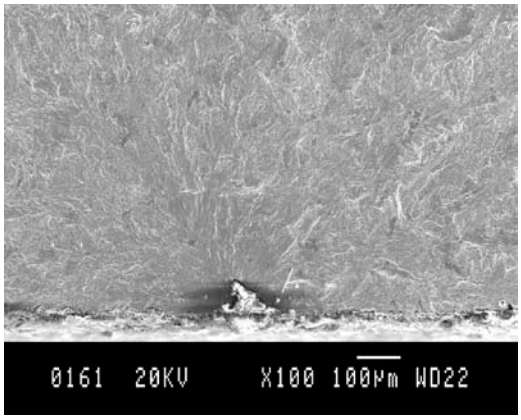

Specimen 10b X 100

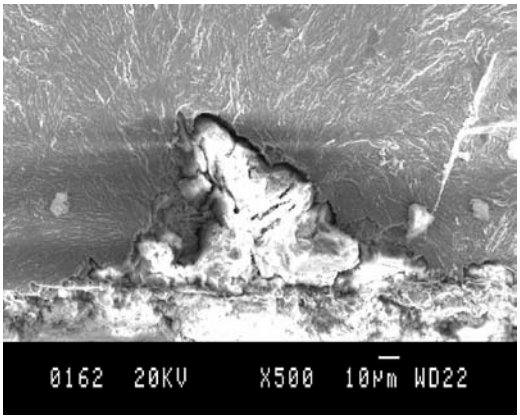

Specimen 10b X 500

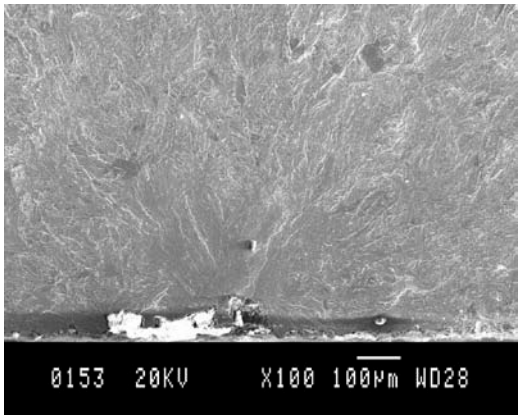

Specimen 11a X 100

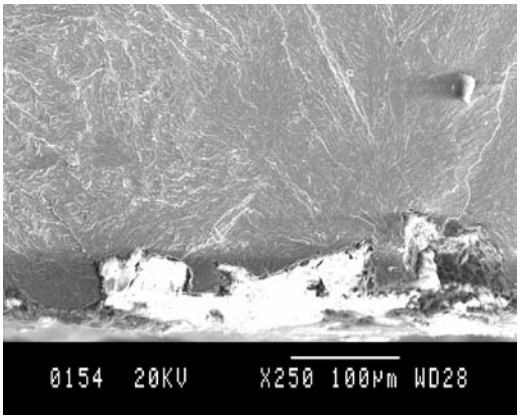

Specimen 11a X 250

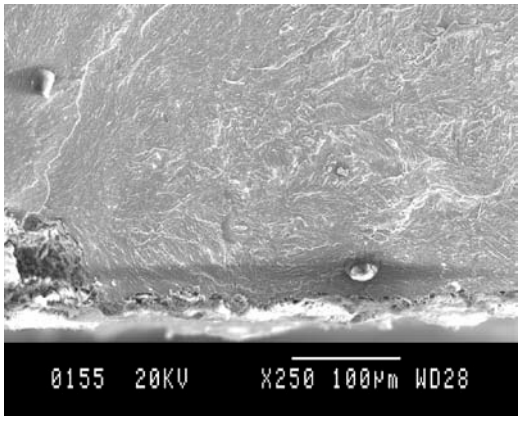

Specimen 11a X 250

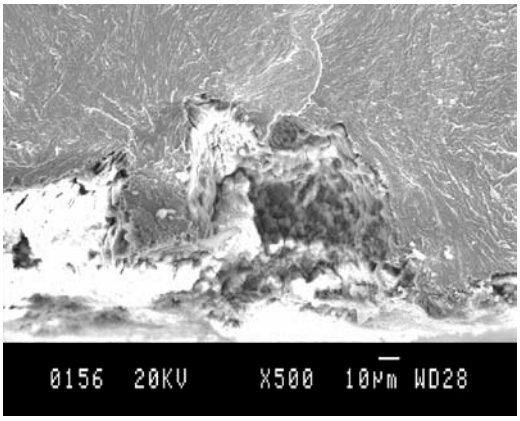

Specimen 11a X 500

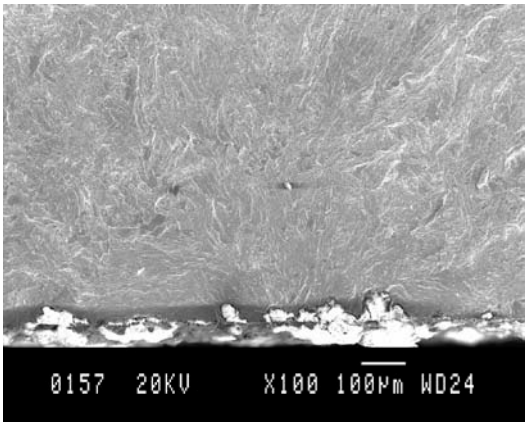

Specimen 11b X 100

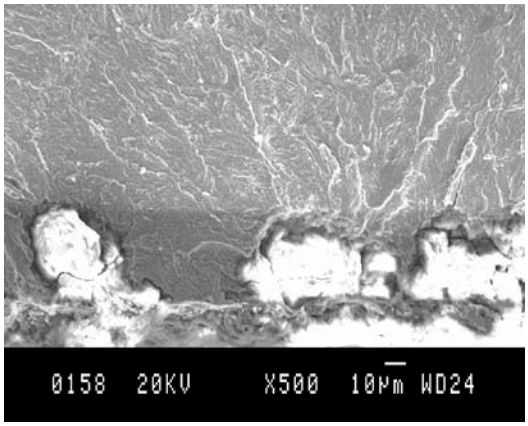

Specimen 11b X 500

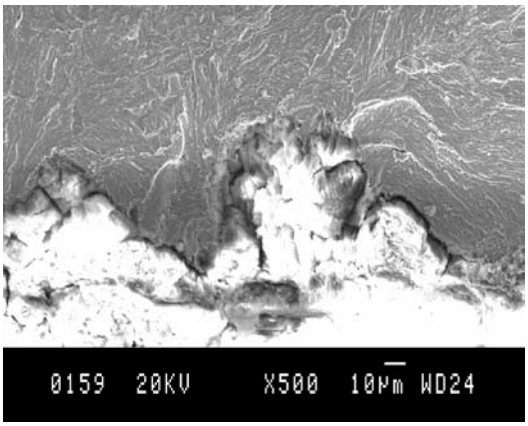

Specimen 11b X 500

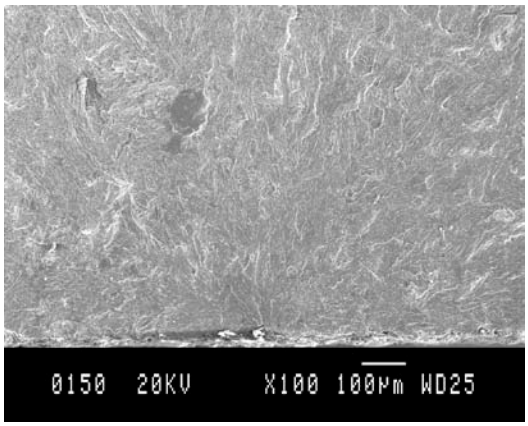

Specimen 12a X 100

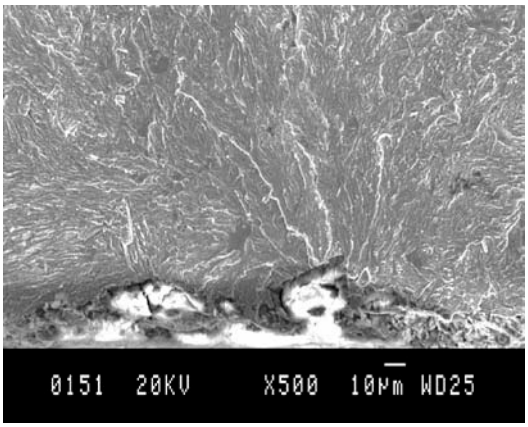

Specimen 12a X 500

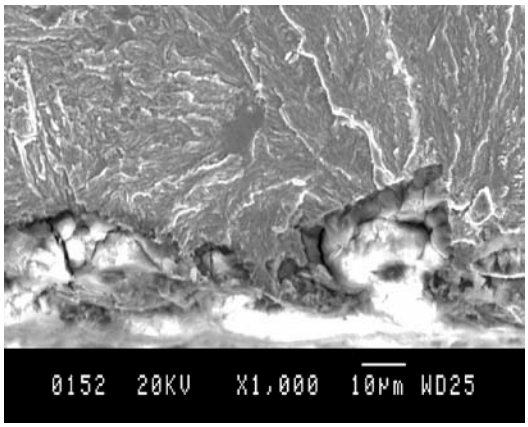

Specimen 12a X 1,000

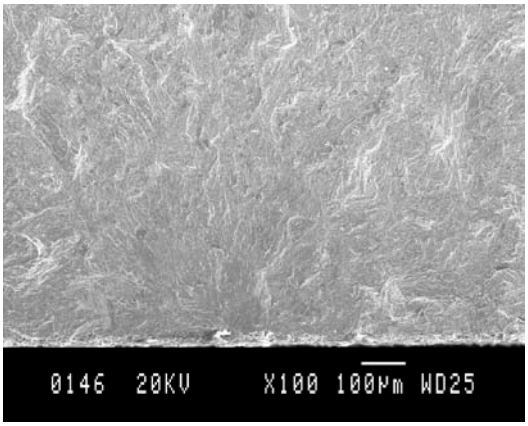

Specimen 12b X 100

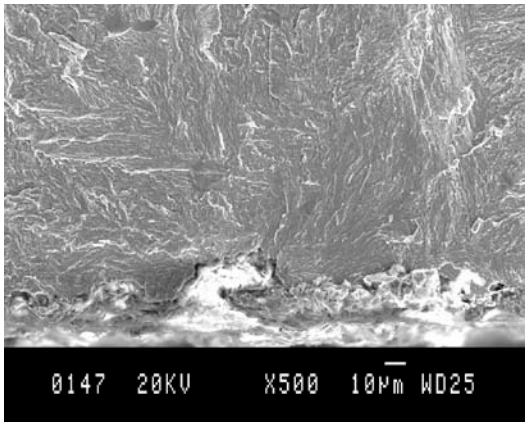

Specimen 12b X 500

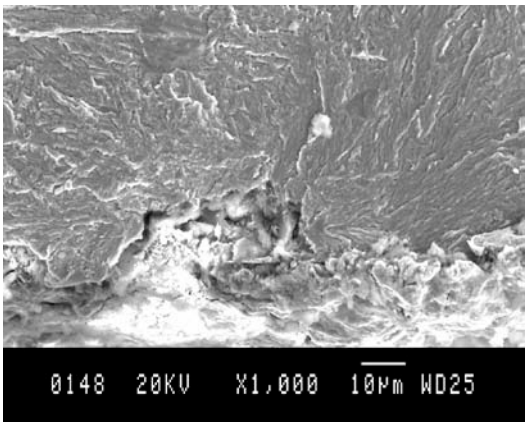

Specimen 12b X 1,000

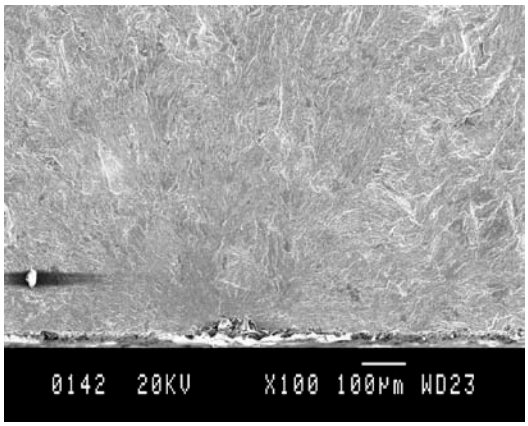

Specimen 12c X 100

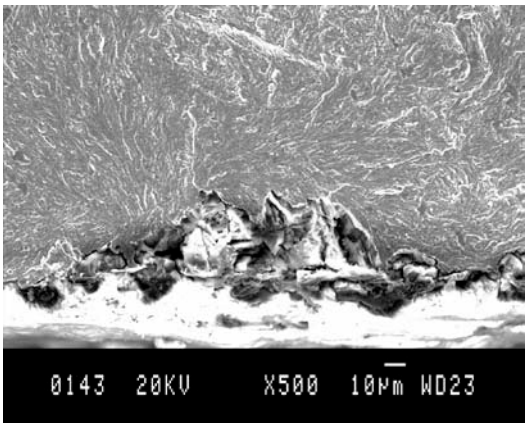

Specimen 12c X 500

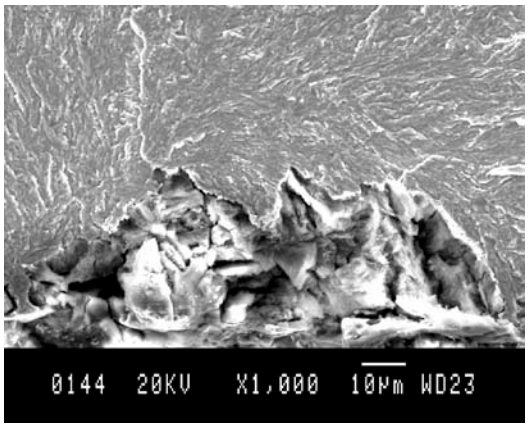

Specimen 12c X 1,000

APPENDIX D: SEM OF SHOT PEENED SPECIMENS

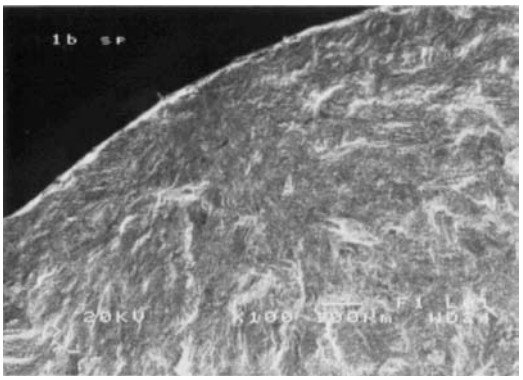

Specimen 1b X 100

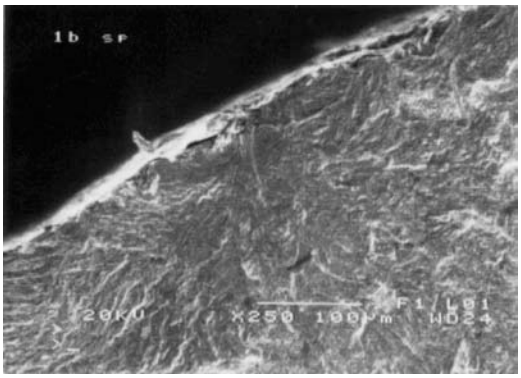

Specimen 1b X 250

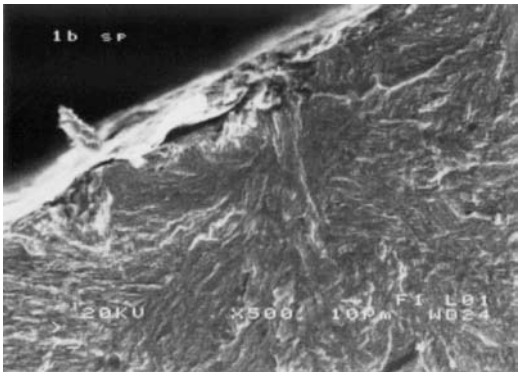

Specimen 1b X 500

Specimen 2b X 100

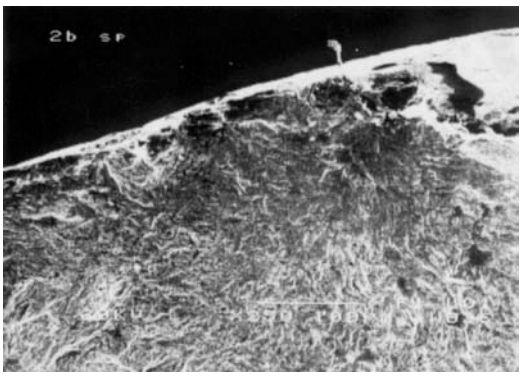

Specimen 2b X 250

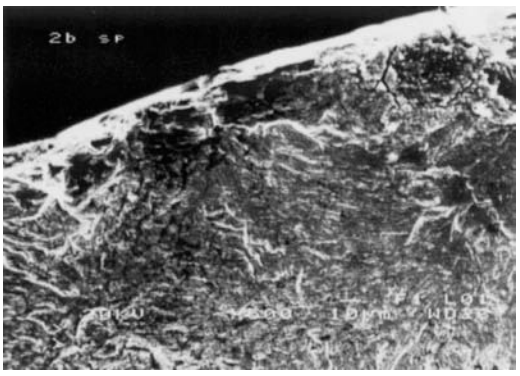

Specimen 2b X 500

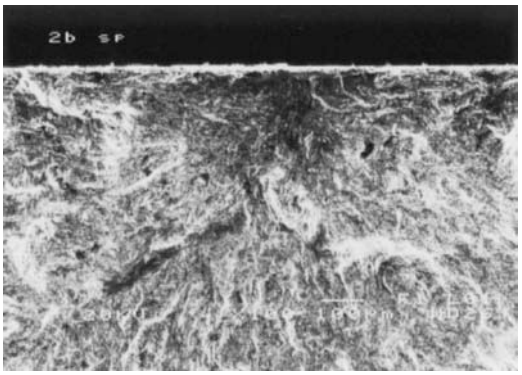

Specimen 2b X 100

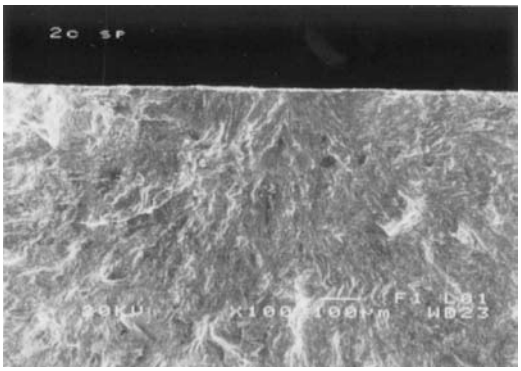

Specimen 2c X 100

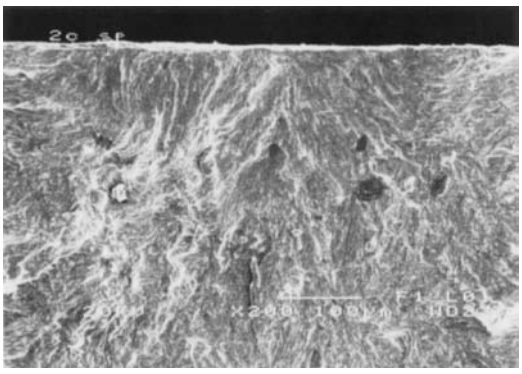

Specimen 2c X 200

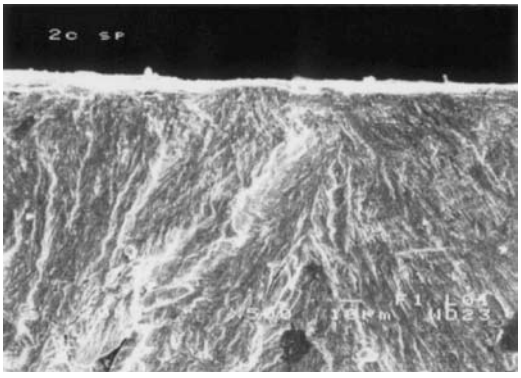

Specimen 2c X 500

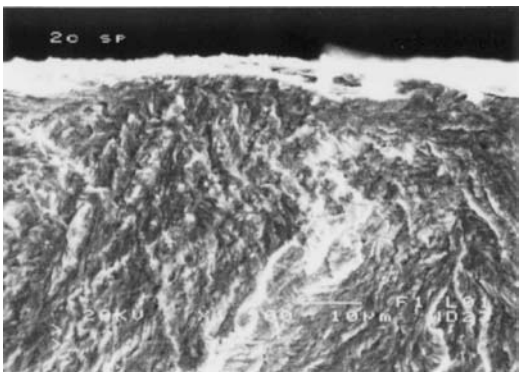

Specimen 2c X 1,500

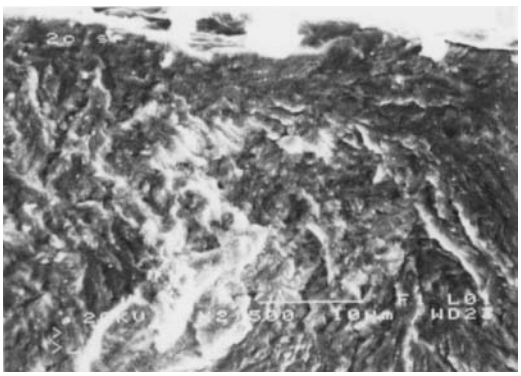

Specimen 2c X 2,500

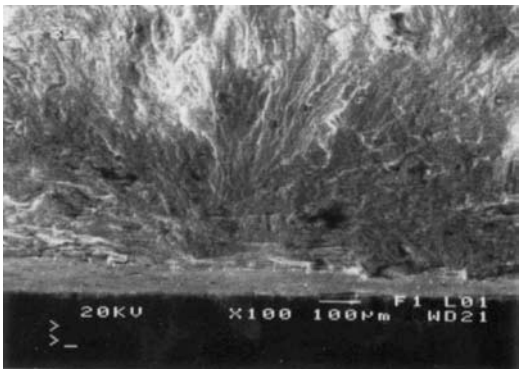

Specimen 3a X 100

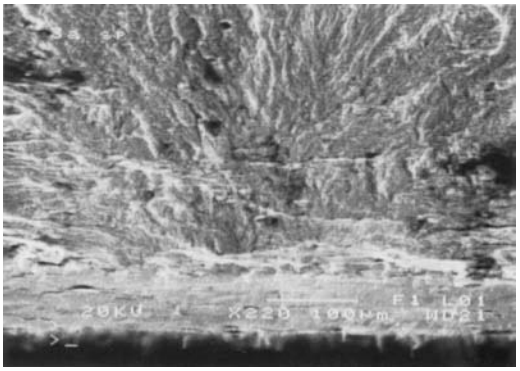

Specimen 3a X 220

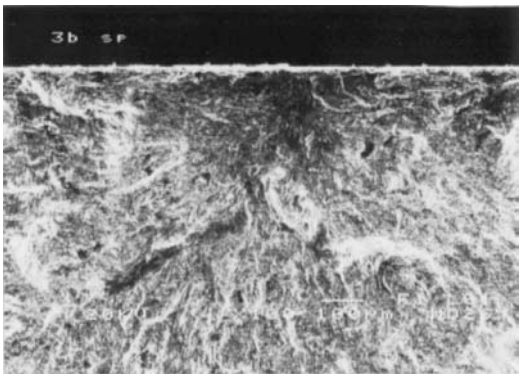

Specimen 3b X 100

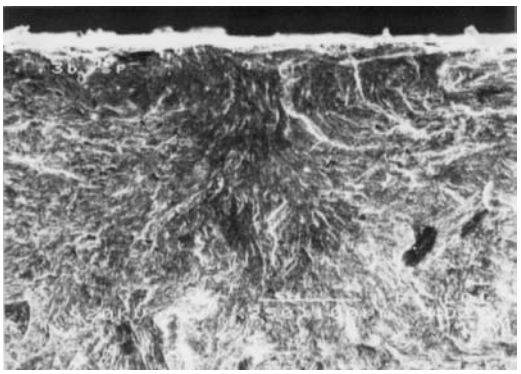

Specimen 3b X 250

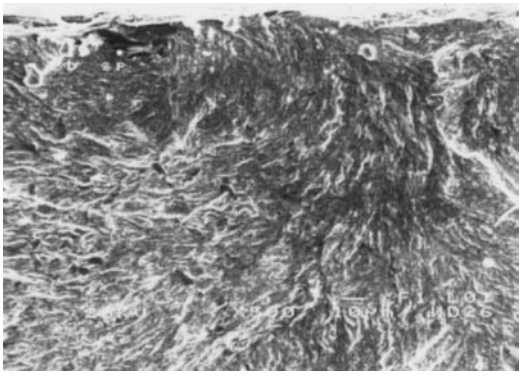

Specimen 3b X 500

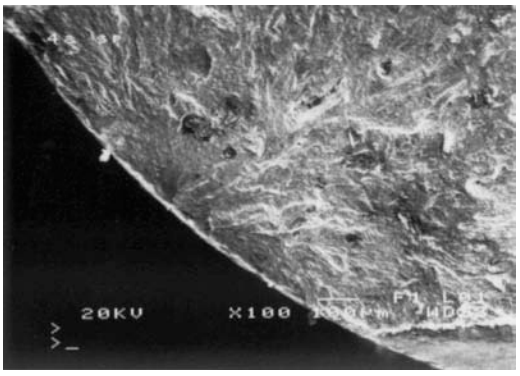

Specimen 4a X 100

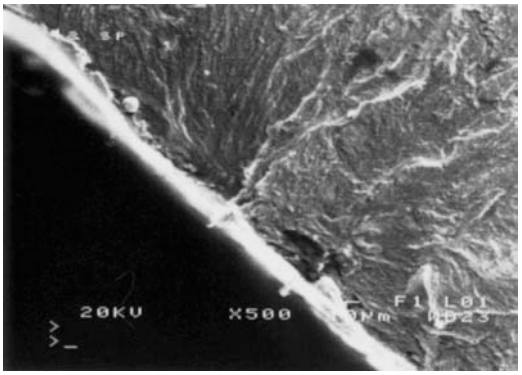

Specimen 4a X 500

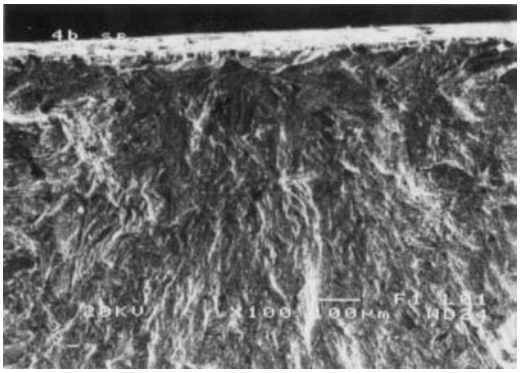

Specimen 4b X 100

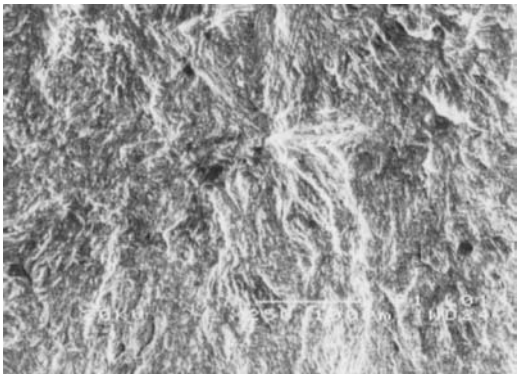

Specimen 4b X 250

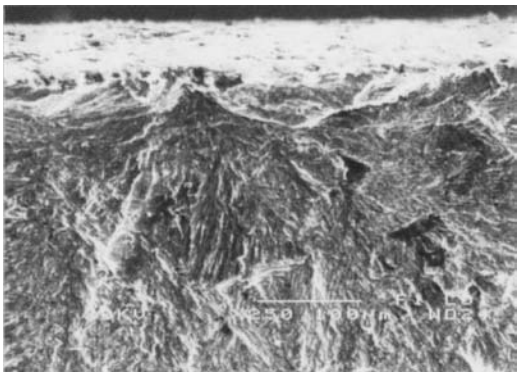

Specimen 4b X 250

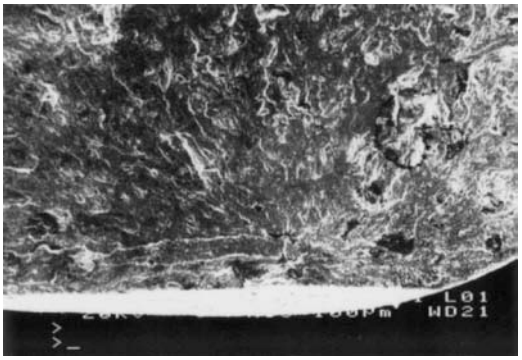

Specimen 5a X 50

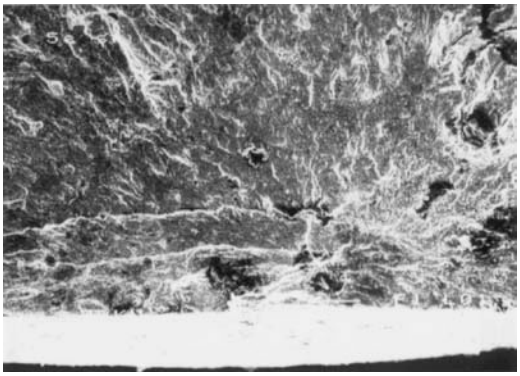

Specimen 5a X 100

Specimen 5a X 250

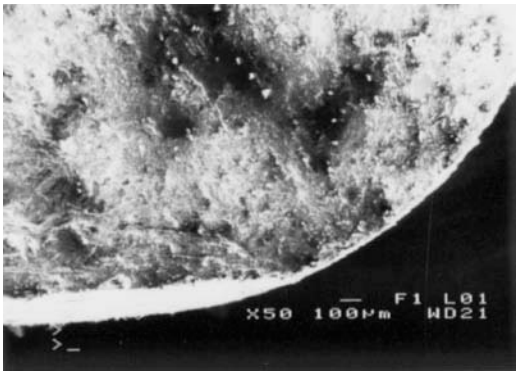

Specimen 6a X 50

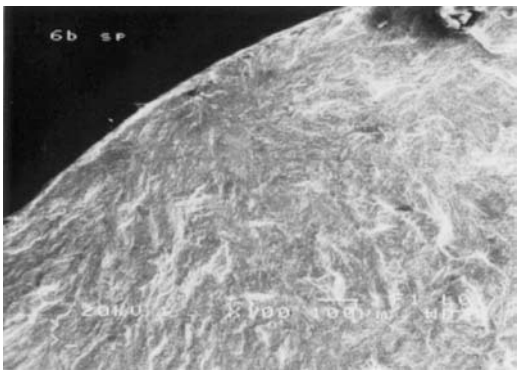

Specimen 6b X 100

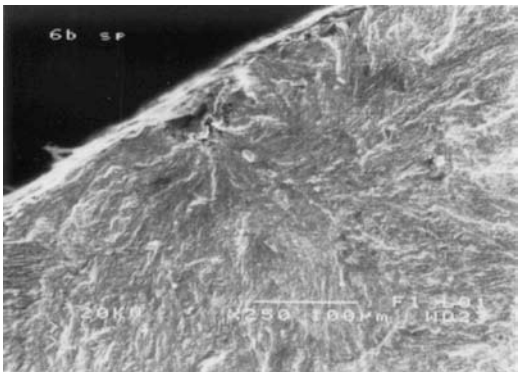

Specimen 6b X 250

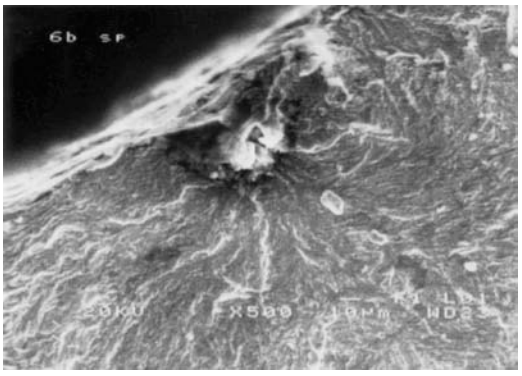

Specimen 6b X 500

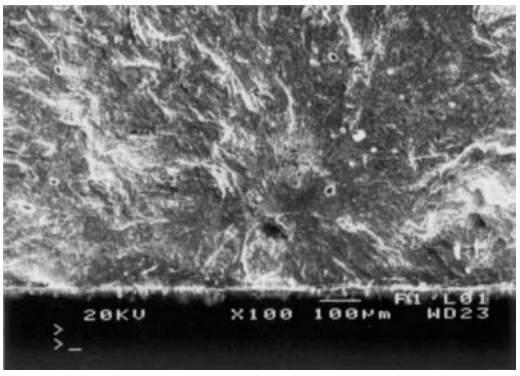

Specimen 7a X 100

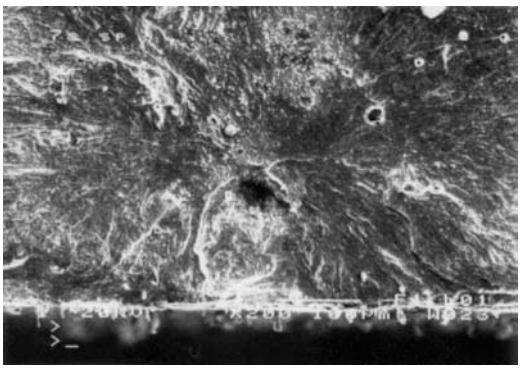

Specimen 7a X 200

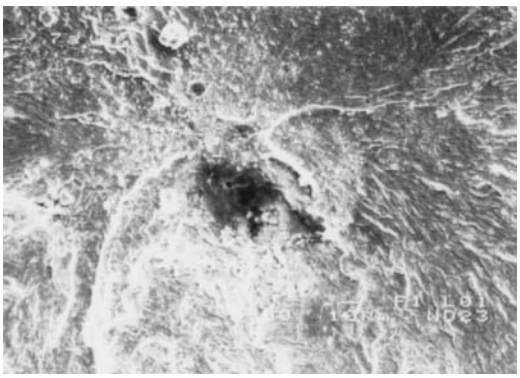

Specimen 7a X 500

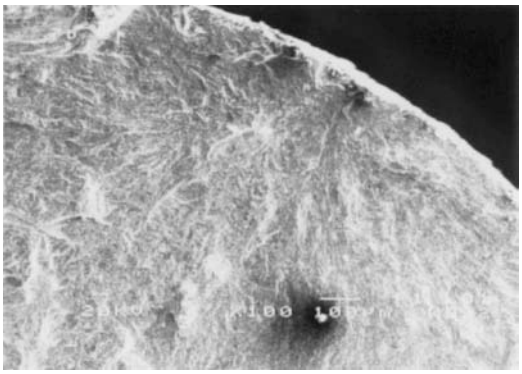

Specimen 7b X 100

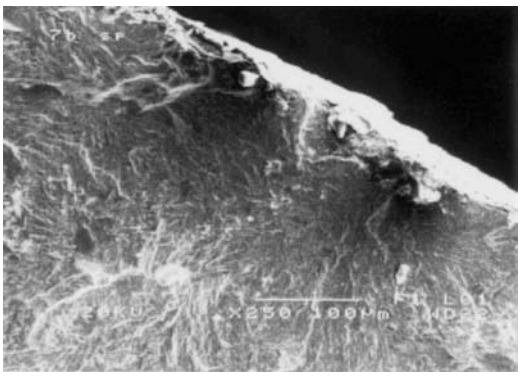

Specimen 7b X 250

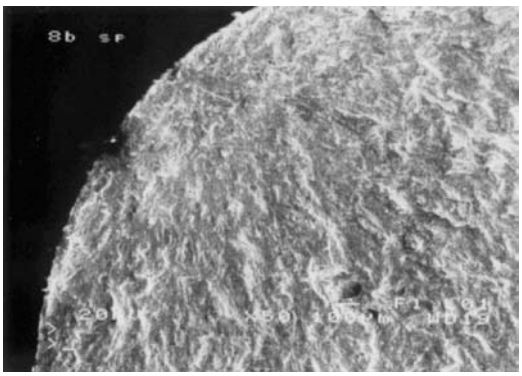

Specimen 8b X 50

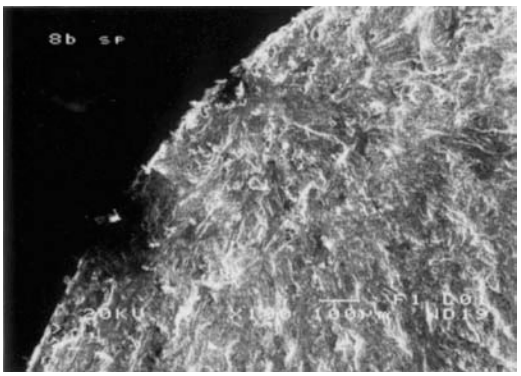

Specimen 8b X 100

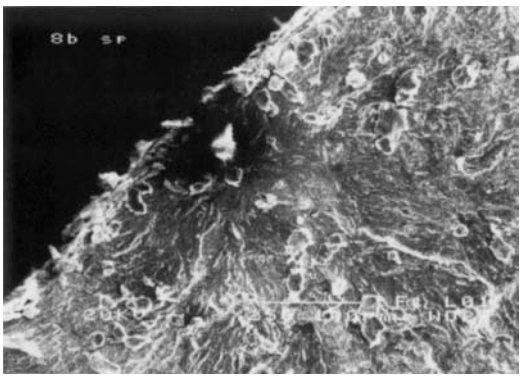

Specimen 8b X 250

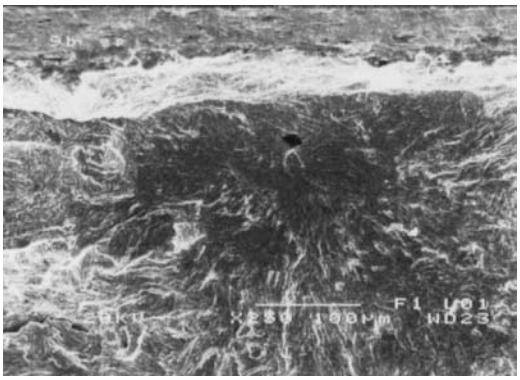

Specimen 9b X 250

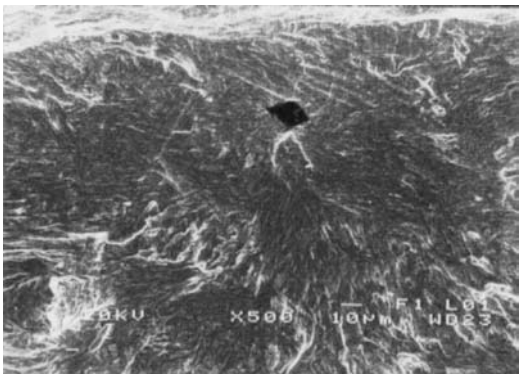

Specimen 9b X 500

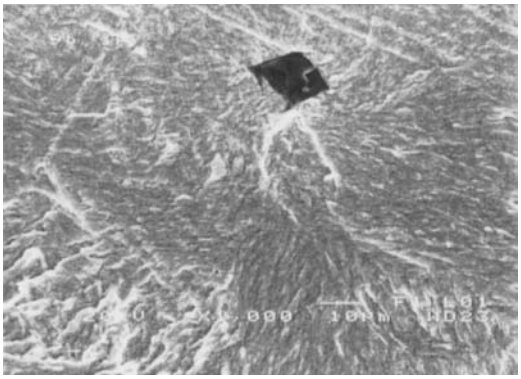

Specimen 9b X 1,000

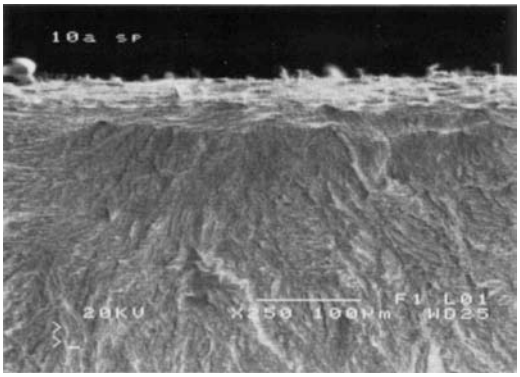

Specimen 10a X 250

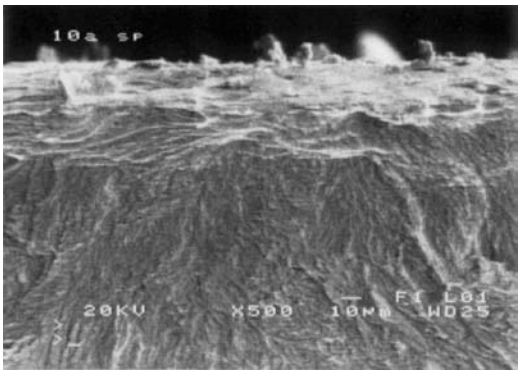

Specimen 10a X 500

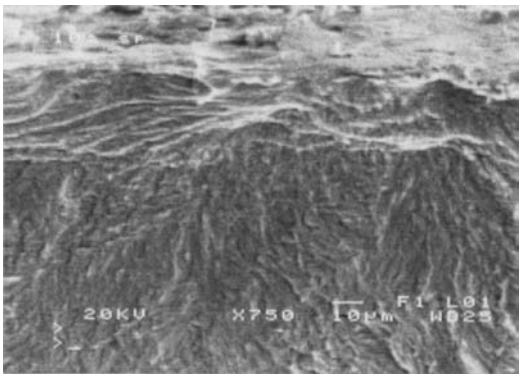

Specimen 10a X 750

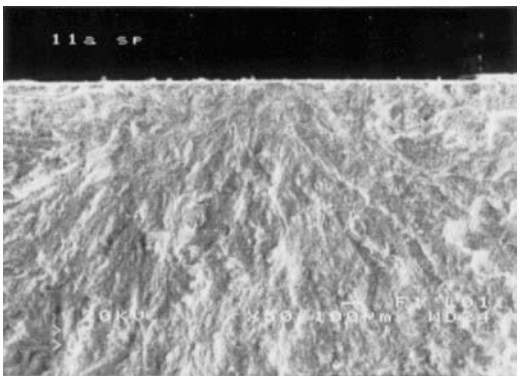

Specimen 11a X 50

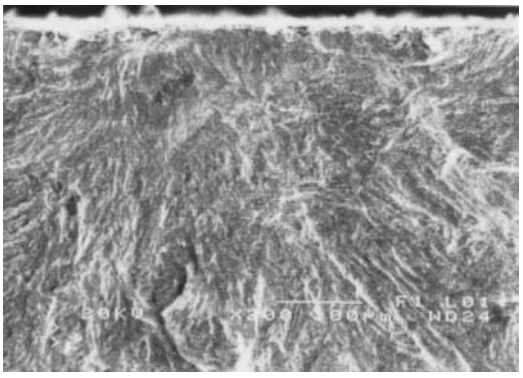

Specimen 11a X 200

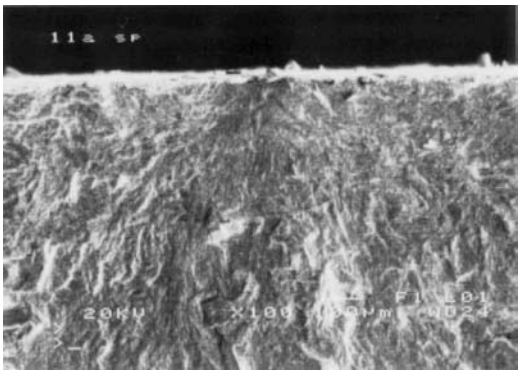

Specimen 11a X 100

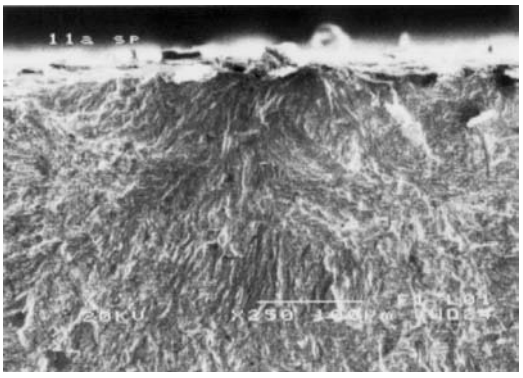

Specimen 11a X 250

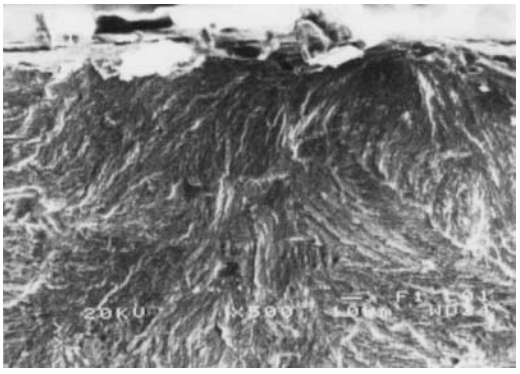

Specimen 11a X 500

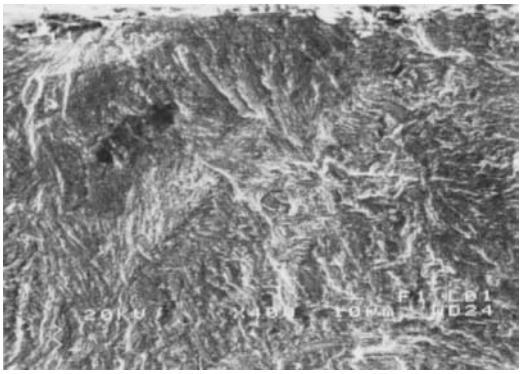

Specimen 11a X 400

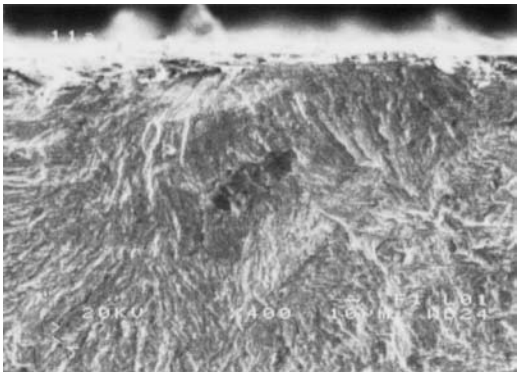

Specimen 11a X 400

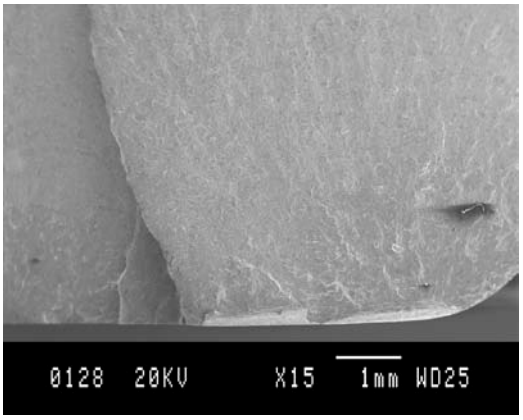

Specimen 1a X 15

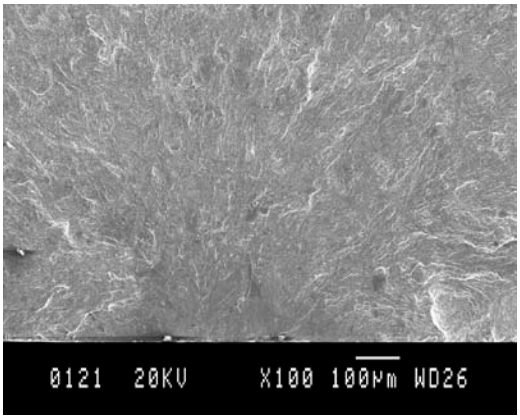

Specimen 1a X 100

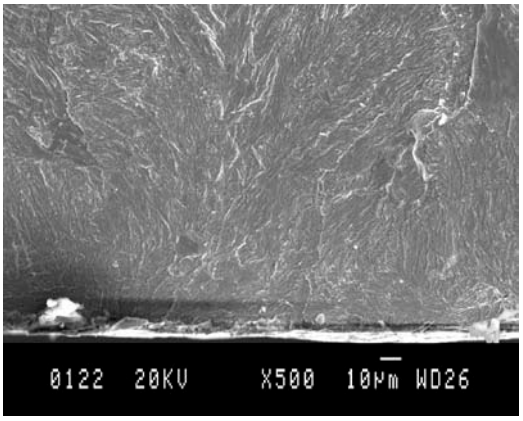

Specimen 1a X 500

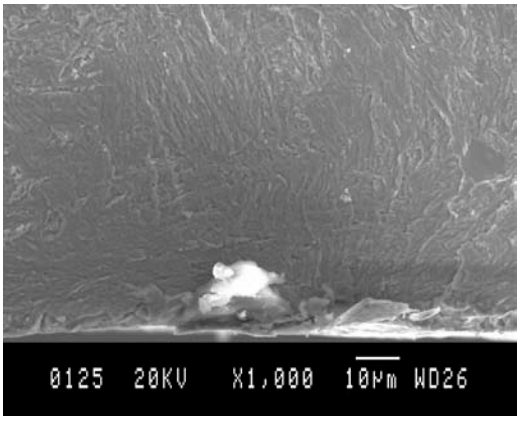

Specimen 1a X 1,000

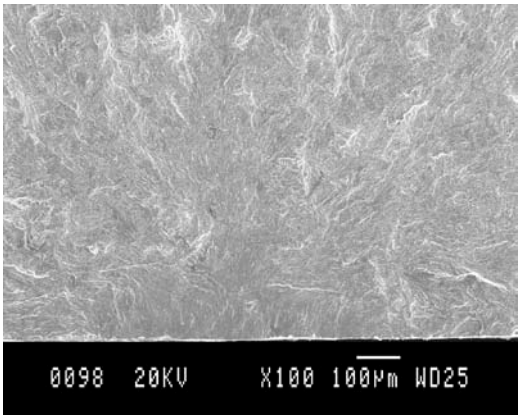

Specimen 1b X 100

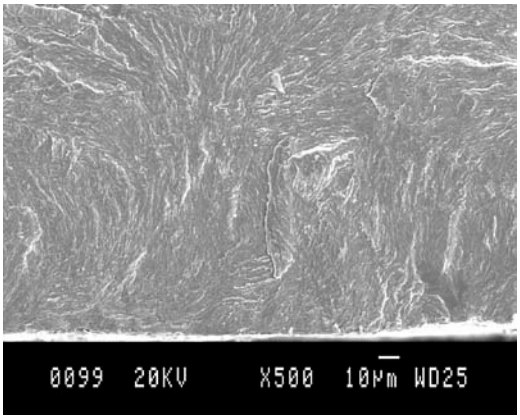

Specimen 1b X 500

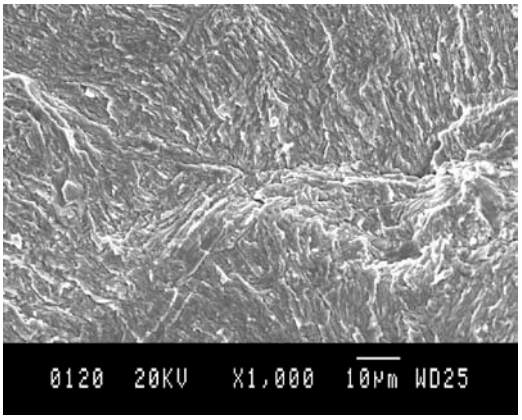

Specimen 1b X 1,000

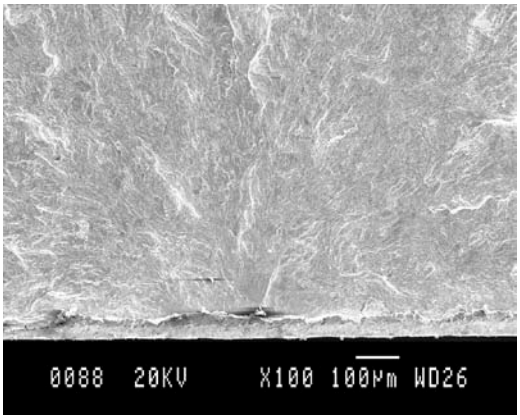

Specimen 3a X 100

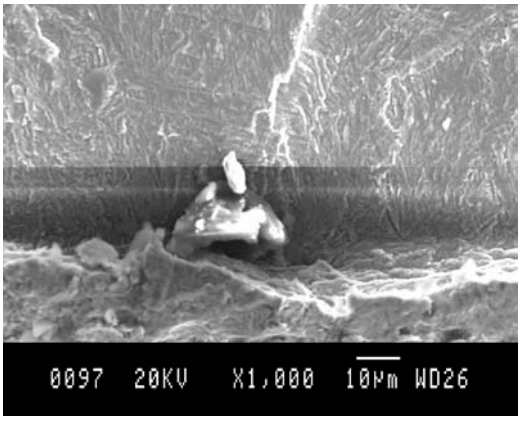

Specimen 3a X 1,000

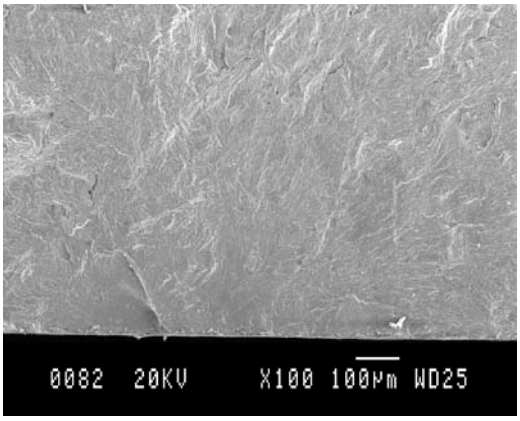

Specimen 4b X 100

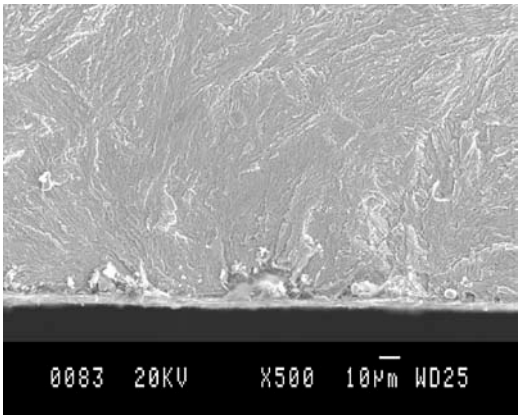

Specimen 4b X 500

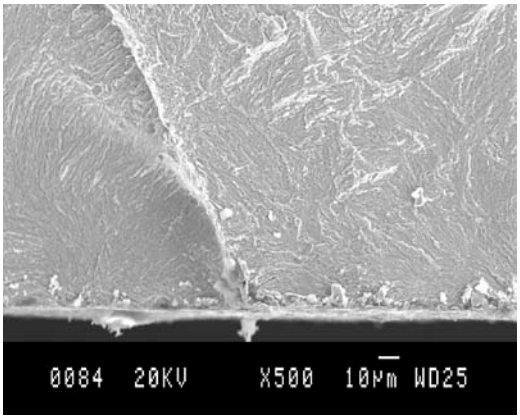

Specimen 4b X 500

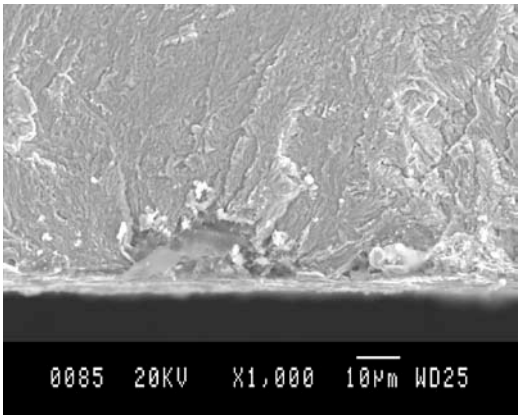

Specimen 4b X 1,000

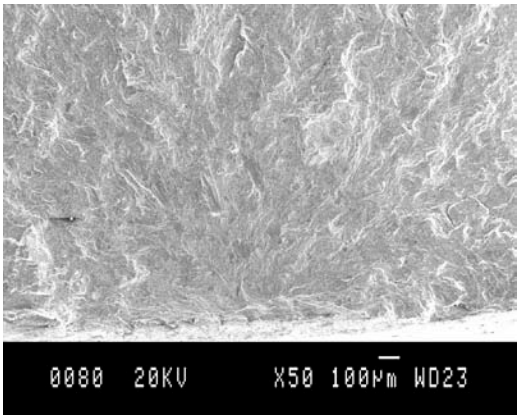

Specimen 7b X 50

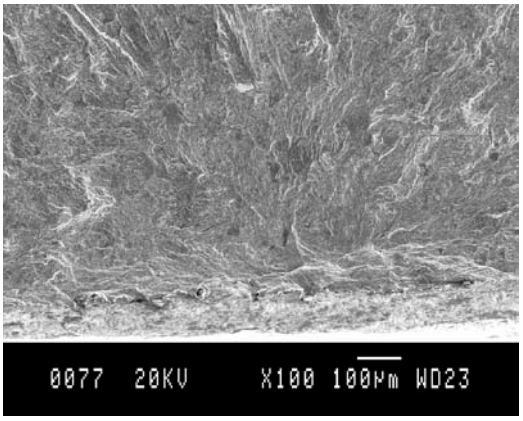

Specimen 7b X 100

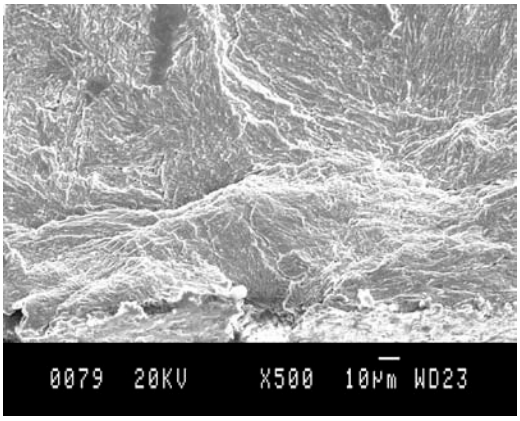

Specimen 7b X 500

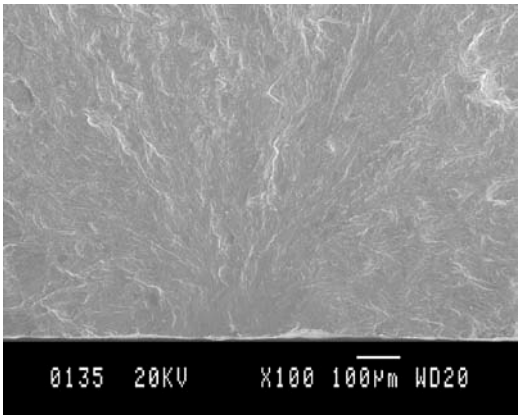

Specimen 8a X 100

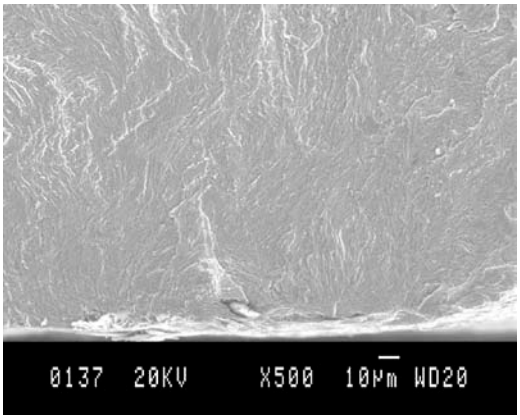

Specimen 8a X 500

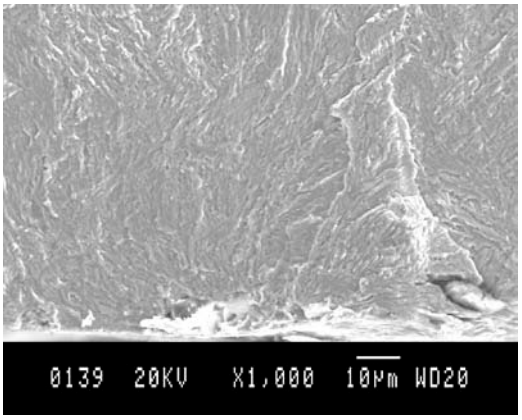

Specimen 8a X 1,000

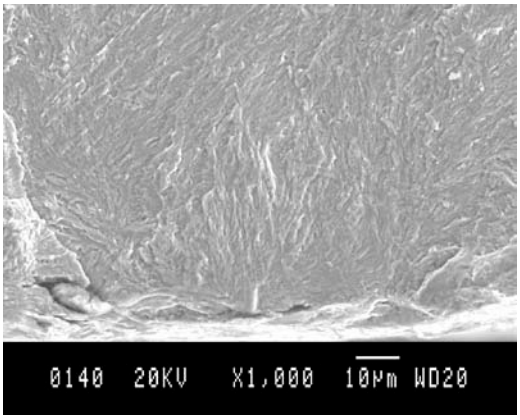

Specimen 8a X 1,000

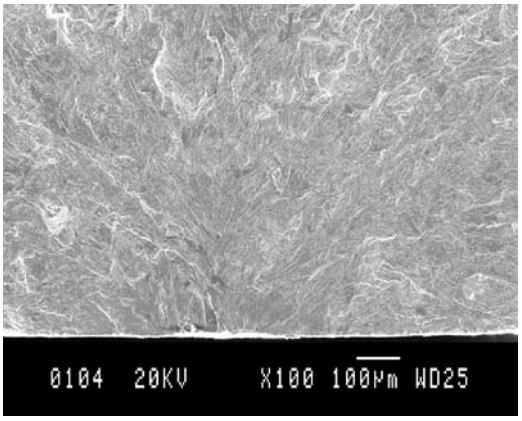

Specimen 8b X 100

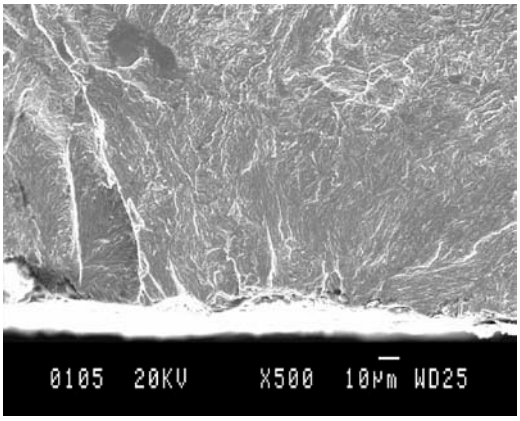

Specimen 8b X 500

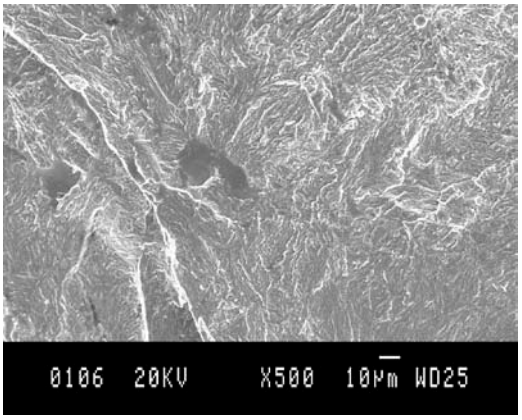

Specimen 8b X 500

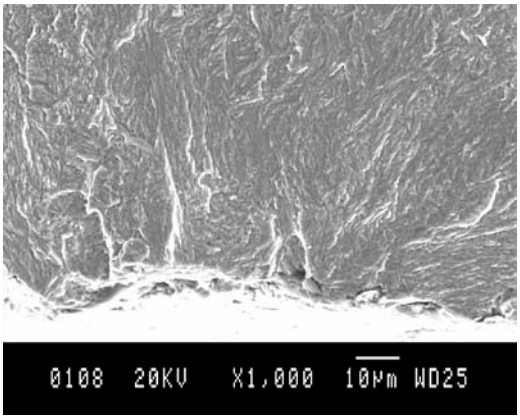

Specimen 8b X 1,000

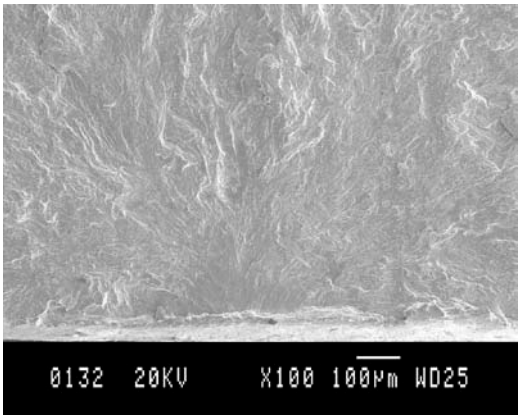

Specimen 11a X 100

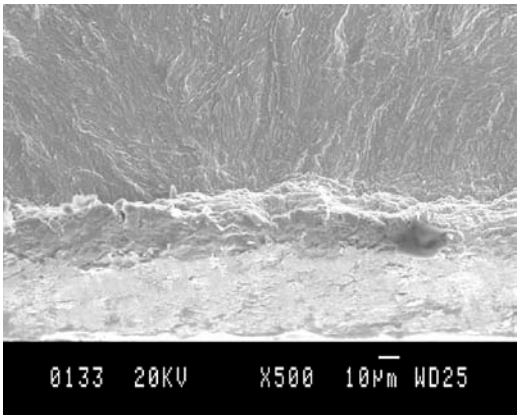

Specimen 11a X 500

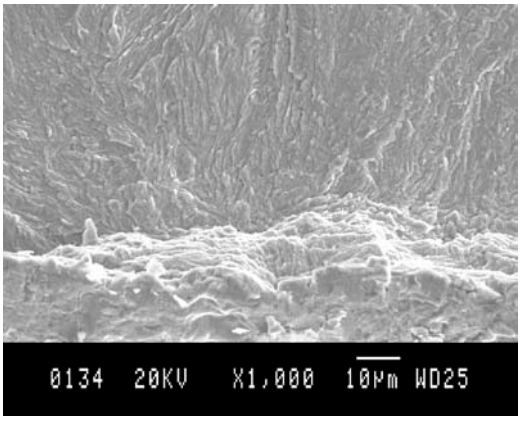

Specimen 11a X 1,000

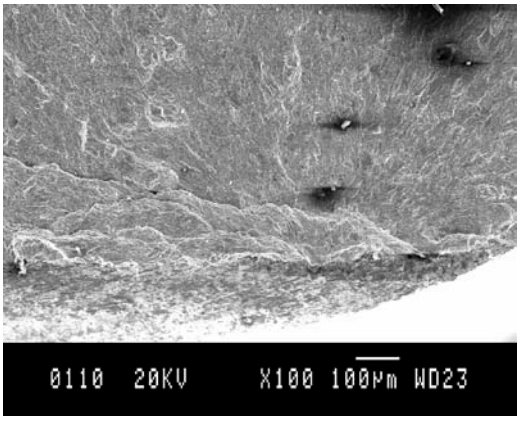

Specimen 12a X 100

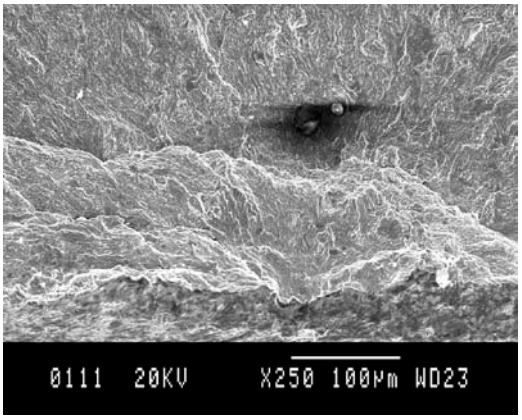

Specimen 12a X 250

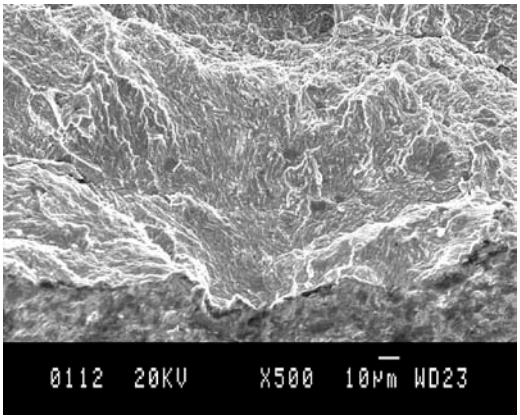

Specimen 12a X 500

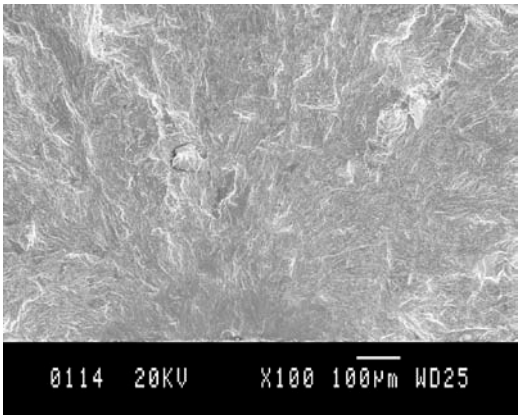

Specimen 12b X 100

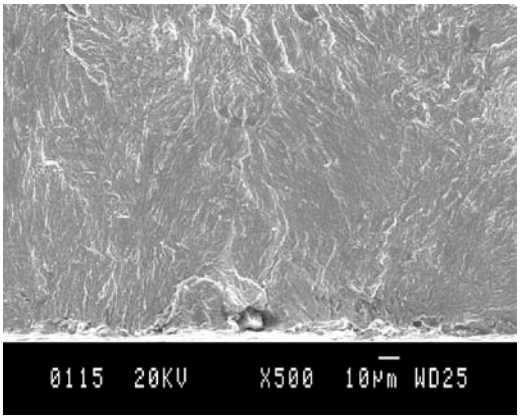

Specimen 12b X 500

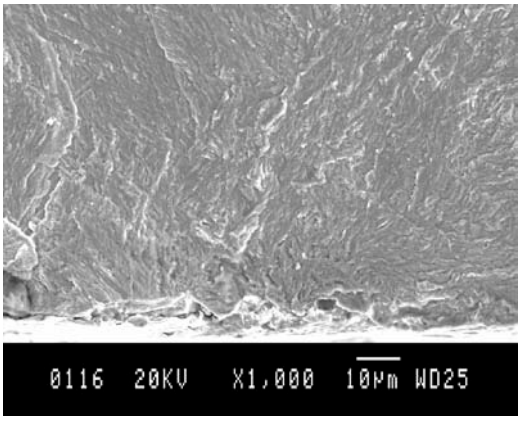

Specimen 12b X 1,000

APPENDIX E: SEM OF GROUND SPECIMENS

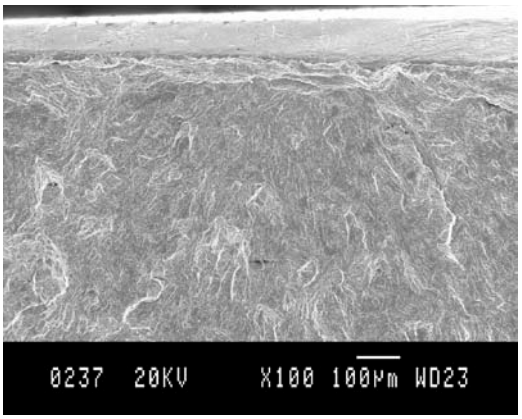

Specimen 3 X 100

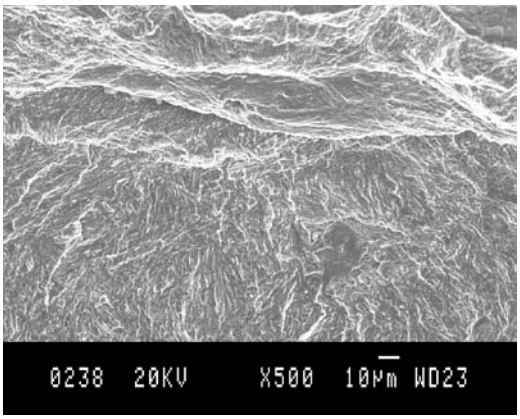

Specimen 3 X 500

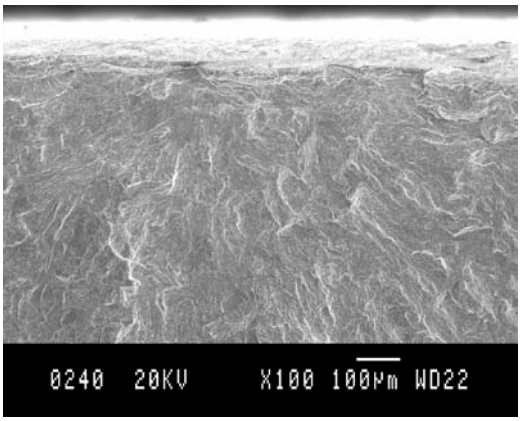

Specimen 4 X 100

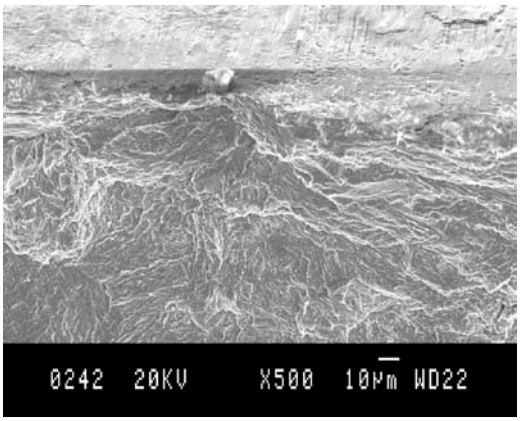

Specimen 4 X 500

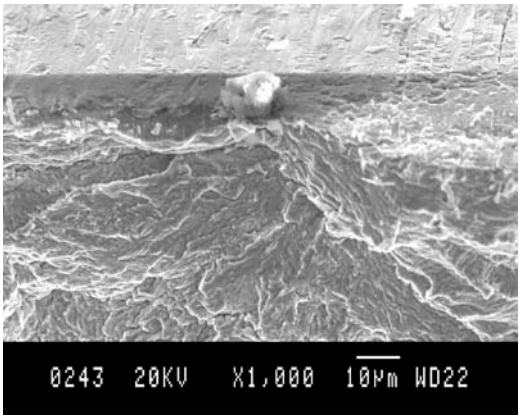

Specimen 4 X 1,000

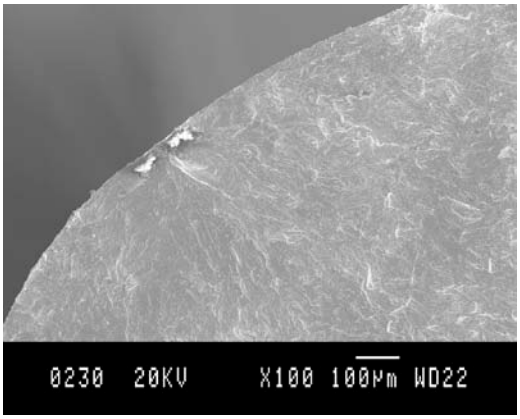

Specimen 6 X 100

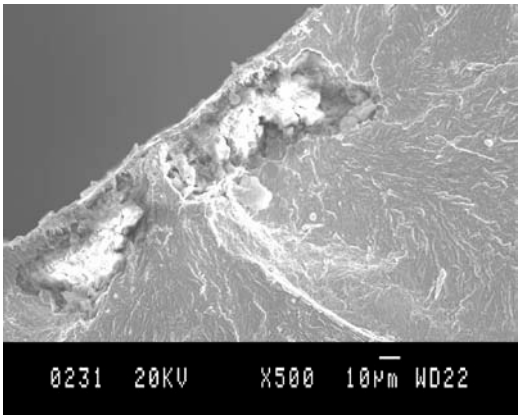

Specimen 6 X 500

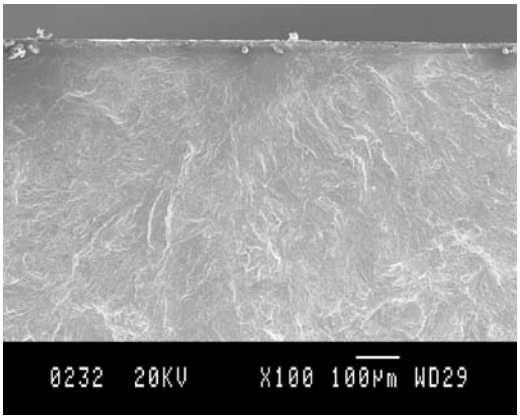

Specimen 7 X 100

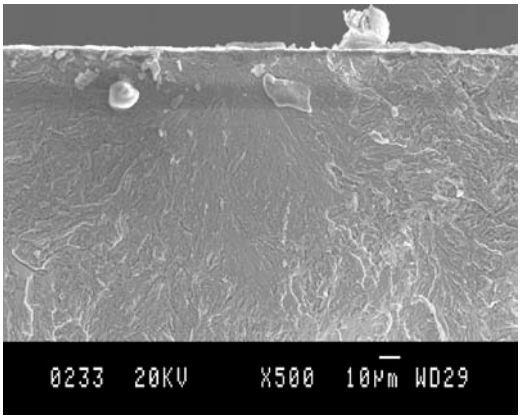

Specimen 7 X 500

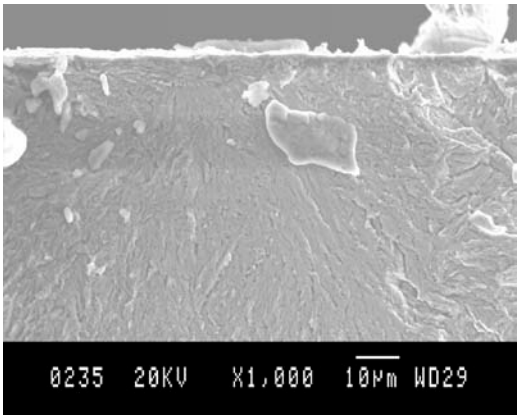

Specimen 7 X 1,000

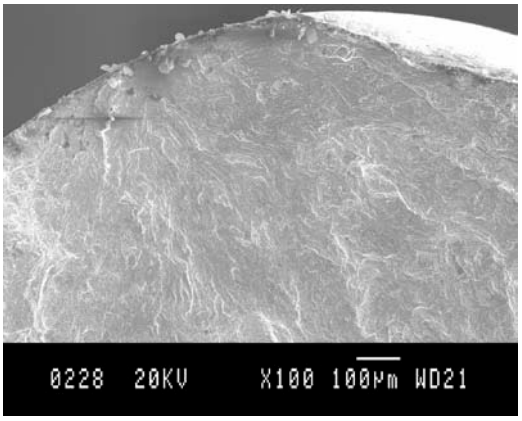

Specimen 8 X 100

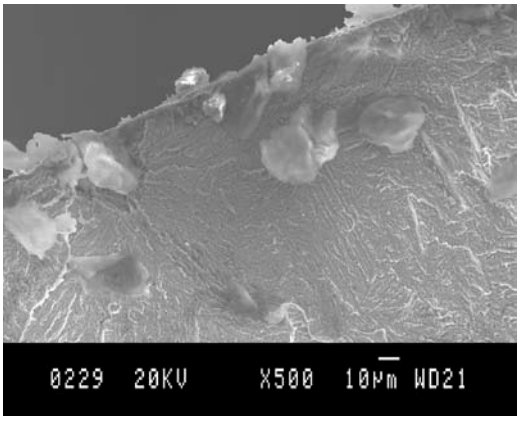

Specimen 8 X 500

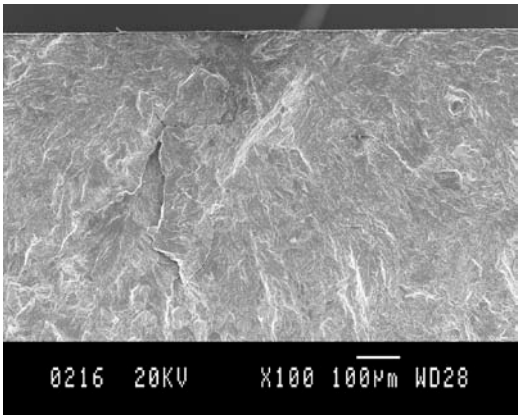

Specimen 9 X 100

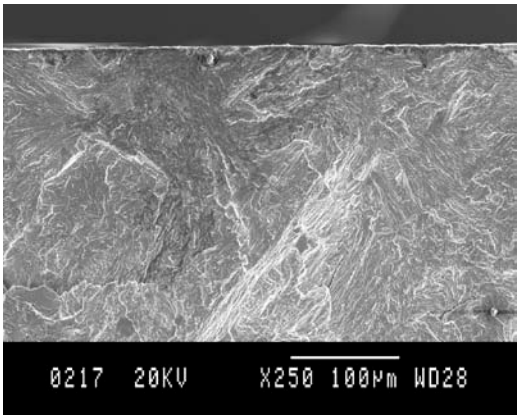

Specimen 9 X 250

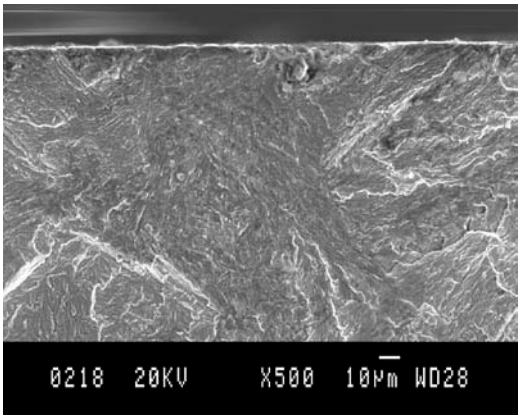

Specimen 9 X 500

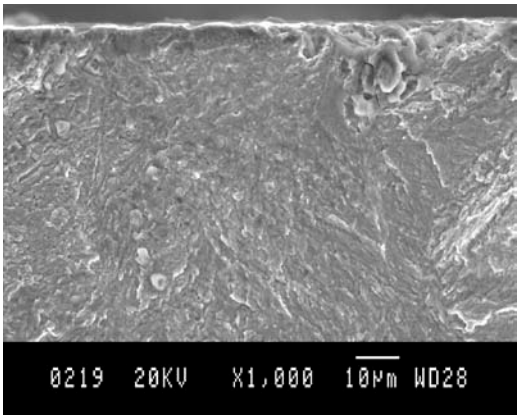

Specimen 9 X 1,000

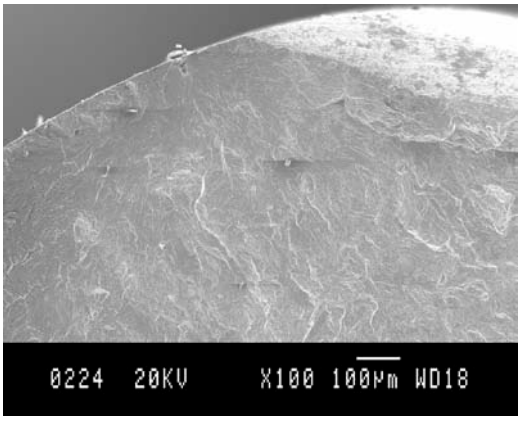

Specimen 10 X 100

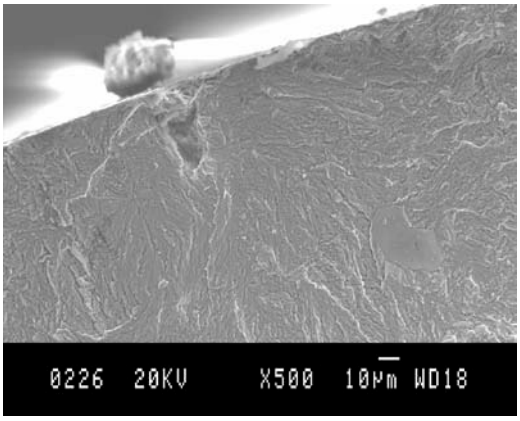

Specimen 10 X 500

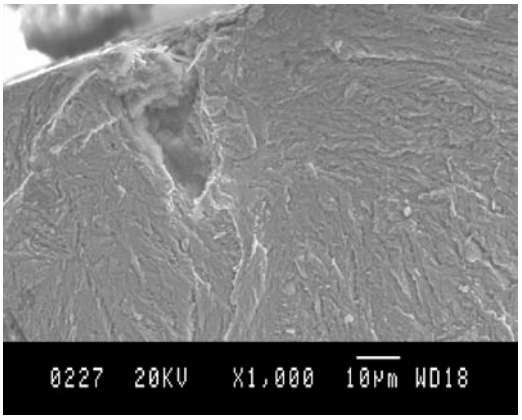

Specimen 10 X 1,000

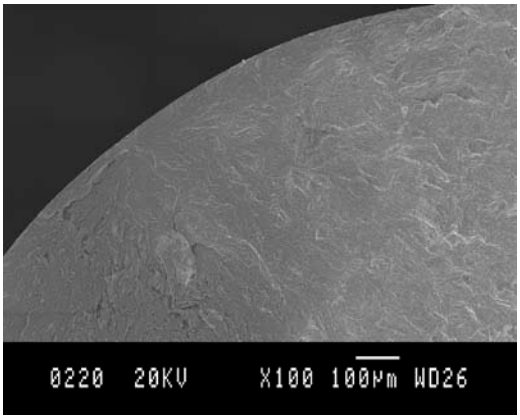

Specimen 11 X 100

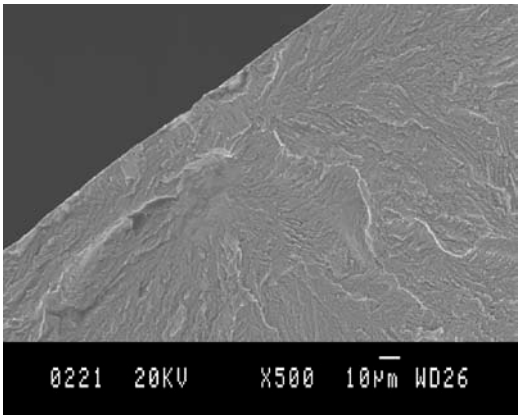

Specimen 11 X 500

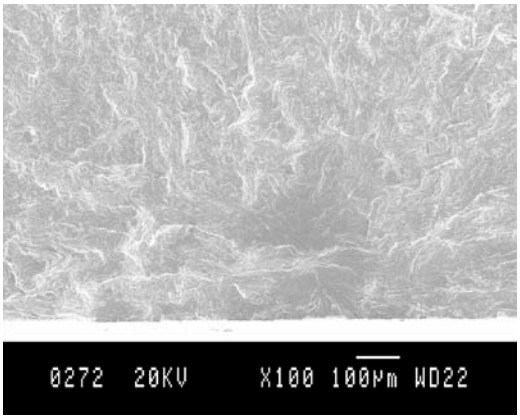

Specimen 12 X 100

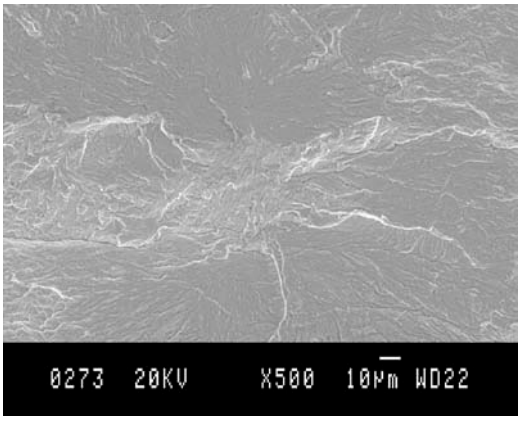

Specimen 12 X 500

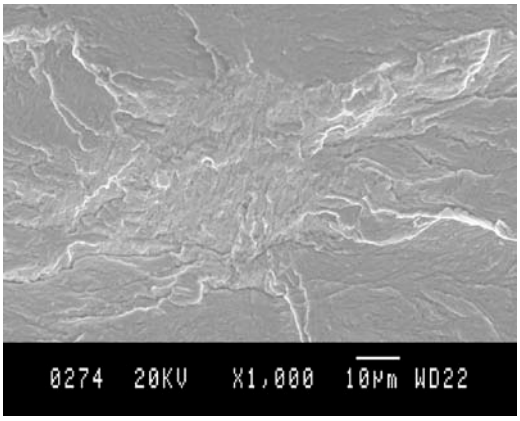

Specimen 12 X 1,000

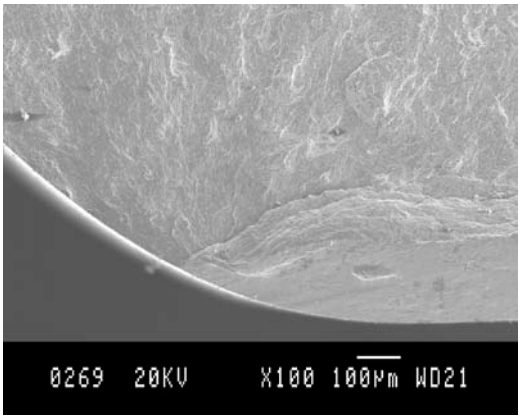

Specimen 13 X 100

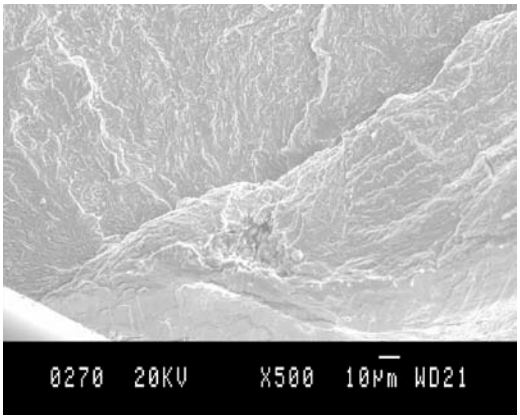

Specimen 13 X 500

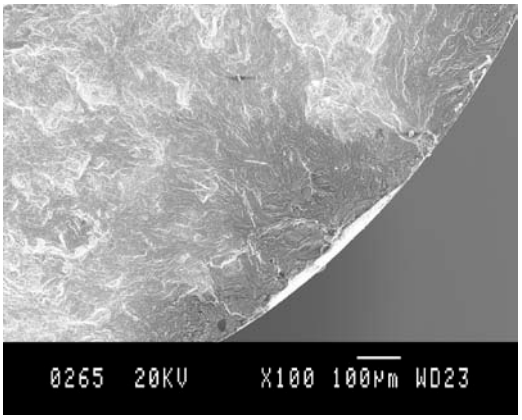

Specimen 14 X 100

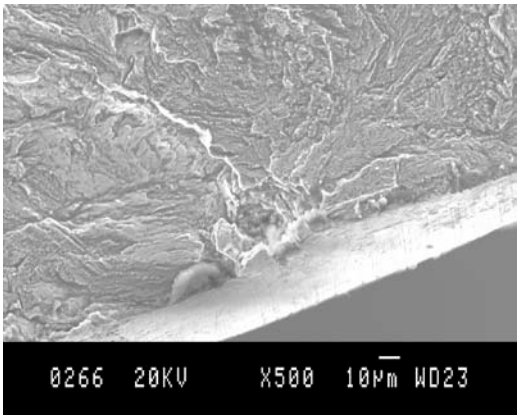

Specimen 14 X 500

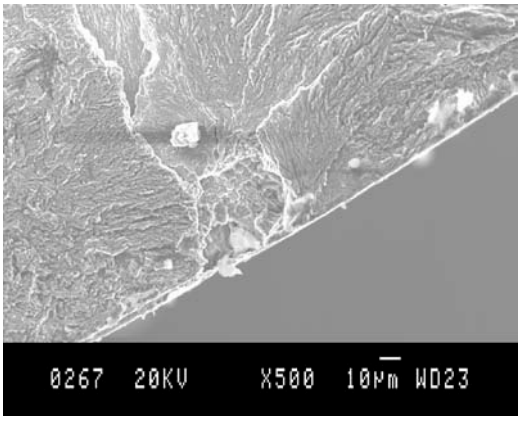

Specimen 14 X 500

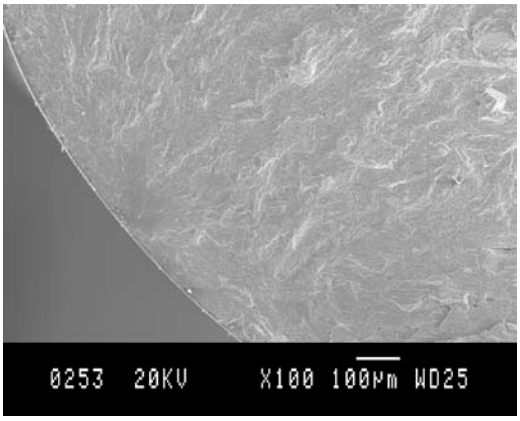

Specimen 15 X 100

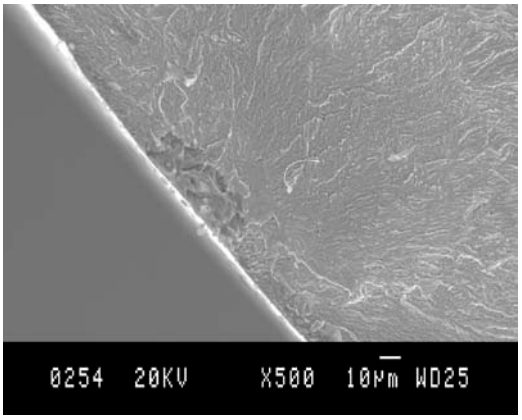

Specimen 15 X 500

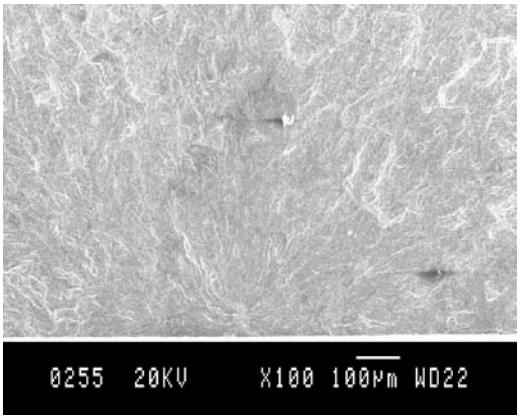

Specimen 16 X 100

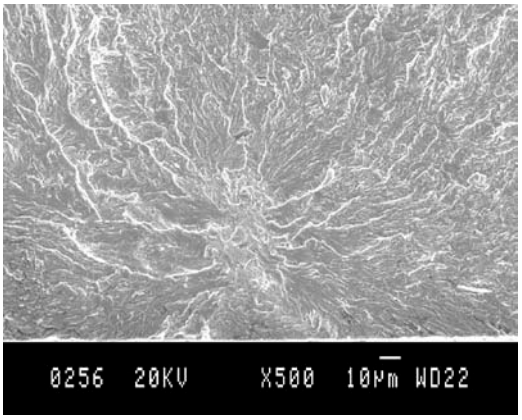

Specimen 16 X 500

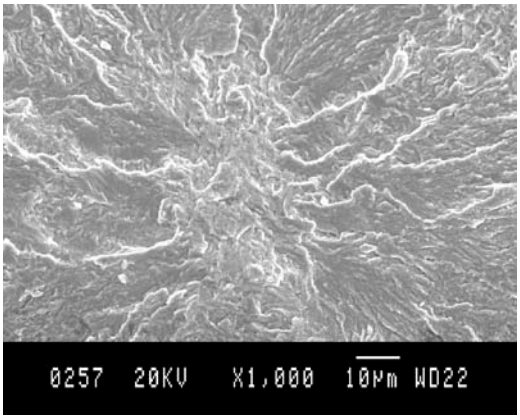

Specimen 16 X 1,000

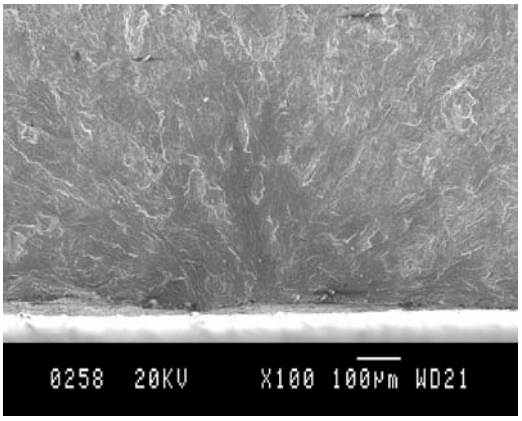

Specimen 17 X 100

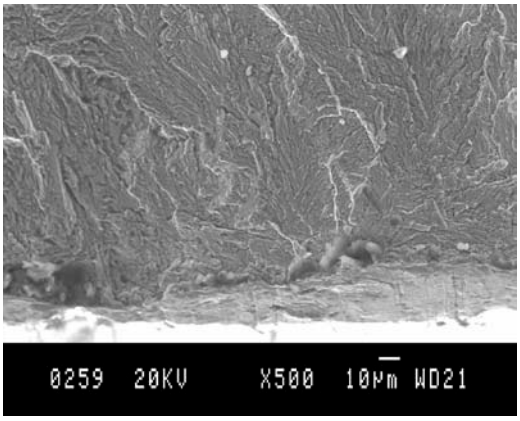

Specimen 17 X 500

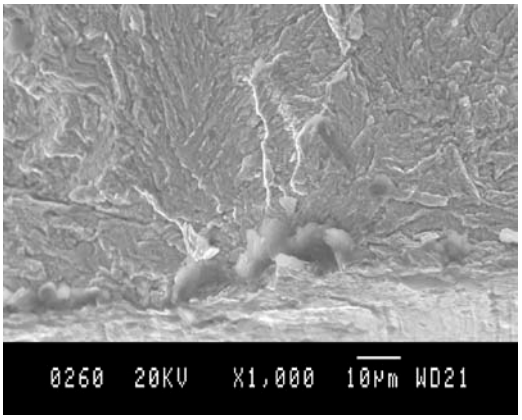

Specimen 17 X 1,000

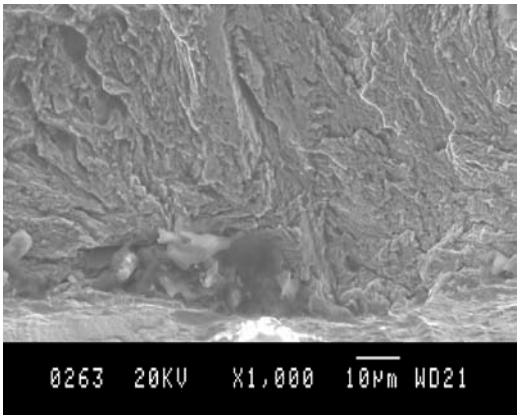

Specimen 17 X 1,000

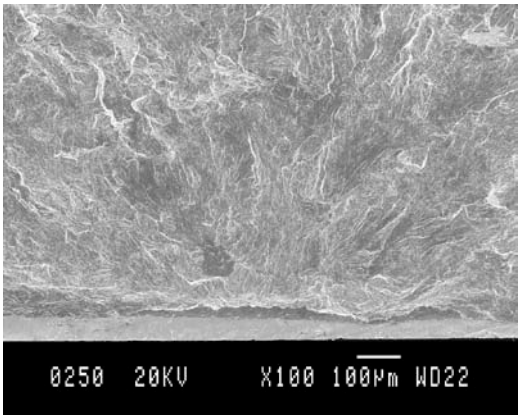

Specimen 18 X 100

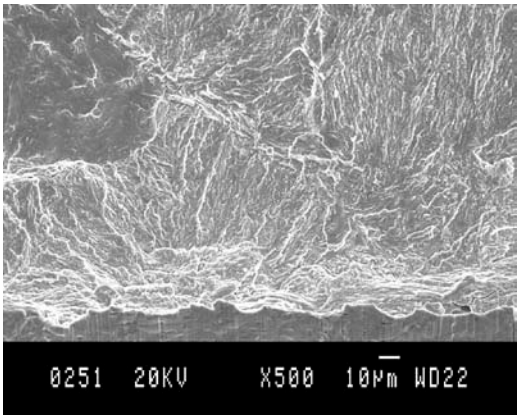

Specimen 18 X 500

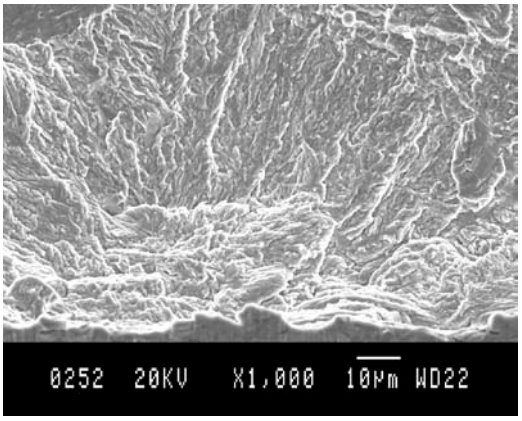

Specimen 18 X 1,000

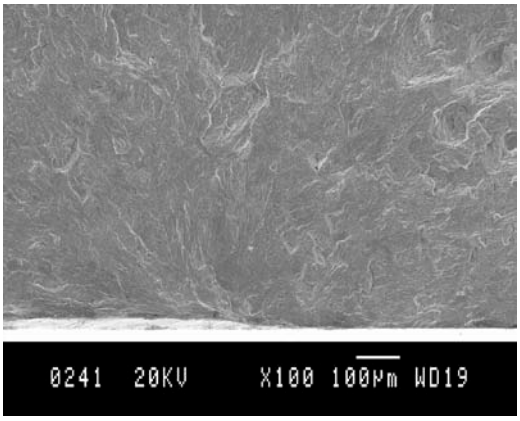

Specimen 19 X 100

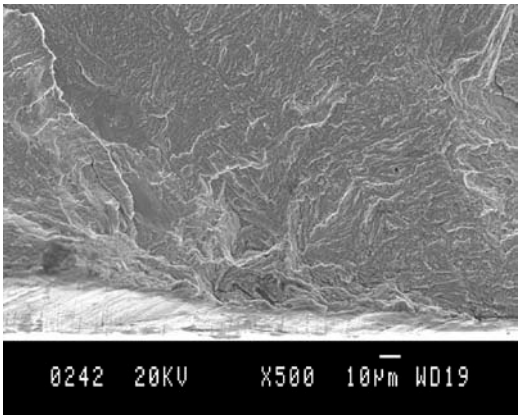

Specimen 19 X 500

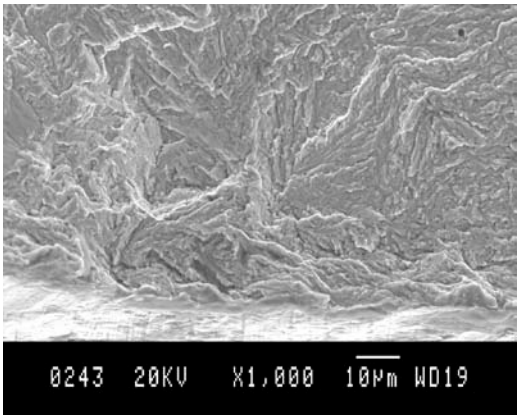

Specimen 19 X 1,000

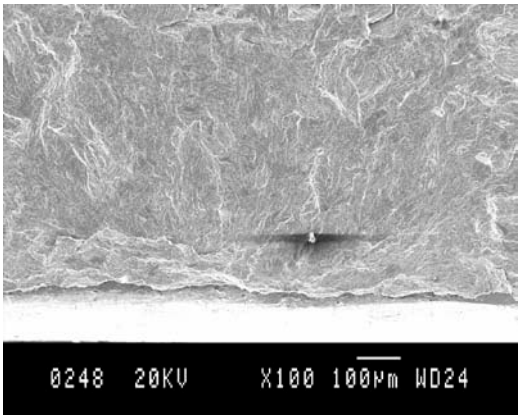

Specimen 20 X 100

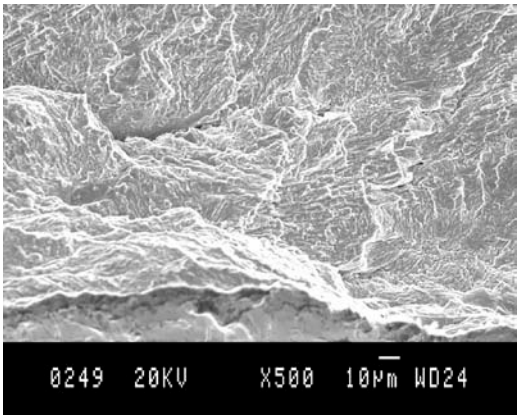

Specimen 20 X 500

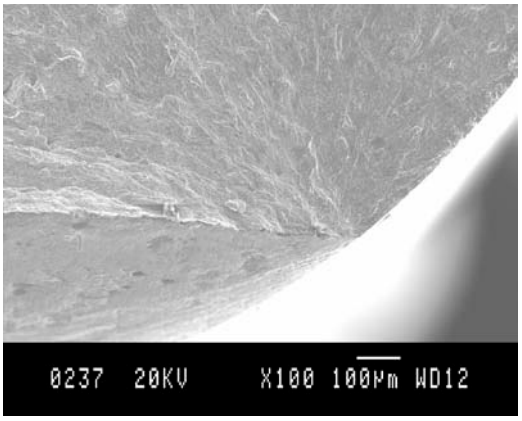

Specimen 21 X 100

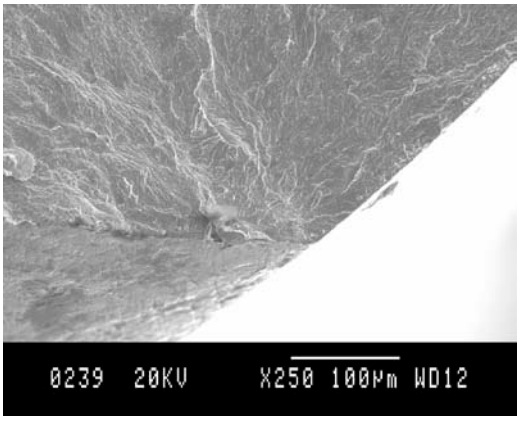

Specimen 21 X 250

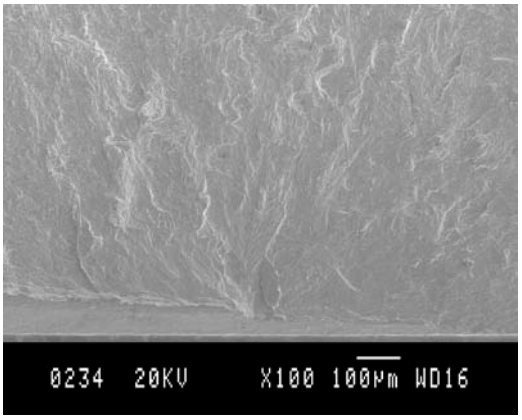

Specimen 22 X 100

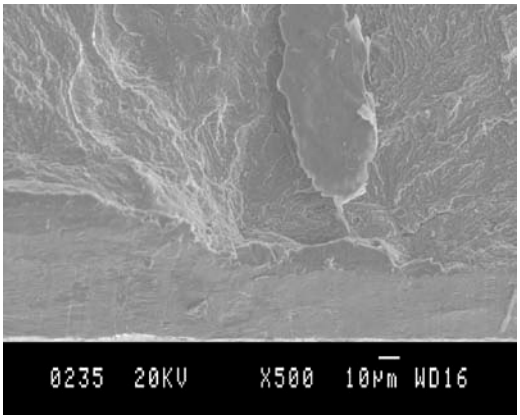

Specimen 22 X 500

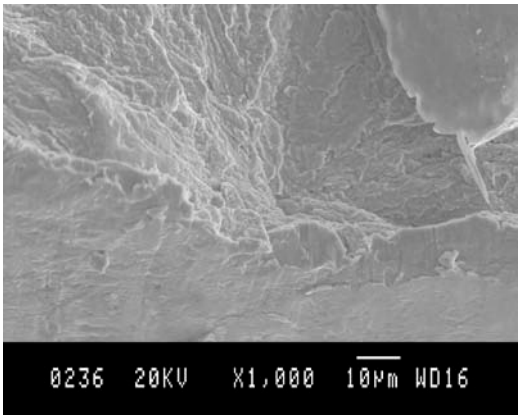

Specimen 22 X 1,000

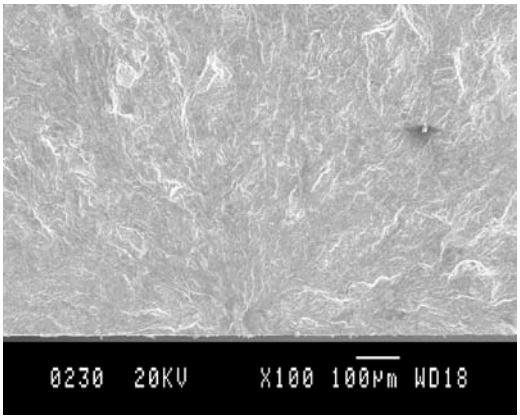

Specimen 23 X 100

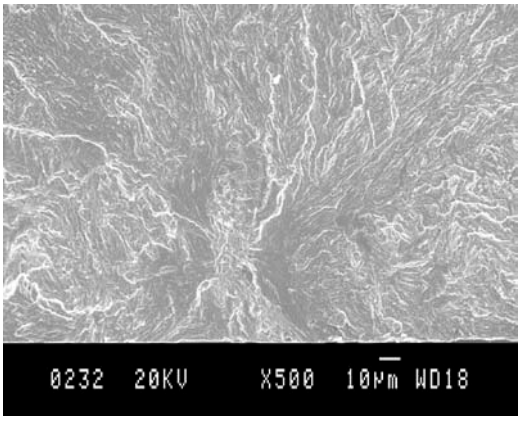

Specimen 23 X 500

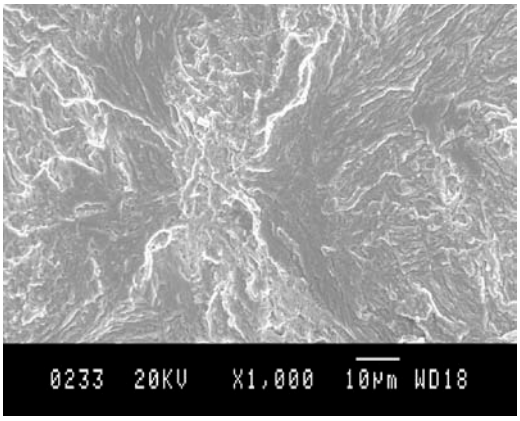

Specimen 23 X 1,000

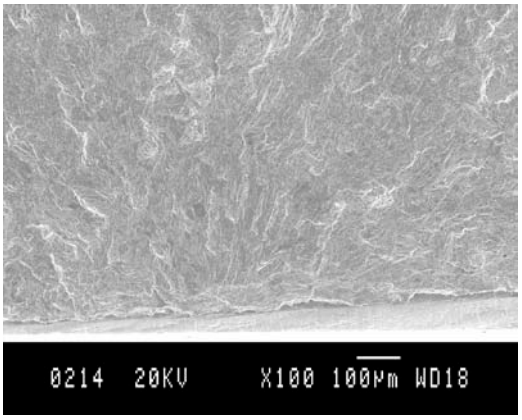

Specimen 24 X 100

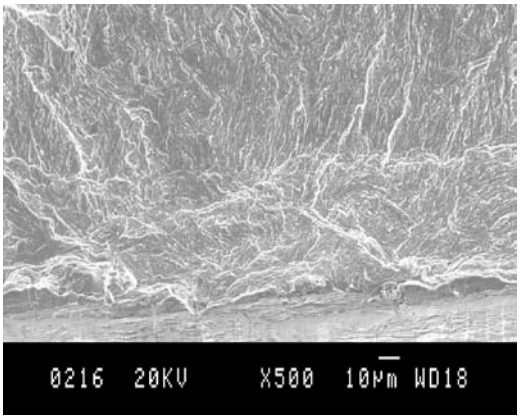

Specimen 24 X 500

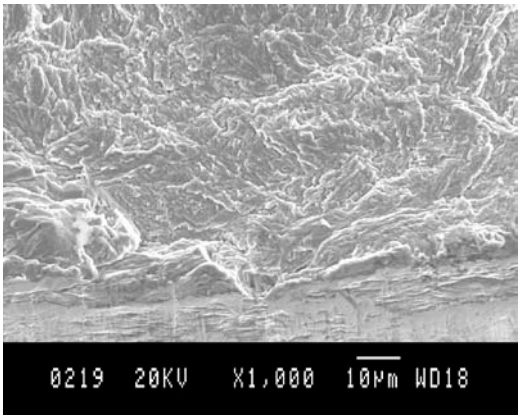

Specimen 24 X 1,000

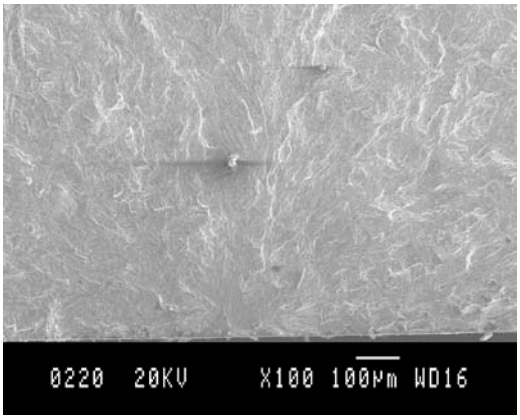

Specimen 27 X 100

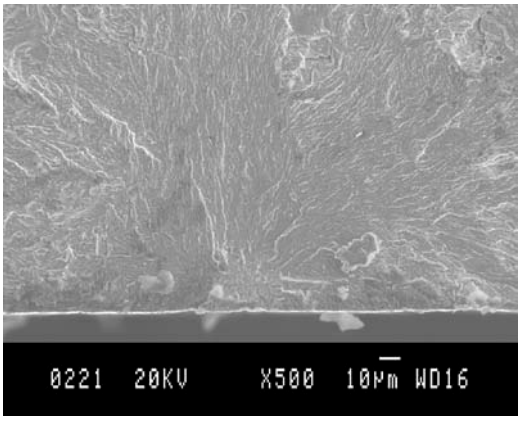

Specimen 27 X 500

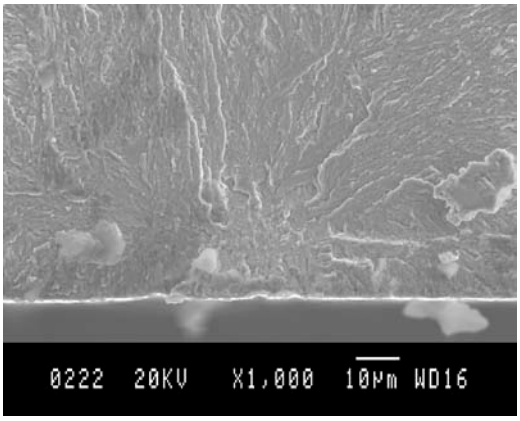

Specimen 27 X 1,000

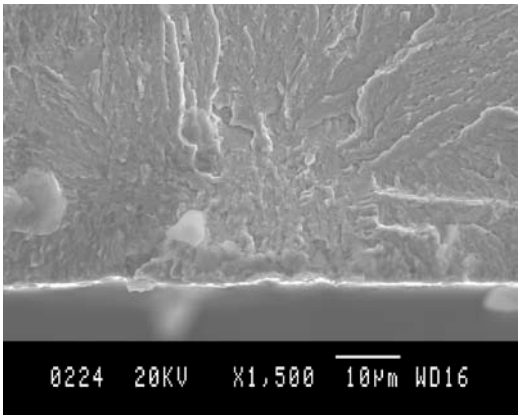

Specimen 27 X 1,500

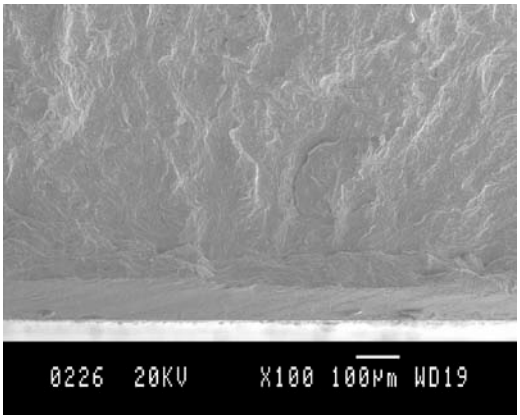

Specimen 28 X 100

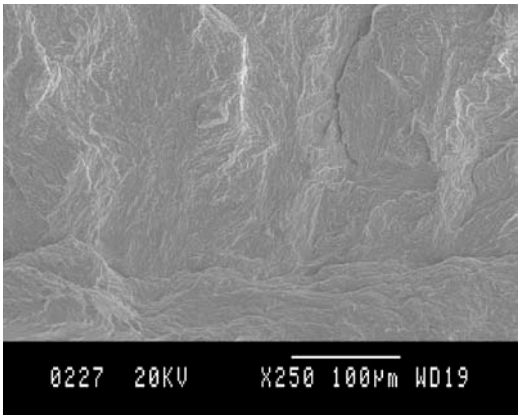

Specimen 28 X 250

APPENDIX F: SEM OF MACHINED SURFACES

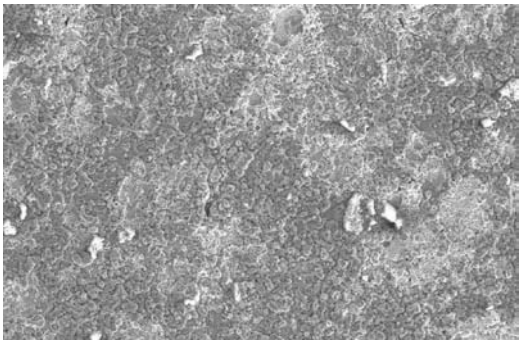

EDWC Specimen X 100

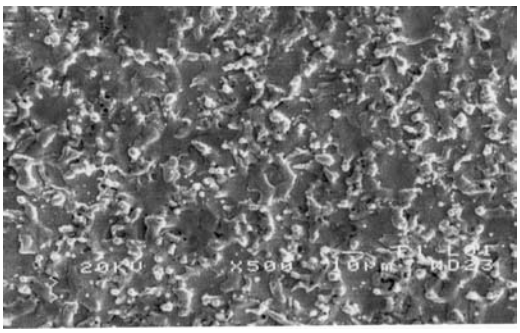

EDWC Specimen X 500

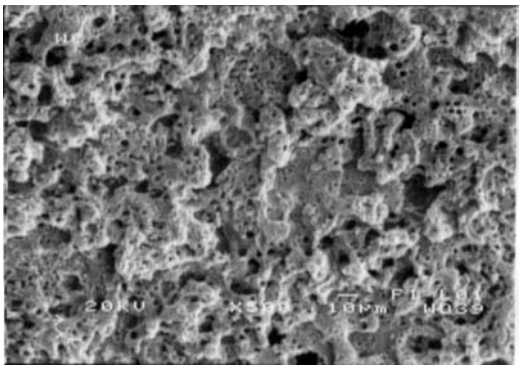

EDWC Specimen X 500

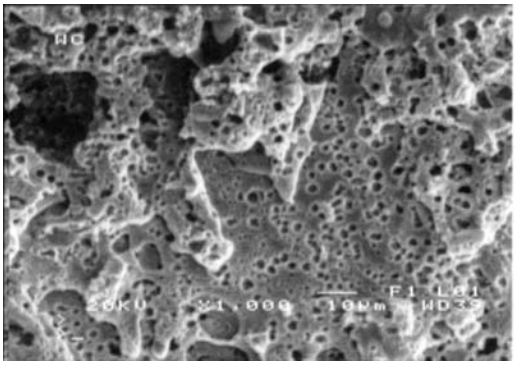

EDWC Specimen X 1,000

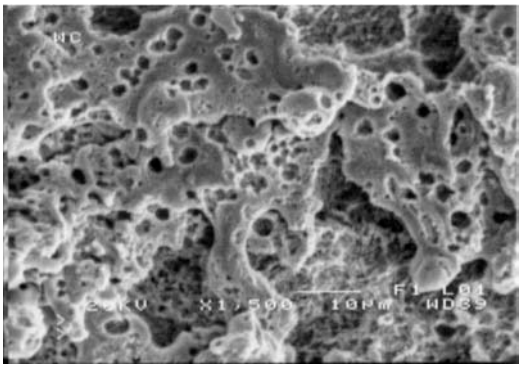

EDWC Specimen X 1,500

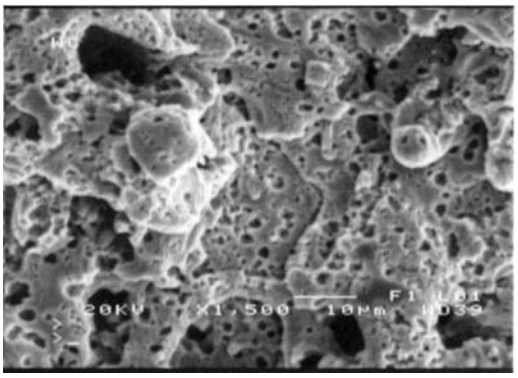

EDWC Specimen X 1,500

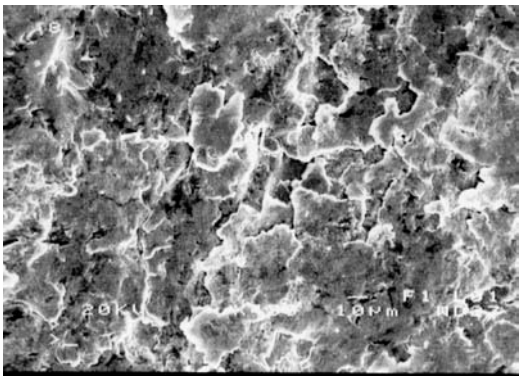

Shot Peened Specimen X 430

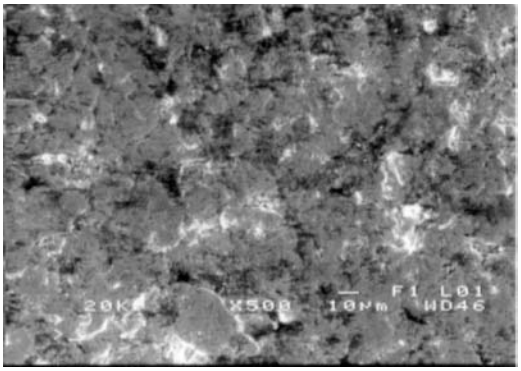

Shot Peened Specimen X 500

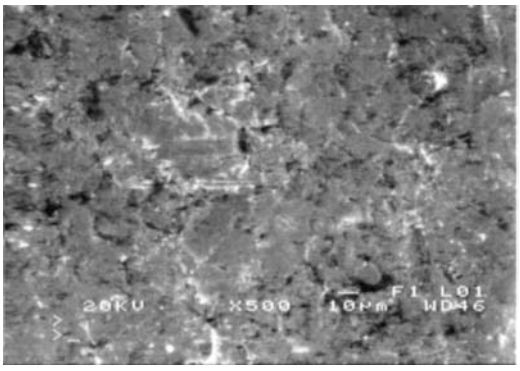

Shot Peened Specimen X 500

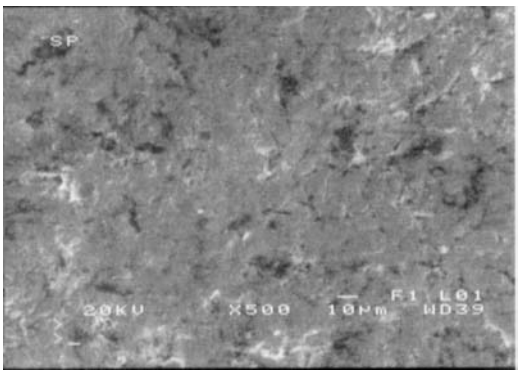

Shot Peened Specimen X 500

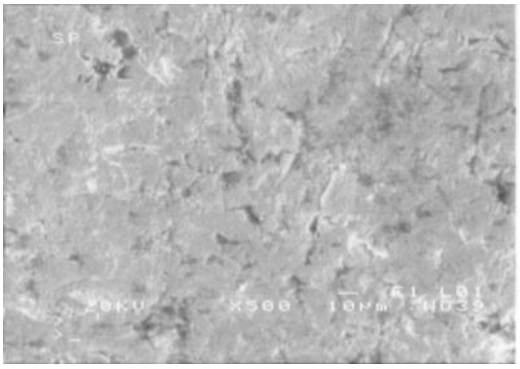

Shot Peened Specimen X 500

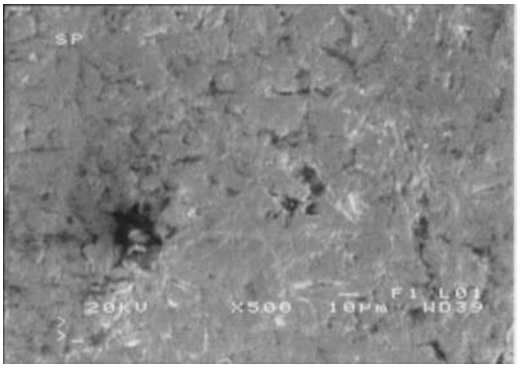

Shot Peened Specimen X 500

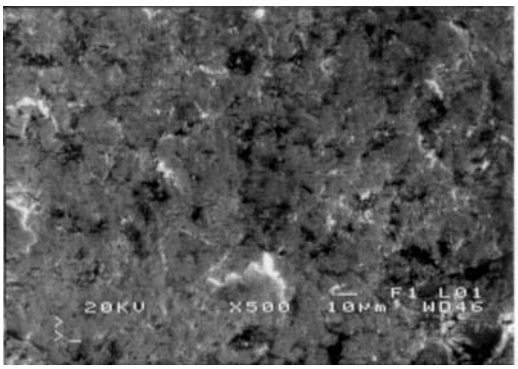

Shot Peened Specimen X 500

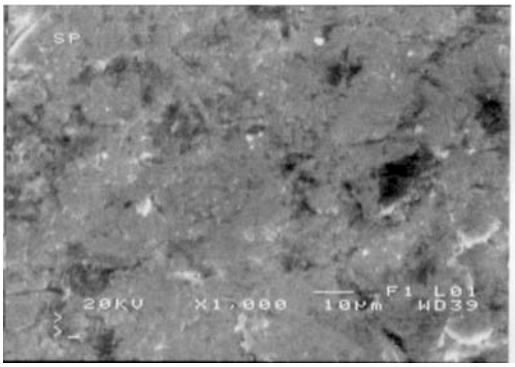

Shot Peened Specimen X 1,000

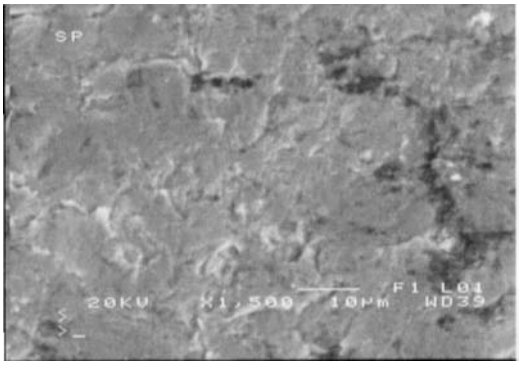

Shot Peened Specimen X 1,500

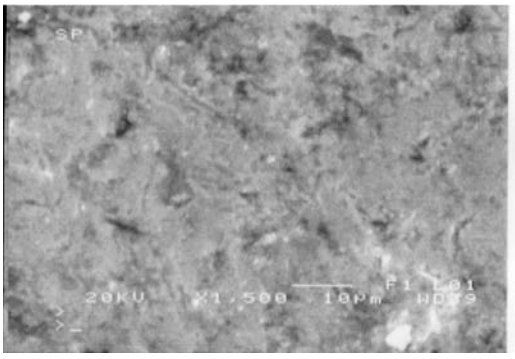

Shot Peened Specimen X 1,500

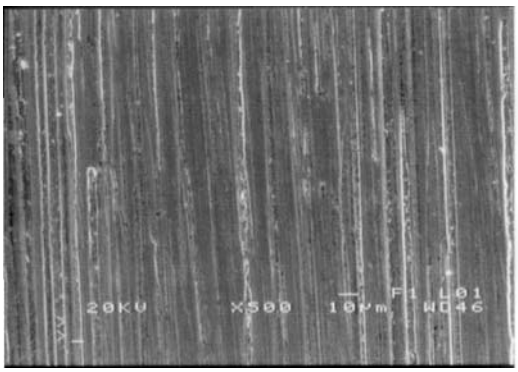

Ground Specimen X 500

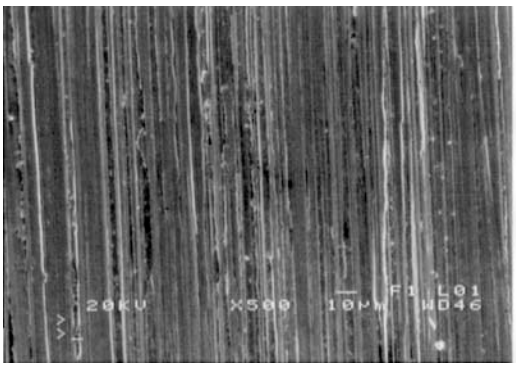

Ground Specimen X 500

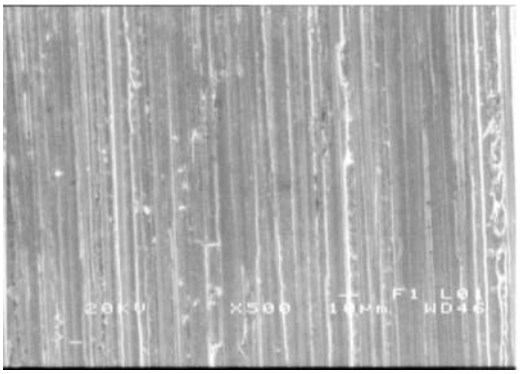

Ground Specimen X 500

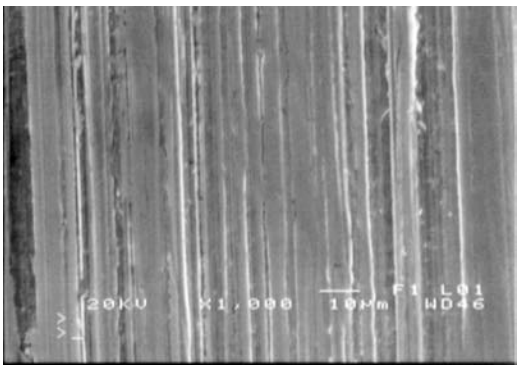

Ground Specimen X 1,000

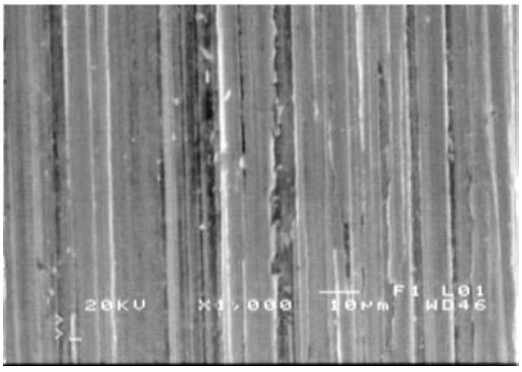

Ground Specimen X 1,000

APPENDIX G: MICROHARDNESS TESTING

Depth (mm)	Hardness (R_c)							
0.03	44.4	49.5	41.8	37.5	46.4	46.2	47.6	38.6
0.06	49.2	50.7	44.9	45.6	48.2	52.5	48.5	45.9
0.09	51.4	50.0	47.5	43.4	49.7	55.1	53.7	45.6
0.12	51.1	52.5	46.9	46.3	50.2	53.5	54.6	44.3
0.15	51.0	54.0	47.1	45.9	50.0	56.2	54.6	44.9
0.18	51.8	53.4	48.2	46.5	50.5	54.0	55.8	44.8
0.21	52.7	54.4	48.8	45.8	49.3	53.0	53.8	46.4
0.24	50.8	51.7	47.9	46.4	51.2	53.4	51.4	45.8
0.27	52.4	50.0	47.4	46.8	50.4	53.8	53.8	46.7
0.30	52.2	53.5	45.8	46.5	50.6	52.5	55.2	46.8
0.33	52.3	52.1	48.2	47.0	49.5	54.7	56.2	47.2
0.36	53.5	52.0	47.9	46.7	51.0	56.5	56.0	48.4
0.39	52.9	54.3	47.2	48.0	51.7	57.4	53.1	49.0
0.42	52.5	52.8	49.8	47.4	52.8	56.1	55.7	49.2
0.45	51.3	53.0	49.3	46.8	52.4	53.2	54.0	49.2
0.48	51.9	54.3	50.2	48.3	52.3	53.2	52.3	49.6
0.51	52.6	56.9	51.9	47.1	51.6	56.0	55.0	52.0
0.54	54.7	55.5	52.1	47.9	49.8	54.5	56.1	50.6
0.57	51.2	55.3	51.7	49.6	51.4	53.4	54.7	50.3
0.60		53.5	51.9	48.4	54.3	53.6	52.8	51.4
0.63		52.9	51.9	50.0	55.3	56.4	55.7	51.8
0.66		52.9	53.2	50.9	55.7	56.8	55.5	51.2
0.69		55.3	51.9	48.5	55.7	54.8	55.4	51.8
0.72		55.4	51.7	48.5	54.0	55.1	56.9	53.2
0.75		53.6	51.4	48.6	55.2	55.1	57.4	53.5
0.78		53.9	53.3	49.3	54.6	53.5	55.0	53.9
0.81		54.1	52.4	50.6	55.1	53.6	54.7	53.1
0.84		53.1	52.2	51.4	56.6	54.0	56.1	52.4
0.87		51.8	53.0	50.7	56.1	53.3	54.9	53.5
0.90		51.9	52.2	49.8	56.5	52.2	53.9	52.3
0.93		53.0	52.6	49.5	55.7	55.5	55.8	52.7
0.96		53.2	51.0	52.7	55.7	53.8	55.1	54.5
0.99		53.5	53.8	53.8	55.5	53.3	55.5	55.2
1.02		54.4	54.3	53.4	54.0	54.8	56.8	54.0
1.05		55.1	54.6	53.7	54.9	56.4	54.2	54.9
1.08		54.2	54.6	54.2	53.5	52.5	55.9	53.6
1.11			53.4	55.5	55.7	55.2	57.4	53.8
1.14			51.4	52.9	56.0	54.5	55.1	54.6
1.17			53.4	53.6	55.5	56.8	53.3	55.1
1.20			52.7	56.3	56.9	55.5	53.9	55.3

Table G1: EDWC Specimens

Depth (mm)	Hardness (R_c)			
0.03	38.9	50.4	49.7	52.5
0.06	41.6	49.3	51.9	55.1
0.09	41.5	50.8	53.3	56.1
0.12	42.6	50.0	53.5	57.2
0.15	42.7	51.1	52.4	57.6
0.18	41.7	51.8	49.0	55.0
0.21	42.0	51.2	51.9	5.6
0.24	42.2	51.3	51.2	51.3
0.27	41.9	49.3	51.1	52.0
0.30	49.1	48.2	50.7	53.6
0.33	49.2	49.2	51.4	53.5
0.36	47.6	50.0	52.4	54.1
0.39	48.0	51.1	50.3	52.9
0.42	49.2	50.1	49.6	54.1
0.45	50.4	52.5	51.1	55.4
0.48	49.2	52.2	50.8	56.3
0.51	49.8	51.6	52.3	52.6
0.54	50.4	50.0	50.5	51.7
0.57	50.4	51.8	51.7	55.2
0.60	51.2	51.9	50.7	56.0
0.63	50.5	53.7	52.4	56.4
0.66	51.7	52.2	51.0	53.6
0.69	51.0	53.2	54.1	50.0
0.72	50.0	54.3	54.0	52.8
0.75	49.1	54.3	54.9	54.2
0.78	49.2	52.0	54.9	53.9
0.81	48.7	54.1	53.6	53.5
0.84	48.3	53.6	52.0	55.3
0.87	49.5	54.9	52.7	54.1
0.90	49.6	52.8	52.0	52.4
0.93	50.3	49.4	53.7	52.1
0.96	53.1	53.3	54.2	55.3
0.99	52.5	52.1	53.2	54.2
1.02	51.0	53.9	53.4	56.1
1.05	52.0	53.0	55.7	53.1
1.08	51.6	55.0	53.1	53.0
1.11	52.5	53.7	53.6	52.6
1.14	51.6	52.4	54.0	52.1
1.17	51.7	50.3	55.4	51.6
1.20	52.6	51.4	55.6	52.0

Table G2: Shot Peened Specimens

Depth (mm)	Hardness (R_c)			
0.03	50.3	44.9	47.3	44.1
0.06	53.0	45.2	48.1	48.3
0.09	54.3	46.6	50.3	49.4
0.12	54.0	46.7	49.3	49.3
0.15	50.4	47.3	49.9	47.8
0.18	47.5	48.0	50.0	51.7
0.21	47.4	48.2	50.5	51.4
0.24	48.5	47.6	49.1	49.2
0.27	48.4	46.4	49.1	48.7
0.30	48.5	49.7	48.7	49.5
0.33	48.5	46.6	49.2	48.9
0.36	48.3	46.5	50.2	47.8
0.39	49.3	47.6	49.6	49.3
0.42	49.4	49.4	49.0	47.7
0.45	50.3	48.0	50.2	49.1
0.48	50.1	48.8	51.7	49.7
0.51	51.8	49.0	51.4	51.4
0.54	51.5	48.0	49.9	53.3
0.57	52.5	48.9	50.5	53.1
0.60	51.5	49.3	51.6	53.7
0.63	49.8	49.9	53.3	52.6
0.66	48.9	50.0	52.2	53.1
0.69	50.7	50.2	50.1	52.9
0.72	45.7	49.5	50.8	52.1
0.75	50.0	49.0	52.9	51.4
0.78	52.2	54.3	56.1	56.7
0.81	53.1	53.3	53.9	54.8
0.84	53.9	53.4	55.5	53.8
0.87	51.0	51.6	51.8	52.7
0.90	52.6	52.1	50.0	54.7
0.93	52.8	51.9	49.9	51.9
0.96	53.7	51.8	52.5	54.7
0.99	53.0	51.8	51.3	53.2
1.02	54.2	53.9	53.3	52.5
1.05	53.4	51.6	53.4	49.4
1.08	54.9	52.1	53.3	50.4
1.11	54.3	53.7	54.4	53.7
1.14	54.5	53.3	53.6	54.1
1.17	53.4	54.0	52.2	52.4
1.20	51.8	51.4	50.4	52.3

Fig G3: Ground Specimens

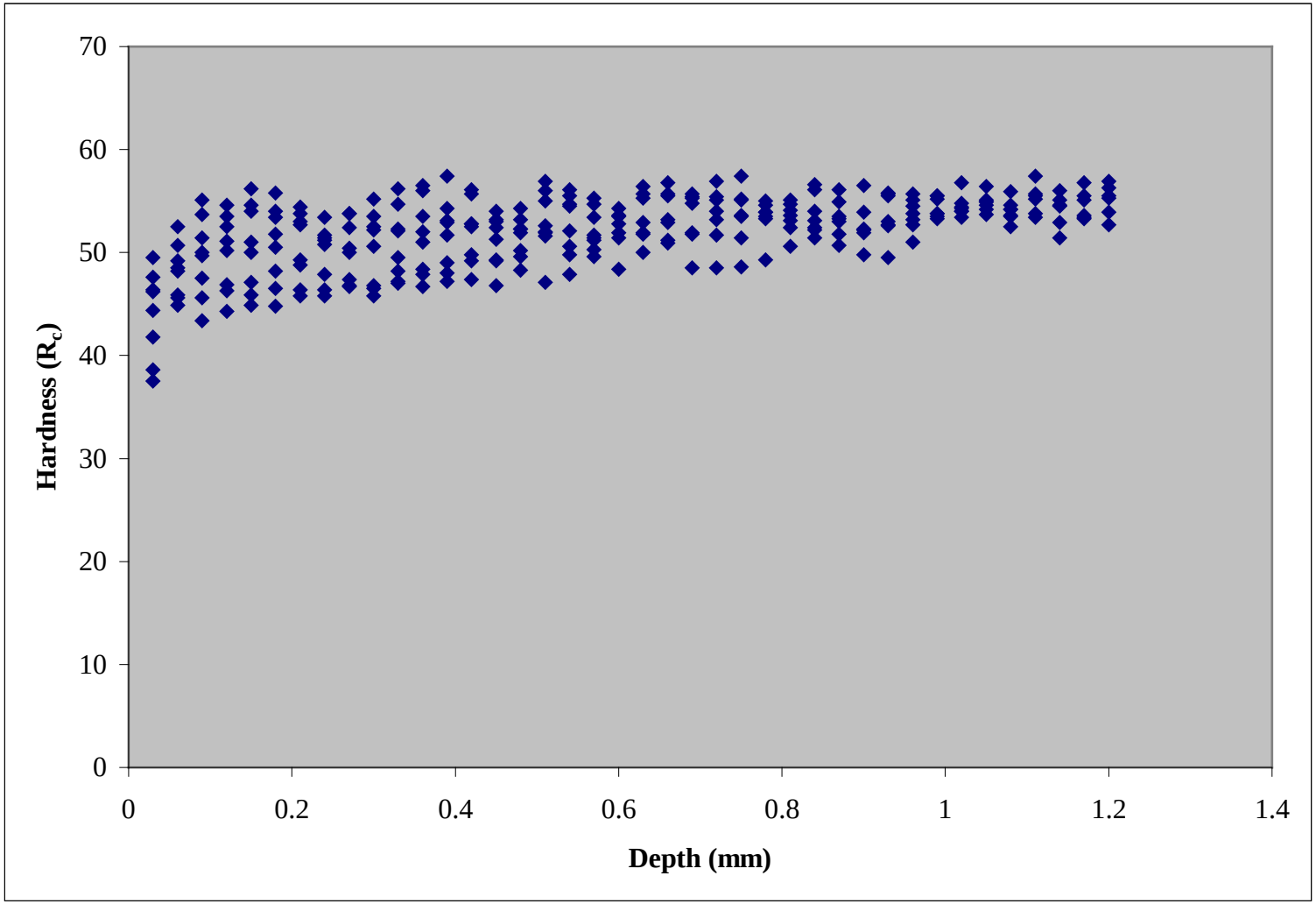

Fig G1: EDWC Specimens

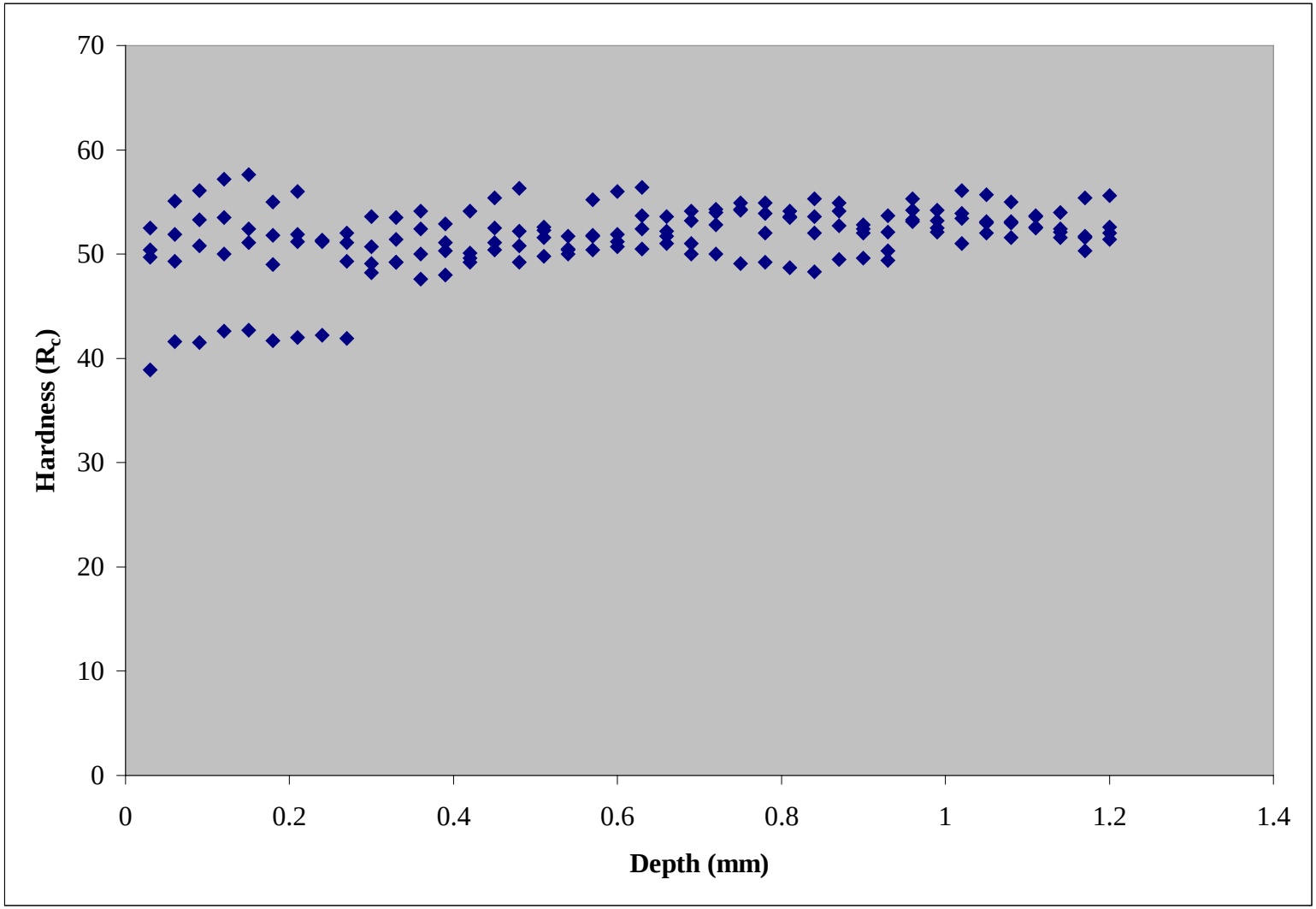

Fig G2: Shot Peened Specimens

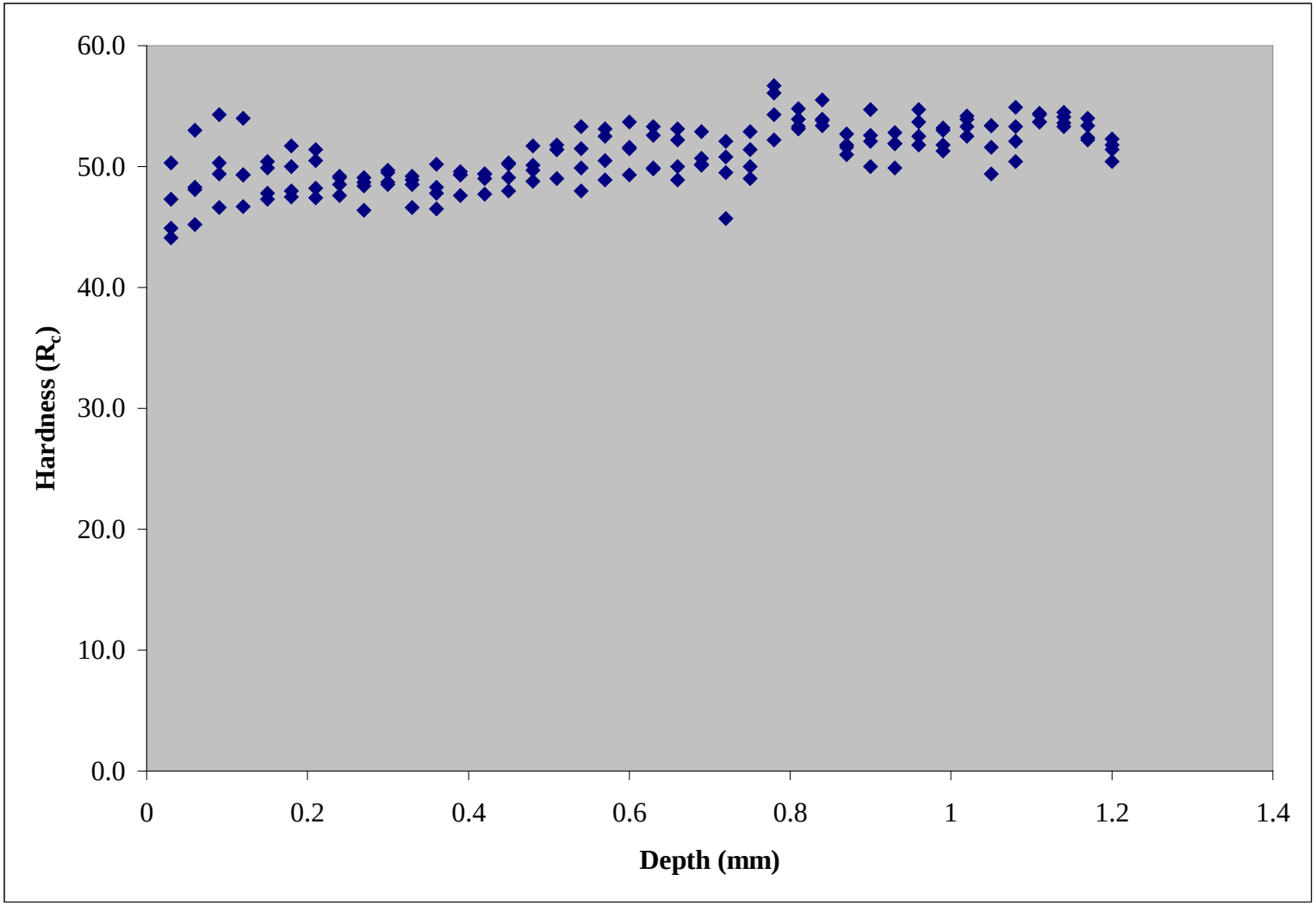

Fig. G3: Ground Specimens

APPENDIX H: SURFACE ROUGHNESS TESTING

EDWC Specimens			Shot Peened Specimens		Ground Specimens	
Length		Width	Length	Width	Length	Width
3.20	3.30	4.30	0.70	0.50	0.15	0.39
2.40	3.10	3.30	0.70	0.70	0.12	0.35
2.60	2.80	3.20	0.94	0.90	0.22	0.42
3.00	3.10	3.20	0.94	0.76	0.15	0.47
3.20	3.20	3.30	0.84	0.91	0.18	0.49
2.60	2.90	3.60	0.87	0.81	0.20	0.44
2.60	3.30	3.20	0.89	1.65	0.17	0.49
2.50	4.20	3.10	0.94	1.40	0.24	0.45
2.90	3.05	2.90	0.86	1.45	0.15	0.51
2.70	4.20	3.25	0.81	1.25	0.28	0.40
3.00	3.30	3.40	0.85	1.60	0.15	0.41
3.00	2.70	2.80	0.70	1.30	0.22	0.38
3.10	4.20	3.30	0.98	1.00	0.19	0.37
3.10	2.95	3.50	1.20	0.85	0.20	0.32
3.40	4.05	3.60	1.40	1.15	0.24	0.38
3.40	3.30	2.95	1.60	0.80	0.20	0.40
3.20	3.95	2.50	0.75		0.18	
3.80	4.50	2.95	1.30		0.22	
3.75	4.40	3.05	1.40			
3.45	3.60	3.30	1.30			
2.60	3.40	3.60	1.20			
3.00	2.90	4.20	1.05			
2.85	3.40	4.10	1.10			
2.50	2.90	3.60	0.80			
2.75	3.05	3.00				
3.80	3.05	3.40				
2.95	3.00	3.70				
3.45	2.80	3.60				
2.70	3.80	3.70				
2.90	3.10	2.90				
3.45	3.15	3.40				
2.80	3.50	3.00				
2.90	3.40	2.80				
3.20	3.30	2.60				
3.70	3.00	2.60				
3.60	3.55	2.90				
3.20	3.40	2.95				
3.45	3.80	2.80				
2.80	3.00	3.30				
3.60	3.20	2.90				
3.40	3.15	3.00				
3.20	2.40	3.30				
3.20	2.50	3.45				
4.40	2.90	3.40				
3.00	2.95	2.80				
3.45	2.50	2.90				
2.80	3.40					
2.95	3.10					
3.05	3.60					
2.75	2.75					

Table H1: Surface Roughness Test Results